Durham E-Theses

Vapour sensing applications and electrical conduction mechanisms of a novel metal-polymer composite

Hands, Philip James Walton

Vapour sensing applications and electrical conduction mechanisms of a novel metal-polymer composite

A thesis submitted for the degree of
Doctor of Philosophy

Philip James Walton Hands

2003

Supervisor: Professor D. Bloor

University of Durham
Department of Physics

PERATECH Ltd
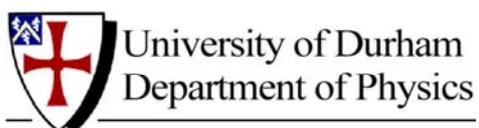
Declaration

I confirm that no part of the material offered has previously been submitted by me for a degree in this or any other University. If material has been generated through joint work, my independent contribution has been clearly indicated. In all other cases, material from the work of others has been acknowledged and quotations and paraphrases suitably indicated.

Signed …………………………………….

Candidate

The work reported in this thesis was carried out by the candidate. Any work not carried out by the candidate is acknowledged in the main text.

Signed …………………………………….

Ph.D. supervisor

Abstract

A novel metal-polymer composite is presented, comprised of a micron-sized nickel powder dispersed within a silicone polymer matrix. The composite is intrinsically electrically insulating, but displays a dramatic increase in conductivity under compression, tension and torsion. The electrical response to applied compression is characterised. Combined with electron microscopy, the large sensitivity to compression is shown to be due to the uniquely spiky morphology of the filler particles. Low mechanical energy mixing techniques are essential for retaining these sharp tips. In addition, wetting of the nickel particles by the silicone polymer is highly effective, resulting in negligible inter-particle contact between metallic grains even at very high loadings and compressions.

Current-voltage characteristics are highly non-linear, displaying peaks, hysteresis, negative differential resistance, trap-filling and radio frequency emission. Evidence points towards an inter-particle conduction mechanism dominated by field emission and Fowler-Nordheim tunnelling, made possible by localised field enhancements at the sharp tips. A novel mechanism of grain charging and the 'pinching-off' of conduction pathways is also suggested.

Granular forms of the composite display dramatic increases in resistance when exposed to organic solvent vapours, transduced by a polymer swelling mechanism. Responses are dependent upon vapour concentration, and differential responses are obtained with other polymers, indicating excellent potential for applications in artificial olfactory devices (electronic noses). Polymer-solvent interactions follow both Fickian and anomalous diffusion characteristics, and follow basic trends predicted by solubility parameters.

Contents

Section A: Electrical characterisation of QTC

Section B: Vapour sensing applications of QTC

List of figures and tables

4

5

6

7

1 General introduction

1.1 *What is a metal-polymer composite?*

Metal-polymer composites and their related applications have been extensively researched in both academia and industry for over 40 years throughout the world. Often, the incentive behind such research is the desire to create new materials, combining many of the electrical properties of metals, whilst retaining the rheological characteristics of a polymer.

Typically, metal-polymer composites consist of a conductive powder mixed into a non-conductive polymeric matrix. Filler powders vary greatly in their shape, size and composition. Metallic filler powders are often chosen, offering a wide variety of electrical and magnetic properties [1]. Examples include silver [2], gold [2], copper [3], nickel [4] and zinc [5]. However, carbon-black and other furnace-blacks are usually favoured [6-8] due to their low cost, wide availability and good conductive properties. More recently, carbon nano-tubes have also incorporated into such composite systems [9] [10]. Filler particle sizes range from the nano-scale to hundreds of microns, and have wide morphological variety [4] [11]. Shapes include filamentary strands, fibres, spherical balls, oblate and prolate spheroids and flat discs.

The insulating matrix may be formed from any non-conducting material, but is usually a polymer. Examples include poly(ethylene), poly(urethane) and natural rubber. The polymer is normally non-conducting, but conducting polymers have also been used [12] [13]. Polymers are primarily chosen according to their wetting ability and mechanical properties. Polymer blends are also often used [14] to help obtain a composite with the desired physical and electrical characteristics.

The presence of conducting particles within a metal-polymer composite will impart improved electrical properties upon the material. These properties can be adjusted by simple alteration of the respective component materials, or by changing the loading ratio of filler in the polymer. One important property of such composites is their change in resistivity when subjected to mechanical distortions [15]. Compressing the composite causes the conductivity to increase, whilst conversely, stretching causes a decrease in conductivity. In addition, they display sensitivity to changes in temperature, often displaying a positive temperature coefficient of resistance (PTCR) effect [16].

1.2 Examples of current applications

Perhaps the most obvious application of a metal-polymer composite is as a pressure sensor or transducer [17]. Such devices can be used in electrical systems for pressure sensing or switching, including also biometric [18] and robotic [19] [20] applications. The PTCR effect is also exploited in resettable fuses, for current surge protection and thermostats. In addition, these types of composites can also be used as conductive adhesives [1] [21], antistatic materials and also in electromagnetic interference (EMI) shielding applications [22] [23]. More recently, it has been shown that certain metal-polymer composites change their conductivity in the presence of chemical vapours [24] [25]. Such composites may therefore be utilised as sensing devices, and can be incorporated into artificial olfactory systems or "electronic noses".

1.3 Who are Peratech, and what have they invented?

Peratech is a high-tech materials development company, based in Darlington, UK. In 1997 they invented a new form of metal-polymer

composite, which they have named QTC (Quantum Tunnelling Composite). It is made using a patented manufacturing process [26], which gives rise to a composite with unique electrical properties.

Fig. 1.1: The family of QTC materials

The composite is intrinsically electrically insulating, but drastically increases its conductivity over many orders of magnitude, when subjected to any variety of mechanical deformation, such as compression, tension, bending or torsion. This is contrary to most standard composites whose conductivity increases only under compression, whilst tension results in a conductivity decrease [27]. At very large strains however, an irreversible conductivity increase is sometimes observed in standard composites (figure

1.2). Under such extreme conditions, severe and irreversible narrowing (or 'necking') of the polymer occurs, as the material's behaviour changes from elastic to plastic. The result of this narrowing may then give rise to a permanent conductivity increase, as metallic particles are pushed closer together.

QTC however, is unique in that it displays a fully reversible conductivity increase with increasing tension at low strains as well as the extreme high strain case described above. In addition, QTC displays extreme sensitivity to such deformations, changing its resistivity over many orders of magnitude. This is far in excess of the ranges displayed by standard, conventional metal-polymer composites.
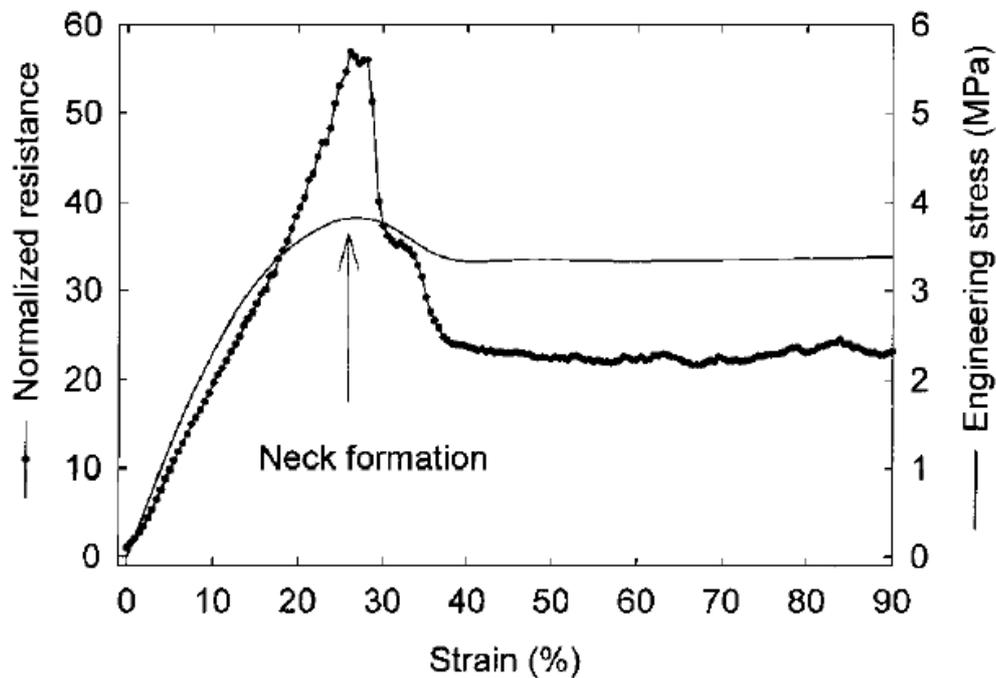
Fig. 1.2: *Change in resistance under tension for*
a carbon-filled ethylene-octene composite [28]

Peratech have developed a variety of different types of QTC materials, some of which can be seen in figure 1.1, all of which display the same properties as the standard composite. Different fillers have been used, usually consisting of different forms of nickel powder, but also including dendritic copper. Polymer type has also been varied. The standard composite uses silicones, but other examples include poly(urethane), poly(butadiene), poly(iso-butyl acrylate) poly(vinyl alcohol) and poly(acrylic acid). Usually the above combinations are made in a bulk material form. However, a granular and an open-cell foam form of many of the above can also be made. QTC granules are discussed in more detail in section B of this thesis, for use in vapour sensing applications.

In addition to QTC, certain other metal-polymer composites have also been reported to display unusual electrical behaviour under compression and tension. Kost *et al.* [15] claim a conductivity decrease under both compression and tension, but offer no explanation of the effect. Shui and Chung [29] report observations of a conductivity increase with applied tension, whilst under compression, a conductivity decrease is seen. The cause of this effect is thought to be an increase in filament alignment within the composite when under tension. The result being the complete opposite effect to the properties displayed by QTC. No other material has yet been reported to display the same electrical trends as displayed by QTC under compression and tension. In addition, the increase in conductivity in response to bending and torsion is also thought to be unique.

In 1998, Peratech approached the Department of Physics at the University of Durham in an attempt to fully understand the unusual properties of their composite. Since that date, QTC has been the subject of intense collaborative research between the University and Peratech, and numerous research projects have been completed on the subject. The work carried out

within the University has helped shed light upon the material's unique conduction mechanisms, and also assisted in the development of new commercial applications for the composite.

1.4 Aims and objectives of PhD

This PhD thesis follows previous work carried out by the author as part of a fourth year MSci Master's research project. It will therefore draw and build upon some of the ideas and conclusions presented in that document. In order to assist the reader, the results to this previous work are also summarised. In addition, the results of other parallel research projects studying QTC materials will be detailed where appropriate.

The content of this thesis can be divided into two sections. Firstly, the electrical properties of QTC are characterised and investigated, exploring the fundamental conduction mechanisms taking place within the composite. In order to study these properties, a variety of the composite's characteristics are studied, including current-voltage characteristics, response to compression and microstructural analysis of the material.

The second section of this thesis is devoted to the development of a commercial application of QTC. Specifically, the chemical vapour sensing properties of QTC are investigated. Its potential as both a quantitative and qualitative sensor within an artificial olfactory device or "electronic nose" is evaluated by a series of experiments exposing various forms of the composite to different concentrations of solvent vapours.

Section A: Electrical characterisation of QTC

2 Theory of electrical conduction in metal-polymer composites

In this section of the thesis, the electrical characterisation of Peratech QTC is discussed, together with some proposed conduction mechanisms of the metal-polymer composite. It begins with a review of current theories behind similar physical systems, and is followed by a summary of previous research undertaken upon the Peratech composite. An experimental and results section then follows, detailing the research carried out in this project. Conclusions are then presented, together with a proposed model of electrical conduction for the QTC material.

The current theories behind electrical conduction within metal-polymer composite systems differ widely between composite types. No single theory can accurately predict the observed behaviour of all metal-polymer composites. However, this area is principally dominated by two main theories: Percolation Theory and Effective Medium Theory. A number of highly specialised tunnelling theories have also more recently been developed. However, for the majority of materials developed, Percolation Theory leads the way in its ability to most accurately predict physical behaviour in the widest variety of metal-polymer composite materials. Good reviews of conduction mechanisms within metal-polymer composites have been written by Strümpler and Glatz-Reichenbach [30] and Roldughin and Vysotskii [31].

2.1 Percolation Theory

The concept of Percolation Theory was first introduced by Broadbent and Hammersley in 1957 [32]. It was developed as a general model of the random motion, or percolation, of a 'fluid' through a 'medium'. Up until that time, such systems were modelled only by conventional diffusion theory. The 'fluid' and 'medium' can be interpreted in a wide variety of different ways: for example, disease spreading throughout a community, molecules penetrating a solid, or electron migration in an atomic lattice. It can also be used to model the electrical interconnectivity of conductive grains within a metal-polymer composite, although this application was not developed until many years later.

(a)   *(b)*
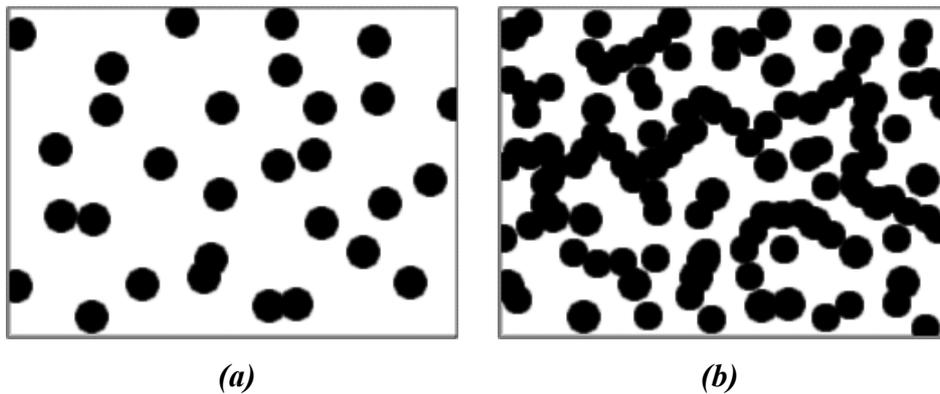
Fig. 2.1: *Two diagrams representing a metal-polymer composite*
(a) below, and (b) at its percolation threshold

Consider a sample of electrically non-conducting polymer, into which is mixed a small quantity of conductive particles (fig 2.1(a))**.** The conductive grains are distributed randomly throughout the polymeric matrix, but are at a sufficiently low concentration for inter-particle contact to be negligible. If one assumes that electrical conductivity is only possible via conducting

particles that are in direct contact with each other, then, at this stage, the overall conductivity of the composite is low.
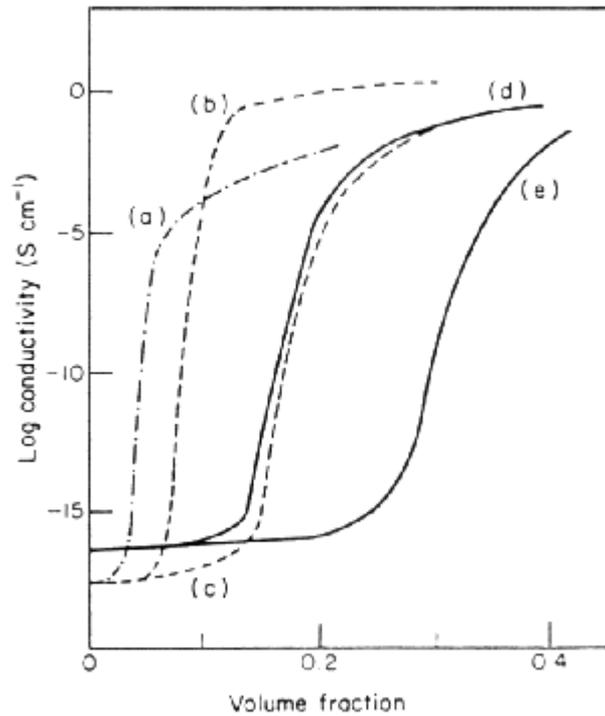
Fig. 2.2: *Percolation curves for carbon-black loaded (a) PE;*
(b) & (c) PMMA; (d) & (e) PVC-co-vinyl acetate [33]

If one continues to randomly add more conductive particles into the system, the number of conductive grains in direct contact with each other increases. Eventually, at some critical concentration, a conductive pathway is formed, spanning the length of the sample, enabling electrical conduction to occur (fig 2.1(b)). This critical point is known as the percolation threshold. The overall conductivity of the sample now rises very rapidly with increasing filler concentration as more percolating pathways are formed within the

16

composite. This gives rise to a step-like pattern of conductivity against filler concentration, as can be seen in figure 2.2.

Percolation Theory predicts that the relationship between the direct-current conductivity (σ_{DC}) of a metal-polymer composite and the concentration of the conductive filler particles, *p*, is given by equation 2.1.

$$\sigma_{DC} \propto \left(p - p_c \right)^t \qquad (2.1)$$

where p_c is the percolation threshold concentration, and the value, *t*, can vary according the exact model of percolation used. Equation 2.1 yields unphysical values for the conductivity for $p < p_c$, and therefore only holds for concentrations above the percolation threshold (figure 2.3).

Due to the statistical nature of Percolation Theory, Monte-Carlo simulations are often used to model metal-polymer composite systems [34]. These simulations, along with other computer modelling techniques, have shown the value of *t* to usually have a value of between 1.6 and 2.4 for three-dimensional systems [35-37]. However, experimental observations do not always concur, ranging from 2.17 [36] to 3.1 [38]. The discrepancy in the value of this parameter is due to that fact that Percolation Theory cannot perfectly predict the behaviour of all metal-polymer composite systems. A number of modifications to the theory have since been developed. These new theories attempt to introduce other variables, such as particle shape and size (with varying degrees of success), in an attempt to fit the theory to experimental observations. Different approaches to the standard statistical model are used in each case, including thermodynamic and geometrical approaches. A good review of these modified percolation theories can be found by Lux [39].
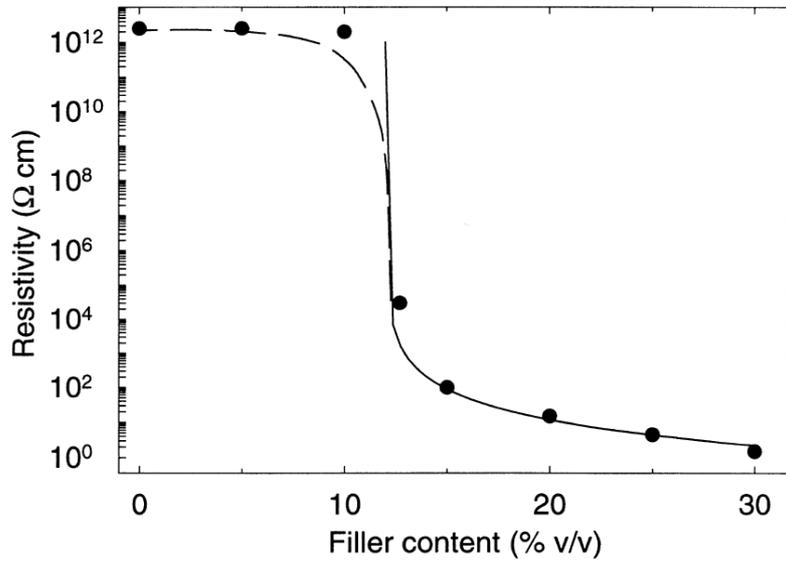
Fig. 2.3: *Theoretical fit of Percolation Theory (solid line) to experimental data for carbon black-filled ethylene-octene elastomers [27]*

Table 2.1 shows experimental measurements of percolation thresholds for a variety of different filler particle shapes and sizes. Certain trends can be observed. For example, the percolation threshold is reduced as particle size is reduced [3] [34]. Aspect ratio also has an effect. Long filamentary fillers with high aspect ratios tend to have lower percolation thresholds compared to shorter fibres with low aspect ratios [3] [40]. In addition, percolation thresholds are reduced for irregular and more highly structured particle shapes when compared to spherical particles [3] [36]. Using Monte-Carlo simulations, Wang and Ogale [34] calculated (and also verified experimentally) that percolation thresholds will fall if filler powders have a narrow size distribution (low polydispersity), and also have a non-uniform distribution within the polymer.

Composite	Filler particle shape/size	Expt. p_c (volume %)	Ref.
Cu – Styrene-butadiene rubber (SBR)	5 μm spheres	11	[3]
	175-250 μm spheres	40	
	Fibres – aspect ratio 5:1 (1 mm x 175-200 μm)	25	
	Fibres – aspect ratio 15:1 (3mm x 175–200 μm)	10	
	150 – 250 μm "Grape-like"	24	
Carbon-black (CB) – Poly(carbonate) (PC)	Fibres – aspect ratio 12.5:1	15	[40]
	Fibres – aspect ratio 24:1	6	
Ni – Poly(ethylene) (PE)	Monodisperse	23	[34]
	Polydisperse	43	
Carbon-black (CB) – poly(ethylene terephtalate) (PET)	"Highly structured" 30 nm	1	[36]
Graphite – Epoxy resin	Flakes/discs aspect ratio 100:1 (dia: 10 μm, thick: 0.1 μm)	1	[41]
Carbon nanotubes – Epoxy resin	Curved tubes aspect ratio ~1000:1 (dia: 10 nm, length: few μm)	0.02 – 0.04	[9]

Table 2.1: *Experimentally determined percolation thresholds (p_c) for a variety of different filler particle shapes and sizes*

Percolation theory remains a successful model for describing the macroscopic trends of electrical conduction within metal-polymer composites [2] [3] [8] [10] [42]. However, strictly speaking, the model only applies if the conductivity ratio (σ_h/σ_l) of the high (σ_h) and low (σ_l) conductivity phases is infinite. Percolation theory is also unable to accurately predict behaviour very close to and below the percolation threshold. In practical terms, it appears to work most effectively for composites made with smooth, spherical or ellipsoidal filler particles, randomly distributed and with little aggregation. For many other composite systems, heavy modification of the theory is often required to fit the data, and in some cases Percolation Theory is wholly inadequate [37] [43]. Differences in manufacturing and processing techniques can often be the cause of discrepancies between theoretical and experimental results. Currently, no single percolation theory can accurately predict all of the results to all experimental studies of metal-polymer composites.

2.2 Effective Medium Theory

Effective Medium Theory (EMT) was developed to address the inability of Percolation Theory to accurately model conduction close to and below the percolation threshold [44]. The modelling of metal-polymer composites with EMT was initially dominated by two theories: the Maxwell-Wagner Equation and the Bruggeman Symmetric and Asymmetric Media Equations. In these models, each conductive grain within the composite defines a site, and sites are linked together by a distribution of resistances. A model consisting of a random and disordered resistor network is therefore built. EMT then replaces all of the random resistances with an average value. The multiphase mixture of conducting and insulating materials is therefore replaced by a single homogeneous "effective" medium. It describes an ordered, symmetric and regular lattice that has the same macroscopic

properties as the inhomogeneous mixture. Because of this, EMT predicts no sharp percolation threshold, and most effectively models metal-polymer composites where the conductivity ratio (σ_h /σ_l) of the high (σ_h) and low (σ_l) conductivity phases is finite.

EMT introduces a correlation length, defined as the length over which field fluctuations within the composite become negligible. EMT is only applicable for samples with a very much larger length scale than the correlation length [45]. In such systems, field fluctuations become 'averaged' or 'smoothed', allowing the composite to be represented as a single "effective" medium.
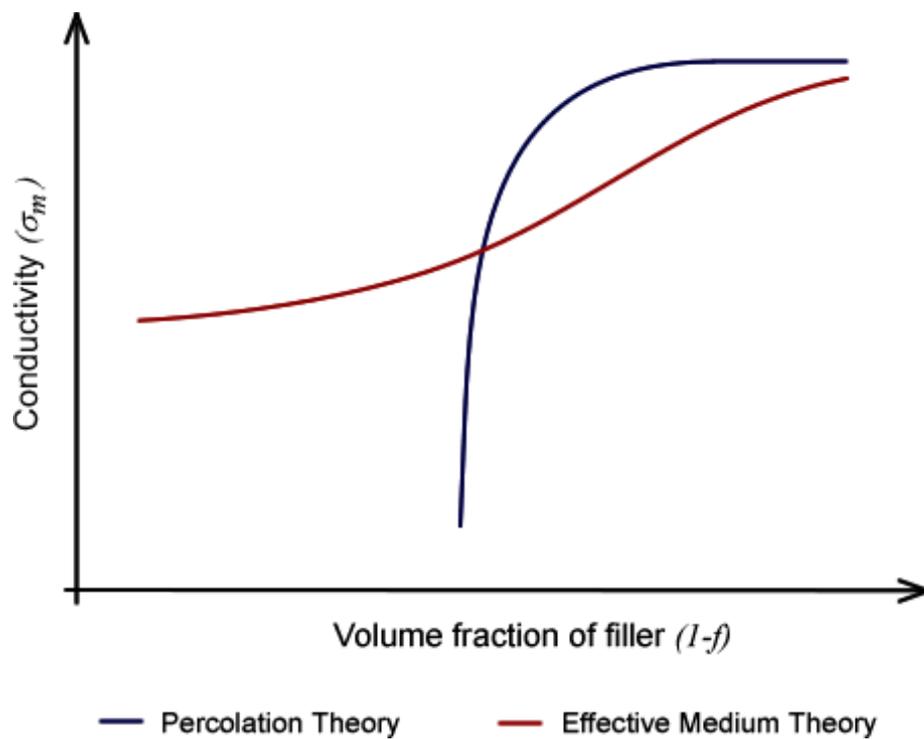
Fig. 2.4: Comparison of Percolation Theory and Effective Medium Theory

In 1987, McLachlan [46] introduced a Generalised Effective Medium (GEM) equation (equation 2.2), which united Percolation Theory and Effective Medium Theory (including also the Maxwell-Wagner Equation and the Bruggeman Symmetric and Asymmetric Media Equations). The term f represents the volume fraction of the low conductivity component, and f_c is the critical fraction of the low conductivity component at which a percolating network is first formed. The subscripts l and h denote the low and high conductivity components respectively, whilst m represents the effective medium, and t is an exponent.

$$\frac{f\left(\Sigma_l - \Sigma_m\right)}{\Sigma_l + \left[f_c/(1-f_c)\right]\Sigma_m} + \frac{\left(1-f\right)\left(\Sigma_h - \Sigma_m\right)}{\Sigma_h + \left[f_c/(1-f_c)\right]\Sigma_m} = 0 \qquad (2.2)$$

$$\Sigma_l = \sigma_l^{1/t} \qquad \Sigma_h = \sigma_h^{1/t} \qquad \Sigma_m = \sigma_m^{1/t}$$

Substitution into the GEM equation of an infinite conductivity ratio (i.e. $\sigma_l = 0$ and $\sigma_h =$ finite) causes the equation to reduce to the more simple form of Percolation Theory [47] [48]. A proof of this can be found in Appendix A.

The exponent, t, is related to the shapes of the conductive grains, and can be expressed in terms of an effective demagnetisation factor, L. For ellipsoids orientated in the direction of the current, $t = f_c/(1-L)$, where L is equal to 1/3 and 1/2 for spheres and flat discs respectively [46]. For randomly orientated ellipsoids, $t = mf_c$ where m is a variable dependant upon both L and the aspect ratio of the conductive grains. In the extreme cases of thin rods and flat discs, m tends to infinity. However, for more complex systems and particle shapes, the variable, m, and the demagnetisation factor, L,

cannot be calculated analytically, and must instead be calculated from fits to experimental data [46] [48], an example of which can be seen in figure 2.5.
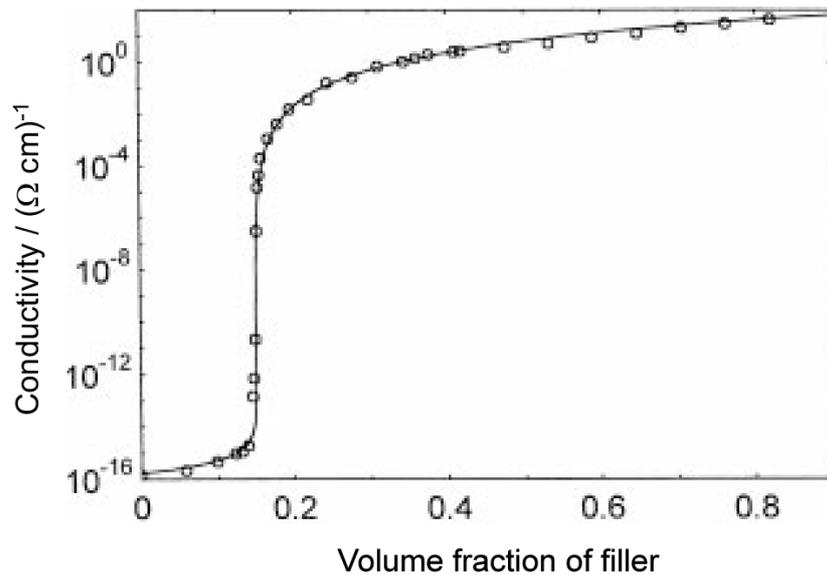
Fig. 2.5: *GEM equation fit (solid line) to experimental data (circles) of graphite-boron nitride composites (f_c=0.150, t=3.03) [49]*

The advantage of the GEM equation over other models of conductivity is that it can easily compensate for variations in conductivity due to particle shape, size and orientation. This means that General Effective Medium Theory is more widely applicable to modelling conductivity in metal-polymer composites than Percolation Theory. It is for this reason that the GEM equation has become the most generally applicable formula for modelling conduction in metal-polymer composites [50-52].

2.3 Tunnelling mechanisms

The classical view of conduction in metal-polymer composites requires that adjacent conductive filler particles be in direct physical contact with each other before conduction from one grain to another may occur. Without this continuous percolating chain of conducting particles, electrical conduction cannot occur due to the insulating properties of the surrounding polymer. This model is sufficient to describe long-range connectivity and macroscopic trends of conduction, however at a microscopic level, contact between metallic grains is not always necessary for conduction to occur.

Experimentally, it has been shown that it is possible for electrons to cross narrow insulating gaps between conducting particles within a metal-polymer composite [2] [53] [54]. This can occur via a number of different quantum tunnelling and field emission processes, and are described in more detail in the sections below. Usually, electron tunnelling may only occur where conductive grains are separated by very narrow insulating gaps. Experimentally, tunnelling has only ever been proven to occur at separations less than 1 nm [54]. However, Dani and Ogale [55] claim that the theoretical limit is closer to 10 nm. Nevertheless, it is logical to assume that tunnelling models dominate over the classical model only in samples that have a high concentration of conducting element, where only thin layers of insulating material surround the conducting particles. In materials with lower filler content, tunnelling effects are negligible, and a classical view of conduction via inter-particle contact is sufficient. Tunnelling is therefore only usually used to describe behaviour in the narrow region close to the percolation threshold, where conventional theories are inadequate.

However, tunnelling mechanisms are not necessarily restricted solely to near-percolating systems. Reports have suggested that in certain metal-

polymer composite systems the incorporation of tunnelling is essential in any effective model of conduction [56] [14]. In such systems, tunnelling probabilities are enhanced in some manner. Many modern models now successfully use a combined percolation-tunnelling model to more accurately describe conduction within metal-polymer composites [57-64].

2.3.1 Simple elastic tunnelling

The simplest model of a quantum tunnelling conduction mechanism in a metal-polymer composite consists of multiple rectangular potential barriers, representing the insulating regions between conducting grains (figure 2.6). Each barrier is formed due to the differences in the relative positions of conduction bands within a conductor and an insulator.
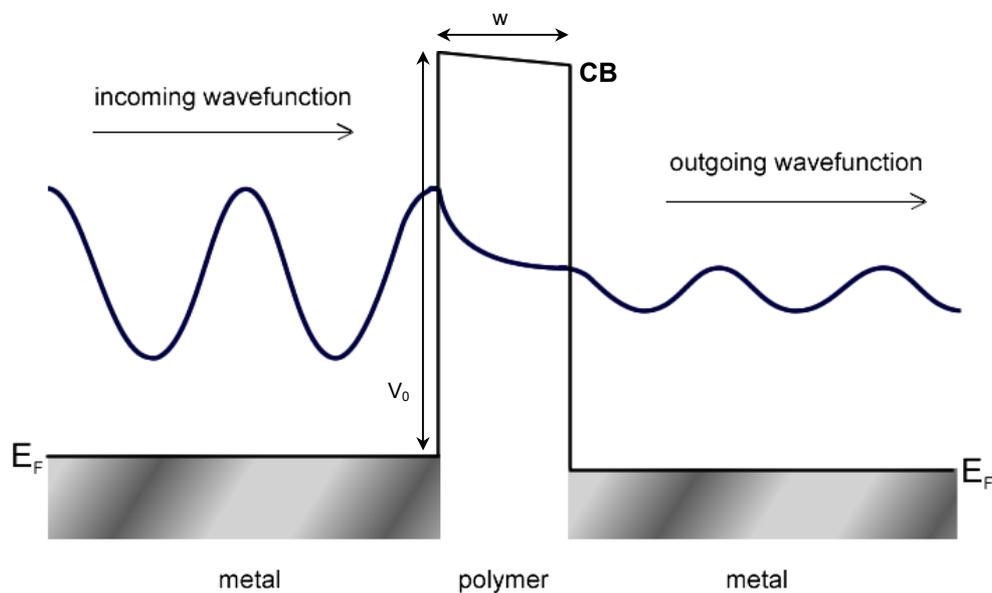
Fig. 2.6: *Simple rectangular barrier model of electron tunnelling between metallic grains in a metal-polymer composite with a small applied potential*

Exponential decay of the electron wavefunction within the barrier implies that tunnelling probability is exponentially dependent upon the thickness of the barrier (w). The resistivity of a single tunnel junction (ρ_t) will therefore share similar barrier width dependence (equation 2.3).

$$\rho_t = \rho_0 \exp\left(\frac{\pi w}{2} \sqrt{\frac{2mV_0}{\hbar^2}} \right)$$

(2.3)

where m is the mass of the tunnelling electron, V_o is the barrier height and ρ_0 is the intrinsic resistance of the metal with no barrier. A metal-polymer composite, in which a tunnelling conduction mechanism dominates, will therefore display resistivity that is highly dependent upon the separation of conducting particles.

Simple tunnel barrier charge transfer mechanisms result in composites with Ohmic current-voltage characteristics. Conductivity is also temperature independent [65] [66]. However, phonon assisted tunnelling is also possible, enabling the promotion of electrons to energies beyond that of the tunnel barrier height. Such a mechanism will therefore display DC conductivity (σ_{DC}) with a temperature dependency of the following form:

$$\sigma_{DC} = \sigma_0 \exp\left[-\left(\frac{T_0}{T} \right)^\alpha \right]$$

(2.4)

where T_0 is the characteristic temperature: a parameter depending upon the density of states at the Fermi level. The constant α has a value between ¼ and 1, depending upon the complexity of the resistor network model used.

2.3.2 Fluctuation induced tunnelling

The theory of fluctuation induced tunnelling (also sometimes referred to as quantum fluctuation augmented tunnelling) was developed by Sheng *et al.* in a series of papers [67-69] studying the transport properties of the composite carbon-poly(vinyl chloride). Their research implied a tunnelling mechanism of conductivity between adjacent carbon black particles, which was temperature activated. This is contrary to the standard model of simple tunnelling, which displays temperature independence.

In Sheng's model, the height and width of barriers between conducting particles are subject to fluctuations due to thermal effects. Electrons in the vicinity of the barriers, at the surface of the conducting grains, are thermally excited. The uncertainty in these electrons' position is therefore increased due to their increased kinetic energy. Such positional fluctuations affect the internal electrical fields between adjacent grains. This effectively reduces the barrier heights and narrows their widths. Increasing the temperature will increase the size of the fluctuations, and therefore tunnelling through the barrier becomes more likely at higher temperatures. At very low temperatures (< 45K), thermal fluctuations become negligible, and the fluctuation induced tunnelling model reduces to the more simple model of elastic tunnelling [36]. Using a parabolic model of the potential barrier (see section 2.4.1), the following equation was derived for the current-voltage characteristics of composites displaying fluctuation induced tunnelling:

$$J = J_0 \exp\left[-\frac{T_1}{T+T_0}\left(1-\frac{E}{E_C}\right)^2 \right] \qquad (2.5)$$

where J is the current density, E is the applied electric field, E_c is the critical field (defined as the field at which the barrier effectively disappears), T_1 is

the temperature below which conduction is dominated by simple tunnelling through the barrier, and T_0 is the temperature above which thermally activated conduction over the barrier can occur.

At high fields, it is predicted that fluctuations in both barrier height and width will also give rise to a non-linearity in current-voltage characteristics. The above equation is insufficient on its own to fully explain the observed non-linearities. In 1995, Paschen *et al.* [70] successfully extended Sheng's model to also include thermal activation of charge carriers over the potential barrier and the thermally activated tunnelling of charge carriers with energies above that of the Fermi level.

Numerous papers [36] [63] [71] attribute conduction within their composites to be due at least partly to fluctuation induced tunnelling. It is for this reason that fluctuation induced tunnelling has been perhaps the most highly successful model of tunnelling conduction within metal-polymer composites to date. However, the theory is limited as it is applicable only to homogenous systems with relatively small inter-particle barrier heights [72].

2.3.3 Resonant tunnelling

Consider a double (or multiple) quantum barrier structure which contains, between the two barriers, a quantum well of narrow confinement. If the well is sufficiently narrow, it can sustain only a single electron energy level, known as a resonant energy level. The total transmission coefficient for the system is roughly the product of the transmission coefficients for each individual barrier. However, at energies near to resonance, the total coefficient rises dramatically to its maximum value of 1. This implies complete transmission, regardless of the opacity of each of the barriers. This phenomenon is known as resonant tunnelling.

(a)

- $V < V_{th}$
- Resonant state above electron sea
- Negligible current

(b)

- $V_{th} \leq V \leq V_{pk}$
- Resonant state within electron sea
- Current rises rapidly

(c)

- $V > V_{pk}$
- Current falls as move away from resonance

- $V \gg V_{pk}$
- Current increases according to single barrier tunnelling model
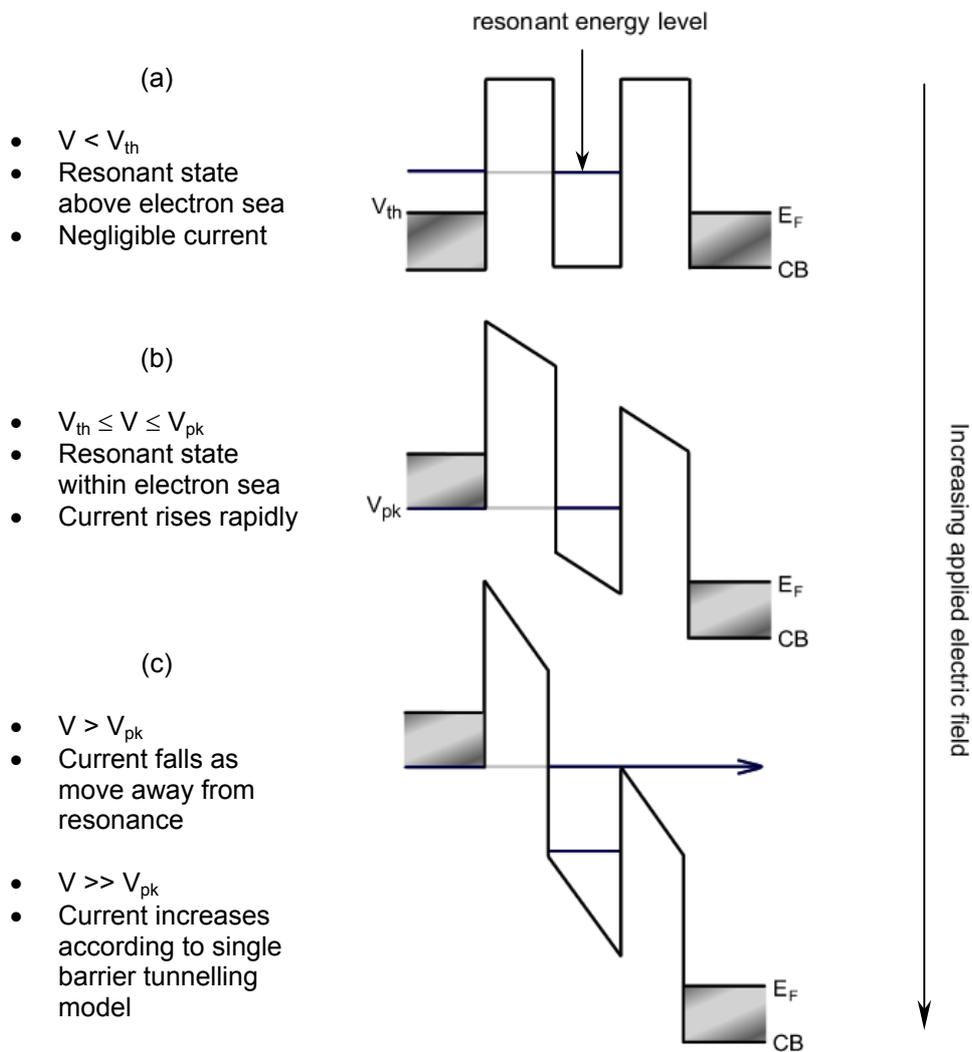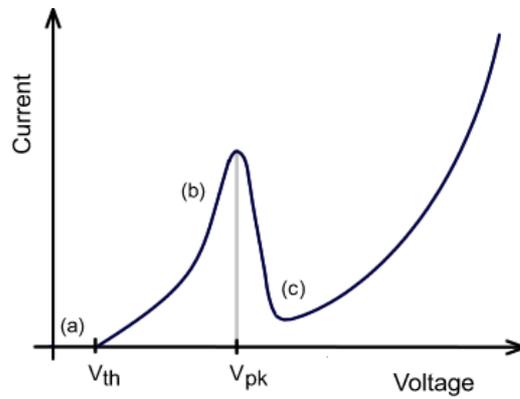
Fig. 2.7: *Current-voltage characteristics of a resonant tunnel diode*

A semiconductor resonant tunnel diode uses the principle of resonant tunnelling to obtain current-voltage characteristics that are shown in figure 2.7. At point (a) and just below the threshold voltage, V_{th}, the position of the resonant energy level is such that it lies above the metallic electron sea. As the applied voltage approaches point (b), the position of the resonant centre is shifted such that it now lies within the conduction band of the injecting metal. If the applied voltage continues to be increased beyond V_{pk}, the resonant level shifts below the level of the conduction band, away from resonance. At point (c), a current minimum is reached. Further increases in voltage will shift the structure such that only one barrier obstructs conduction. Current therefore increases with applied voltage as is typical for single barrier tunnelling.

Pike and Seager [73] show that impurities within a tunnel barrier may act as resonant centres, thus improving tunnelling probabilities. Although not well documented, it is therefore possible that resonant tunnelling phenomena may occur within metal-polymer composite systems, where similar double (or multiple) quantum barriers exist.

2.4 Charge injection

Until this point, the polymer regions of metal-polymer composites are considered to be wholly insulating. However, no material is a perfect insulator, and so, for a complete theory of conduction within such a system, one must also consider conduction mechanisms within the polymer. An insulator can be made to carry appreciable currents at room temperature if contacts are such that charge carriers can be injected into the material [54]. Well-chosen materials and surface irregularities will also enhance the probability of charge injection [74]. Detailed treatment of charge injection into insulators was first carried out by Mott and Gurney in 1948. Some

examples of relevant charge injection mechanisms are detailed below. A good review of charge injection has been written by Lampert and Mark [75].

2.4.1 Field emission and the Schottky effect

For a more realistic model of tunnelling between adjacent conducting particles within a metal-polymer composite, one must consider the physics of thermionic emission, field emission and the Schottky effect.
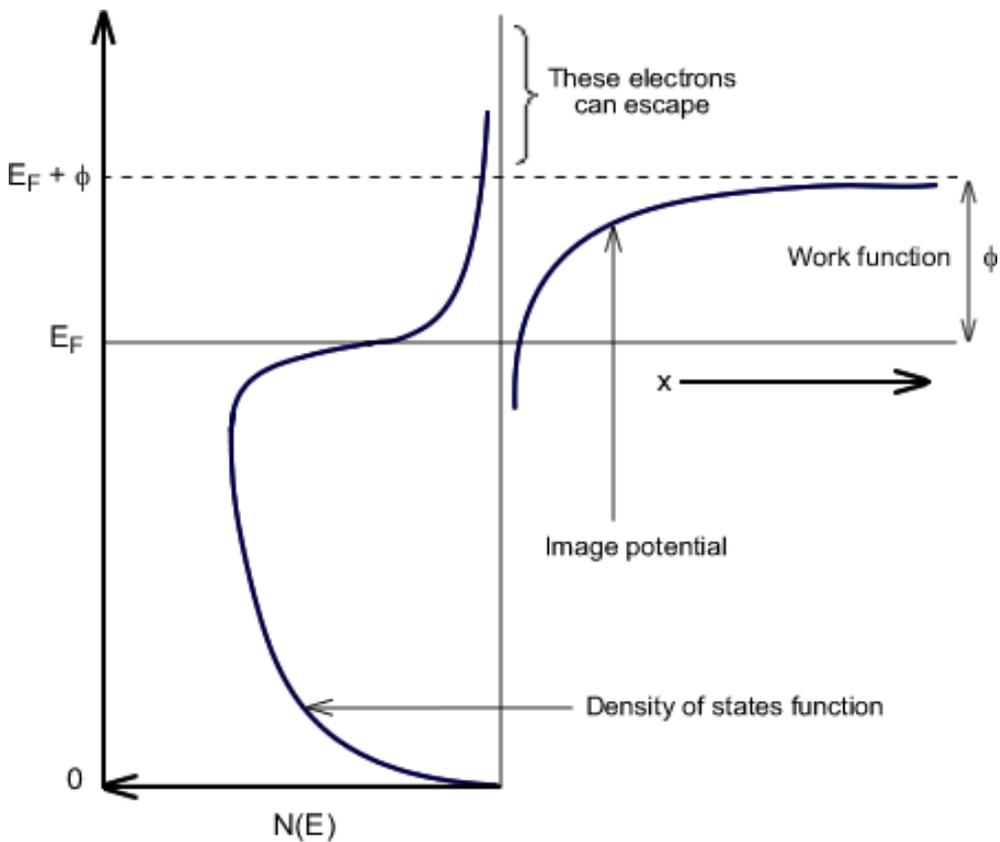
Fig. 2.8: Thermionic emission occurs when electrons have
sufficient energy to overcome the work function

At zero Kelvin, electrons fill energy levels up to and including the Fermi level, E_F, in a manner according to the density of states function, $N(E)$. For a metal, the position of this Fermi level is within the conduction band of the material, and electrons are bound within the volume of the metal. Electrons may only escape from the metal if they possess sufficient energy to overcome the work function, φ. The origin of this minimum energy requirement arises when one considers the potential experienced by an electron that has just been ejected from the metal, at a distance x beyond the surface. An attractive electrostatic image force of magnitude, $e^2/(16\pi\varepsilon_0 x^2)$ pulls the electron back towards the metal. Only electrons with energy sufficient to overcome this image force will therefore be able to escape. Such 'hot' electrons will lie in the tail end of the electron energy distribution. The mechanism by which electrons are released from the bulk of the material into a vacuum or an insulator in this manner is called thermionic emission [76] [77] (figure 2.8).

The maximum current density (J_{th}) that can be injected via thermionic emission at a metal-insulator junction is given by the Richardson-Dushman equation [76] [77]:

$$J_{th} = A_R \left(1 - \sigma\right) T^2 \exp\left(-\frac{\phi}{k_B T}\right)$$ (2.6)

where A_R is the Richardson-Schottky constant (120 A cm^{-2} K^{-2}) and σ is a reflection coefficient for electrons attempting to enter the insulator. The equation therefore includes consideration of the insulator's ability to accept electrons. However, the pre-multiplying factor of (1-σ) is often neglected for simplification purposes. The term T^2 accounts for the thermalisation of electrons as they approach the injecting electrode. In order for the electrons
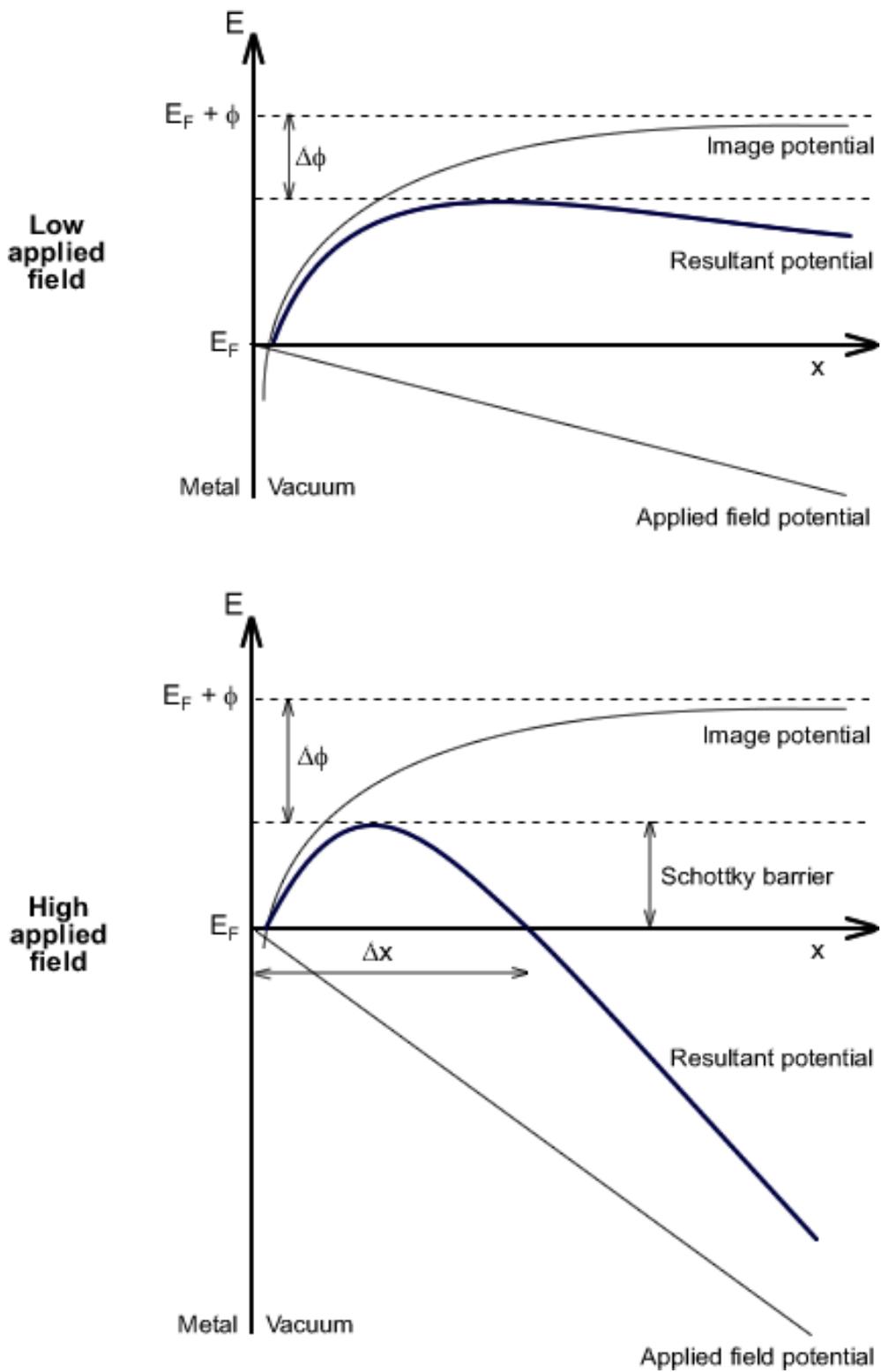
Fig. 2.9: The Schottky effect. In the presence of an applied electric field, the work function (ϕ) is lowered by an amount Δϕ

to escape, they must not only overcome the work function, but also have sufficient energy to survive the energy dissipating collisions with other electrons whilst within the range of the electrode's image force.

The Schottky effect has the result of lowering the work function of the material by an amount $\Delta\varphi$, and consequently also lowers the minimum electron energy required for emission. At high applied fields, the resultant potential may become sufficiently distorted for it to feature a maximum, turning over to reach a value of E_F at a distance Δx away from the surface of the material. When this occurs, a potential barrier (or Schottky barrier) for electrons exists between the metal and freedom from the surface. In this situation, electrons with energy lower than $(E_F + \varphi - \Delta\varphi)$ may tunnel through the barrier and escape from the surface of the metal. As the E-field is further increased, the Schottky barrier may become sufficiently reduced for it to disappear completely. From this point onwards current through the junction is said to be emission-limited.

Current-voltage characteristics of a single metal-vacuum field emission junction follow the general form of equation 2.7 [53].

$$J = AE^n \exp\left(-\frac{B}{E}\right) \qquad (2.7)$$

where J is the current density, E is the field across the junction and A, B and n are constants. The constant n usually has a value of between 1 and 3. Not to be confused with the Richardson-Schottky constant, A is a function of the tunnelling frequency (the number of attempts to cross the barrier per second). The exponential term represents the transparency of the barrier, or the probability of a successful field-emission event. It is dependent upon E

because the probability of barrier penetration depends upon the area under the barrier, which in turn depends upon the applied electric field. Schottky emission occurs in the field range of 10 to 1000 kV cm^{-1} [78].

In a metal-polymer composite, Schottky emission will occur from the metallic particles at the metal-polymer interface. A mirror situation also occurs at the adjacent polymer-metal interface. The resulting potential barrier is shown in figure 2.10, and is often approximated as being parabolic in shape. The absence of the Schottky effect and no image force correction simplifies this barrier shape to the rectangular barrier model in figure 2.6.
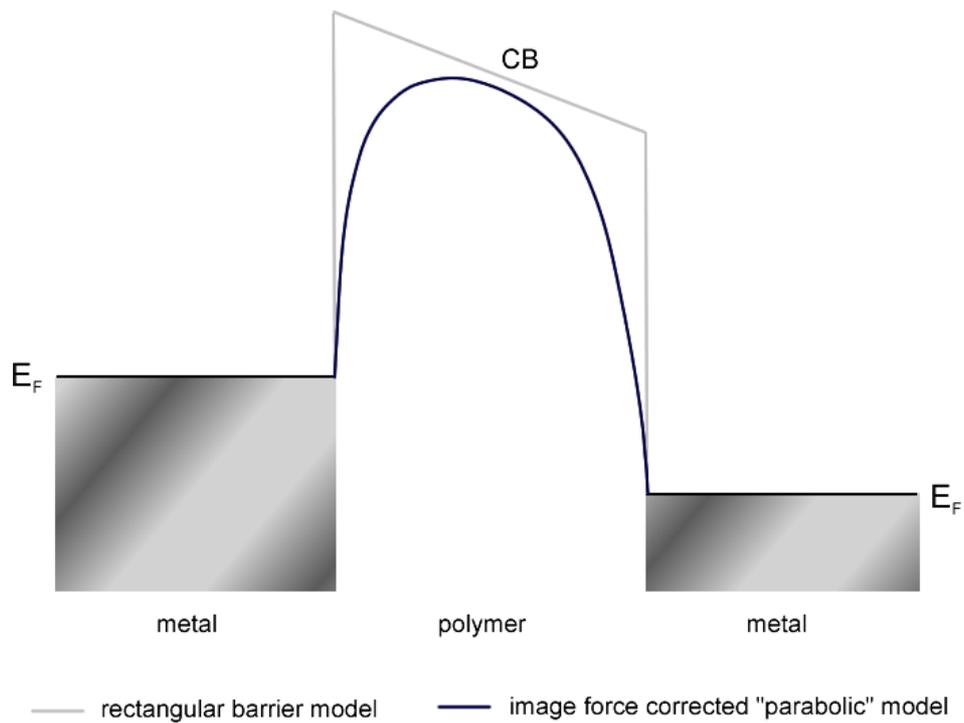
Fig 2.10: *Schottky effect in metal-polymer composites: the rectangular barrier is lowered and corrected to a "parabolic" shape*

Radhakrishnan [62] said that current-voltage characteristics of a single metal-polymer junction, dominated by Schottky emission, can be described effectively by the following equation:

$$J = A_R T^2 \exp\left(-\frac{\Delta}{k_B T}\right) \exp\left(\frac{\beta E^{1/2}}{k_B T d^{1/2}}\right) \tag{2.8}$$

where J is the current density, E is the applied electric field potential, A_R is the Richardson-Schottky constant (120 A cm^{-2} K^{-2}), T is the temperature, k_B is the Boltzmann constant, Δ is the Schottky barrier height, β is a constant and d is the thickness of the insulator. Origin of the pre-multiplying term $A_R T^2$ arises from the same source as that described for equation 2.6 (i.e. thermalisation of electrons in the vicinity of the injecting electrode). (Note however, that the (1-σ) term has been neglected in this equation). The first exponential term, $\exp\left(-\Delta/k_B T\right)$, accounts for thermal activation of electrons over the Schottky barrier, whilst the second exponential, $\exp\left(\beta E^{1/2}/k_B T d^{1/2}\right)$, represents electron tunnelling through the barrier.

Radhakrishnan [62] rewrites equation 2.8 to extend the formula to multiple Schottky barriers, in the case of a metal-polymer composite. His equation includes terms representing the average grain size, loading volume fraction and physical dimensions of the sample, and his treatment assumes regular and uniformly dispersed filler particles. This effective medium approach is highly successful in modelling conductivity data for many carbon black and metallic loaded polymer composites. The results prove that a model of conduction in metal-polymer composites need not invoke the formation of contacts between metallic grains.

2.4.2 Fowler-Nordheim Tunnelling

Field emission from a metal surface may also take on another form. Fowler-Nordheim emission occurs when electrons tunnel through the Schottky barrier, out of the bulk of the metal, directly into the conduction band of the neighbouring material (figure 2.11). High local fields are required in order to distort the potential barrier to this extreme. However, careful choice of the two material types and their contact potential can also be used to promote this type of mechanism.
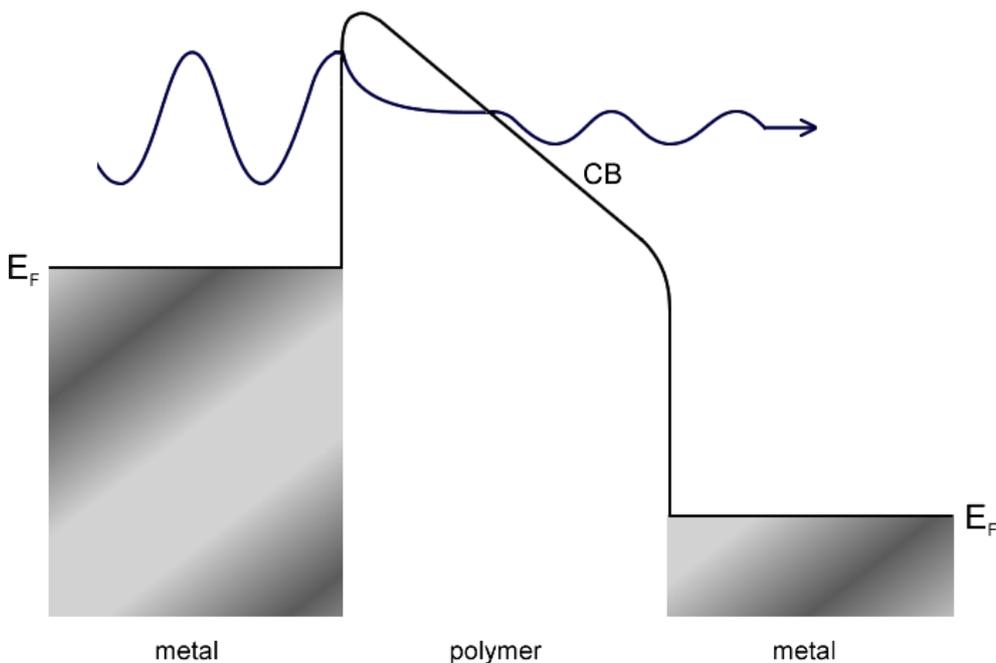
Fig. 2.11*: In Fowler-Nordheim tunnelling, electrons from the metal are injected directly into the conduction band of a neighbouring insulator*

Current-voltage characteristics of Fowler-Nordheim junctions follow the same general formula as described in equation 2.7. The analogy to standard

field emission is clear, however, in the case of Fowler-Nordheim tunnelling, the values of the constants, *A, B* and *n* will differ. Specifically, *n* = 2, which introduces a quadratic dependency of the current upon the applied field. This is accounted for by the influence of Child's law upon the system, which must be considered if electrons are tunnelling into the conduction band of the insulator (see equation 2.12, section 2.5). A rectangular barrier model, which combines the free-electron gas model for metals with the WKB approximation (i.e. the assumption that the properties of the medium vary slowly on a scale comparable to the wavelength of the electron), gives rise to the following equation [74]:

$$J = \frac{AE^2}{\phi} \exp\left(-\frac{B\phi^{3/2}}{E}\right)$$

(2.9)

ϕ is the work function of the polymer and is included because equation 2.6 is only applicable for field emission into a vacuum. Specifically, the constants *A* and *B* can be defined by the following equations:

$$A = \frac{e^3}{8\pi h}$$

(2.10)

$$B = \frac{8\pi (2m)^{1/2}}{3he}$$

(2.11)

where *e* and *m* are the electron charge and mass respectively, and *h* is Planck's constant. Where tunnelling through a dielectric is concerned, *m* should be replaced by m^*, the effective mass.

Numerical simulations of Fowler-Nordheim field emission from irregularly shaped metallic particles have been published by Isayeva *et al.* [74]. The

results confirm that Fowler-Nordheim tunnelling is more probable in regions of small-scale irregularities on the surface of metallic grains, where the electrostatic field is enhanced. Fowler-Nordheim tunnelling is therefore predominantly a high-field effect.

2.5 Space-charge limited currents

Appreciable electrical current can be made to pass through a conventionally insulating polymer if an appropriate charge injection process has occurred [54]. Once injected, the charge is referred to as "space-charge". The motion of space-charge through the conduction band of an insulator is hindered by the presence of electron trapping sites. Electrons may move between such sites by mechanisms including hopping, thermal activation and the Poole-Frenkel effect. From 1955 onwards, the simplified theory of space-charge limited currents was developed by a number of different authors, most notably Rose and Lampert [75], working on the basic assumptions of charge injection as developed by Mott and Gurney several years earlier. A brief description of this theory follows, as applied to shallow trapping in insulators.

In all non-perfect crystal structures, defects exist within the lattice matrix. These defects can be in the form of chemical impurities (substitutional or interstitial) or crystal deformations such as dislocations, dangling bonds, Schottky defects and Frenkel pairs. Such abnormalities give rise to the formation of carrier traps within the crystal lattice.

Chemical impurities within a host lattice will have differing energy levels, ionisation energies and electron affinities compared to neighbouring atoms. If the electron affinity of an impurity (or guest) atom is greater than that of its host, then the impurity will act as a trapping centre for passing electrons.

Conversely, a trap for holes is formed when the impurity has an electron affinity less than that of the host material. The depth of these carrier traps depends upon the difference between the ionisation energies of the guest and the host.

Physical deformations in the crystal lattice will modify energy levels in the area surrounding the defect. This occurs when the regular bonding between adjacent lattice points is disturbed. Consequently, vacant orbitals, which lie within the forbidden energy gap between conduction and valence bands, are often made accessible. Carriers, in the form of either holes or electrons, can fall into such a vacant orbital (or vacuum energy level) and become trapped.
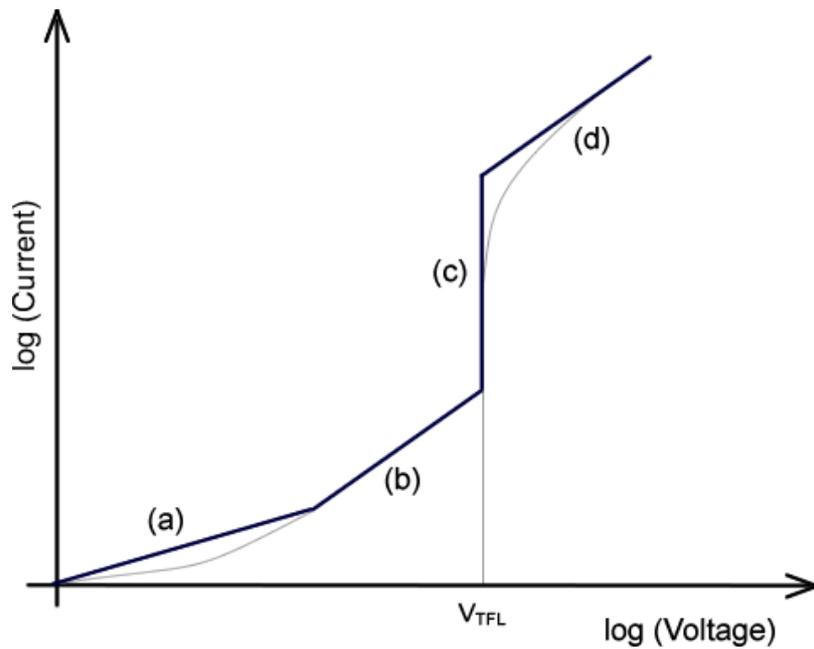
Fig. 2.12: *Space-charge limited current-voltage graph (showing the trap-*
filled limit voltage, V_{TFL}) for a material with a single trap level:
(a) Ohmic region, (b) Child's law due to shallow trapping,
(c) Trap-filled limit, (d) Child's law after trap saturation

40

When electrical current initially passes through a material containing trapping sites, Ohmic behaviour is displayed (figure 2.12(a)). However, beyond a certain current, electrons begin to fall into the vacant energy levels and do not contribute to conduction. If a constant voltage is maintained across the sample for a length of time, a gentle increase in the generated electrical current is observed. This is due to increasingly more traps having being filled by charge carriers, allowing more current to pass through without hindrance. Space-charge is now trapped within the sample, the material is said to display space-charge limited current (SCLC) behaviour and Child's law is obeyed (figure 2.12(b)). (In practice, regions (a) and (b) are often indistinguishable, their two gradients becoming blurred into one gentle curve [79]). The observed current continues to rise (with $V \propto I^2$) until the sample becomes saturated and all traps are filled. Any further increases in the applied voltage would cause new carriers to be introduced from the electrodes that cannot be trapped. This results in a sharp increase in the observed current-voltage characteristics (figure 2.12(c)). The material is now said to have exceeded the trap-filled limit. Sometimes traps may exist at many different energy levels, causing the current to pass through several distinct and sudden rises. Beyond the trap-filled limit, the dramatic current rise is limited by the new intrinsic resistivity of the material, after trap saturation. Child's law is again obeyed, and the current displays quadratic dependence upon the applied voltage as before in region (b). Regions (d) and (b) in figure 2.12 therefore have the same gradient as each other. However, in practice region (d) is rarely observed, often blurring into a curve with region (c) [79].

Due to the amorphous nature of polymers, the insulating regions of metal-polymer composites contain a very high density of defects and impurities with a wide distribution of trap energies and depths. The effects of trap

filling are therefore smoothed out, sometimes obscuring the observations of trap-filled limits. The current-voltage characteristics are therefore dependent upon trap energy distribution and depth. However, in the case of shallow trapping and partially or filled traps, equation 2.12 can be applied [76]. This is known as the Mott-Gurney equation, or Child's law for solids (Note the difference to Child's law for a vacuum, where $J \propto E^{3/2}$) [80].

$$J = \frac{9}{8} \mu \varepsilon \varepsilon_0 \frac{E^2}{L^3} \qquad (2.12)$$

where J is the current density, E is the applied electric field, L is the length of the insulator, ε_0 is the permittivity of free-space and ε and μ are the permittivity and permeability of the insulator respectively.

The Mott-Gurney equation is derived from a statement of continuity of charge motion. The assumption is made that the carrier concentration gradient within the insulator is negligible, such that there is no contribution to current flow due to charge diffusion. The sole contributor to charge motion is therefore the drift current, driven by the applied field. Ideal Ohmic electrodes are also assumed, i.e. ones that inject infinite charge density at the electrode-insulator contact. The barrier to charge injection is therefore assumed to be small.

For a more comprehensive account of SCLC behaviour, the reader is referred to an excellent account written by Pope and Swenberg [76].

2.5.1 De-trapping and the Poole Frenkel effect

Upon heating, sufficient energy can be supplied to a trapped electron, exciting it out of a trapping site and into the conduction band. The electron

then becomes free to drift throughout the material as a charge carrier, and can be detected as a small current. This thermal de-trapping technique can be used to probe trap depth and to analyse trap density profiles within a material. The mechanism associated with thermally induced de-trapping shares strong similarities with thermionic emission. A modified version of the Richardson-Dushman equation (equation 2.6) can therefore be applied, which adjusts the potential barrier function from the Schottky barrier to the barrier created by the wall of a trapping site.

Electron de-trapping may also occur when trap-filled samples are exposed to large electric fields. An applied field will generate an offset between opposite walls of the trapping site potential well. At sufficiently high fields, this offset may become large enough for a loss of confinement to occur, releasing the electron from its trap (figure 2.13). This field-induced de-trapping phenomenon is known as the Poole-Frenkel effect. It is also important to note that electrons close to the point of de-trapping may also tunnel out of their traps into the conduction band of the insulator. The potential barrier to escaping the trap will lower and narrow as the applied field increases, increasing the offset and distorting the potential of the system.

Strong similarities can be seen between the physics of the Poole-Frenkel effect and that of Schottky emission. At high fields, the wall on the lower potential side of an electron trapping site will have a similar shape to that of the Schottky barrier as seen in figure 2.9. Current-voltage characteristics consequentially show great similarities to equation 2.7 for Schottky emission (and also equation 2.9 for Fowler-Nordheim tunnelling), the only difference being in the constant, B.

Low/zero applied E field

Conduction band electrons are trapped in local minima potential wells, caused by defects and impurities within the insulator.

CB ——————⌒⌒⌒—————— CB

Medium/high applied E field

The walls of the potential well become sufficiently distorted for containment of the electron wavefunction to be lost. Electrons of sufficient energy may escape (or tunnel) out of the trap.

Fig.2.13: *Field-induced electron de-trapping (Poole Frenkel effect)*

2.5.2 Hopping

In a highly defective material, trapping sites may often exist in close proximity to one another. In such a system, electrons may be able to move from one trapping site to another by a process known as "hopping" (figure 2.14).
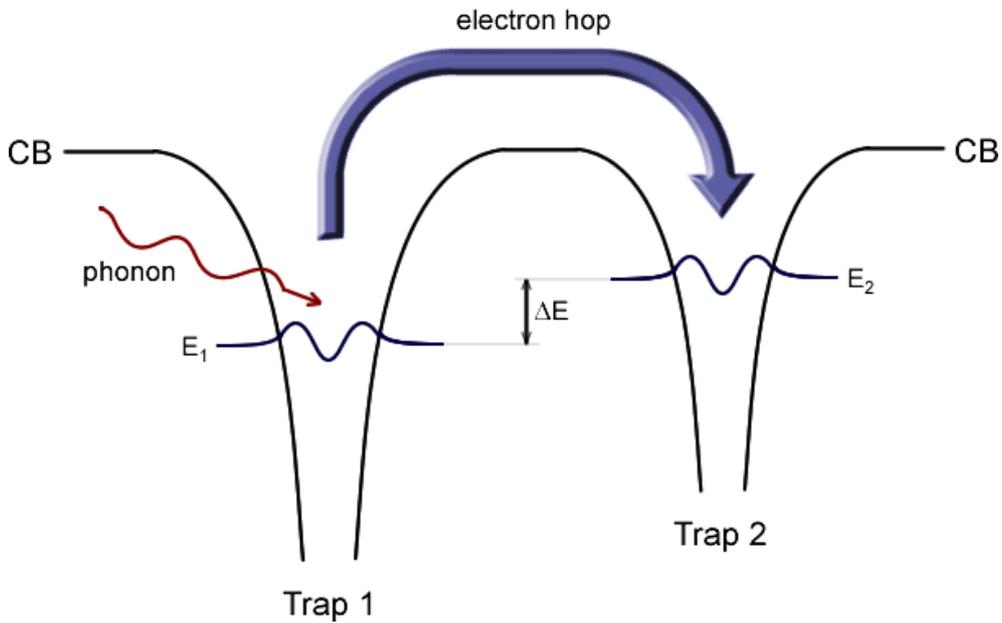
Fig. 2.14: *Electron hopping between adjacent trapping sites*

Thermally assisted hopping requires the absorption of a phonon to gain sufficient energy to overcome the barrier between adjacent trapping sites. A phonon is also then emitted once the charge carrier has fallen back into the next trap. At lower temperatures when phonon energies are insufficient to permit thermally assisted hopping, charge carriers may move to adjacent trapping sites of similar energy via tunnelling. It is more likely that an electron will find a trapping site with a similar energy at a distance beyond that of its closest neighbours. The distance of the "hop" is therefore variable, and hence the process is known as variable range hopping. The range of the hop is dependent upon the energy difference, ΔE, between the two trapping sites. Any slight increase (or decrease) in energy for the trapped electron as it is transported from trap 1 (at energy E_1) to trap 2 (at energy E_2) is accounted for by the absorption (or emission) of a phonon. Hopping conduction mechanisms are therefore temperature-dependent. The

process is entirely analogous to phonon-assisted tunnelling, and thus the two mechanisms share the same temperature dependence, as given by equation 2.4. The characteristic temperature (T_0) is given by ($\Delta E / k_B$). The constant, α, is often calculated from best fits to experimental data, but in theory can take on a number of values, depending upon the exact model of hopping used:

Short range hopping:	$\alpha = 1$
2D variable range hopping:	$\alpha = 1/3$
3D variable range hopping:	$\alpha = 1/4$

In addition to the transfer of charge between trapping sites, hopping theories may also be applied to the conduction of charge from one metallic grain to another within granular metals [81] [82]. Other authors [55] [72] have extended this theory further, suggesting hopping between adjacent grains in metal-polymer composites. However, Celzard *et al.* [78] suggest that this is only feasible in a composite constructed using nano-sized conducting particles. They argued that in a system with larger, micron-sized filler particles, excessively long hopping distances are required, and the conducting grains are too large to be considered as trapping sites from which hopping can take place. More likely perhaps is a hopping assisted tunnelling conduction mechanism, as suggested by Sarychev and Brouers [83], whereby tunnelling of electrons between grains is assisted by hopping between trapping sites within the polymer layers. Miyauchi and Togashi [65] also observe a similar conduction mechanism in polymer-grafted carbon black composites. In their system, at low fields, a temperature-dependent hopping mechanism is proposed, whilst at high fields temperature independence is observed, indicating a tunnelling mechanism (figure 2.15).
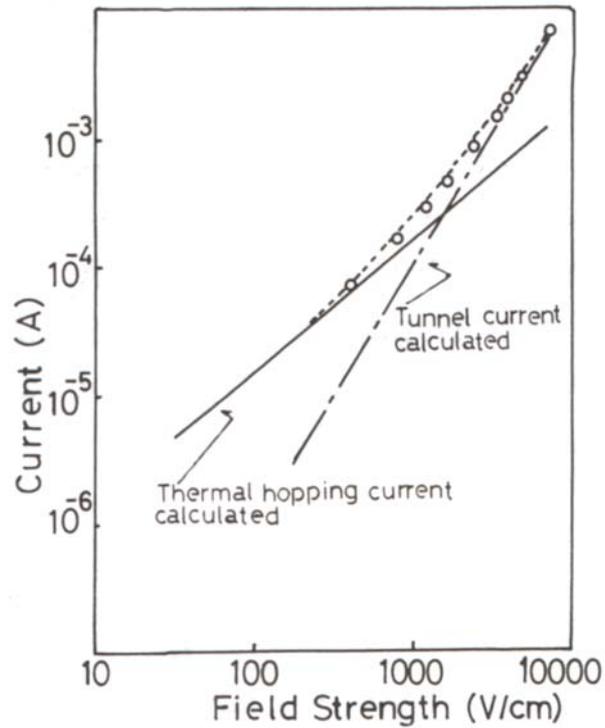
Fig. 2.15: *Field-dependent hopping and tunnelling conduction mechanisms in a polymer-grafted carbon black composite [65]*

The effects detailed above (SCLC, trapping and hopping) are concerned with electrical conduction within the "insulating" regions of metal-polymer composites. These effects will undoubtedly have an impact upon the electrical characteristics of many metal-polymer composites, in particular those well below their percolation threshold. Such effects have been successfully incorporated into models of conduction for metal-polymer composites [14] [62]. A possible result of such a model is that the resistivity of metal-polymer composites can, in some cases, depend upon the electrical history of the material. For example, if a large current has recently been passed through a sample, then trapping sites may have

become filled, causing a change in the observed current-voltage characteristics.

2.6 Ionic conduction processes

In certain metal-polymer systems, conditions may be such that ionic species exist within the polymer regions of the composite. An additional conduction mechanism through the polymer (in addition to SCLC and hopping) may therefore be possible.

Under an applied potential, positive and negative ionic species will migrate towards the cathode and anode respectively. In a metal-polymer composite, additional "micro-electrodes" will exist in the form of the charged metallic particles. After prolonged exposure to an electric field, there may be a build-up of ionic species at or near to the electrodes. Evidence of this type of build-up is often in the form of a residual polarity over the sample, once all applied fields have been removed. Once in position, this build-up of space-charge may screen internal electric fields, inhibiting current flow [84]. Conduction in this situation is dominated by electron and hole injection from the conducting particles into the polymer, neutralising the ionic species. Any residual ionic polarity across the material may also give rise to a small transient current [84] once all applied potentials have been removed, as ionic species within the composite migrate back, neutralising each other.

Celzard *et al.* [78] report samples with time-dependent current-voltage characteristics and very slow recovery times in returning to their original conductivity (5 to 15 days). Such a long recovery is considered to be too slow for an entirely space-charge build-up effect, and therefore these effects are claimed to be a strong indication of an ionic conduction mechanism. They also claim that in a combined electronic and ionic conduction

mechanism (where conduction is electronic within the conducting particles, but ionic in the regions between them) the current-voltage characteristics will be in the form of the following equation:

$$J = AE^n \exp(BE) \qquad (2.13)$$

where A and B are constants, and n has a value very close to 1. The formula is calculated from a best fit to the data, and has not been derived analytically. However, it does also confirm earlier data produced by Cashell *et al.* [84] who also report an ionic conduction mechanism in their carbon black filled cis-poly(butadiene) composites.

In a more recent paper, Celzard *et al.* [66] also report composites displaying increasing resistance with increasing applied pressure. This they considered to be further evidence of ionic processes. At low loadings, it is thought that the application of pressure causes a reduction in the volume of the polymer, thus inhibiting the diffusion of ionic species. However, at higher loadings, closer to the percolation threshold, this effect becomes insignificant compared to the increase in conductivity caused by the improved connectivity of conducting grains under applied pressure.

2.7 Grain charging

Conduction between metallic grains may occur by a wide variety of mechanisms, as described above. However, none have yet considered the response of the metallic particles themselves.

In a study of granular metals in which inter-particle contact is considerable (comparable to a metal-polymer composite at a loading well above its

percolation threshold), Sheng *et al.* [81] [82] [85] considered the energy required to charge (and discharge) metallic grains. A type of hopping conductivity was proposed, whereby electrostatic charge builds up on a metallic grain and is then discharged to its neighbour once the electrostatic potential exceeds the charging energy of the next grain.

The amount of electrostatic energy required to transfer one electron from a charged grain to a neutral grain (E_c) is given by the following relation [81]:

$$E_c = \left(\frac{e^2}{d} \right) \cdot F\left(\frac{s}{d} \right) \qquad (2.14)$$

where e is the electronic charge, d is the average grain size and s is the average grain separation. The function *F(s/d)* depends upon the shape and arrangement of the grains. This inverse proportionality between charging energy and grain size implies that the greatest charging energy is required for the smallest grain size. Upon application of an electric field, charging energies are reduced [86], due to the increased kinetic energy possessed by electrons as they approach metallic grains.

In practice, thermal fluctuations often exceed the energetic requirements of grain charging, unless grains are sub-micron in size. Composites using nano-sized particles are therefore expected to have higher resistivities than those made using larger, micron-sized particles. It is of interest to note that this conclusion is contrary to the predictions of Percolation Theory, which finds that smaller particle sizes generate lower percolation thresholds and therefore make composites with higher conductivities.

In the case of very high charging energies and very small (nano-sized) particles, electrons may become trapped upon certain metallic grains when there is insufficient energy to transfer the charge to their neighbour. The trapped charge then acts as a barrier, hindering the passage of charge for nearby conduction routes. This phenomenon is known as a coulomb blockade. Currents in such systems can fall when they might normally be expected to rise. Unusual electrical characteristics therefore result. A more detailed discussion of this topic can be found in reference [87].

3 Summary of previous work

The purpose of this section is to summarise the results of a variety of research projects that have been carried out on the electrical properties of QTC materials over the past four years. These results have been collected from several different authors carrying out a variety of research projects, including earlier work carried out by the author himself. At the time of writing, the results to these projects were not in the public domain, due to non-disclosure agreements. Therefore, for the purposes of completion and to aid the reader in their understanding of the behaviour of QTC materials, the following summary of results has been included.

Type	Particle size / μm	Surface Area / m^2/g	Loading ratio metal:polymer by mass	Morphology	
123	3.0 - 7.0	0.4	6.00 : 1	Spiky	Particulate
255	2.2 - 2.8	0.7	3.43 : 1	Spiky	Filamentary
287	2.6 - 3.3	0.6	4.00 : 1	Spiky	Clumpy
210	0.5 - 1.0	1.5 - 2.5	1.20 : 1	Smooth	Filamentary
110	0.8 - 1.5	0.9 - 2.0	1.66 : 1	Smooth	Particulate

Table 3.1: *Summary of powder types used in previous experiments*

Table 2.1 details the different varieties of nickel powder used to manufacture QTC samples, as detailed in the supplied data sheets. A more detailed explanation of the differences between these metallic powder types, including information regarding their source, can be found in section 4.2.

3.1 Mechanical properties

3.1.1 Response to applied pressure

The mechanical response of QTC materials to applied compression has been briefly characterised [88]. Figure 3.1 shows plots of the force required to achieve various percentages of compression for a number of QTC types. In the graph, each data set corresponds to a different filler powder type.
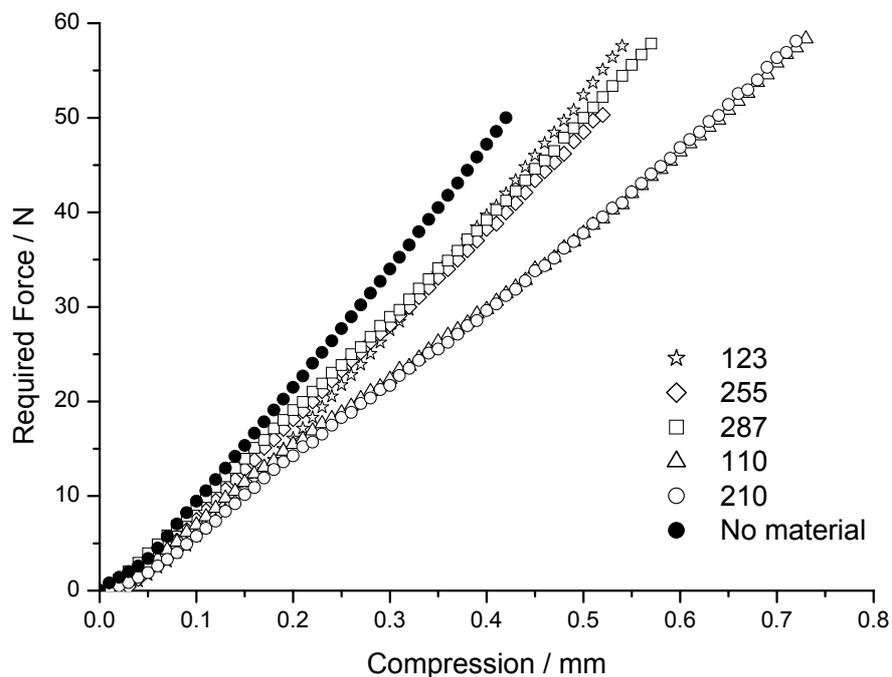
Figure 3.1*: Mechanical response of QTC materials to compression [88]*

Types 123, 255 and 287 correspond to nickel powders with spiky surface morphologies, whereas types 110 and 210 correspond to nickel powder with smoother surface characteristics.

It can be seen that there is a clear grouping of the data sets between materials made using spiky shaped powders, and those made with smooth powders. The shape of filler particles used in the manufacture of QTC clearly has an effect upon the elastomeric properties of the overall composite. Further effects of the shape of nickel powder upon the properties of QTC are described in the experimental section of this thesis.

3.1.2 Viscoelastic relaxation

An important physical characteristic of QTC is viscoelasticity. The silicones used in QTC composites have elastomeric properties. Thus, when a non-compliant force is applied, such as a free mass resting on, or hanging from the sample, the material slowly relaxes with time, gradually reducing in thickness. This gradual, but persistent movement is often referred to as "creep", and is characteristic of a viscoelastic response.

QTC materials display electrical sensitivity to deformations of their structure [89] [88]. In the case of viscoelastic relaxation, gradual stretching or compression of the composite will cause conducting metallic particles within the bulk to become more closely packed. The electrical resistance of a QTC sample therefore slowly decreases with time whenever mechanical loads are placed upon it [88]. This effect can be seen clearly in the graph in figure 3.2.
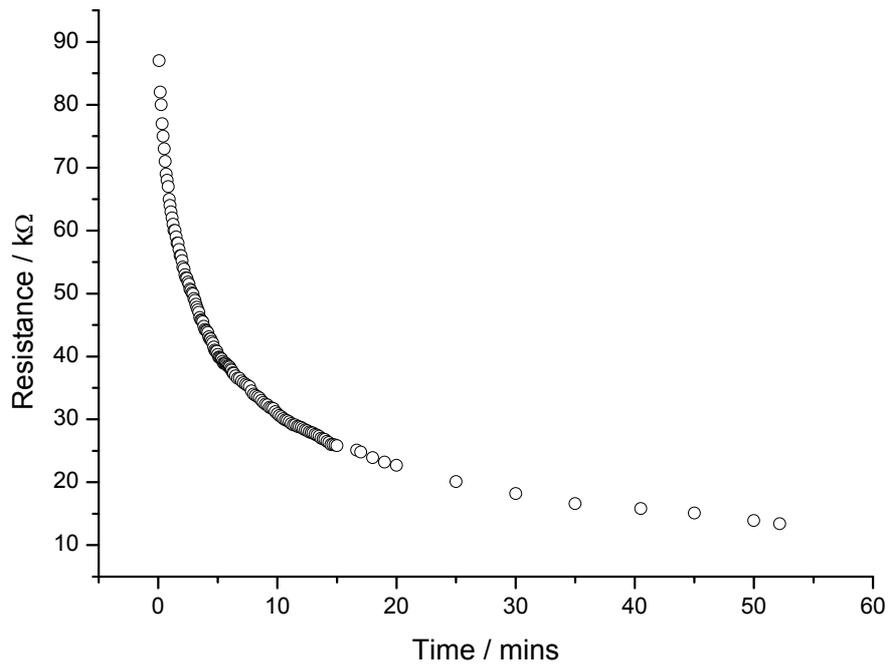
Fig. 3.2: *Viscoelastic relaxation and its associated effect upon*
electrical resistivity for type 287 QTC under compression [88]

3.2 Electrical response to tension and compression

Compressing QTC materials will cause the resistivity of the composite to decrease. This phenomenon is common to all metal-polymer composites. It is due to neighbouring conductive filler particles becoming more closely packed, thus increasing the density of conductive pathways within the composite. However, the Peratech material displays far greater sensitivity to applied pressure compared to all known competitors. In the most sensitive samples manufactured, resistivity can be made to change by more than seven orders of magnitude under only finger pressure [88] [90].
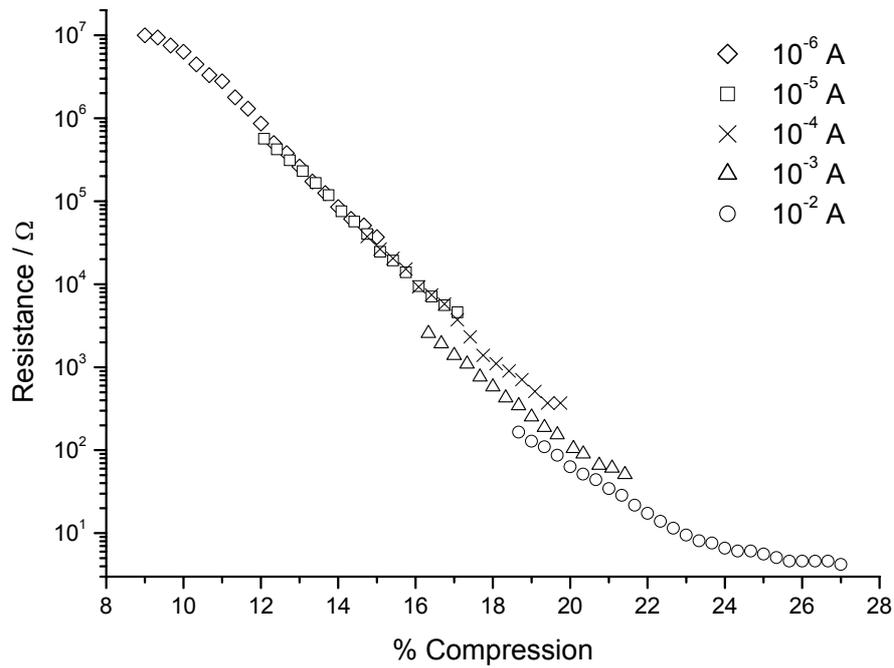
Fig. 3.3*: Electrical response of QTC to compression [90]. Different currents have been used to show the full dynamic range of resistance*

Percolation theory and effective medium theory are inadequate on their own to model such extreme sensitivity to pressure in a metal-polymer composite. It has been proposed that inter-particle conduction is instead dominated by some variety of quantum mechanical tunnelling process. This hypothesis has been confirmed by experiment [88]. Morphologically smooth metallic particles were compared with spiky shaped particles. Composites made with these two types of filler powders were tested for electrical sensitivity to applied pressure and overall resistivity. The results showed that spiky particles gave rise to composites that were more sensitive to applied pressure, and generally more conductive than composites made from smooth shaped particles (figure 3.4).
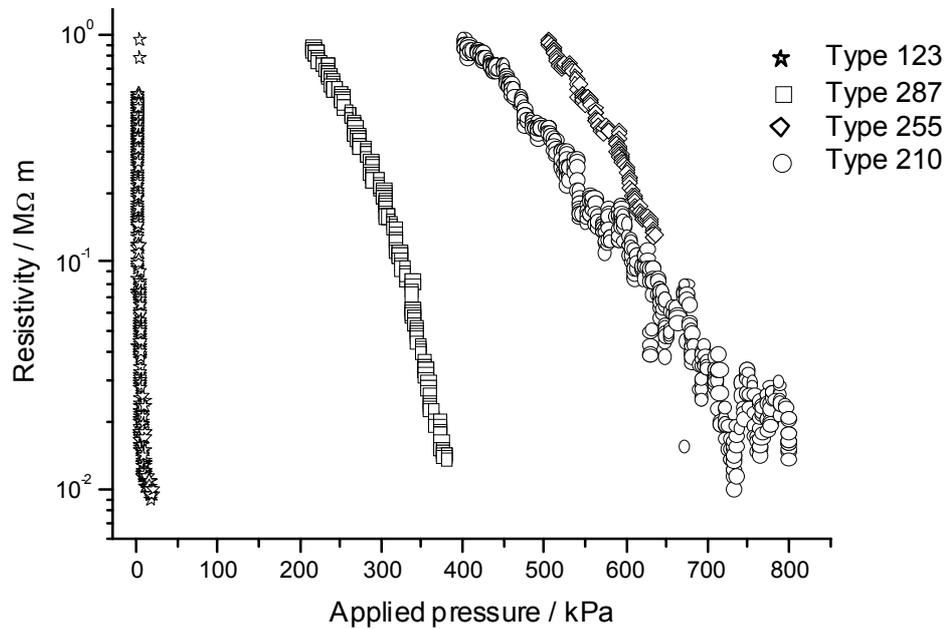
Fig. 3.4*: Electrical response to compression for QTC*
made with spiky and smooth filler powders [88]

Percolation theory cannot account for this difference in sensitivity between spiky and smooth powder types. However, in a tunnelling model, the spikes are thought to increase charge density, and thus give rise to more favoured conditions for field emission and tunnelling mechanisms to occur.

QTC materials also display an electrical response to tension [26] [89] [91]. However, contrary to conventional composites, conductivity increases when tension is applied (figure 3.5). Complex internal mechanical distortions are thought to be responsible for this. It is also possible that stretching QTC in one direction causes compression in a direction perpendicular to the applied tension (a phenomenon described by the Poisson ratio of the material). Alternative conductive pathways are therefore formed in this new direction, giving charge carriers an alternate route for conduction in the composite.
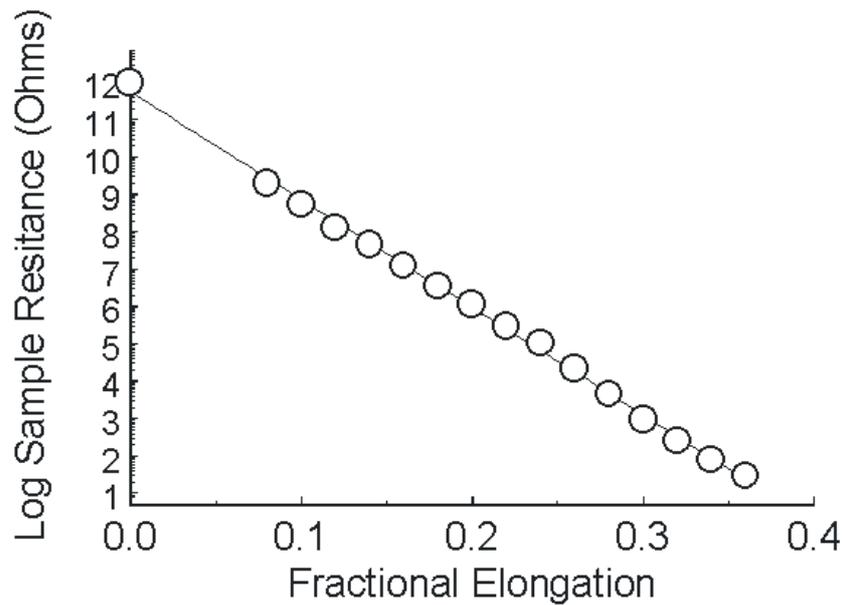
Fig. 3.5: *Electrical response of QTC to tension [89] [26]*

QTC also displays an increase in conductivity when subjected to torsion and bending. The reason for this is due to induced compressions and tensions occurring elsewhere in the material. However, a detailed investigation of the response has not yet been undertaken.

3.3 Trap filling and space-charge limited currents

Space-charge limited behaviour can be seen to take place within QTC materials [88]. This manifests itself in the form of continual upwardly drifting currents whilst a constant voltage is applied. Current-voltage characteristics also show similar behaviour at low applied electric fields. For example, figure 3.6 shows the material passing through what appears to be a trap-filled limit, resulting in a sudden increase in the measured current.
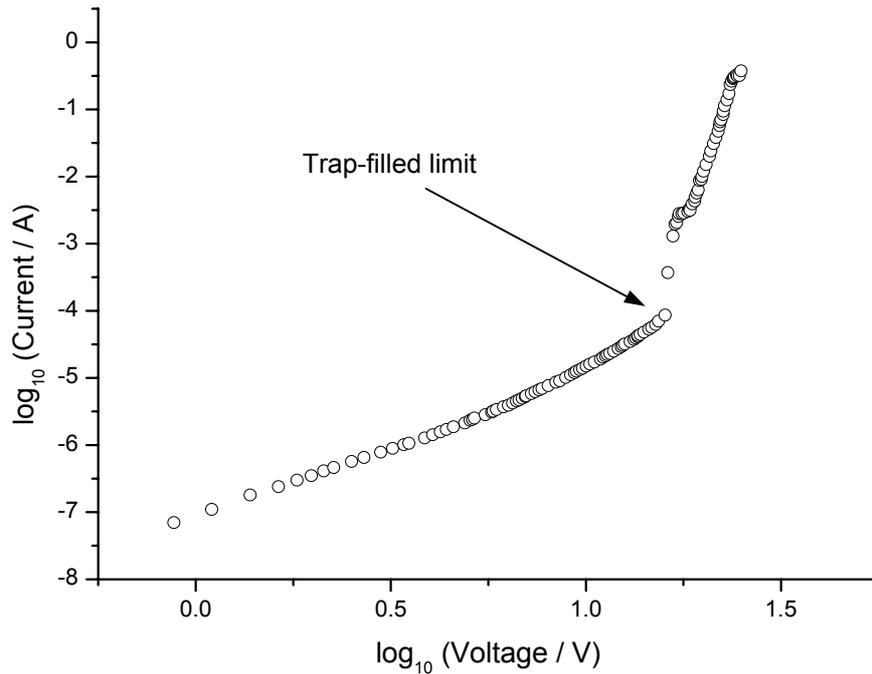
Fig. 3.6: *Space-charge limited behaviour in type 255 QTC [88]*

The cause of such space-charge limited behaviour is thought to be due to the highly amorphous structure of the polymeric matrix from which QTC is constructed. A high density and wide variety of trapping sites therefore exist within the Peratech material, which can be represented by a broad continuum of trap energies. In addition, peaks may occur within this continuum representing dominant trapping energies due to the presence of nickel acting as an impurity within the silicone matrix.

It is possible that one might argue that sudden rises in current, such as that displayed in figure 3.6, are not truly representative of SCLCs. If one refers to the theoretical graph shown in figure 2.12, one would expect to see four regions of differing gradients. Regions (a) and (b) are often blurred together, and region (c) is clearly observed in our material. However, the

presence of region (d), accounting for Child's law after trap saturation, is not observed. However, regions (c) and (d) are sometimes also blurred together, and may not be seen at all. The other effects that are clearly present within QTC may also obstruct our observation of this region. The evidence for SCLCs is therefore inconclusive.

3.4 Current-voltage characteristics

The current-voltage characteristics of QTC materials are highly unusual [88] [91]. Figure 3.7 is a typical example, and shows highly non-linear behaviour and hysteresis. In this figure, peaks can be seen in both the voltage increasing and voltage decreasing plots. However, the positions of these two peaks are usually displaced from one another, such that the peak on the voltage-increasing plot occurs at a higher voltage than the peak that occurs during the voltage decreasing section of the cycle.

As the voltage is decreased, the current remains almost voltage independent, until lower fields are approached. At this point a rise in the current is observed, sometimes occurring extremely rapidly, and peaking at values above 3A. This is sometimes higher and sometimes lower than the peak observed at higher fields. The cause of this "secondary" peak and the observed negative differential resistance is uncertain at present.

It has also been noted that repeated voltage sweeps give rise to different current-voltages compared to those obtained on the first cycle [88]. Once an initial cycle of voltage increasing and decreasing has been completed, peak positions in subsequent cycles are shifted in an as yet unquantified manner. Also, if the compression is sufficiently large and previous voltage sweeps have been high enough, it is possible to switch the Peratech material into a more highly conductive state [88]. In this state, QTC displays Ohmic

behaviour up to currents as high as 3A. The result of these findings is that QTC displays electrical history-dependent behaviour.
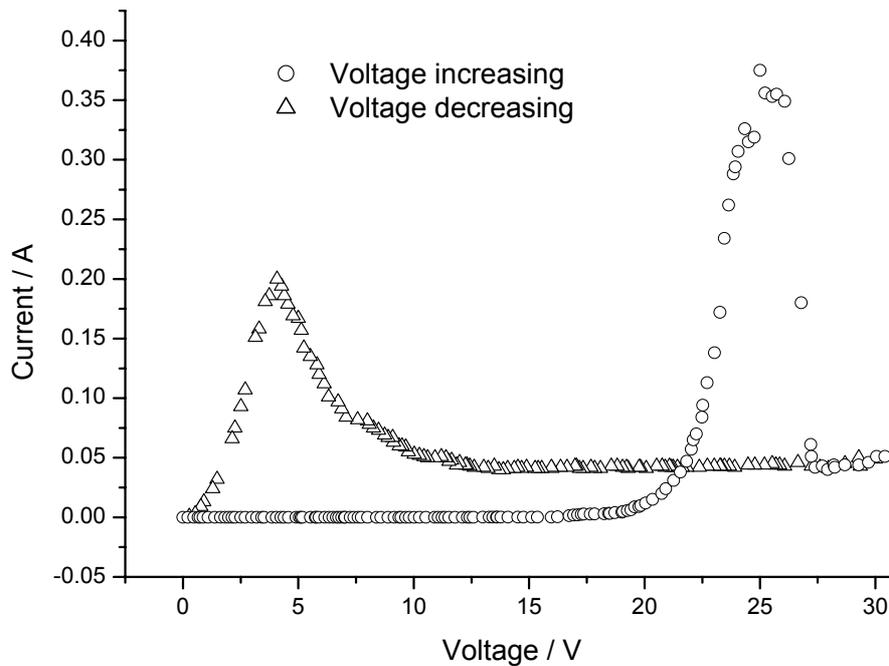
Fig. 3.7: *Typical current-voltage characteristics of type 255 QTC [88]*

The non-linear rise in current with increasing voltage might be attributed to space-charge effects within the composite. However, the cause of peaks in the current-voltage characteristics is uncertain. A PTCR effect was originally thought to be the cause. Experiments showed peak currents as large as 3A occurring within QTC samples (combined with voltages anywhere between 3V and 25V). Such large currents caused substantial Joule heating within the composite. Indeed, temperatures would sometimes increase to the point of localised melting within the composite. Under elevated temperatures, the composite will of course expand. However the

61

polymer has a coefficient of expansion greater than that of the nickel powder. Consequently, upon heating, metallic particles will become pushed further apart by the more rapidly expanding polymer. This in turn will decrease the conductivity of the composite, resulting in the observed current decrease. Whilst the current remains low, joule heating is reduced, and eventually the polymer contracts again as it cools. The conductivity then increases again, and the current rises to form the second peak occurring on the voltage decreasing cycle.

This thermostatic effect occurring at high powers may have commercial application, and investigations into the application of QTC as a reusable fuse by use of the PTCR effect have taken place.

3.5 EMI shielding

An undergraduate team project was undertaken [92], which investigated the potential of QTC as an electromagnetic interference (EMI) shielding device for use at microwave frequencies. A granular form of QTC was chosen to carry out these measurements, further details of which can be found in chapter 7 of this thesis.

QTC granules were impregnated onto cloth substrates at different loadings by use of a polymeric binder. A klystron source generated microwaves of a narrow frequency range, measured to be 9.307 (± 0.156) GHz. This was then used to direct microwaves onto the QTC impregnated fabric. Crystal receivers on either side of the sample compared the incident power with the transmitted power, enabling a percentage transmission to be calculated. The degree of transmission could then be compared to the loading of QTC within the fabric, and also to the resistance of the QTC granules. The results can be seen in figures 3.8 and 3.9.
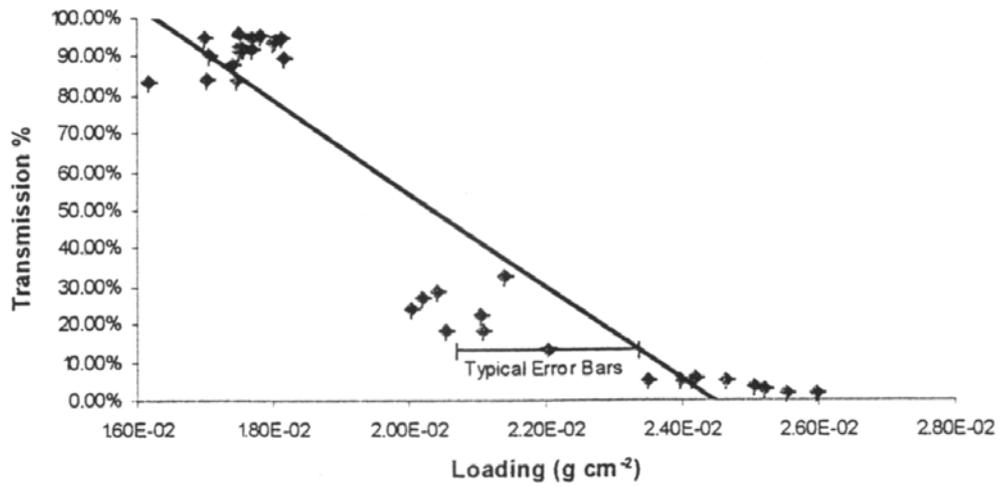
Fig. 3.8: *Percentage of microwave transmission against*
loading of QTC within the fabric substrate
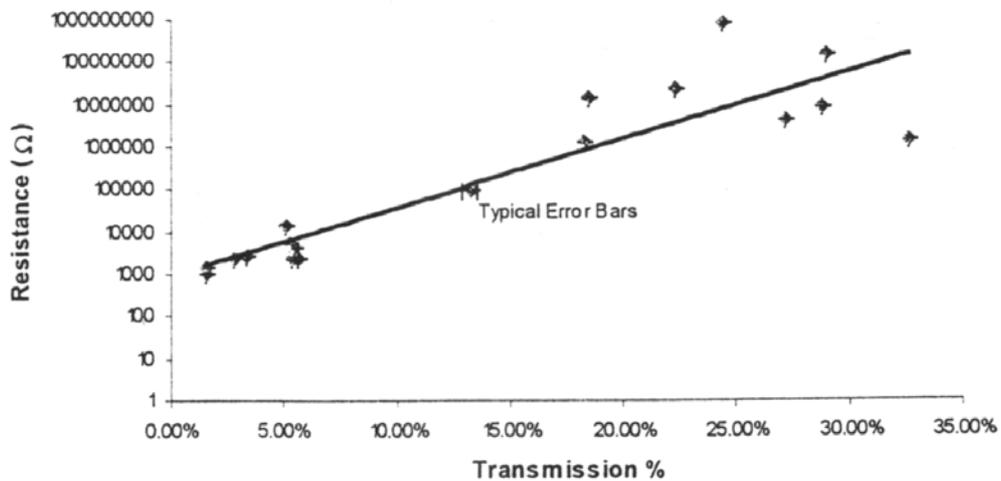
Fig. 3.9: *Resistance of fabric impregnated granular QTC*
against percentage of microwave transmission

Figures 3.8 and 3.9 show that QTC does indeed possess EMI shielding
capabilities, with percentage transmission decreasing as the loading of QTC

within the fabric increases. The percentage transmission also appears to be dependent upon the resistance of the QTC sample. Greater transmission was observed for samples with the largest resistances. This implies that the conductivity network within QTC is at least partly responsible for the absorption of microwaves.

It is important to note that these are only basic EMI shielding measurements, working at only a single microwave frequency. In addition, only transmission percentages are shown in these results. A more detailed investigation must also measure the percentage reflected from the surface of the sample, so that the degree of microwave absorption can be calculated.

3.6 Radio frequency emission

It has been observed that under certain conditions, QTC emits electromagnetic radiation at radio frequencies (RF). Emission appears noisy, and at first was thought to occur almost randomly, whenever a current passed through the material. However, upon closer investigation with a simple antenna [93], it was discovered that RF emission was strongest whenever the composite was in a dynamic state. Changes in applied voltage, or mechanical distortion, such as tension or compression, gave rise to increased emission levels. Conversely, when the composite was in a steady state, with no changes in voltage or compression, RF emissions were low. The nature of the emission was broadband and noisy, containing no specific intensity peaks.

The cause of such emission was initially uncertain. However, results show similarities to emission caused by spark discharging. A more detailed discussion of the causes of RF emission within QTC, along with proposed conduction mechanisms within the composite, can be found in chapter 6.

4 Microstructural analysis of QTC materials

4.1 Introduction

This purpose of these experiments was to investigate the microstructure of QTC materials. Previous work [88] has implied that the spiky metallic particles used to manufacture QTC are responsible for the unique electrical properties of the material. However, verification that the metallic particles within QTC still retain their spiky characteristics after the mixing process has not yet been sought.

In addition, it has been hypothesised that the patented manufacturing process, utilised by Peratech, which uses minimal mechanical energy to mix the composite, is essential in order to retain the high sensitivity to applied pressure which characterises QTC. Electron microscopy enables a detailed examination of the microstructure of QTC, including the morphology of nickel particles once they have been mixed into the polymer. Comparison with samples manufactured using different types of nickel powder and higher amounts of mechanical energy can also be made.

4.2 Experimental

Electron microscopy facilities were kindly provided by Dr. Ken Durose and Mr. Andrew Yates of the University of Durham Semiconductors and Ceramics Research Group. Secondary electron images were taken using a Jeol JSM IC848 scanning electron microscope. This facility was also equipped with a thin windowed PGT Avalon EDX system. Transmission electron microscopy was performed using a Jeol JEM 200CX.

Scanning electron microscope (SEM) analysis was first performed upon the five different types of raw nickel powders in order to confirm their morphology. These powders were supplied by Inco Speciality Powders, details of which can be found in table 3.1. Powder types are referred to as type 123, 255, 287, 210 and 110, as named by Inco.

Using the five different types of nickel powder, Peratech manufactured standard samples of QTC according to their patented process [26]. The silicone polymer used in each case was Alfasil 2000, supplied by Alphas Industries. Loading ratios (by weight) of metal powder to polymer are detailed in table 3.1 and have been calculated so that all samples contain the same surface area per gram of composite [88].

The five different QTC samples were then examined using scanning electron microscopy. Compositional analysis of the samples using the technique of Energy Dispersion of X-rays (EDX) was also carried out (accelerating voltage for EDAX was 20 kV) whilst samples were being imaged in the SEM. In addition, thin microtomed samples from the type 287 QTC composite were examined using a transmission electron microscope (TEM).

Three further samples were also provided by Peratech that had been manufactured using differing amounts of mechanical energy. The quantity of mechanical energy is assumed to be proportional to the length of time in the mixer and the mixing speed. Due to the nature of the mixing process employed at Peratech, the exact amount of mechanical energy used to manufacture each sample is difficult to quantify precisely. Sample A was made using the standard technique of low mechanical mixing energy (slow mixer speed for minimum mixing time), whilst sample B was made using a high mixing speeds for a longer period of time. A third composite, sample

C, was also made in which the nickel powder had been pre-crushed using a mortar and pestle before mixing into the silicone polymer. These QTC samples were all made using type 123 nickel powder at a loading of 6:1 by weight (nickel:polymer). At loadings as high as this, standard percolating theory suggests that these composites should all lie above the percolation threshold. The above samples were therefore analysed in the SEM for evidence of percolation and for signs of microstructural differences.

QTC samples often appear to have a shiny surface, which becomes more pronounced as the age the sample increases. This may be caused by the migration of certain chemical species during the curing process or perhaps by oxidation. In order to avoid the possibility of such surface contaminants obscuring the image, samples were first cryo-fractured before viewing in the SEM. By immersing them in liquid nitrogen for a few seconds, samples were cooled below their glass transition temperature (T_g). They could then be easily snapped, revealing a clean fracture interface, which was then presented to the electron microscope.

Due to the intrinsically highly resistive nature of the composite, it was also necessary to sputter QTC samples with a thin layer of gold before imaging. This prevented image blurring due to the build-up of static charge whilst in the electron microscope.

Clear images of the metal particles in the QTC samples were very difficult to obtain due to the presence of a thin polymer layer surrounding the nickel particles. High accelerating voltages (35 kV) were utilised in the SEM in such cases, in an attempt to probe deeper into the material, through the polymer layer. However, for some samples, a high accelerating voltage was still insufficient to obtain a clear image of the nickel particles within the polymer. In such extreme cases, a silicone digester was used to try and

dissolve the polymer layer without damaging the nickel particles contained within. QTC samples of dimensions 15mm x 15mm x 1mm were each placed in approximately 5ml of Ambersil silicone digester, supplied directly from Ambersil. Samples and digester were agitated in a sonic bath for 5 days, and then repeatedly filtered and washed using distilled water. The residues were dried at 50°C for approximately 1 week, before being taken to the SEM for imaging.

4.3 Results and discussion

Raw nickel powders

The images shown in figures 4.1 – 4.5 show typical results obtained for the five different raw nickel powders under examination in the SEM. These results confirm that the microstructure of the five nickel powder types is similar to that described in the data sheet literature provided by Inco, and listed in table 3.1.

Type 123 nickel powder consists of discrete spiky balls. Type 287 appears to be very similar to type 123, but is slightly more agglomerated, resulting in a clumpy structure. Type 255 is yet more agglomerated with even greater numbers of spiky particles joined together into long filamentary structures.

Type 110 powder is smooth and approximately spherical in shape, with only a small amount of agglomeration present. In comparison, the other smooth powder, type 210, is more filamentary in structure. It is also confirmed that types 210 and 110 have a generally much smaller particle size than their spiky counterparts.
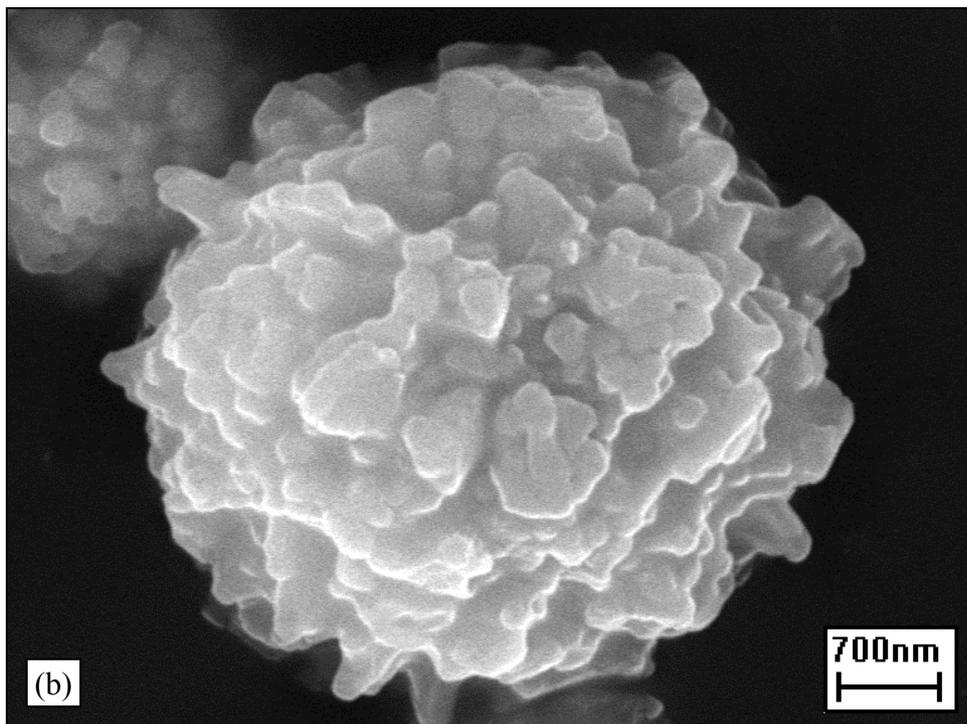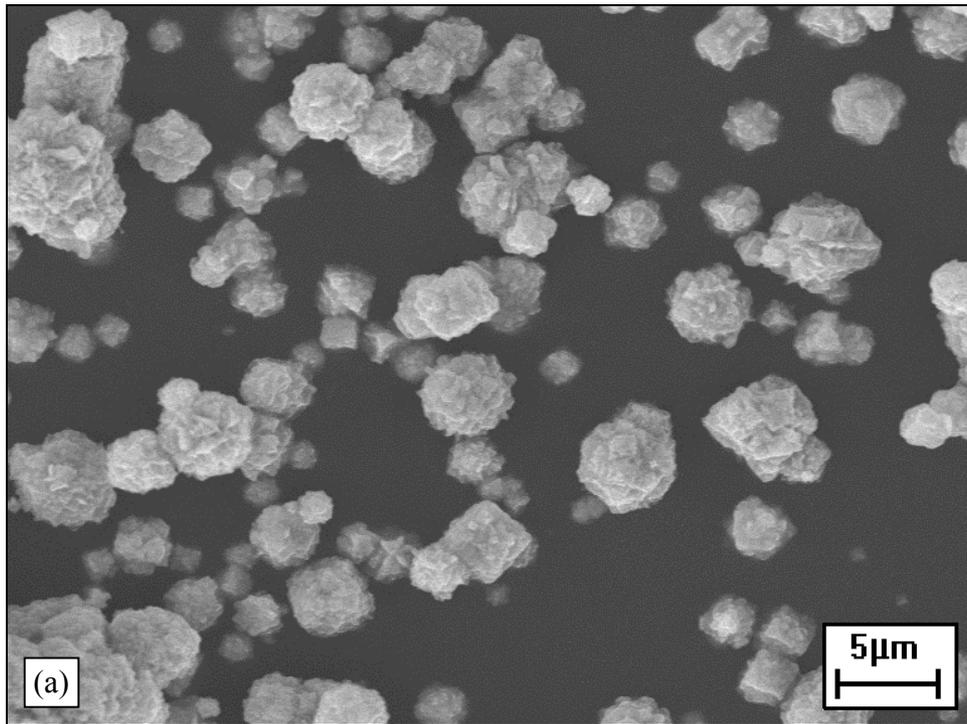
Fig. 4.1: *SEM images of type 123 nickel powder,*
magnification factors (a) 2000x, (b) 15000x
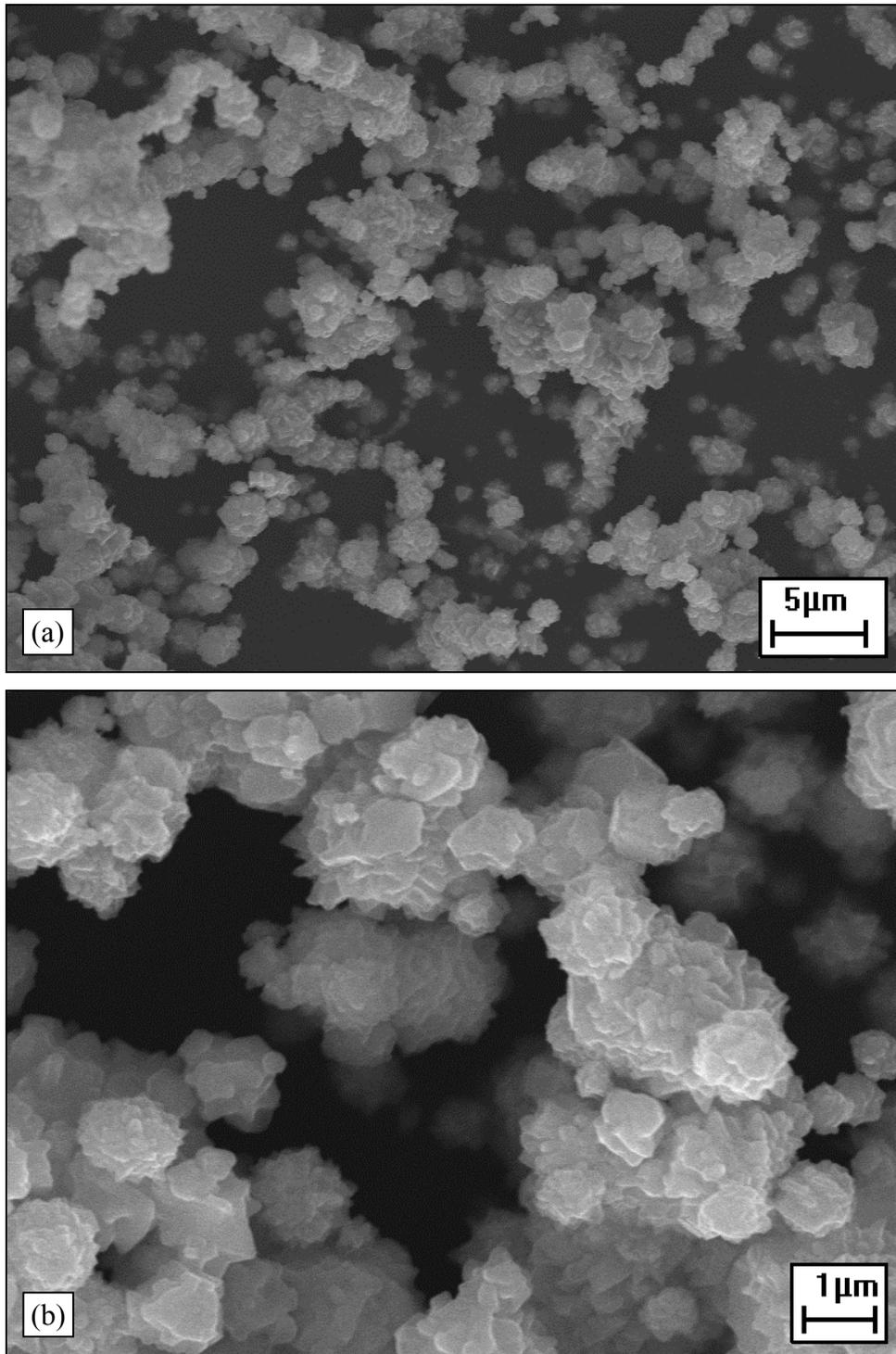
Fig. 4.2: *SEM images of type 287 nickel powder,*
magnification factors (a) 2000x, (b) 8000x
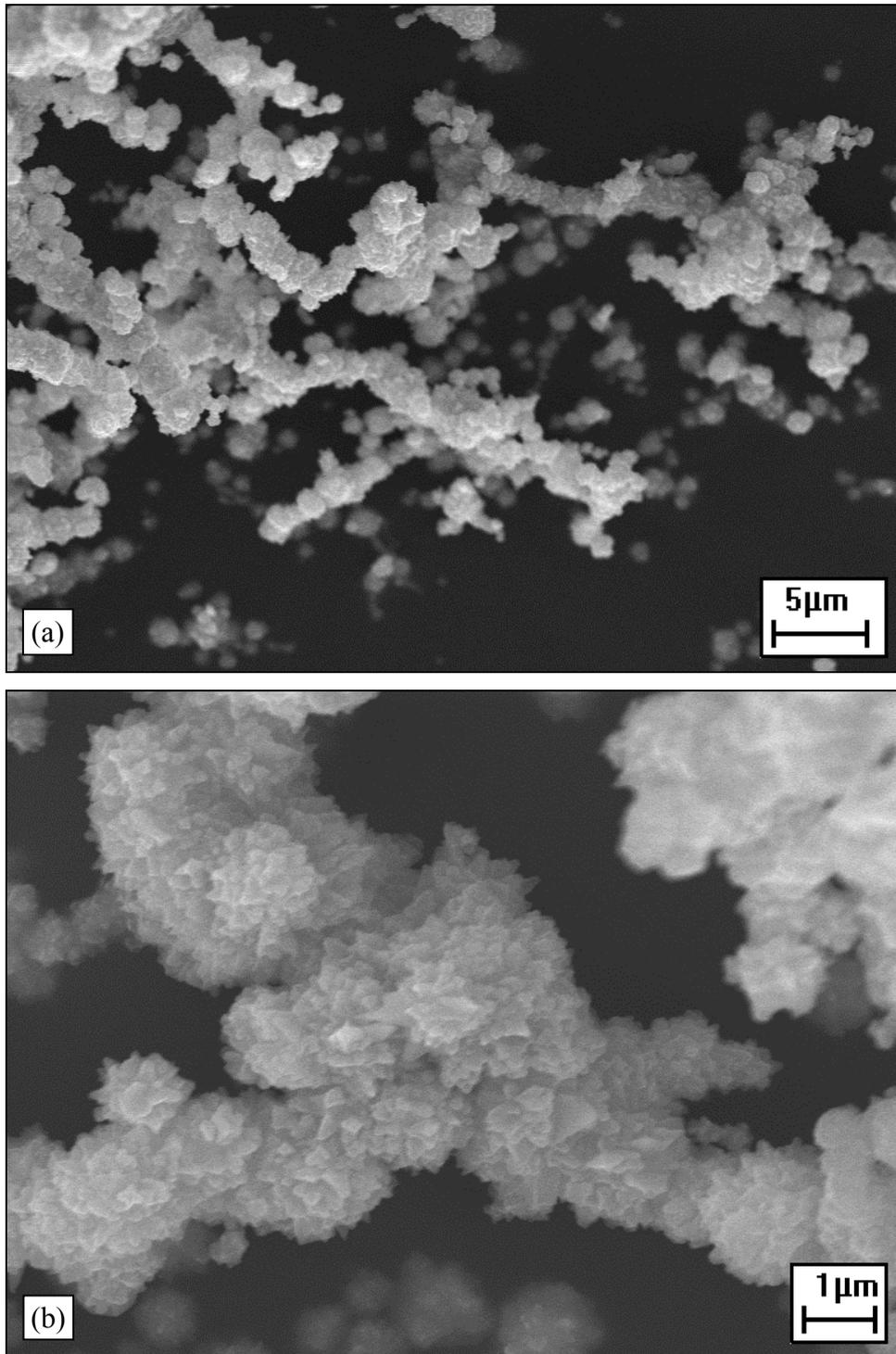
Fig. 4.3: *SEM images of type 255 nickel powder,*
magnification factors (a) 2000x, (b) 8000x
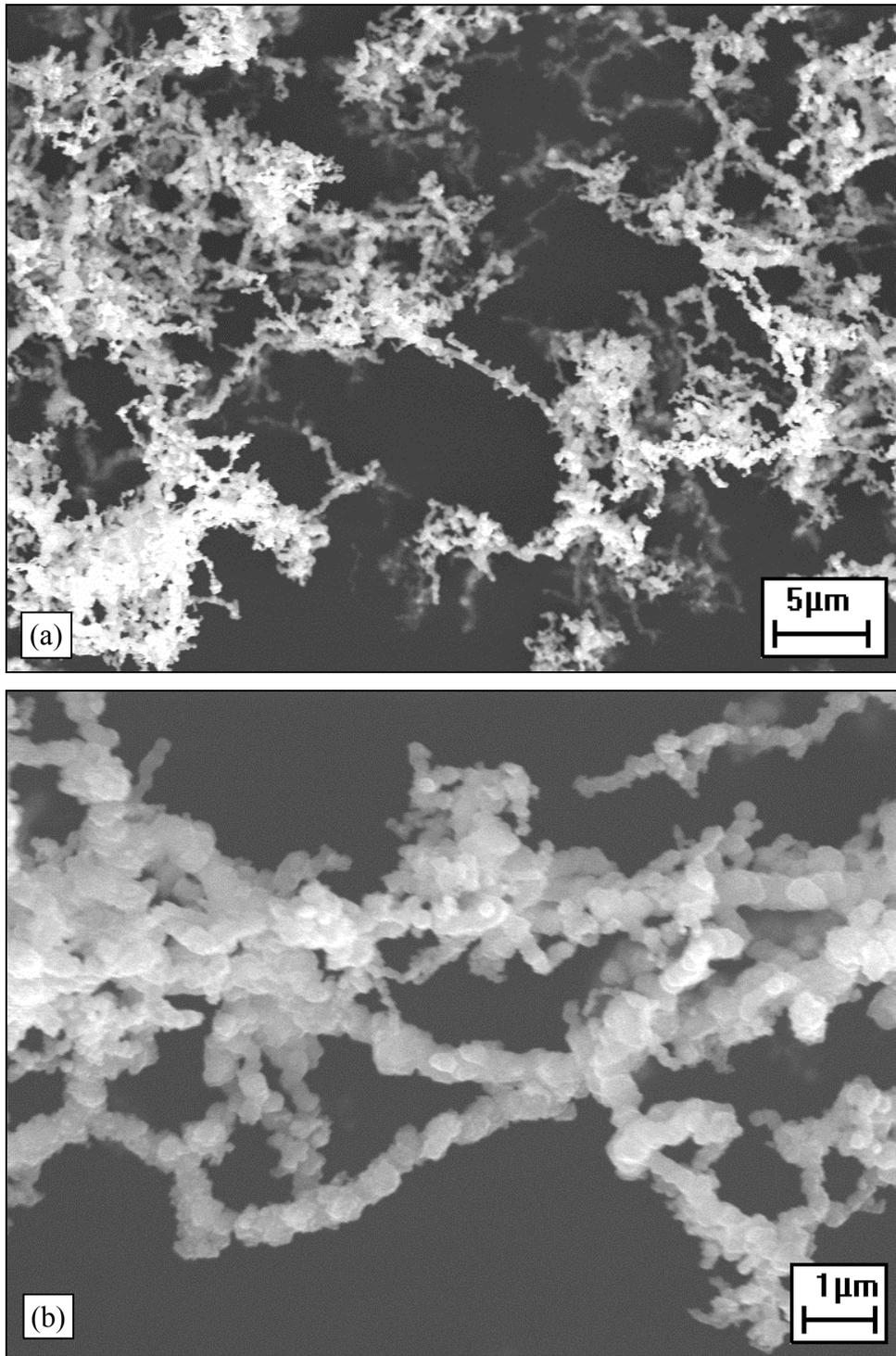
Fig. 4.4: *SEM images of type 210 nickel powder, magnification factors (a) 2000x, (b) 8000x*
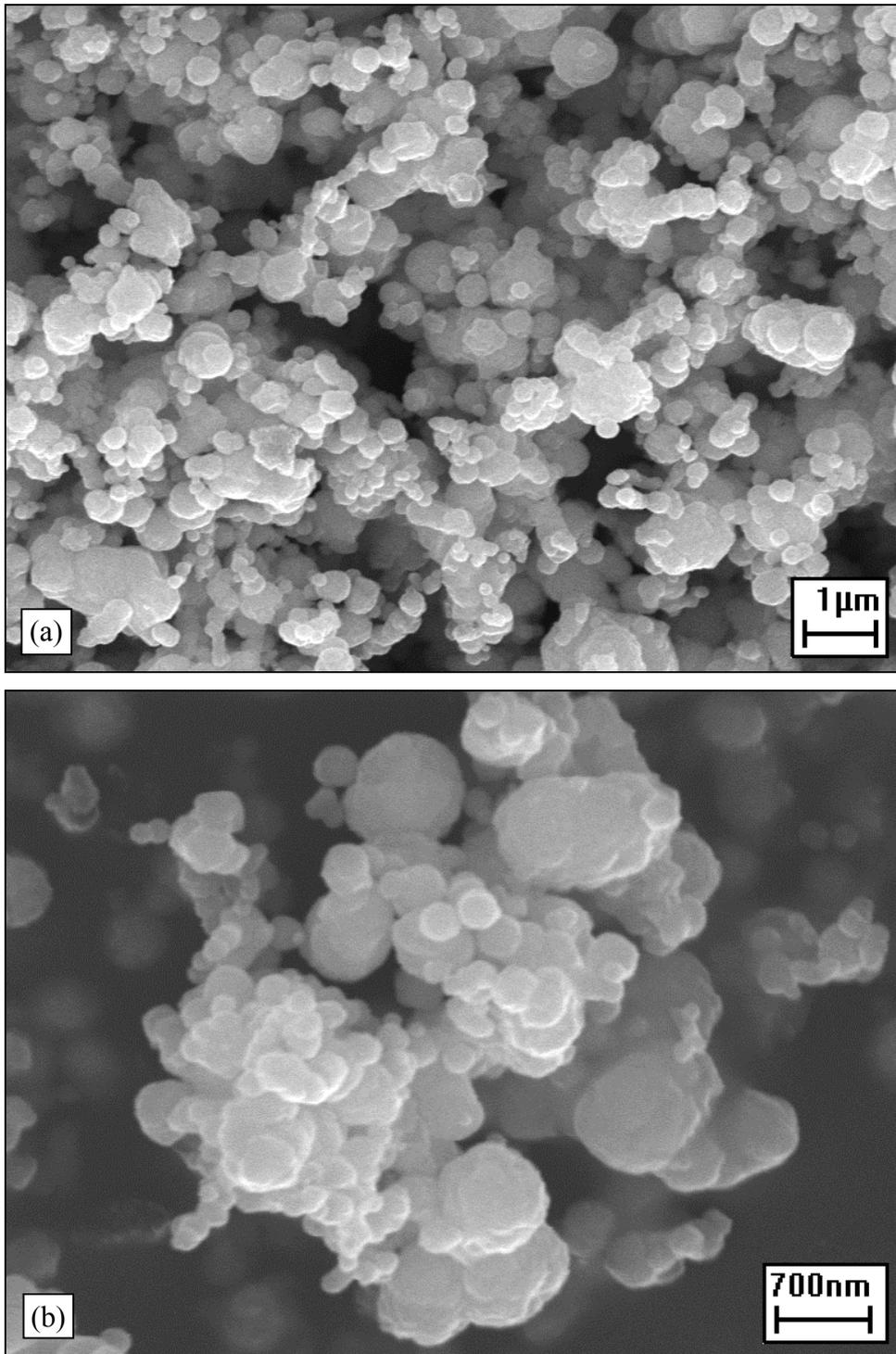
Fig. 4.5: *SEM images of type 110 nickel powder,*
magnification factors (a) 8000x, (b) 15000x

QTC made using different powder types

EDX results for the five QTC samples, made from nickel powders of different particle morphologies, are almost identical to each other. Typical results (for the type 287 QTC) can be seen in figure 4.6. K_α and K_β peaks have been identified, indicating the presence of carbon, oxygen, nickel, silicon and gold as expected. The lack of other peaks suggests that no elemental impurities exist within QTC (or at least that they exist in sufficiently low concentrations for their peaks to fall within the noise of the experimental apparatus).
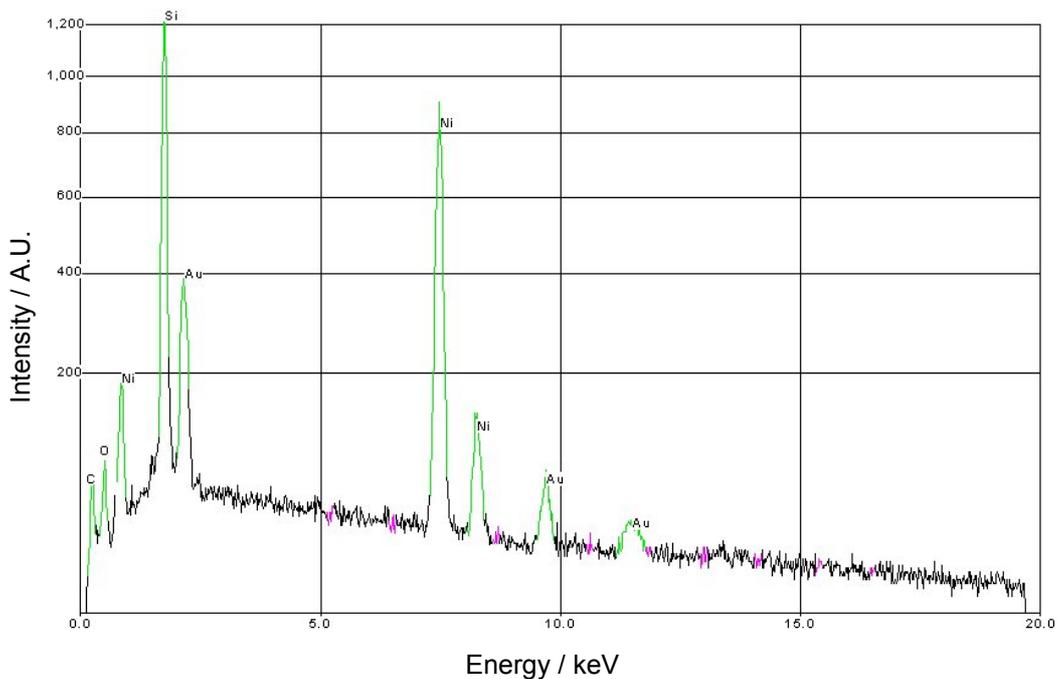
Fig. 4.6: *EDAX results for type 287 QTC (20 kV accelerating voltage)*

Figures 4.7 - 4.11 show typical SEM images of QTC made from the five different nickel powder types, 123, 287, 255, 210 and 110. These images

are all taken at a magnification of 1500x. The distribution of nickel particles within all five samples is random and homogeneous, implying an effective mixing process. Mechanical energy during mixing has been kept to a minimum, resulting in a composite with very few air bubbles and voids.

The cryo-fractured surface was rough, indicating good adhesion between the nickel particles and the polymer [27]. The polymer appears to have completely wetted the surface of the nickel particles very efficiently, resulting in virtually no inter-particle contact. Therefore, in an uncompressed state, percolating pathways do not exist, thus accounting for QTC's intrinsically high resistivity.
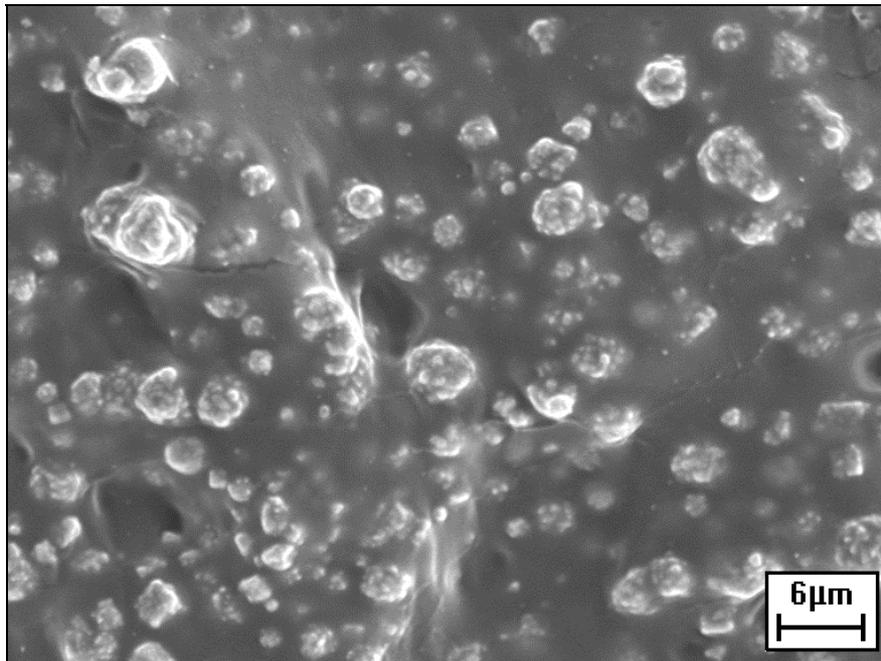
Fig. 4.7: *SEM image of type 123 QTC at 1500x magnification*
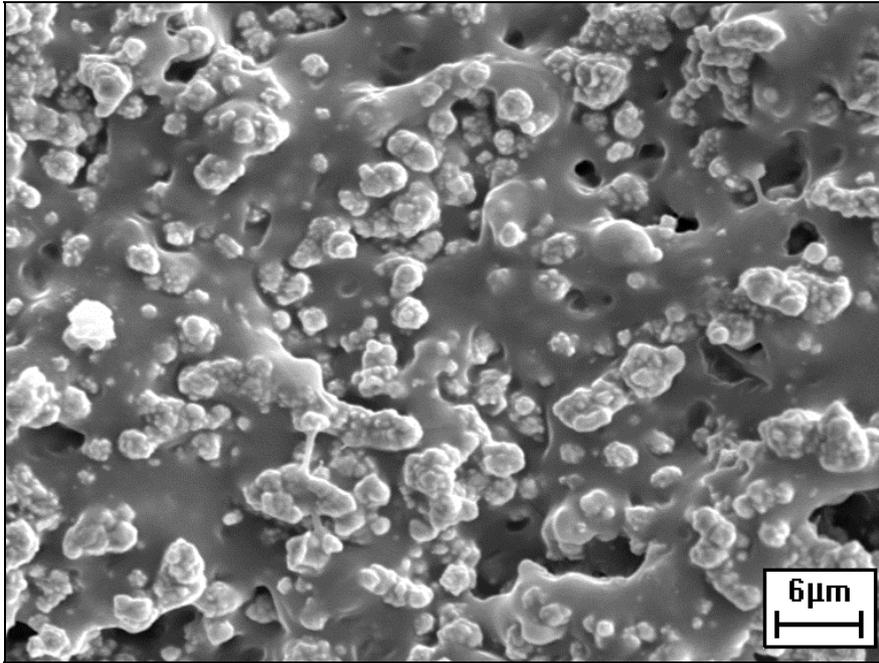
Fig. 4.8: *SEM image of type 287 QTC at 1500**x** magnification*
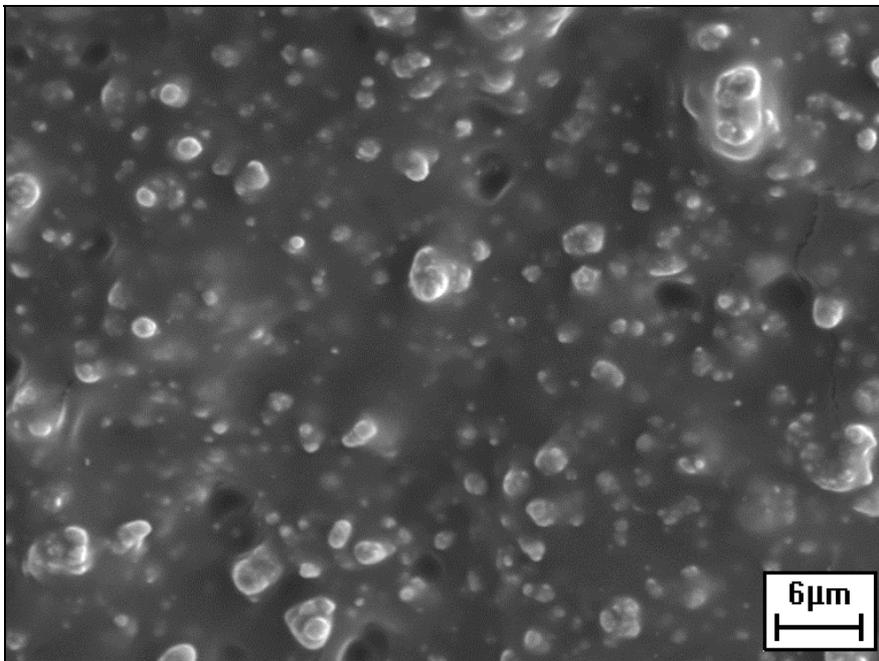
Fig. 4.9: *SEM image of type 255 QTC at 1500**x** magnification*
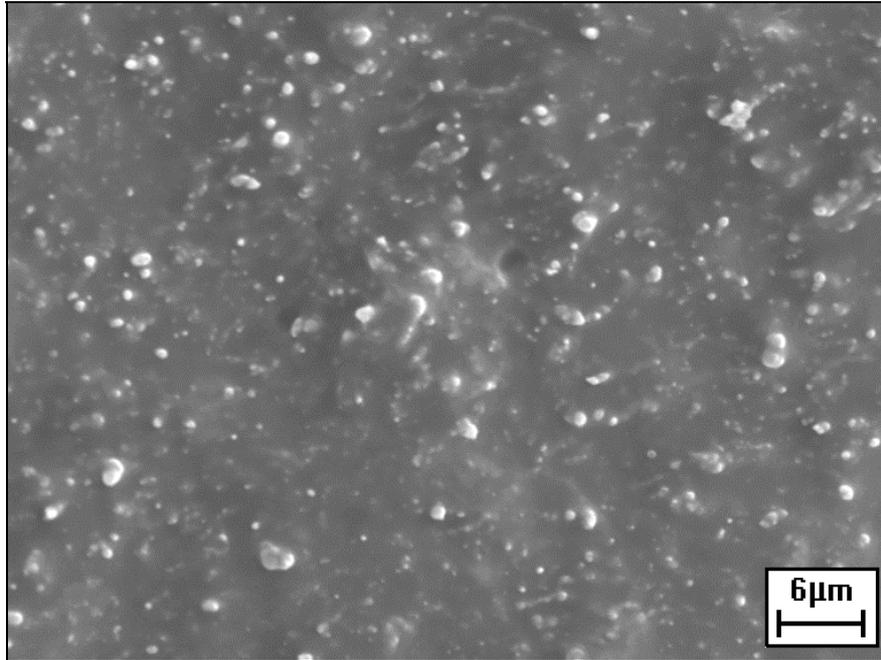
Fig. 4.10: *SEM image of type 210 QTC at 1500x magnification*
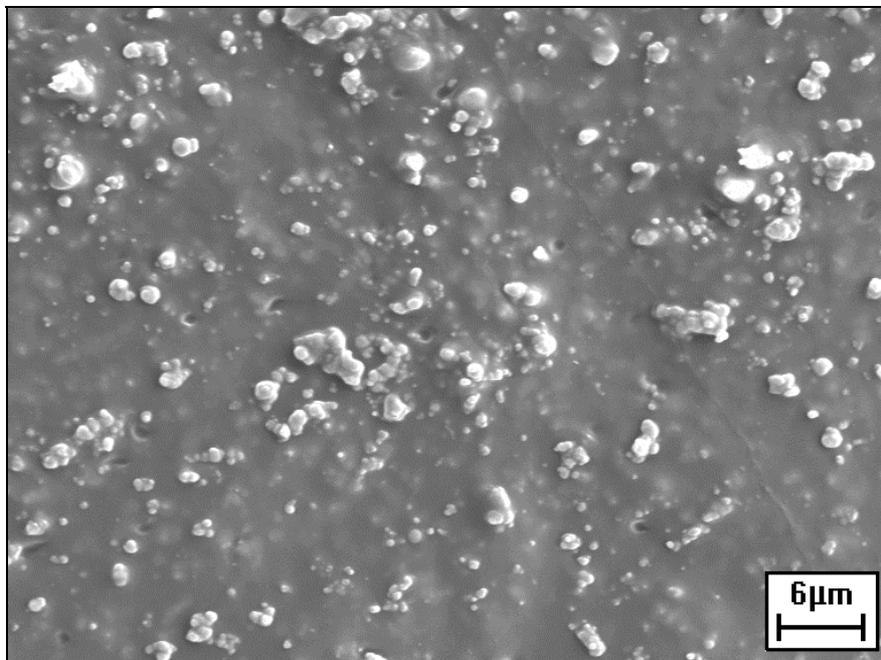
Fig. 4.11: *SEM image of type 110 QTC at 1500x magnification*

Types 255 and 210 QTC both appear to have lost much of the filamentary structure associated with their nickel powder type. It is likely that such delicate structures have been destroyed during the mixing process. The resulting composites therefore now appear to be very similar in structure to QTC samples made from the more particulate varieties of nickel powders.

It can be seen that QTC types 123, 255 and 287 have maintained their more irregular and spiky surface structure after mixing into the polymer. This confirms the earlier hypothesis [88] that it is the presence of spikes that are responsible for the improved electrical sensitivity to applied pressure as seen in types 123, 287 and 255 QTC composites. If the spikes had been destroyed in the mixing process, then clearly this hypothesis could not be true.

The exact condition of spikes on the surface of these particles is difficult to determine at 1500x magnification. In addition, the highly effective wetting of nickel particles by the polymer causes an imaging problem. In all samples, thin residual layers of polymer persistently remain on the particle surface, coating them and thus blurring the image. Therefore, when higher magnifications were used on the type 287 material, as seen in figure 4.12, the accelerating voltage in the SEM was increased to 35kV, in an attempt to probe slightly deeper into the composite and to obtain clearer images.

Figures 4.13 and 4.14 show TEM images of type 287 QTC at high magnifications. Clearer images were possible with this technique compared to SEM. This was due to the sample being a thin microtomed film, compared to the uneven fracture interface as viewed in the SEM samples. A true cross-section of the material therefore results, sometimes cutting directly through metallic particles. Image blurring caused by thin layers of polymer persisting on the metal particles, is therefore less of a problem.
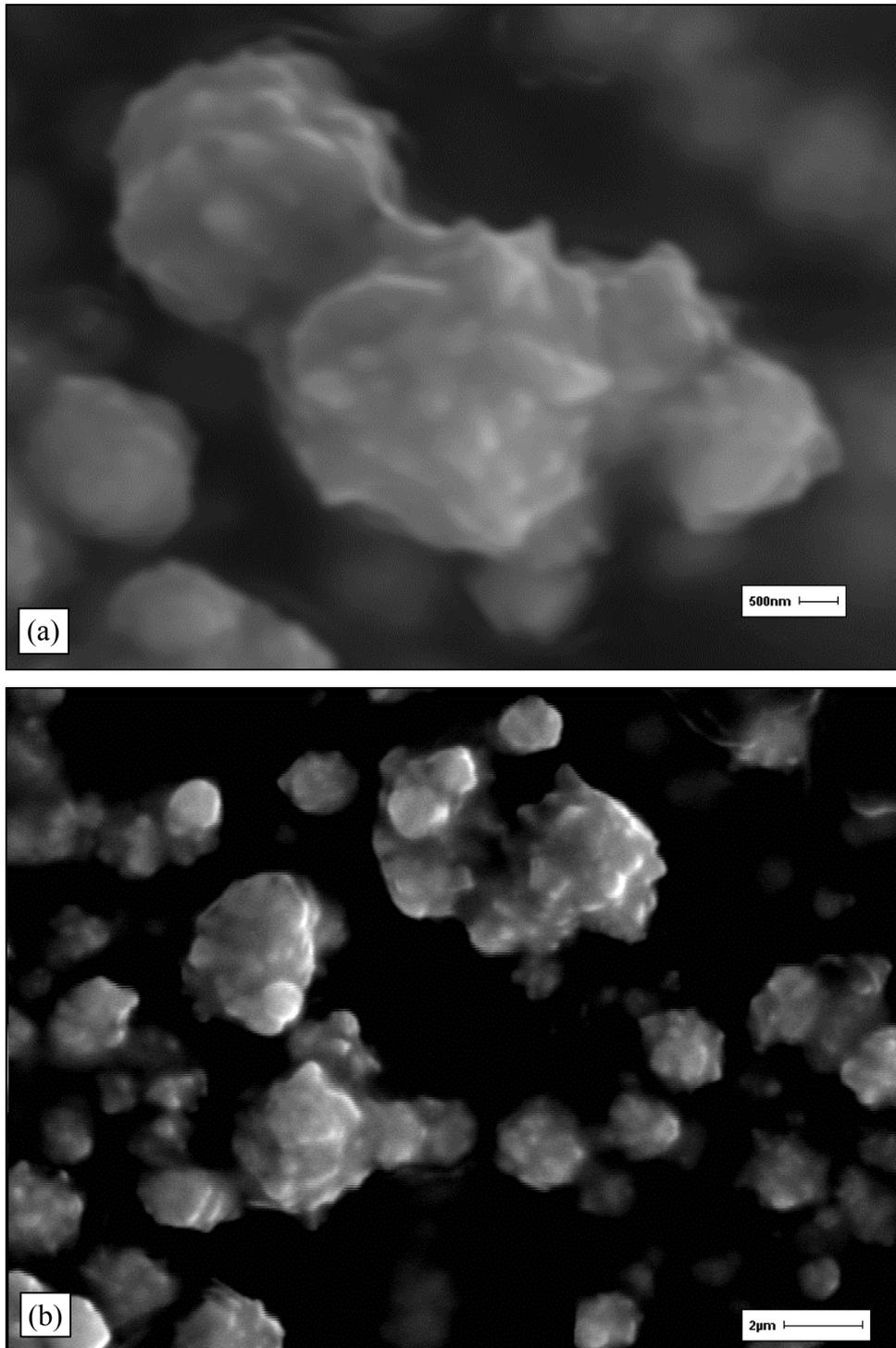
Fig. 4.12: *SEM images of type 287 nickel powder, using 35kV accelerating voltage and magnifications of (a) 9500x, (b) 5000x*
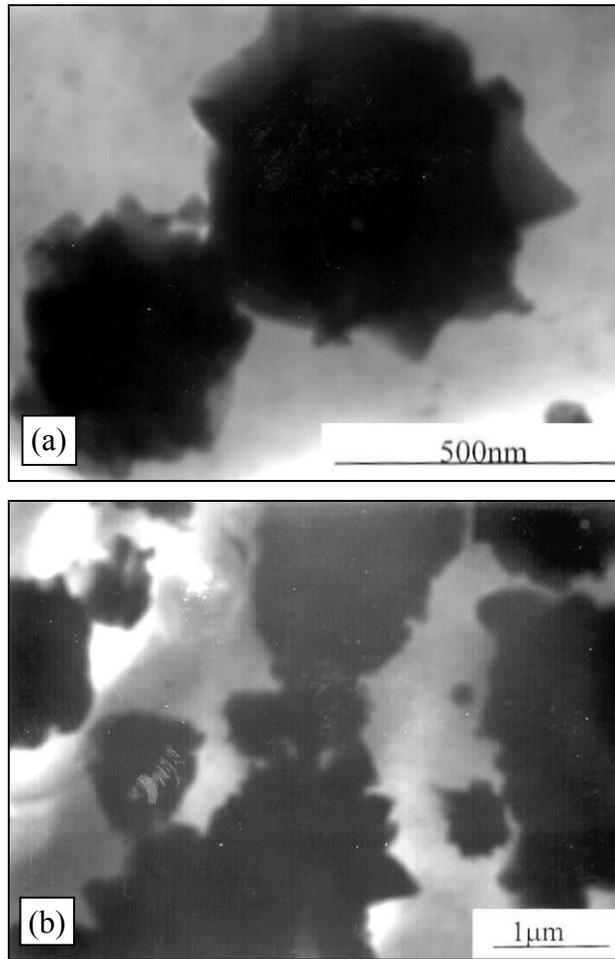
Fig. 4.13: *TEM micrographs of type 287 QTC material*

It is important to note that the persistent nature and good adhesive properties of the silicone coating implies that conduction via a standard percolating mechanism is unlikely. Even under high compressions and loadings, a thin insulating barrier between metallic particles will persist.

Highly irregular structures including spikes on the surface of the nickel particles are clearly visible in many of the figures. Figure 4.14 shows tips with radii of approximately 1nm or less. Features such as this will

significantly enhance local fields, allowing high field conduction mechanisms such as field emission or Fowler Nordheim tunnelling to become potential candidates for models of electrical conduction.

It is also interesting to note that the mixing process has not destroyed these delicate spiky structures. The low mechanical energy used to manufacture QTC is thought to be responsible for this.
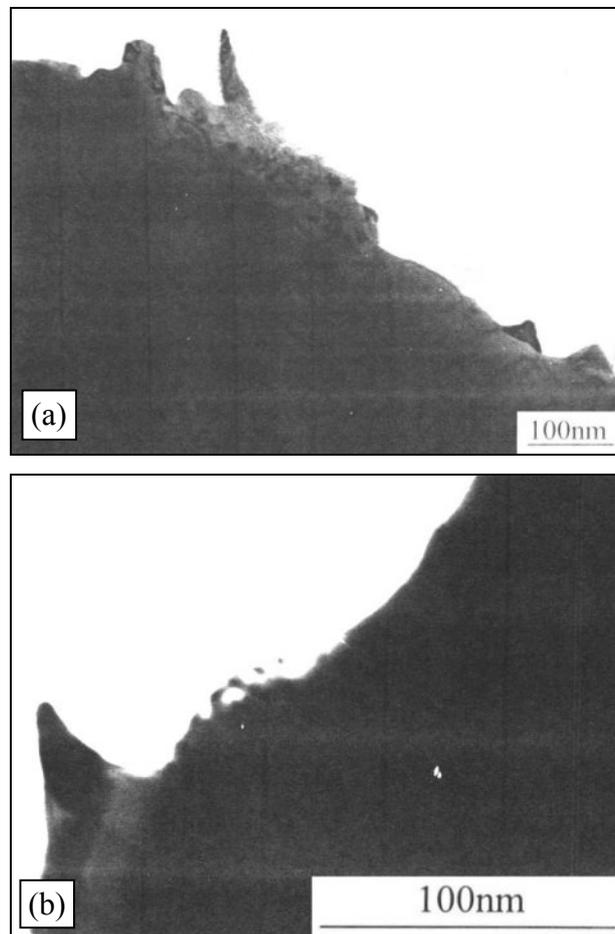
Fig. 4.14: *TEM micrographs of type 287 QTC material,*
showing individual spikes on the surface of nickel powder particles

QTC made using different amounts of mechanical energy

Images of three samples made using different mechanical energy are shown in figures 4.15, 4.16 and 4.17. Both the sample made using high mechanical mixing energy (sample B), and the sample made with pre-crushed nickel (sample C), were particularly difficult to image clearly. For this reason, silicone digester was employed to try and dissolve away the surface layers of silicone from the composite. Some remnants of the silicone are clearly still visible in many of the images. However, this technique enabled clearer images of the surface of the nickel powders to be obtained.

Samples B (figure 4.16) and C (figure 4.17), made using high levels of mechanical energy, appear to contain a few smaller, fragmented particles which are less frequently observed in sample A (figure 4.15). It is thought this is clear evidence of the destructive results of using high mechanical energy during the mixing process. Metallic grains will rub against each other in an abrasive fashion, causing fractures and breakages.

Sample B, mixed using high levels of mechanical energy, shows nickel particles with a relatively smooth surface morphology. Most of the type 123 powder's characteristic spikes appear to have been destroyed during the mixing process. This effect cannot be attributed to the solvent attack of the silicone digester. Sample A, mixed using the standard technique of low mechanical energy, clearly still shows highly complex and spiky features on the surface of the nickel particles.

Sample C, made using pre-crushed nickel, shows yet further smoothing of the nickel particles. Surface irregularities have been reduced in comparison to samples A and B.
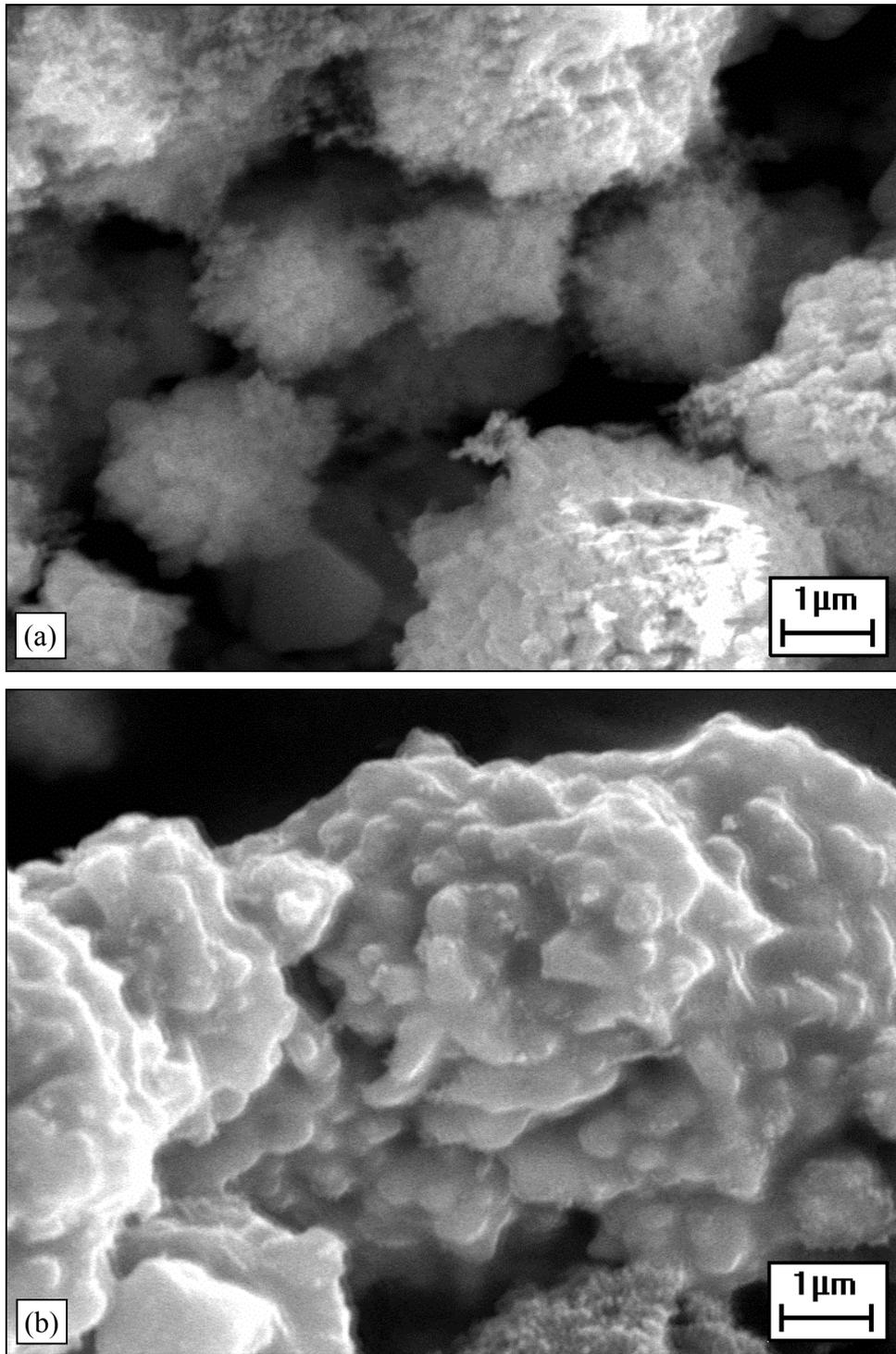
Fig. 4.15: *Type 123 QTC made using low mechanical energy (sample A), dissolved in silicone digester, magnification 10000x*
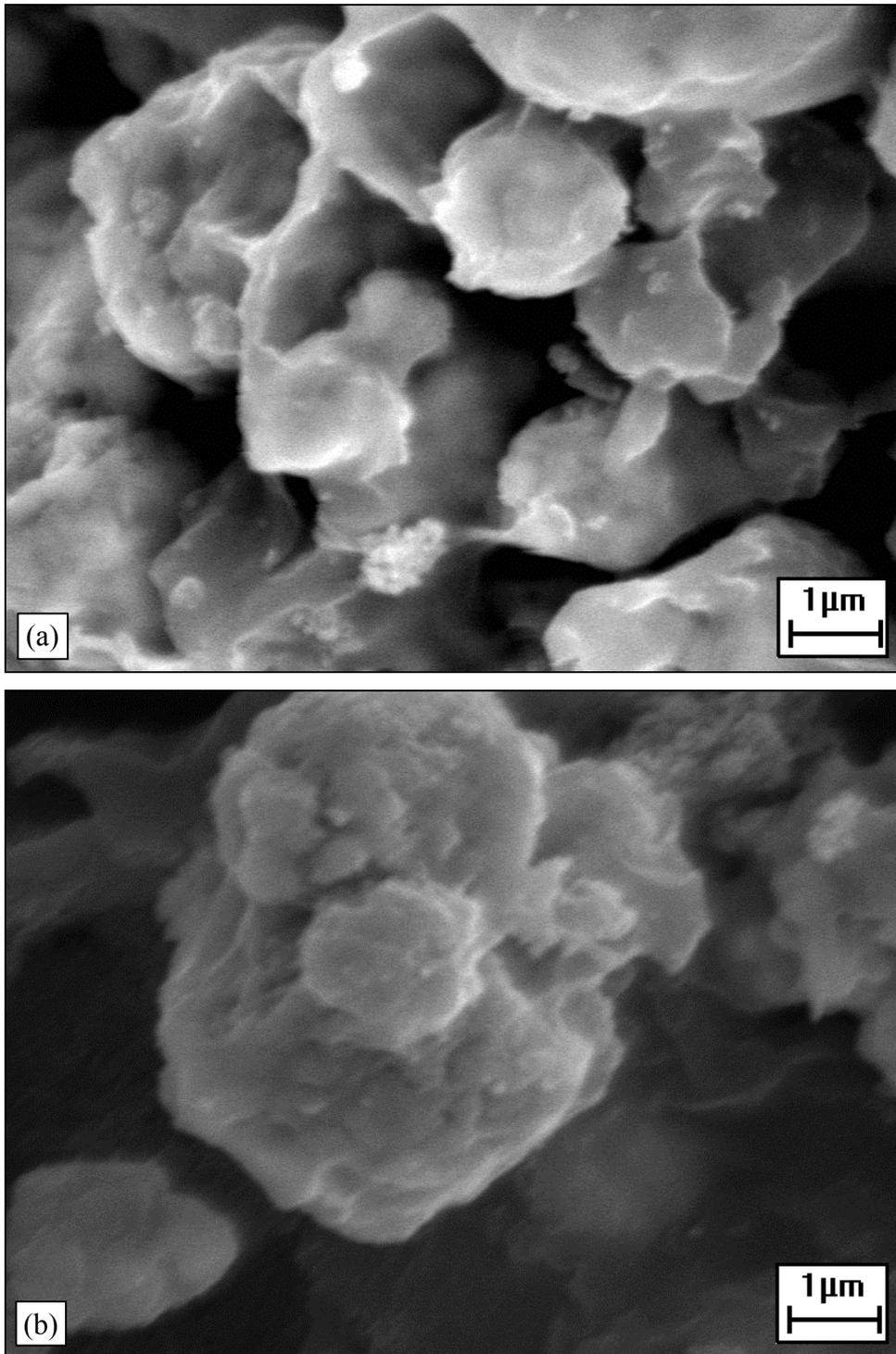
Fig. 4.16: *Type 123 QTC made using high mechanical energy (sample B), dissolved in silicone digester, magnification 10000x*
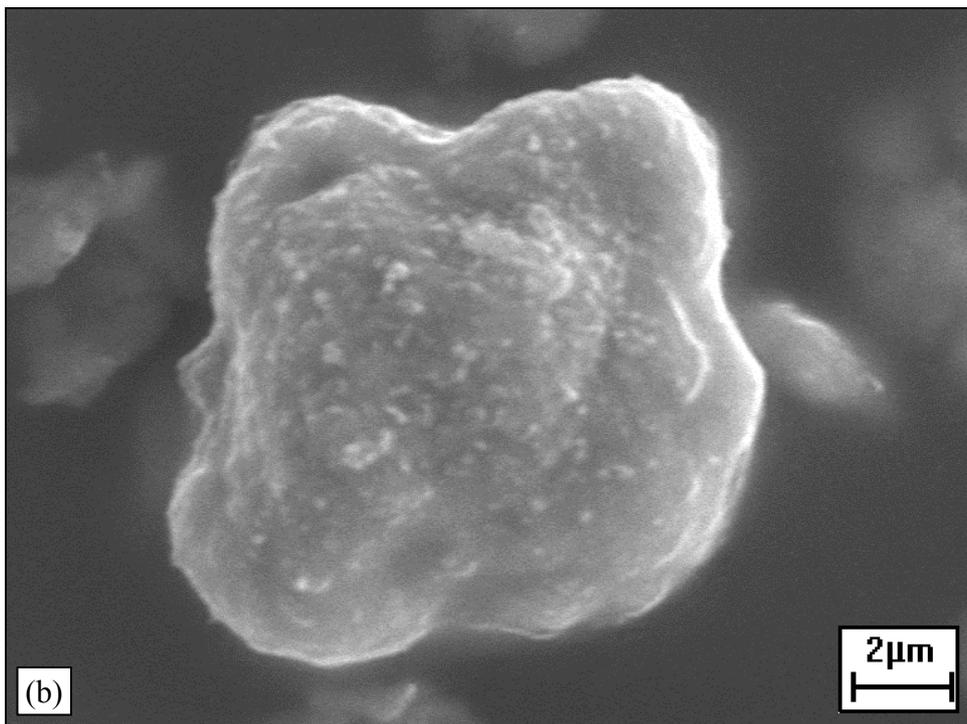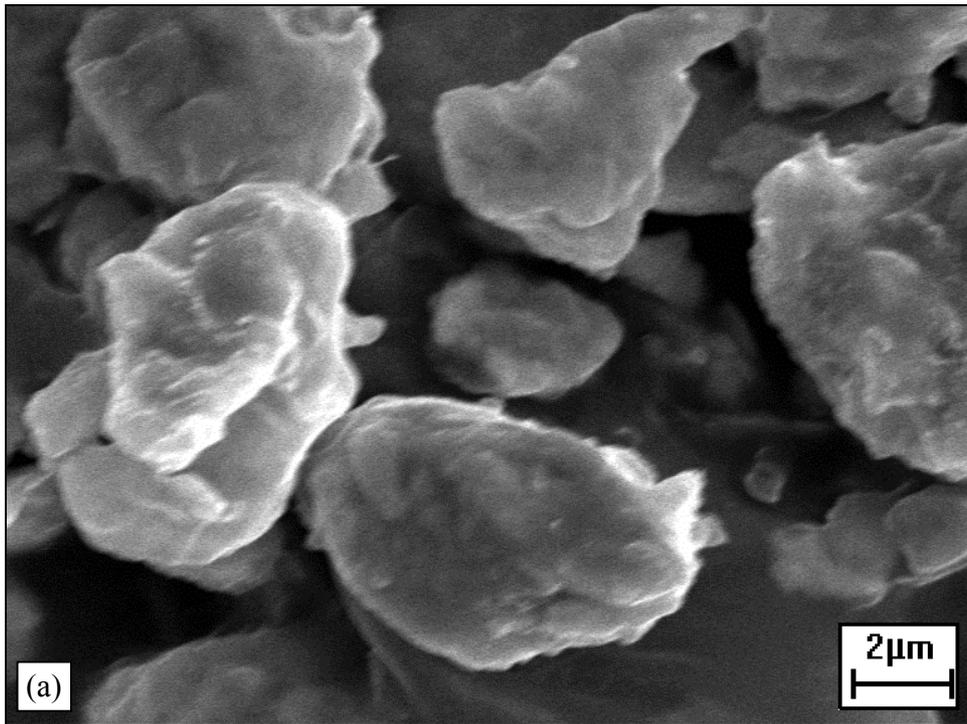
Fig. 4.17: *Type 123 QTC made using pre-crushed nickel powder (sample C), dissolved in silicone digester, magnification 20000x*

It is clear from these results that the low mechanical energy mixing process, as employed by Peratech in their manufacture of QTC, is essential in order to maintain the spiky surface morphology of the nickel particles in the composite.

4.4 Conclusions

QTC composites consist of a mixture of micron-sized spiky nickel particles within a silicone polymer matrix. The distribution of metallic grains within the polymer is random, but homogenous. The polymer appears to have wetted the surface of the nickel particles highly efficiently. A thin layer of polymer persistently remains on the surface of the nickel, hindering clear imaging in the electron microscope. Inter-particle contact is negligible, even at high loadings, where predicted percolation thresholds are exceeded. This implies that conventional percolating theories of electrical conduction are unlikely to be applicable to QTC.

The spiky surface characteristics of types 123, 287 and 255 nickel powders are retained after mixing into polymer. It has been confirmed that the patented low mechanical energy mixing process, employed by Peratech, is essential in order to protect these delicate structures. The high degree of wetting by the polymer is also thought to protect the delicate spiky structure of nickel particles within, preventing damage being caused to the nickel particles. Upon mixing at higher mechanical energies, spikes are mostly destroyed and other surface irregularities become smoothed out. In addition, small shards of fractured metallic particles are visible in the composite. This is caused by the increased friction generated between abrasive metallic particles when mixed at higher energies. It is also thought that the use of low mechanical energy is responsible for the very low quantity of observable air voids within the composite.

5 Effect of metallic loading upon the sensitivity to applied pressure

5.1 Introduction

Metal-polymer composites display different resistances and sensitivities to applied pressure at different metallic loadings. For many applications it is desirable to manufacture QTC with maximum sensitivity to applied pressure. It is therefore necessary to characterise the electrical behaviour of the composite under compression at a variety of different loading ratios.

By evaluating the resistivities of samples at different loadings, a plot that is analogous to a percolation curve for conventional composites can be obtained. It was hoped that this experiment would therefore also be able to provide evidence either for or against a conduction mechanism based upon Percolation Theory.

5.2 Experimental

QTC samples were supplied by Peratech. Two sets of samples were manufactured, using types 123 and 287 nickel powders and silicone rubber at a variety of different loadings. The specific type of silicone used was again Alfasil 2000, supplied by Alfas Industries. Type 123 samples were made at the following loading ratios by weight: 4:1, 5:1, 6:1 and 7:1 (nickel:silicone). Type 287 samples were made at the following loading ratios by weight: 3:1, 3½:1, 4:1, 4½:1, 5:1 (nickel:silicone).

Disc shaped samples of QTC (5mm diameter and 1mm thick) were tested for their sensitivity to applied pressure using a Lloyd automated

compression facility located at Peratech. This machine enabled samples to be compressed to forces up to 100N, at variable compression rates, whilst simultaneously monitoring the force exerted upon the sample. A constant current source (consisting of preset values of 1uA, 100uA and 10mA) was used to apply current to each sample during compression. Compression rate was set at 0.5 mm min^{-1}. The apparatus had a PC interface allowing remote experimental control and data collection. Picoscope software used serial communication with the equipment via an analogue to digital converter unit. The resulting voltage and force were both recorded as a function of time, and a plot of resistivity as a function of applied pressure was calculated.

Scanning electron microscopy (SEM) was also used to confirm the microstructure of samples manufactured at different loadings. Samples were cryo-fractured as described in section 4.2 before being imaged. High accelerating voltages (35 kV) were again used in order to peer through surface layers of polymer, which may obscure from view the nickel particles embedded within the composite. It was hoped that the results would indicate any potential differences between the structures of samples, which might also account for any observed electrical sensitivity differences.

5.3 Results and discussion

As has been described in chapter 3, QTC displays non-ohmic behaviour. Consequently, plots of resistivity against applied pressure curves for different current sources will not be identical to one another. To illustrate this, figure 5.1 shows typical results of resistivity against applied pressure for the three different currents used.

Unusually, the results in figure 5.1 show that sensitivity to applied pressure increases as the current decreases. The reason for this is thought to be due

to increased grain charging at higher currents. Alternatively, high currents may generate space-charge in the polymer. In either case, the result is restriction in electron movement through the conducting network. A more detailed description of these effects is given in chapter 6.
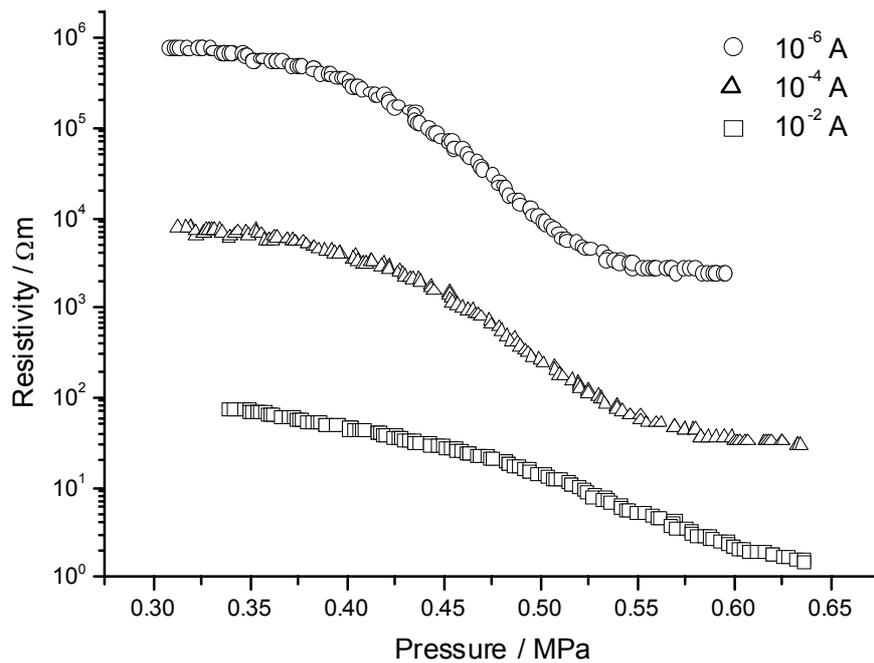
Fig. 5.1: *Resistivity against applied pressure for 287-type QTC*
at loading of 4½:1 by mass, at different current sources

Results for the 10 mA tests appeared smoother and more repeatable than the results obtained at other currents. This appears to be an intrinsic characteristic of the current source, and is not a property of QTC. 10 mA was therefore chosen as the standard current source value, used for comparing resistivity against applied pressure for QTCs made using different loadings (figures 5.2 and 5.3).
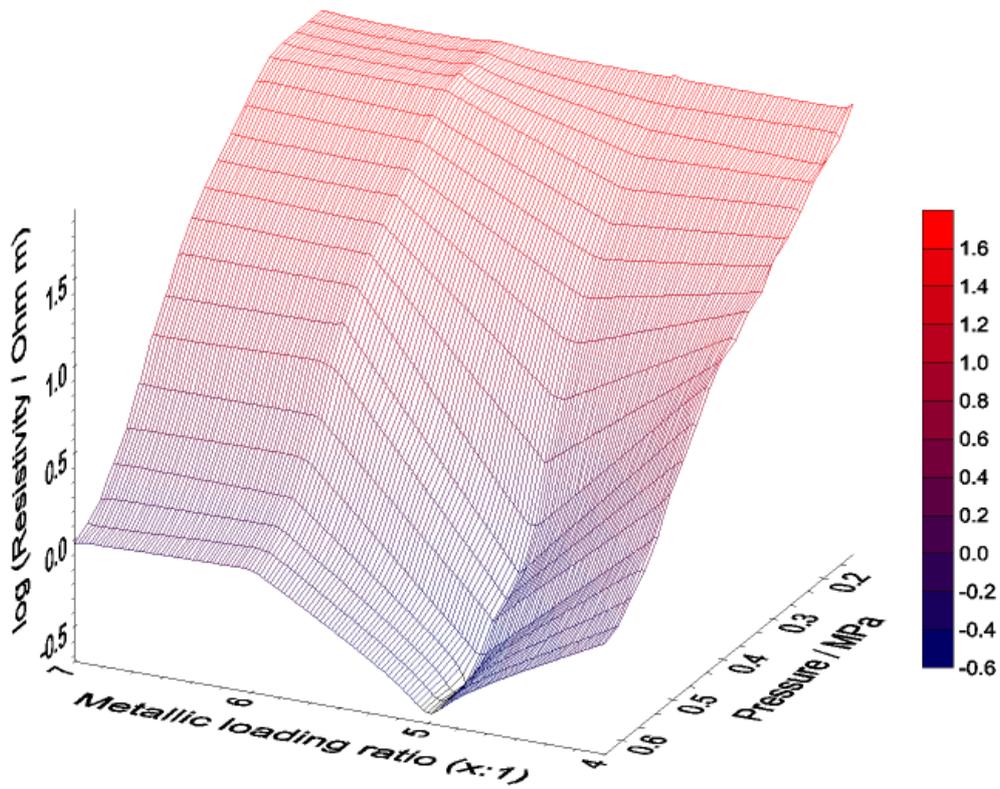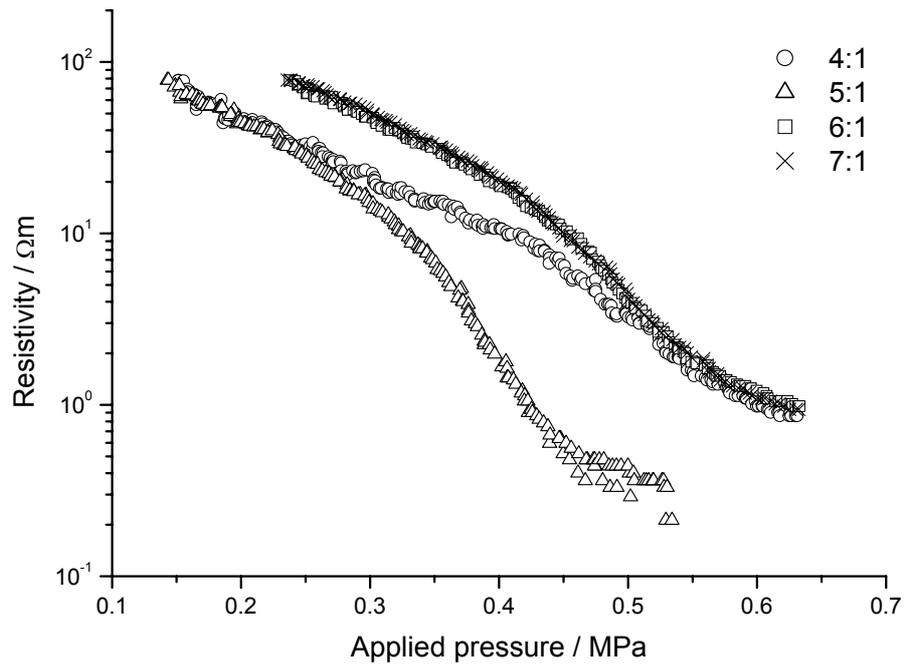
Fig. 5.2: *Sensitivity of type 123 QTC to compression for*
different metallic loadings (10mA constant current)
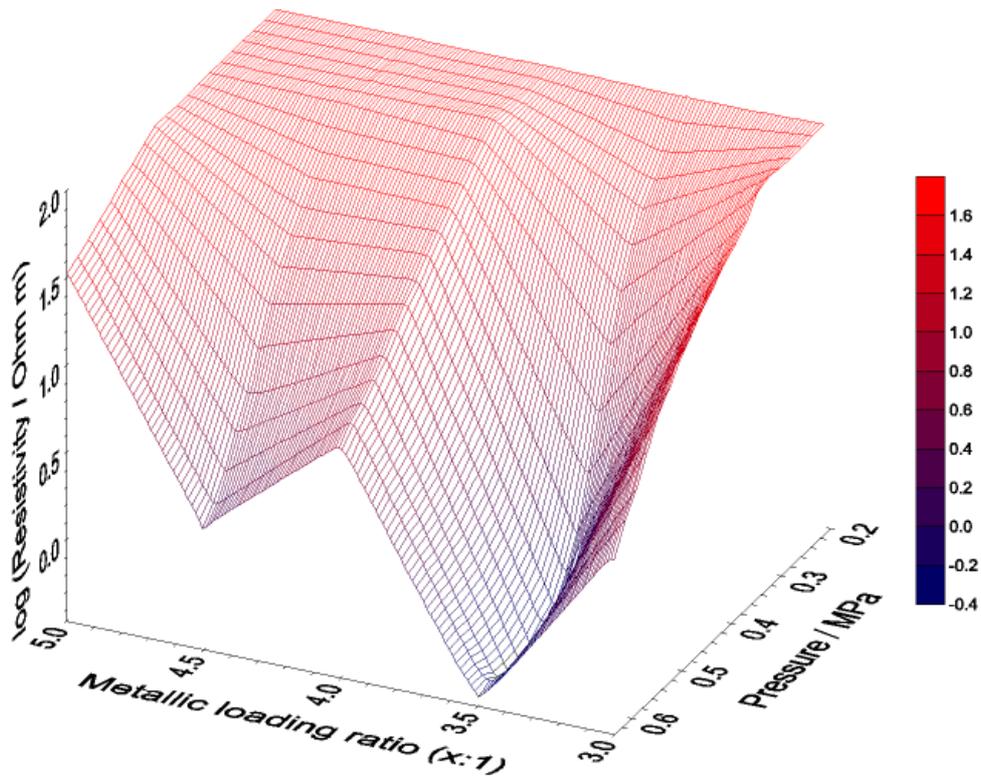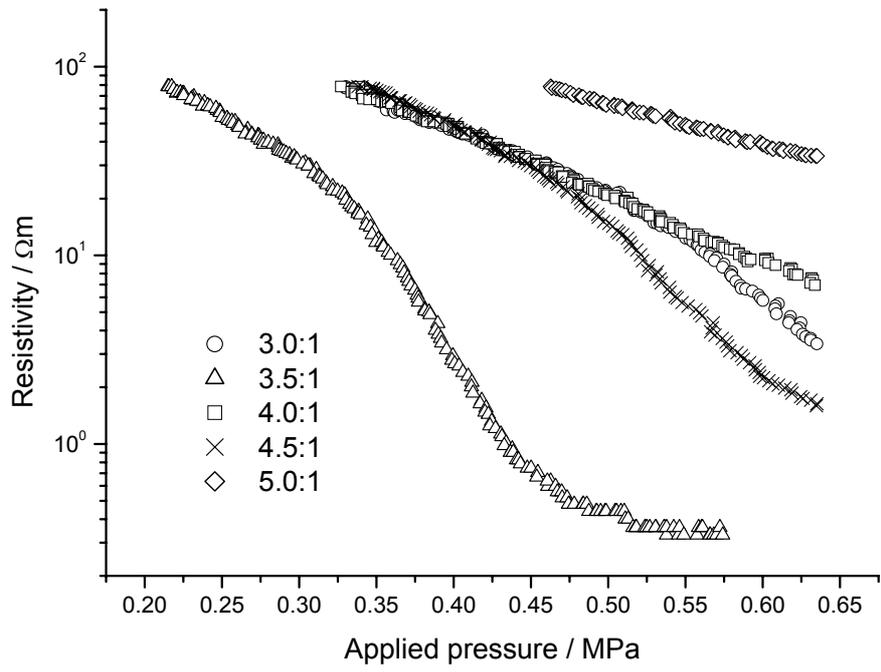
Fig. 5.3: *Sensitivity of type 287 QTC to compression for different metallic loadings (10mA constant current)*

By observing the steepness of the curves in figures 5.2 and 5.3, it can be seen that the most highly sensitive QTC samples (i.e. the ones that display the greatest change in resistance for the smallest change in applied pressure) are those made at the optimum loadings of 5:1 for type 123 QTC and 3½:1 for type 287 QTC. It is interesting to note that these loadings both lie in the middle of the ranges tested in this experiment.   Conversely, the least sensitive samples were found to be at loadings of 4:1 for type 123 and 5:1 for type 287.   These loadings are the lowest and highest loadings tested respectively.

The most highly conductive samples (at a given applied pressure) also coincide with the most highly sensitive samples (i.e. 5:1 for type 123 and 3½:1 for type 287).   However, the most highly resistive samples of types 123 and 287 QTC (at a given applied pressure) are, in both cases, the most highly loaded samples.   This surprising result is completely contrary to standard percolation theory, where one would expect the greatest resistivity from the lowest loadings.   No percolation-style curve can be seen for either composite type within the loading-resistivity planes of figures 5.2 and 5.3. We therefore conclude that QTC does not exhibit percolative behaviour.

These data illustrate that for types 123 and 287 composites, there is no obvious relationship between either the overall conductivity of the sample, or the sensitivity to applied pressure, and the metallic loading of QTC. The loading of metallic fillers within QTC materials is clearly a more complex problem than the simple percolative (or effective medium theory) trends displayed by conventional composites. However, one cannot ignore the fact that at high loadings, an increase in filler density will result, thus resulting in improved electrical interconnectivity within the network.   Therefore, it is proposed that at high loadings, an additional factor is causing a decrease in sensitivity and overall conductivity.

It was hypothesised that the delicate spiky structures, shown to be crucial to obtaining the enhanced sensitivity displayed by QTC, were perhaps being damaged within the more highly loaded samples. This might be caused by the increase in the amount of abrasive contact between particles when mixing at high loadings. At low loadings, interparticle contact during the mixing process is reduced. Abrasive contact is therefore decreased, resulting in a composite with filler particles that retain their spiky structure.

To test the above hypothesis, scanning electron microscopy was performed on the same samples used in the above sensitivity experiments. The purpose of this was to establish whether or not spikes had indeed been damaged in the samples that displayed reduced sensitivity. The results for type 123 composites at high and low loadings are shown in figures 5.4 and 5.5.

Figure 5.4 shows typical images of type 123 QTC at a metallic loading of 4:1 (nickel:polymer) by mass, the lowest loading used for this powder type. The results clearly show significant irregular surface structure on the surface on the nickel particles. Spiky surface features have been reasonably well retained after the mixing process, confirming also the results of chapter 4. It should also be noted that the most sensitive sample, loaded at 5:1, also displayed nickel particles in a similar condition to this sample.

Figure 5.5 shows typical images of type 123 QTC at a metallic loading of 7:1 (nickel:polymer) by mass, the highest loading used for this powder type. This composite also displayed unusually low electrical sensitivity to applied pressure. The results indicate a general smoothing of nickel particles within the composite, which becomes more noticeable as the loading ratio is increased. The unique spiky morphology that is characteristic of QTC nickel particles has been largely destroyed during the mixing process.
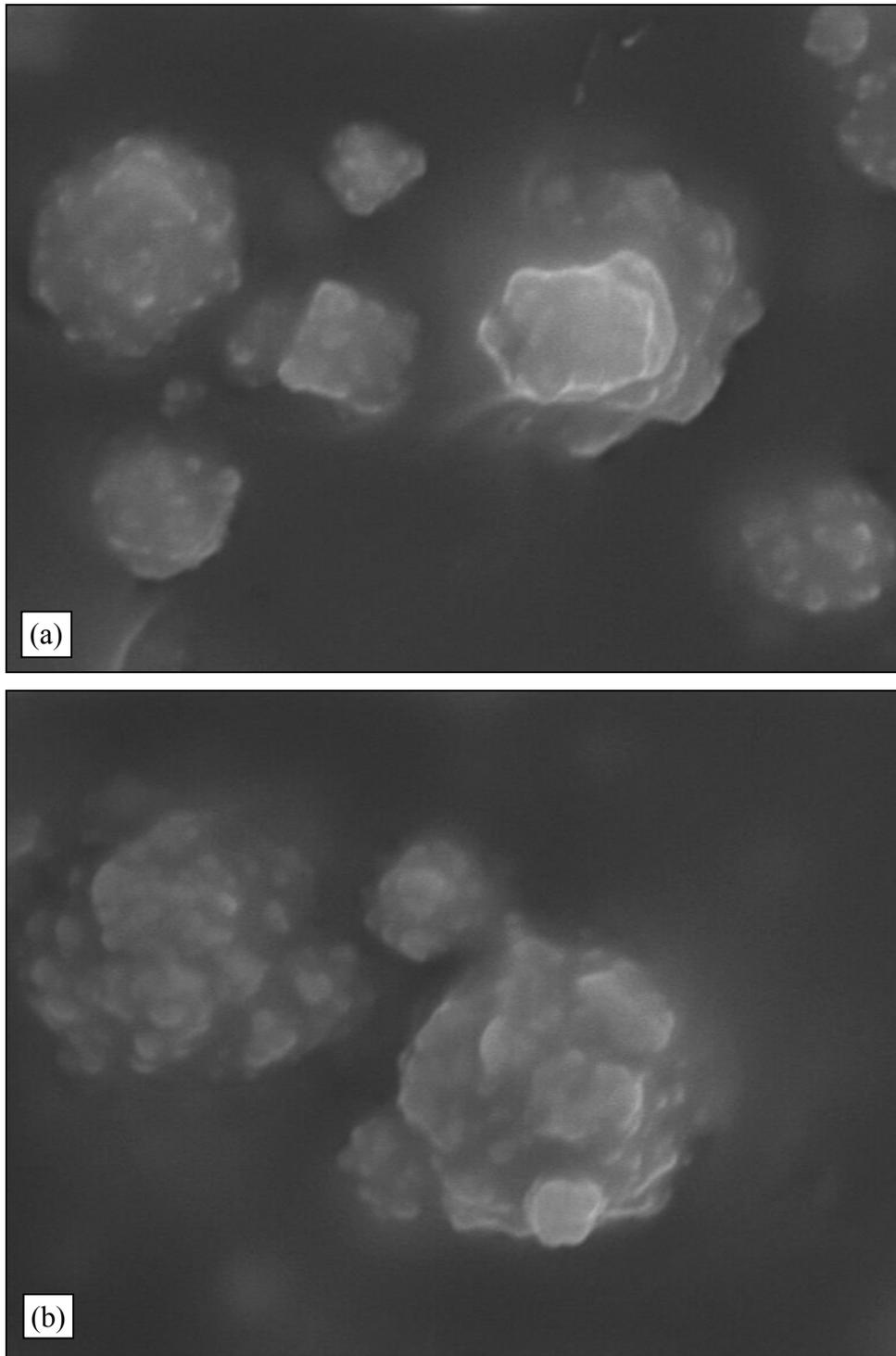
Fig. 5.4: *SEM images of type 123 QTC loaded at 4:1 (nickel:polymer) by mass, magnification 7000x*
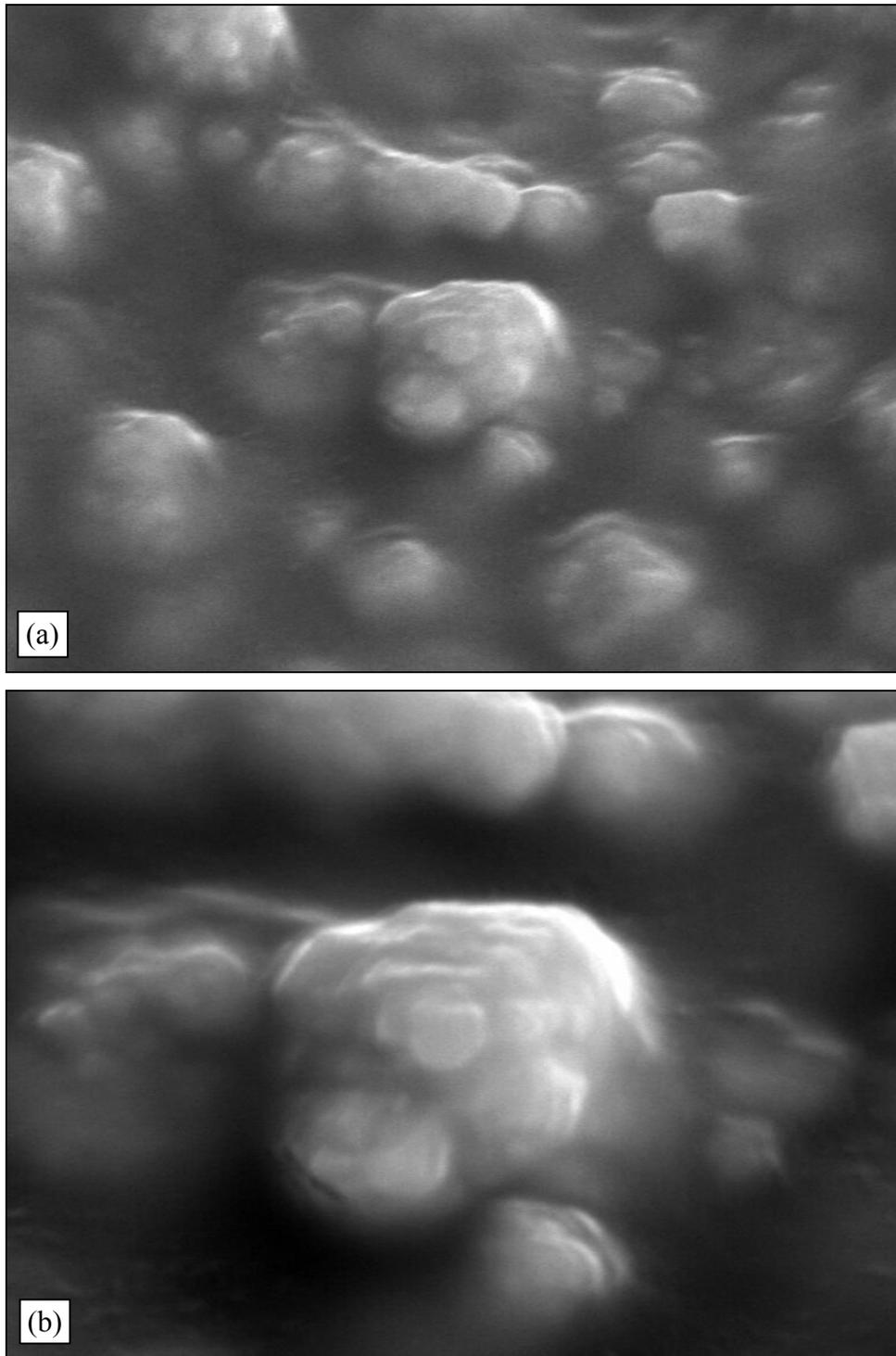
Fig. 5.5: *SEM images of type 123 QTC loaded at 7:1 (nickel:polymer) by mass, magnification (a) 5000x, (b) 10000x*

These SEM images confirm our hypothesis of increased loading leading to increased abrasive contact during the mixing process, which in turn, leads to composites with reduced electrical sensitivity to applied pressure. The results also confirm the importance of spikes as an essential part of the conduction process within QTC.

5.4 Conclusions

QTC materials display trends of increasing conductivity with increasing loadings over only a limited range of low loadings. At a critical loading ratio (5:1 for type 123 and 3½:1 for type 287), both conductivity and sensitivity to applied pressure reach a maximum. Further increases in metallic loading are detrimental to the performance of the composite, resulting in unusually low conductivities and decreased sensitivity to applied pressure. It was hypothesised that the reason for such behaviour in highly loaded samples, is due to increased abrasive contact between metallic particles during the mixing process. SEM analysis confirmed this hypothesis, and verified that at high loadings, metallic grains have indeed suffered irreversible damage to their delicate spiky structure.

Optimum performance of QTC materials is therefore obtained when one is closest to the critical loading ratio. At this point, loading ratios are high enough for the composite to exhibit good conductivity, but remain low enough to prevent damage being caused to the spikes during manufacture.

The above experiment provides further evidence of the importance of spiky filler particles in order to generate highly sensitive QTC samples, and that the spikes are crucial to explain conduction mechanisms within the composite.

6 Electrical conduction mechanisms within QTC materials

6.1 Introduction

One of the principal aims of this thesis is to try and ascribe a specific physical mechanism (or combination of mechanisms) to describe electrical conduction within QTC materials. As the name of the material suggests, it has been hypothesised that quantum tunnelling is responsible in some way. This chapter attempts to verify that hypothesis, by drawing upon conclusions presented in chapters 3, 4 and 5, and also by investigating the electrical characteristics of QTC materials.

Electrical characterisation experiments in this section consist mostly of the measurement of current-voltage characteristics under a variety of different conditions. A number of conduction mechanisms will then be presented, along with discussions of how well they describe the data. Arguments for and against each one will be put forward, concluding in what is thought to be the most probable mechanism (or mechanisms) responsible for electrical conduction within QTC.

6.2 Experimental

Initially, current-voltage studies were carried out manually using a Weir 4000 DC voltage source combined with a Keithley 2000 multimeter. A two point contact method was used to apply voltages and to measure current. A four-point probe method might ideally have been more accurate, but is impractical when one considers the small thickness of the typical samples being tested, particularly when compression needs to be simultaneously

applied to the composite. Voltage sweeps were carried out over the full range of the source's capabilities, ranging from 0V to 30V.

Contacts to the QTC sample under test were achieved with a clamp assembly, which was developed in-house (figure 6.1). Stainless steel electrodes were mounted on a micrometer screw gauge, which provided variable amounts of compression to the composite. A Mitutoyo 940-241E digital force gauge then monitored the exact force being used to compress the sample.
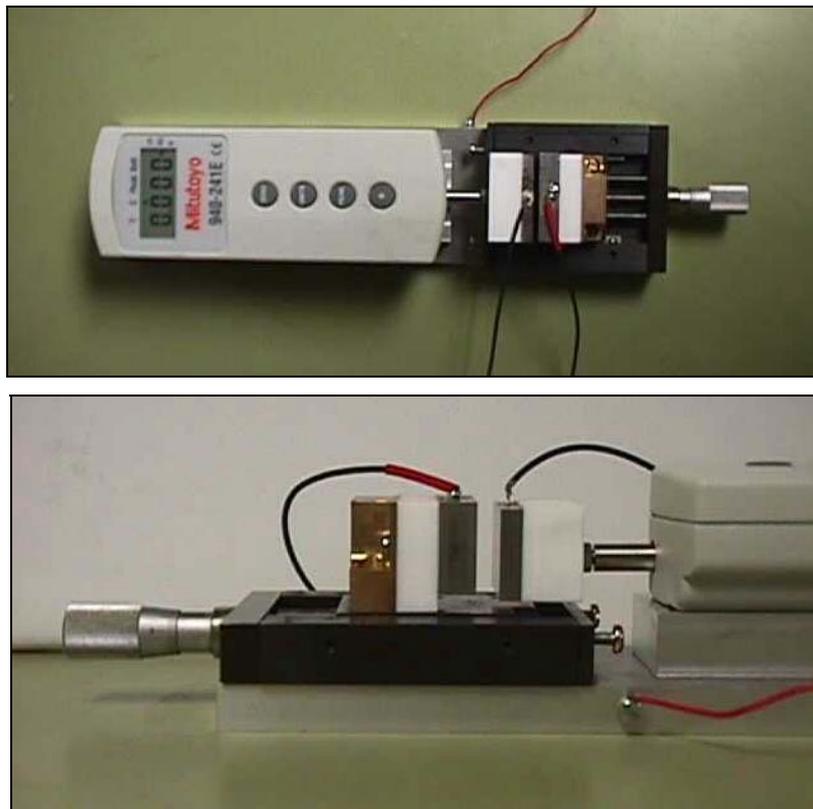
Fig. 6.1: The clamp assembly used to compress QTC samples whilst performing electrical characterisation experiments

QTC samples were of the type 123 and 287 variety, made using either Alfasil 2000 (supplied by Alphas Industries) or Silcoset 153 (supplied by Ambersil) silicone polymer. Electrical results were highly similar for each combination of the above, so no differentiation is made later in the text. Unless stated otherwise, samples of QTC used for testing were disc shaped with approximate diameters and thicknesses of 10mm and 1mm respectively. Exact dimensions were determined using vernier calipers and a micrometer screw gauge. Samples were lightly sanded before testing using wire wool. This was to remove the shiny oxidised layer, which was often present on the surface. Samples were also allowed to relax under compression for at least 15 minutes before the experiment began. This reduced the contribution to current drift caused by viscoelastic relaxation.

The acquisition of a Keithley 2420 high current sourcemeter allowed current-voltage characteristics to be obtained more reliably than the previous manual technique could provide. The sourcemeter enabled a voltage source to be applied to the sample whilst simultaneously measuring the current. GPIB communication between the sourcemeter and a personal computer via LabView software also enabled automated acquisition of data and for experimental parameters to be set remotely. Voltage ramping speed and the number of repeat cycles could now be accurately controlled, along with the maximum and minimum voltage settings.

The surface temperature of the sample could be monitored using a Digi-Sense DualLogR 91100-50 thermometer and infra-red probe, supplied by Cole-Parmer, which was mounted to the clamp assembly. Serial communication between the thermometer and a personal computer enabled automated logging of temperature readings, whilst simultaneously performing electrical characterisation. The exact temperature of the sample was difficult to determine as the infra-red probe was focussed upon only a

very thin section of QTC, sandwiched between two electrodes. These electrodes not only hindered access for the probe to the sample's surface, but also acted as efficient heat sinks. Temperature readings must therefore not be interpreted as actual values, but instead merely reflect the relative changes caused by Joule heating within the sample. Internal temperatures within the composite may reach much higher values than those recorded.

6.3 Results and discussion

In this section, data will first be presented for all electrical characterisation experiments, together with a description of the observed electrical behaviour. After the data has been presented, a discussion of the reasons for the observed behaviour will be presented. Different electrical conduction mechanisms will be proposed, together with arguments for and against each one, based upon the evidence given by the experimental results.

Repeated cycles of applied voltage sweeps, increasing and decreasing at rates of 0.1V per second, between 0V and 10V were performed on a type 123 QTC sample under medium compression (10N applied over a standard 10mm diameter disc-shaped sample of thickness 1mm). The resulting current-voltage characteristics can be found in figure 6.2.

Three sequential voltage sweeps are shown in figure 6.2(a) on linear axes. The first sweep to be carried out was sweep 1, which displays a large hysteresis. The current in the voltage increasing direction remains low, and follows a higher path on the return journey. Subsequent voltage sweeps (sweeps 2 and 3) also result in loops, but with a smaller degree of hysteresis. Additionally, the gradient of the loops increases as more sweep cycles are completed, implying that the conductivity of QTC rises as the number of voltage cycles increases.
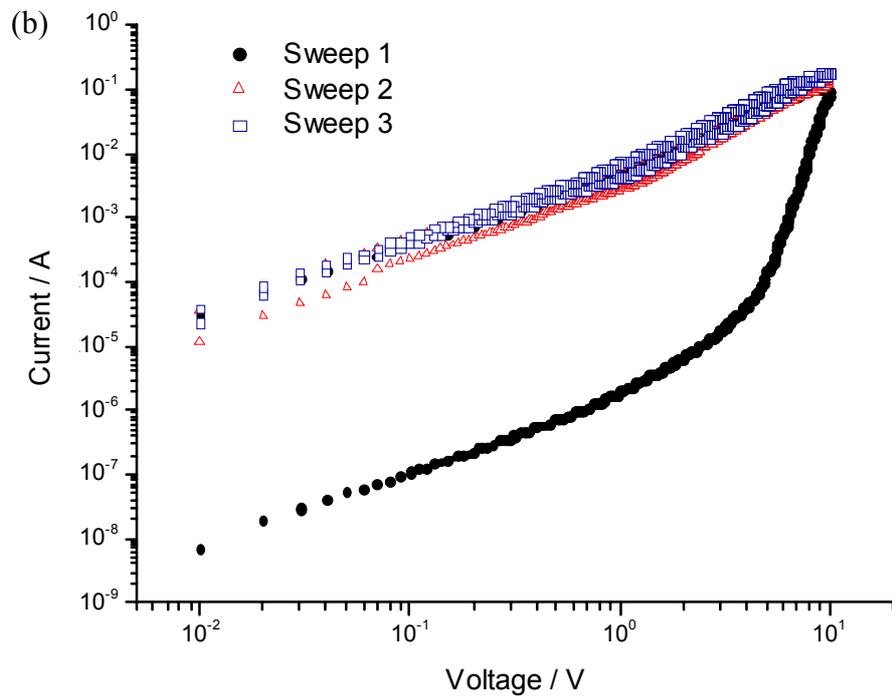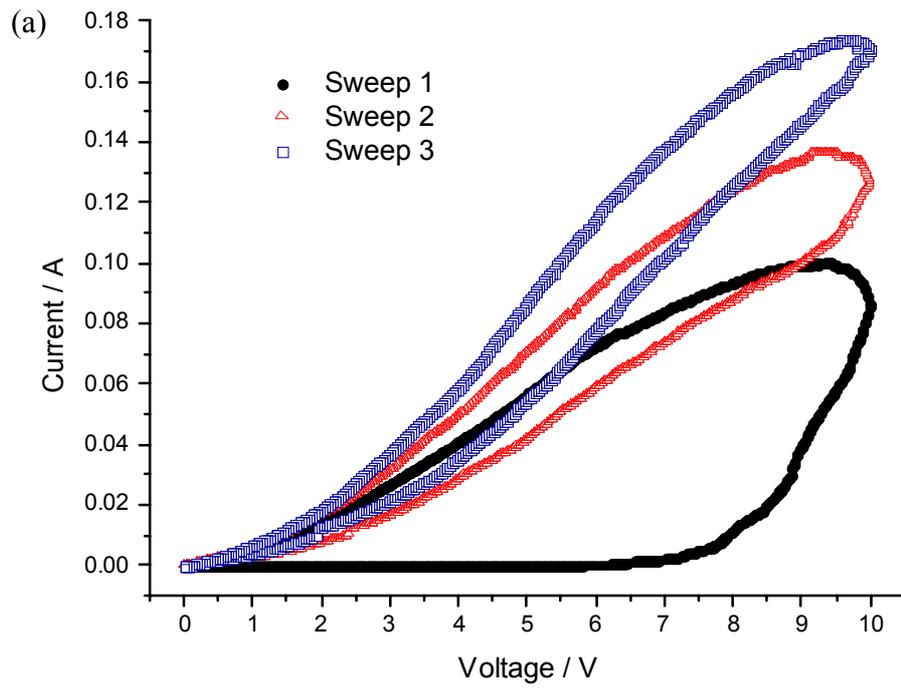
Fig. 6.2: *Current-voltage characteristics of type 123 QTC*
(lower voltage regime), plotted on (a) linear and (b) logarithmic axes

101

It is interesting to note that in figure 6.2(a), after reaching the maximum voltage of 10V, the current continues to rise for a short while, even though the voltage is now decreasing. This has been observed to be a time dependent phenomenon. Cycles completed at faster sweep rates display less hysteresis than those carried out at a slower rate. This is in agreement to previous observations [88], whereby under a constant voltage, currents perpetually drift upwards. Current drift of a similar nature in this experiment would cause hysteresis like that observed in figure 6.2, and also accounts for the gradual steepening of the loops.

Plotting of the above data on logarithmic axes draws attention to the relative similarity of gradients during repeat cycles, compared to that of the initial voltage increase. This offset illustrates the typical differences in conductivity between initial voltage sweeps and subsequent sweeps. Logarithms of the data from sweeps 2 and 3 (including also the voltage-decreasing sweep of sweep 1) were taken, and a linear fit gave rise to a gradient of 1.400 ($\pm$ 0.004). This implies the following current-voltage relation for repeat sweeps at this compression:

$$I = AV^{\alpha} \qquad\qquad (6.1)$$

where A = 5.93 ($\pm$ 0.40) x 10^{-3} AV$^{-\alpha}$, and α = 1.400 ($\pm$ 0.004).

Figure 6.3 shows the results of more repeat voltage sweeps carried out on a fresh sample of type 123 QTC. However, in this experiment, the maximum voltage was set to the higher value of 30V. Sample dimensions were slightly smaller in this experiment (diameter 3mm, thickness 1mm), however the force was reduced to only 2.5N, resulting in only a slight increase in applied pressure compared to the previous experiment.
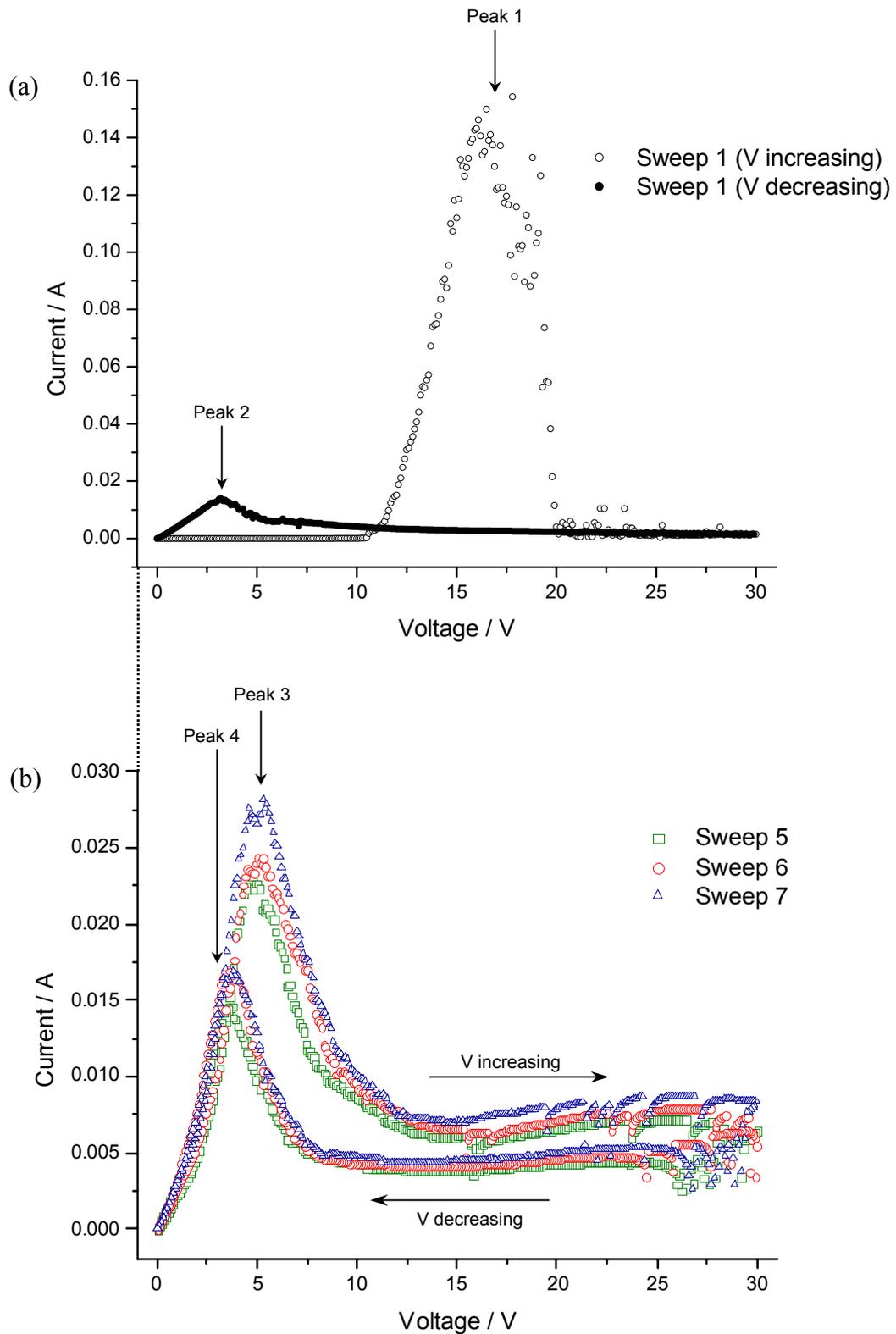
Fig. 6.3: *Current-voltage characteristics of type 123 QTC (higher voltage regime): (a) initial sweep, (b) repeat sweeps*

When a sweep up to a higher voltage is applied, a peak can be observed in the current-voltage characteristics as the voltage increases (peak 1). A further increase in the applied potential results in the fall, and eventual flattening of the measured current. These regions of negative differential resistance and of voltage independence are often quite noisy. Downward jumps in the current are often seen, and repeatability is difficult to obtain. An AM radio, tuned to a value outside broadcasting frequencies, showed that RF emissions were also very active during this region of relative voltage independency. This rather crudely demonstrates the general observation that RF emissions are often observed alongside noisy current-voltage characteristics.

When the direction of voltage sweep is reversed, current measurements begin to become less noisy than those taken in the upward direction. Current remains largely insensitive to the applied voltage, remaining at a relatively constant level. However, once the voltage has fallen to approximately 10V or 5V, the current begins to rise, displaying a second negative differential resistance regime. A peak is reached (peak 2), before current begins to fall again as the applied voltage approaches zero.

During the first sweep carried out on a fresh sample of QTC, the positions of peaks 1 and 2 are displaced from one another, as shown in figure 6.3(a). However, if one immediately recycles the voltage sweep, a change occurs. Upon all subsequent cycles, the peak observed during the upward sweep (peak 3) occurs at a much lower voltage than before. In comparison, the peak occurring during the voltage-decreasing sweep (peak 4) does not change its position from sweep 1.

If, after repeatedly cycling the composite, the material is removed from the experimental apparatus and is gently mechanically exercised for a few

minutes, or just left alone for several hours, the material returns to its original state. A voltage sweep results in characteristics reverting back to those shown in figure 6.3(a), followed by 6.3(b) upon further repeat sweeps. Such history dependent effects are therefore not permanent.

Peak height was found to be dependent upon the rate at which voltage sweeps were carried out. This effect was first discovered during an earlier similar experiment of repeated voltage sweeps using the manual voltage source (figure 6.4). The results show peak heights of widely varying sizes. Unfortunately, the exact rate at which sweeps occurred could not be controlled accurately using the manual voltage source. Nevertheless, a trend can clearly be seen of increasing peak height with slower sweep rates.
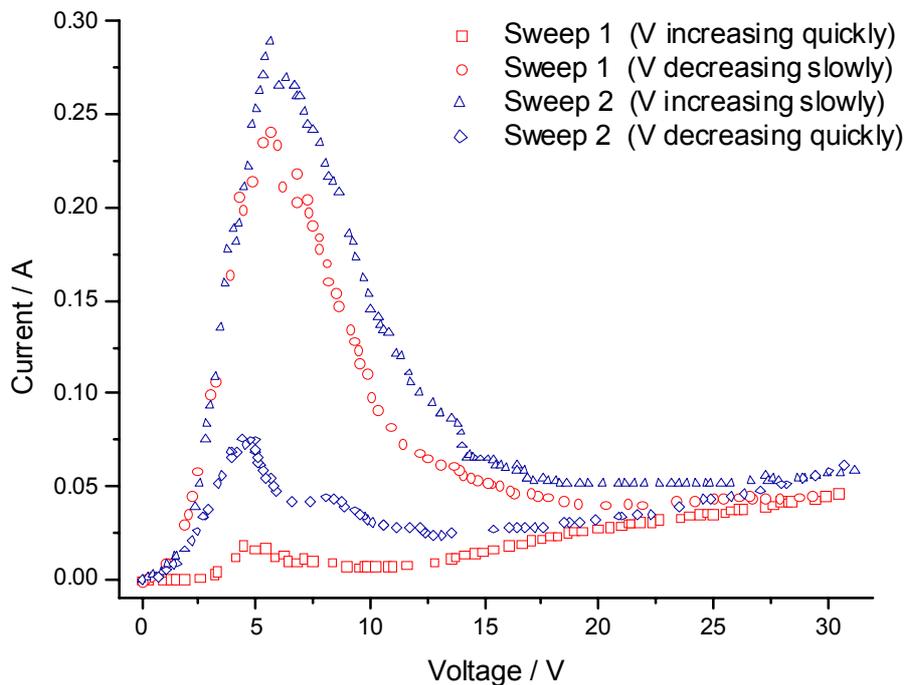
Fig. 6.4: *Current-voltage characteristics of type 287 QTC under different voltage sweep rates*

In these early experiments, peaks 3 and 4 were indistinguishable from each other in their relative positions. This was simply due to the lack of accurate control of the rate of change of voltage due to the manual source. Once again, currents continually drift upwards with time during the experimental cycle, thus giving rise to the sweep rate dependency of the peak size. In the negative differential resistance regime during a voltage-decreasing sweep, a step down in voltage resulted initially in a current decrease (concurrent with standard Ohmic principles). However, if the voltage remains constant for just a few moments after the decrement has been made, the current quickly begins to drift upwards again. If the sweep rate is slow enough, the current can drift upwards beyond that of its previous value, resulting in the negative differential resistance trend observed in these figures. However, at faster rates of voltage decrease, the current does not get the opportunity to rise so far, and thus the peak is both narrowed and reduced in height.

When the rate at which the voltage changes is kept constant, current-voltage characteristics are reasonably repeatable between subsequent cycles, as shown in figure 6.3. However, repeat experiments with the same sample a few hours later, or with a fresh sample, are unfortunately not quite so consistent. The most notable change that one observes when testing multiple samples is that of relative peak size. Peaks occurring during voltage-increasing sweeps are sometimes bigger, but also sometimes smaller than peaks occurring during voltage-decreasing sweeps. The former is clearly the case in figure 6.3, however this result is not observed for all samples. In addition, the degree of upward current drift often differs between samples. However, it should be noted that the same phenomenological trends are observed throughout all samples.

Repeatability of results is difficult to obtain between samples due to the number of physical variables that must be kept constant between

experiments. In the laboratory, accurate control is required of compression, temperature, applied voltage, rate of change of voltage and electrical history. In addition, accurate control of the manufacturing processes is required. This is necessary in order to achieve consistency in metallic loading, quantity of mechanical energy used during mixing, distribution of metallic particles and curing conditions. Finally, there will be slight variations in the specifications of raw materials used to make QTC, resulting in further inconsistencies. It is impossible to have total control over all variables. Subsequently, electrical results are sometimes difficult to reproduce from sample to sample. To combat this problem, variations in experimental parameters have been minimised to the limit that the equipment allows. Unfortunately, microscopic deviations in the experimental conditions can often result in large differences in the macroscopic electrical properties. This may be interpreted as chaotic behaviour within QTC materials.

We now attempt to explain the trends observed in electrical characterisation experiments. Chapter 5 has already shown that QTC does not display the standard trends of percolation theory and effective medium theory. These theories can also offer no credible explanation on their own of the composite's unusual current-voltage characteristics. We therefore turn to alternative theories to explain these processes. A series of conduction mechanisms will be considered, together with their ability to describe observed experimental behaviour. Incidental experimental data is also presented, where appropriate, to help illustrate these discussions.

PTCR effect

Initially, the peaks observed in current-voltage characteristics were attributed to a PTCR effect, as described in section 3.4. When currents as

high as 3A pass through the composite (standard sized sample, approximate applied voltage, 10V), surface temperatures greater than 100 °C have been recorded, sometimes even causing localised melting and permanent degradation of the polymer. Under such extreme conditions, before melting occurs, resistivity readings increase, concurrent with a PTCR effect (resistance falls when actual melting occurs, implying an NTCR effect). Readings taken from the force gauge show an increase in the required force when temperatures become elevated, indicating thermal expansion. Differences in the results between initial and repeat voltage sweeps might be explained by a preliminary period of warming. The thermostatic effects of self heating and cooling would be the cause of the observed peaks.

However, thermostatic behaviour is unlikely to occur so consistently from sweep to sweep. Voltage sweeps performed at different rates (figure 6.4) would give rise to changes in heating and cooling rates. This, in turn, would result in shifts in both peak position and peak height, as heating and cooling rates are changed. However, this effect is not observed. In addition, figure 6.3 shows the same effect occurring at currents as low as 15mA (combined with only 3V applied voltage). Such low powers are insufficient to cause heating on this scale. Indeed, no measurable change of the surface temperature was detected throughout the experiment shown in figure 6.3. One may argue that internal temperatures may indeed be higher than the surface value, and that the PTCR effect therefore occurs internally. However, a composite with such a high metallic loading and under compression is likely to have good thermal conductivity. Internal heating effects are likely to be quickly transported away, and any changes in temperature should be measurable at the surface. The PTCR effect is therefore not considered as an important mechanism when discussing the shape of current-voltage characteristics under normal conditions, such as those in figures 6.3 and 6.4.

Trap filling and space-charge limited currents

The cause of the perpetual upward current drift with time is thought to be due to the filling of traps with injected charge within the composite. As trapping sites fill with conducting electrons, fewer sites become available to trap later electrons. Thus, the restriction to the flow of charge is decreasing with time, and the current drifts upwards. It is quite likely that the observations in figure 6.2 of hysteresis loops, and the trend of loop gradients increasing with the number of cycles, are also due to this same trap filling effect. Such space-charge limited currents (SCLCs) therefore also explain how the rate of voltage change affects the size of observed peaks in current-voltage characteristics.

As trap filling occurs, a build-up of a space-charge layer may develop. This inhibiting layer decreases current drift, and measurements become more consistent. Figure 6.2(b) clearly shows this effect, whereby the initial voltage-increasing sweep serves as an initial trap-filling sweep, followed by more consistent curves with only relatively small increases in gradient as space-charge accumulates. Other evidence of SCLCs can be seen in figure 3.6. The effect of rapid and sudden current increase occurs regularly in QTC materials, and at many different voltages. It is thought these sudden jumps are due to passing through trap-filled limits of specific trapping sites. In a polymer, many such trapping sites will exist in very large quantities, due to the amorphous nature of the material. The interface between the nickel and the polymer might also be an example of a specific trapping site, existing in high concentrations throughout the composite.

One might argue that the observed sudden rises in current, such as that displayed in figure 3.6, are not truly representative of SCLCs. If one refers to the theoretical graph shown in figure 2.12, one would expect to see four

regions of differing gradients. Regions (a) and (b) are often blurred together, and region (c) is clearly observed in our material. Region (d), accounting for Child's law after trap saturation, is not observed. However, regions (c) and (d) are sometimes also blurred together, and therefore (d) may not be seen at all. Other electrical effects present within QTC may also obstruct our observation of this region. More convincing evidence of SCLCs can be seen in figure 6.5, by re-plotting the 0V to 15V data from figure 6.3(a) on logarithmic axes.
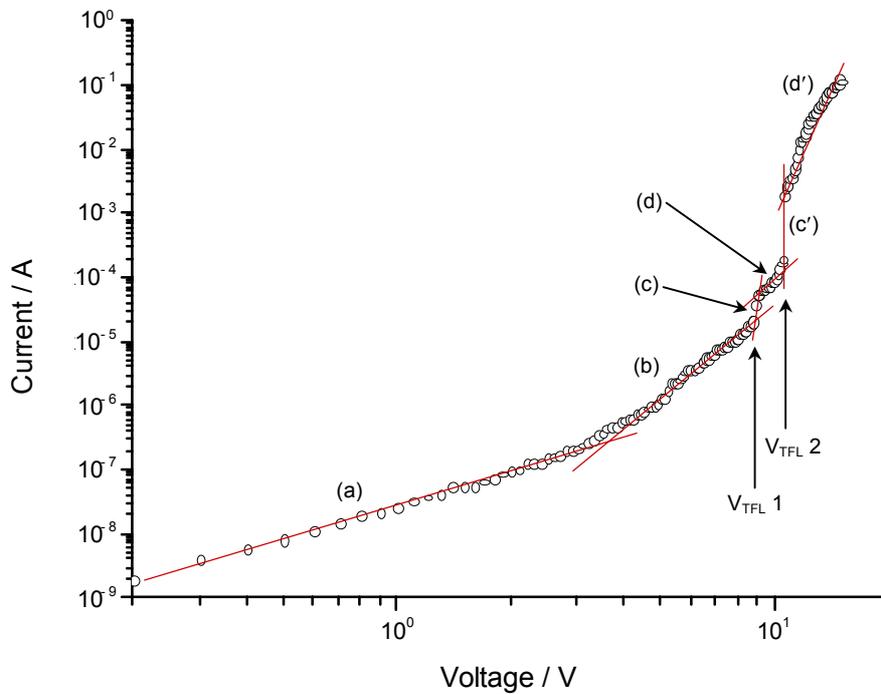
Fig. 6.5: *Evidence for space-charge limited currents in QTC,*
0V to 15V data from figure 6.3(a) is re-plotted on log-log axes
(a) Ohmic region, (b) Child's law due to shallow trapping,
(c),(c') Trap-filled limits, (d),(d') Child's law after trap saturation

Multiple linear regions can be seen in figure 6.5, including two sudden increases in current, conducive to trap-filled limits being exceeded. Gradients of each section are detailed in table 6.1. The coefficients C and m represent the constants obtained for the linear fit on logarithmic scales. These then are used to calculate the values A and α, which correspond to the current-voltage relation as expressed in equation 6.1. The linear gradient m is consequentially equal to the exponent α in this equation.

Section	C	m = α	A [AV$^{\alpha}$]
(a)	-17.435 ($\pm$ 0.013)	1.631 ($\pm$ 0.020)	2.680 ($\pm$ 0.036) x10^{-8}
(b)	-20.373 ($\pm$ 0.148)	4.354 ($\pm$ 0.075)	1.419 ($\pm$ 0.210) x10^{-9}
(d)	-19.642 ($\pm$ 0.640)	4.484 ($\pm$ 0.282)	2.948 ($\pm$ 1.886) x10^{-9}
(d′)	-33.505 ($\pm$ 0.995)	11.731 ($\pm$ 0.391)	2.810 ($\pm$ 2.796) x10^{-15}

Table 6.1: *Fitted coefficients to linear sections of figure 6.5 assuming the formula: $\ln V = C + m \ln I$ and $I = AV^{\alpha}$*

Sections (b) and (d), either side of $V_{TFL}1$, have gradients that are very similar to each other, falling within each other's margin of error. This is in agreement to theory, as Child's law should govern both regions. Unfortunately, gradients within the Ohmic and Child's law regions of the graph have values that are approximately twice the theoretically required values of 1 and 2 respectively, and thus an element of doubt may still remain. However, other complex electrical processes taking place within

QTC, which are not incorporated into the theory of SCLCs, may have distorted the data away from the theoretical result. For example, different gradients will no doubt result if experiments are performed on a fresh sample, compared to one that has electrical history. The above data therefore seems sufficient to give reasonable evidence of the presence of SCLCs and trap filling, confirming our explanation of current drift.

If one assumes that SCLCs exist within QTC, then data from figure 5.1 might also be explained more clearly. It shows a trend of decreasing sensitivity to applied pressure when higher current sources are used. High currents would result in larger amounts of space-charge being present in the polymer. This may hinder charge movement within the composite, resulting in the observed reduction in pressure sensitivity.

A more detailed investigation of trap-filling and space-charge effects within QTC could be provided by de-trapping experiments. Thermal (and voltage) induced de-trapping would shed light upon the exact nature of trap depths and distributions. An estimation of the quantity of charge stored within the composite could also be made as a result of such experiments. Such trapped charge may be in the form of space-charge stored within the polymer regions of the composite, or charge stored on the metallic grains themselves.

Although no charge injection mechanism has yet been proposed, it seems highly likely that trap filling and SCLC effects occur within QTC materials, giving rise to upward current drift. If this indeed is the case, then this opens the door to other mechanisms such as the Poole-Frenkel effect and hopping. High fields are required for the Poole-Frenkel effect, in order for trap potentials to become sufficiently distorted for de-trapping to occur. This is provided by the large field strengths generated at the spikes of the nickel particles within QTC. The high density of traps within the insulating

regions of the composite, also imply that hopping distances will be small, thus increasing the likelihood that inter-trap hopping is occurring. (Further discussion of inter-trap hopping can be seen later in this chapter, along with a discussion of Fowler-Nordheim tunnelling and other charge injection processes). However, it is unlikely that direct, single-step hopping between metallic grains is occurring due to the large hopping distances required [78]. Low temperature conductivity studies of QTC are required to investigate hopping effects more thoroughly.

The overall conduction mechanism within QTC is still incomplete. Although a convincing argument has been put forward to explain current drift, no mechanism for charge injection has been suggested. In addition, there is still no explanation for the cause of the peaks observed in the current-voltage characteristics. Additional mechanisms of conduction within QTC therefore need to be considered, which will help explain the cause of these unusual results.

Resonant tunnelling

It was noted that the peaks shown in figures 6.3(b) and 6.4 were similar in shape to those displayed by the current-voltage characteristics of a tunnel diode. It was therefore considered possible that resonant tunnelling may be occurring in some way within QTC. Resonant tunnelling requires two (or more) potential barriers within close proximity of each other, combined with resonant energy states situated in the region between the barriers. Surface states on the surface of the nickel particles (possibly within the oxide layers) may represent such resonant centres, with the barriers due to the polymer and the Schottky barrier on either side acting as the double barriers (figure 6.6). A triple barrier system may even exist whereby the oxide layer of the neighbouring metal particle also acts as a barrier to the conducting electron.
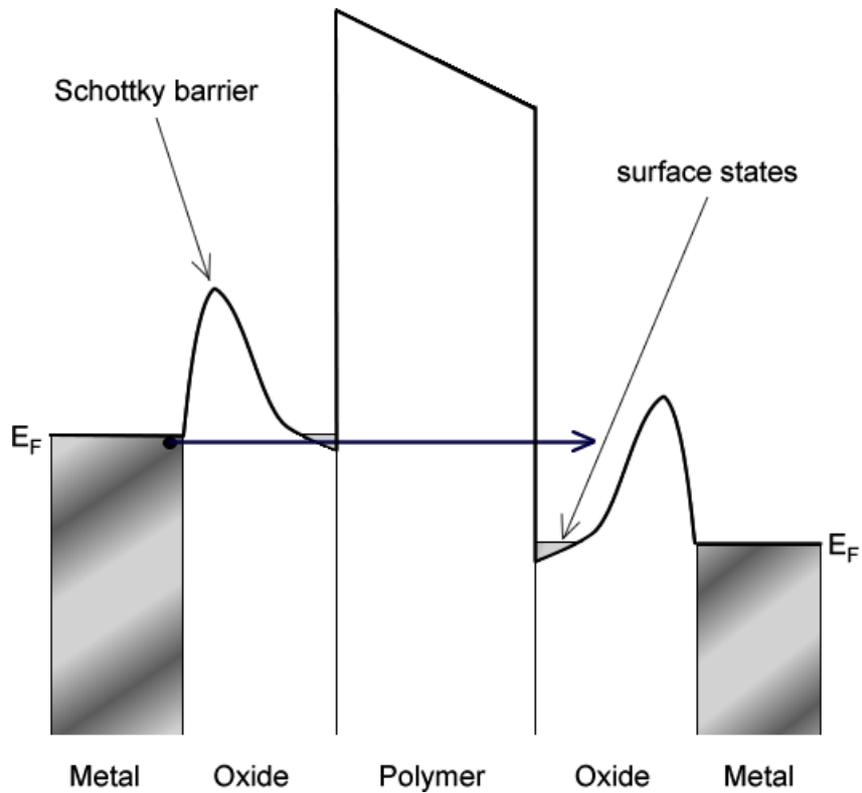
Fig. 6.6: *Possible resonant tunnelling mechanism within QTC,*
using surface states within the oxide regions as resonant centres

There is great uncertainty in the exact energetic alignments of the system described in figure 6.6. If surface states do exist, we have little knowledge of their energy levels or of how broad they are. Barrier heights could be estimated from consideration of the work functions of the polymer, metal and oxide. However upon application of an electric field to the system, enhanced localised fields due to spiky nickel particles add further complexity. Work functions will change due to the Schottky effect. Electrons may or may not pass straight over the second Schottky barrier on the adjacent metal particle. The energies of surface states within the oxide may or may not overlap with each other and with those within the metal.

These factors will also, of course, change with applied voltage and oxide layer thickness. In addition, trapping sites within the polymer may also act as resonant centres, and trapped charge within the polymer may disturb local potentials within resonant tunnel junctions, making the system extremely difficult to model.

There are many problems with a resonant tunnelling model of conduction in QTC. For example, no explanation can be given for the wide separation of peaks during only the first cycle of current-voltage characteristics. Also, resonant energy levels within the oxide surface layers will have widely varying values, accounted for by the natural distribution of oxide layer thicknesses. In addition, potentials across the junctions will have a wide distribution of values, caused by the variation in spike sharpness. It is these oxide thicknesses and potentials between adjacent particles that are critical in controlling resonant tunnelling probabilities. Wide distributions of these parameters therefore result in a smoothing out of resonant positions. Indeed it is highly likely that current peaks would become sufficiently broadened by this effect that the entire process becomes unnoticeable.

If a conduction mechanism of resonant tunnelling is to be believed, then the thickness of the oxide layer present on the surface of the nickel particles will surely affect electrical properties within QTC materials. In a recent study [94], the nickel particles were subjected to acid etching to remove surface oxidation, and also to thermal oxidation in order to thicken oxide layers. These powders, of varying oxide thicknesses were used to make samples of QTC, and then tested for their current-voltage characteristics.

If resonant tunnelling were the dominant conduction mechanism, one would expect thicker oxide layers to create more surface states and a wider distribution of resonant energy centres. Peaks in the current-voltage

characteristics would therefore become broadened, and probably also shifted. The results [94] gave rise to composites that were highly resistive, displaying no measurable peaks. One might suggest that oxide layers were now too thick for tunnelling to occur, however, oxidation temperatures and exposure lengths were insufficient for such drastic oxide layer growth. The lack of peaks in current-voltage characteristics therefore implies that resonant tunnelling is unlikely in QTC materials.

If one removes the oxide layer, one would expect resonant tunnelling to become impossible due to the lack of resonant states. Experimental results [94] showed that etched powders gave rise to composites with reduced conductivity (probably due to the preferential etching of spikes), but still displaying the characteristic peaks of QTC. The current peaks therefore cannot be caused by resonant tunnelling via oxide surface states.

Certain samples also show quite a severe onset to the current peak, displaying sudden rises from milliamps to amps within a few seconds. A resonant tunnelling effect cannot be responsible for such dramatic behaviour within such a disordered system. It is therefore disregarded as a possible mechanism responsible for conduction within QTC.

Metallic bridging

Consider two metallic electrodes separated by a thin insulating region. Microscopic irregularities on the surface of the electrodes will result in localised regions of high field density. In certain cases [95] [96], it has been reported that local fields may become sufficiently enhanced for the electromigration of metallic atoms to occur. For example, the failure of integrated circuits is often caused by electromigration at microscopic discontinuities within the conductor [97] [98] [99]. Atoms from the positive

electrode are pulled out of their positions within the metallic lattice, towards the opposite electrode, resulting in the growth of such surface irregularities. Very shortly, tiny spikes develop on the electrode surface at these positions, which have greater atomic sharpness than the original surface irregularities. This further enhances local fields, and accelerates the electromigration process. Within a few seconds (depending upon the insulator's thickness), the spikes have grown to form extremely narrow (only a few atoms wide) conducting bridges across the insulating region. When contact is made with the opposite electrode, a rise in current through the system occurs, due to the formation of the new conducting pathway. If applied fields are increased, currents will also increase, due to the greater number of metallic bridges being formed. However, such extremely narrow structures will quickly heat up, in a similar manner to a light-bulb filament. Eventually, they will fuse as electrical powers become too large to dissipate, resulting in a fall in the overall measured current.

A bridging mechanism might be proposed as a potential mechanism for conduction within QTC. The spiky structure of the nickel particles within the composite would act as ideal sites for the initial formation of such structures. The formation and then fusing of such bridges as the voltage is increased can explain the observed rise and fall in the measured current. If the voltage is then reduced, bridges may begin to form again, resulting in a second current peak. Repeat voltage cycles then start their current-voltage characteristics curve with residual conducting bridges already being present. Currents are therefore higher on the second cycle, causing fusing to take place at a lower voltage. This therefore accounts for the difference in peak positions between the initial and subsequent cycles. Mechanical exercising of the material will destroy the delicate bridge structures, returning the composite back to its original state of conductivity.

When bridges are almost connected between adjacent metallic islands, dielectric breakdown may occur in the polymer regions near the tips of the nearly completed bridges. Breakdowns would not only cause sudden increases in current, but the spark discharge may also contribute to the radio frequency (RF) emissions that have also been observed (see section 3.6).

Unfortunately, SEM studies of samples that have been electrically cycled many times provide no visual evidence of metallic bridging. Bridges may have been destroyed during the transportation of the sample to the microscope, however remnants of the structures ought to still be visible when viewed under high magnifications.

The primary argument against the theory of metallic bridging is the fact that applied compression and tension should destroy such delicate structures. Conductivity should therefore drop suddenly when such forces are applied, however this is not observed experimentally. An increase in compression between subsequent voltage sweeps simply results in an increase in the overall conductivity. Peak positions remain almost identical to those observed before the compression increase was applied. It is therefore concluded that metallic bridging is not occurring within QTC.

Electrostatic 'Pinching'

In any metal-polymer composite there will exist multiple routes of conduction through the material. The exact mechanism of charge transfer between grains has yet to be identified. However, as the voltage increases, increasingly more routes will become available, as electrons gain sufficient potential to cross the insulating gap between metallic grains.

(a) V increases, charge builds on 'dead-end' pathways

(b) Trapped charge causes 'pinching-off' of successful pathways

(c) Low V potential insufficient to hold charge,
'pinching' reduced, pathways reinstated
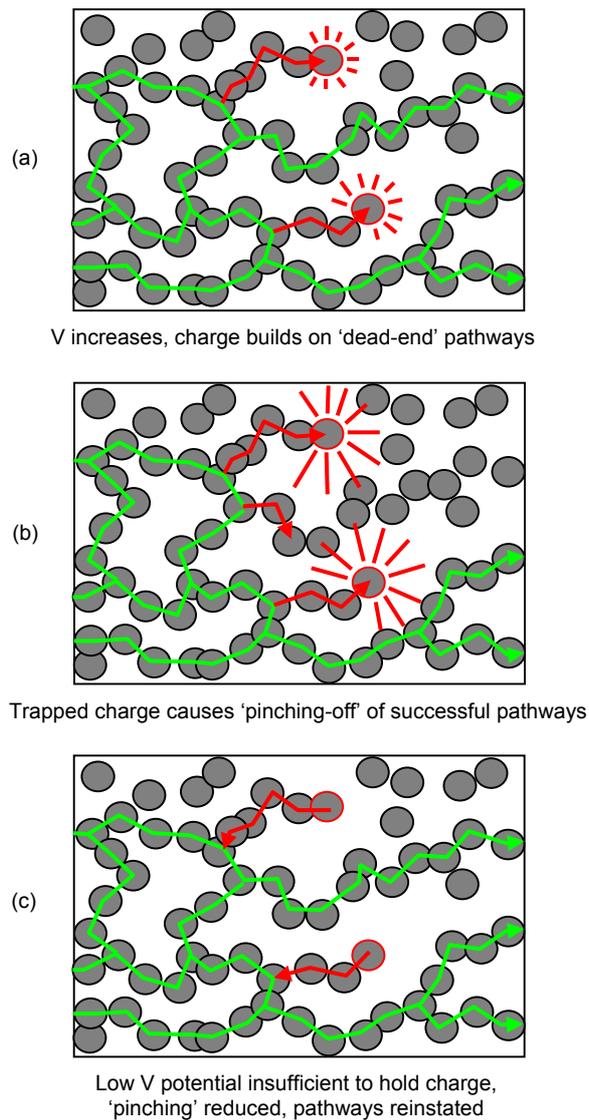
Fig. 6.7: *'Pinching' mechanism of conduction due to grain*
charging of incomplete conduction pathways

For every successful conductive pathway through the composite, there will
also exist many unsuccessful routes, resulting in 'dead-end' channels, where
electrons cannot reach the opposite side of the sample. Upon application of
an electric field, charge will become trapped at the end of these 'dead-end'

channels (figure 6.7(a)). Such trapped charge is unable to leak to a grain of lower potential due to the large distances to neighbouring particles. As time goes on, and the applied field is further increased, more charge becomes trapped in the 'dead-end' pathways, particularly on the final grains in the chain. Electrostatic fields from such trapped charge may become sufficiently high for them to interfere with charge transfer in neighbouring successful conduction pathways (figure 6.7(b)). At this point, charge is prevented from passing through successful conduction routes, due to 'pinching' caused by the trapped charge. Current therefore falls at high fields, as is shown by QTC's current-voltage characteristics. 'Pinching' may also explain the sudden decreases in current observed in the higher voltage region of the upward sweep of current-voltage characteristics in figure 6.3(b).

As the applied voltage is decreased, current remains steady. Trapped charge remains in 'dead-end' channels, and many conduction routes have been 'pinched-off'. Lowering the voltage slowly reduces the strength at which trapped charge is held, allowing small amounts of charge to leak backwards, out of the dead-end channel. However, it is not until the voltage has been lowered substantially that electrostatic fields due to the trapped charge become sufficiently low for 'pinching' to no longer occur (figure 6.7(c)). At this point, the current rises with decreasing field, as successful pathways are reinstated and once again allowed to contribute to conduction.

Repeat cycles of applied voltage will differ from initial sweeps, due to the residual trapped charge that will remain in the sample. In a second cycle, it now takes less voltage to generate sufficient trapped charge in order for 'pinching' to occur. Repeat cycles of current-voltage characteristics therefore display peaks that are shifted to lower voltages than that displayed in the initial voltage-increasing sweep. Charging of dead-end conduction

routes in this manner can therefore explain the hysteresis within the electrical properties of QTC.

'Pinching' can also be used to explain the data in figure 5.1. The graph shows decreasing electrical sensitivity to applied pressure when higher current sources are used. Higher currents would cause increased grain charging, leading to more 'pinching' and fewer conduction routes being available to carry current. This restriction in electron movement may lead to the observed decrease in sensitivity to applied pressure.

There appears to be little evidence to contradict the above theory of electrostatic 'pinching' due to the charging of 'dead-end' channels. It is for this reason that this is the favoured theory for describing the macroscopic trends of conduction within QTC materials. However, one important factor of electrical conduction remains unaddressed. It is still uncertain how charge transfer occurs from metallic grain to another. Evidence from chapter 4 implies that inter-particle contact rarely occurs within QTC. Direct contact between metallic grains is therefore not a suitable charge transfer mechanism. In addition, our theory must include some type of charge injection mechanism to account for the observed trap filling and SCLC behaviour. We therefore turn out attention to other inter-grain conduction mechanisms, which can be combined with the above theory of electrostatic 'pinching' to fully explain charge movement within QTC.

Dielectric breakdown

The uniquely spiky shape of nickel particles within QTC will generate very high local field strengths. It is possible that the dielectric strength of the insulating regions may be exceeded when critical electric fields are applied. Ionisation of the intervening medium would then occur, resulting in

sparking and current flow. Due to the variation of surface sharpness and inter-particle separation, a distribution of breakdown voltages would be present. However, avalanche effects may take place once breakdown has occurred in other regions of the sample.
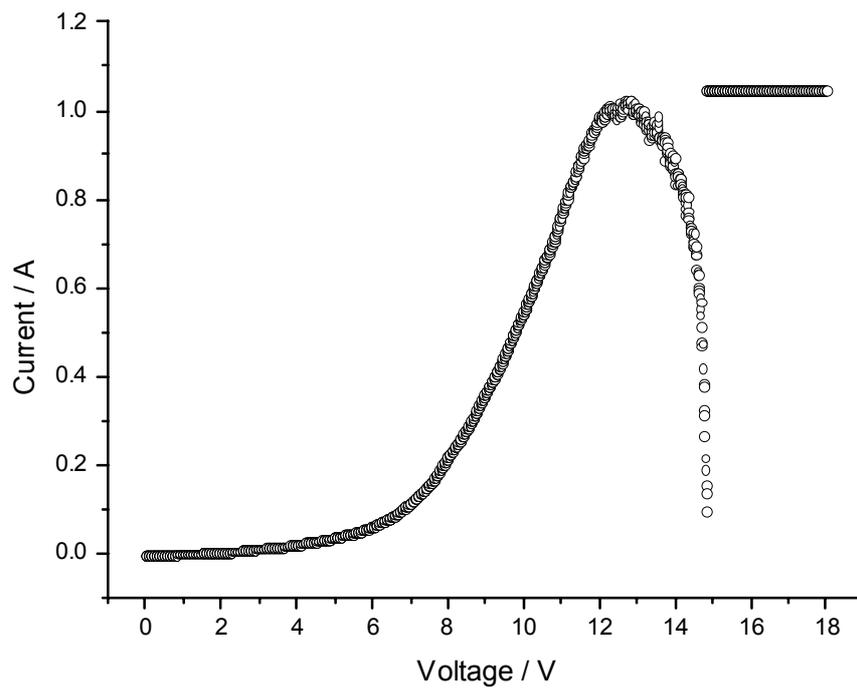
Fig. 6.8: *Possible high field dielectric breakdown within QTC. At 15V, current rises dramatically to beyond the measuring range of the multimeter*

Figure 6.8 shows evidence of dielectric breakdown possibly occurring. An increasing applied voltage sweep resulted in the familiar rise and then fall of measured current. Grains in 'dead-end' channels have become highly charged, resulting in the 'pinching-off' of conduction routes. At a critical voltage, the charge becomes so great that dielectric breakdown occurs within the polymer. The current suddenly increases to beyond 1 amp (the

maximum limit of the equipment's detection in this experiment). The current remains at this high current-limited level throughout the following decreasing voltage sweep, before falling quickly to zero in the last 350mV. Subsequent sweeps have the same high conductivity, appearing Ohmic over the initial 350mV range, before once again exceeding the maximum current limit of the equipment. The sample will not return to its original conductivity state regardless of the length of time left to recover. Permanent damage has occurred within the sample.

Dielectric breakdown might help to explain the high noise levels observed in some electrical measurements, as charging and discharging occurs. It may also account for RF emission within the composite. As changes are made to the system, in terms of compression, tension or voltage, inter-particle separations would be reduced, or critical fields would be exceeded. The effect of either could result in spark discharge and RF emission.

It is important to note that this type of behaviour occurs only rarely in QTC samples, and under extreme conditions. This highly sensitive type 123 QTC sample, loaded at 6:1 (metal:polymer by mass) was subjected to over 10N of compression over a relatively small and thin QTC sample, with approximate diameter and thickness of 3mm and 0.5mm respectively. The consequences of this were high field intensities and currents, resulting in the eventual failure of the sample.

If one estimates compression of 50%, the resulting average field strength through the sample at the point of apparent dielectric breakdown in figure 6.8 (15 V) would be approximately 0.6 kV cm^{-1}. The dielectric strength of the silicones used to manufacture QTC vary in the range from 1.6 x 10^2 kV cm^{-1} to 2.0 x 10^2 kV cm^{-1}. Breakdown therefore clearly cannot occur in this situation. However, the presence of spikes on the surface of nickel particles

within QTC will enhance localised electric field strengths. Assuming breakdown is indeed occurring in figure 6.8, it can be calculated that a field enhancement factor of between 270 and 340 is required to generate the appropriate breakdown field strengths. Calculations of field strengths under more normal conditions (1 to 30 V over 1mm thick, 1 cm diameter samples) imply average fields of between 1×10^{-2} kV cm^{-1} and 0.3 kV cm^{-1}. Multiplying this by the above deduced enhancement factor, gives a value for typical enhanced field strengths of between 2.7 kV cm^{-1} and 1.0×10^2 kV cm^{-1}. Under these more normal conditions, dielectric breakdown is therefore unlikely to occur in large quantities.

The above deduced value for a localised field enhancement factor does not seem unreasonable when compared to the values obtained from experimental and theoretical investigations of field emitters by Edgecombe and Valdrè [100] [101]. Using their calculations and the above predicted range of the enhancement factor (between 270 and 340), QTC nickel spikes can be deduced to have tip length to tip radius ratios of between 300 and 1000. Earlier SEM and TEM analysis has shown that such ratios are also not unreasonable. The work of Edgecombe and Valdrè also implies that in extreme cases, field enhancement factors approaching 30 000 are physically possible, although dielectric breakdown is sure to occur in large quantities in such a system.

Sparking and dielectric breakdown results in irreversible damage being suffered by the intervening medium. Tracking would occur within the polymer regions of QTC, resulting in a permanent change in conductivity. With the exception of occasional results such as that shown in figure 6.8, QTC suffers from no such long-term effects. The vast majority of samples show repeatable electrical properties. It therefore seems unlikely that

dielectric breakdown occurs in large quantities in QTC, except under extreme conditions.

Grain charging and RF emission

RF emission can be explained by simple consideration of grain charging and discharging without the need for dielectric breakdown. When the transfer of charge occurs from one metal particle to another (by whatever mechanism), a small amount of grain charging also occurs. This increases the potential between the charged grain and its nearest neighbour.

Discharging may occur (via any possible mechanism) at any point, up to and including when the grain has become fully charged. However, when discharge does occur, it does so in a sudden burst, neutralising the potential difference between the two neighbouring grains. Sudden movements of charge such as this may also give rise to RF emission. The wide distributions of particle size and separation then account for the observed "white-noise" broad frequency distribution RF emission. In addition, the resonance of charge may occur at the point of discharging, resulting in the oscillation of charge between the two neighbouring grains. This would certainly result in RF emission, which may then also couple with resonances of other nearby metal-polymer-metal junctions, causing further discharging to occur elsewhere in the composite.

As described earlier, RF emission appears to occur synchronously with noisy current-voltage characteristics. This is in agreement with the above theory, because currents will exhibit sharp falls and rises as grains charge and discharge. In addition, discharging (and therefore also RF emission) will occur more frequently whenever changes to inter-grain conditions take place. For example, increases in applied voltage, compression or tension

will increase the probability of discharging. This is in agreement with the observations of RF emissions described in section 3.6 [93].

RF emission in QTC appears to be able to be explained sufficiently by consideration of the charging and discharging of metallic grains. However, this is clearly a complex phenomenon, and requires closer inspection. Detailed analysis of the emission spectrum is required to help determine the mechanisms that are occurring.

Distribution and movement of charge within QTC

Figure 6.9 illustrates a simple model of how potential may vary through a sample of QTC under an applied voltage, ΔV. (For clarity, the diagram does not illustrate the potential barriers generated by the insulating polymer layers, and also ignores any effects caused by 'pinching'). The model relies upon an irregular spacing of metallic grains. This will give rise to a distribution of probabilities that charge transfer (by whatever mechanism) will occur between each of the metallic grains. Figure 6.9 illustrates equi-sized spherical grains, but irregularities in these will contribute further to the distribution of charge transfer probabilities. The result is that when a critical applied voltage is reached, the potential difference between the weakest link in the chain (between grains 4 and 5 in this example) will exceed the requirement for inter-particle charge transfer (figure 6.9(a)). Charge neutralisation will therefore occur between these two grains (figure 6.9(b)), resulting in a shifting in the relative potentials experienced by neighbouring grains. This shift is such that the potential differences between grains 3 and 4, and also between grains 5 and 6, is now increased. These potentials may now exceed the requirement, or require only a small additional increase in applied voltage, for inter-grain charge transfer to occur. Grains 3 and 4 and grains 5 and 6 therefore neutralise (figure 6.9(c)),

resulting in an increase in the potential differences between grains 2 and 3 and grains 6 and 7. This process of neutralising charge transfer continues to occur, migrating outwards throughout the composite.
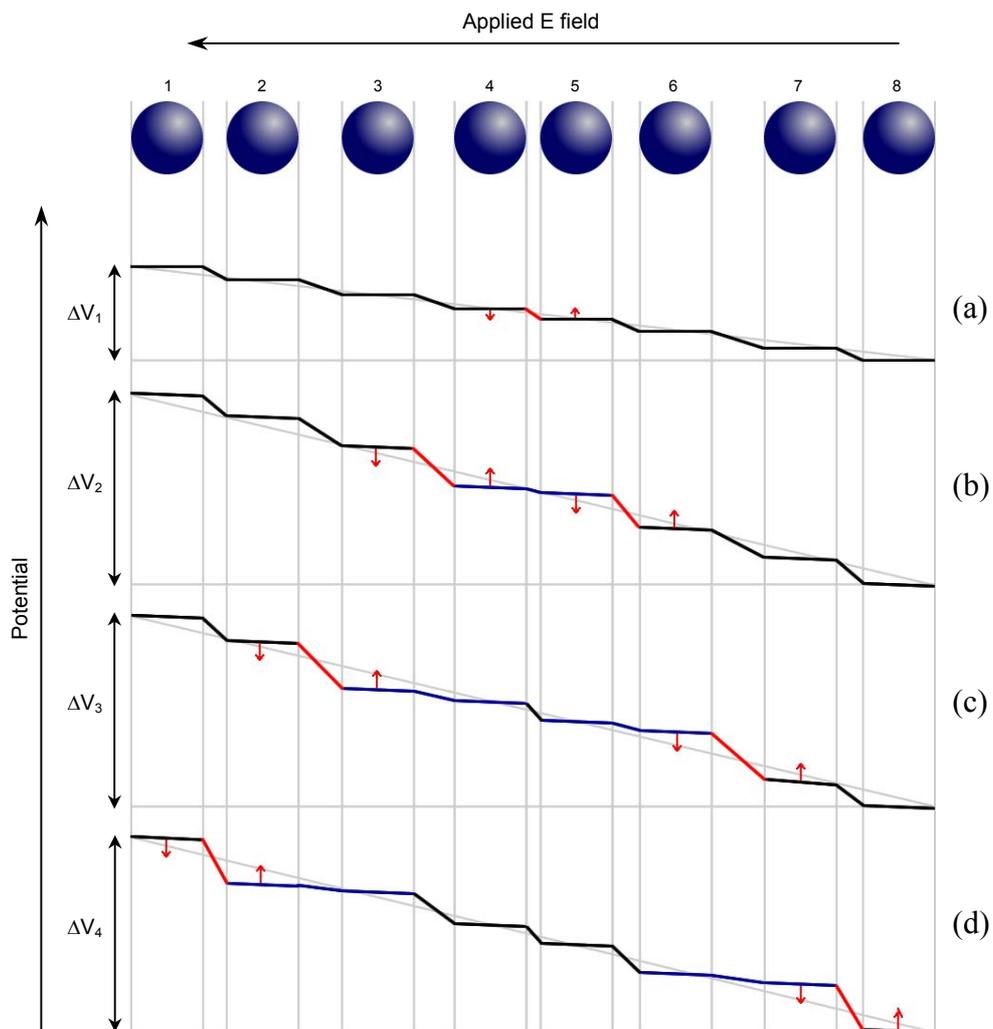
Fig. 6.9: *Simplified model of potential within QTC: (a) applied voltage increases until grains 4 & 5 exceed requirement for inter-particle charge transfer, (b) charge neutralising between 4 & 5 increases potential difference between 3 & 4 and 5 & 6, (c) 3 & 4 and 5 & 6 neutralise, (d) the charge neutralisation process continues to migrate outwards*

Non-uniform particle size, shape and separation distributions are essential in the above model of conduction. The result is a series of sudden bursts of charge movement, as neutralisation occurs between many different grains within many conduction routes at different times. This results in noisy current-voltage characteristics and RF emission. Without such non-uniformity between metallic particles, charge transfer would occur in a more controlled sequential manner through the composite. This would result in smoothly changing current-voltage characteristics with little noise.

Ionic conduction

It is possible that ionic species exist within the free volume of the polymer regions of QTC. Charged metallic grains may act as additional electrodes, supplying these ions with positive and negative charge. It is therefore possible that the migration of such charged species may contribute to electrical conduction within the composite.

The nature of ionic species within QTC will vary according to the type of polymer used to manufacture the composite. Standard QTC samples are made using silicone rubber, which liberates acetic acid during the curing process. The acid will react with nickel to produce ions of nickel and acetate by way of the following chemical reaction:

$$2\left(CH_3COOH\right) + Ni \rightarrow Ni^{2+} + 2\left(CH_3COO^-\right) + H_2 \qquad (6.2)$$
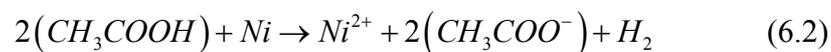
The high surface area of the nickel powder will result in an increase in the rate at which the above reaction takes place. Water will also be present within the system, further contributing to the number of ionic species. However, in order for ionic conduction to be a significant mechanism for charge transfer in QTC, high concentrations of ions must be present. This is

necessary in order to justify the high currents that QTC is capable of maintaining. Large quantities of the species identified by equation 6.2 would result in an observable amount of hydrogen being liberated at the nickel surfaces. A few bubbles do sometimes exist within QTC, however this is caused by mixing of air into the composite during the manufacturing process, and has been significantly reduced as manufacturing techniques have improved. Evidence of significant hydrogen gas liberation during the curing process is not present.

The large surface area of the nickel powders used to manufacture QTC may assist in ionic conduction. Also, the presence of spikes on the metallic particles will give rise to higher localised fields, which in turn may also assist ionic conduction. This would agree with the observation that spiky powders rather than smooth ones are necessary in order to generate the unique properties of QTC. However, if ionic conduction preferentially occurs in these regions close to metallic tips, then the available surface area is small and so the ionic conductivity contribution must be small.

Celzard *et al.* [66] report that under applied pressure, the free volume of the polymer, within which ionic species move, is dramatically reduced. Consequently, in a composite dominated by ionic conduction, conductivity can actually decrease with applied pressure; the opposite trend to that observed in QTC.

Supporting evidence, also opposing an ionic conduction mechanism, is given by the results to electrical characterisation experiments of QTC composites made from different polymers [94]. Many different rubbers and elastomers have been used to make QTC materials, with varying degrees of success. Success is usually defined as the ability for the new composite to display current-voltage characteristics and sensitivity to applied pressure

similar to that displayed by the standard silicone composite. Successful composites have been made from both curing and non-curing polymers, implying that the presence of acetic acid and other ionic species within the system does not have significant effect upon electrical characteristics. If ionic transfer does indeed occur within QTC, it is therefore considered to be a negligible effect.
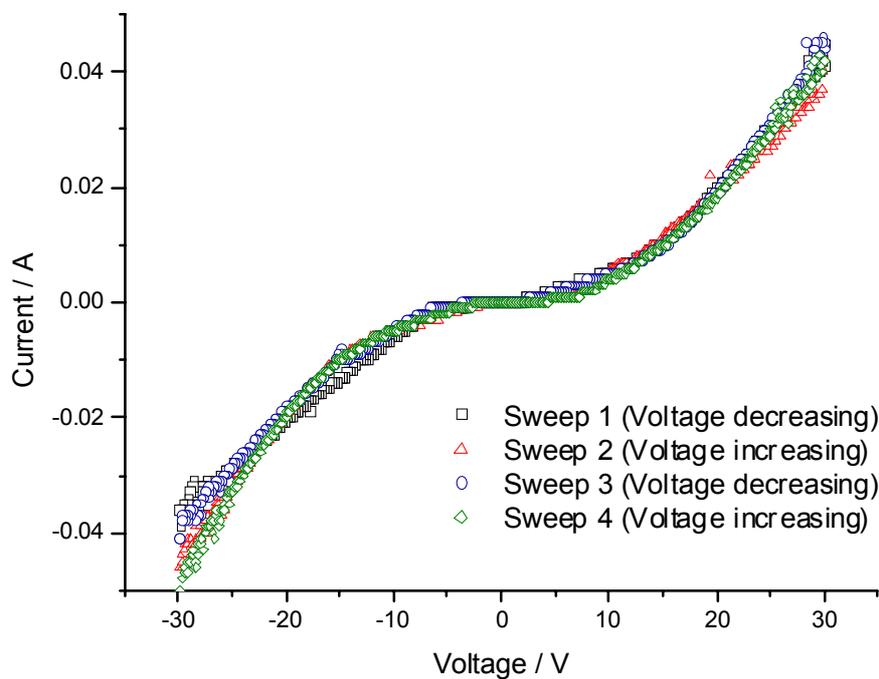
Fig. 6.10: *Current-voltage characteristics under positive and negative bias*

Further evidence against ionic conduction within QTC can be seen in figure 6.10. Sweeps of applied voltage under both positive and negative bias were carried out on a type 123 QTC sample of standard dimensions, loaded at 6:1 (metal:polymer by mass). Alternating bias sweeps such as this would give rise to asymmetric current-voltage characteristics in a composite undergoing

ionic conduction. This would be caused by a residual polarity that is expected to exist across such composites after having conducted in one direction for an appreciable length of time. Therefore, one might expect conductivity under one bias to be greater than under the other. The only conditions under which this effect might not be expected is for fast sweep times, of the order of one second or less. At these higher frequencies of alternating potential, ionic species would not be able to react fast enough to accumulate in large proportions. However, 40 second sweeps were used in this experiment, providing ample time for polarisation to occur. Figure 6.10 shows no observable difference between positive and negative bias, indicating little evidence of ionic conduction.

Cashell *et al.* [84] claim that in an ionic conduction dominated composite, a small transient current may occur through the sample after the applied voltage has been removed, generated by the residual polarity predicted to exist over the composite. Attempts were made to measure such a current in QTC, after repeat voltage cycles from 0V to 30V had been carried out. A Keithley picoammeter, could not detect any transient current.

Cashell *et al.* [84] and Celzard [78] claim recovery periods of several days before total neutralisation of ionic species has taken place, rendering the composite back to its original state of intrinsic conduction. QTC recovers to its original state within a few hours when left unattended, reducing to a few minutes if mechanically exercised. This is perhaps more indicative of SCLC and trap-filling effects, rather than ionic conduction.

Simple tunnelling

An important mechanism of inter-grain conduction that needs to be considered is that of quantum mechanical tunnelling. A simple tunnelling

theory such as that described in section 2.3.1 is the least complicated way to begin our model. In such a system, resistivity of a single junction will vary exponentially with barrier width according to equation 2.3. This implies that a metal-polymer composite with conductivity dominated by tunnelling will also display resistivity with an exponential dependence upon the separation of the metallic particles. Particle separation has a linear relation to the amount of compression and elongation being subjected to the overall composite, providing that one assumes that all of the compression is occurring in the polymer regions, and not in the metal particles. Resistivity will therefore also be exponentially dependent upon the compression. Figure 3.5, which shows such an exponential dependency, is therefore convincing evidence of a tunnelling mechanism of conductivity.

The primary argument against a simple tunnelling model of conduction is the fact that particle separation is too great within QTC for tunnelling to occur. Tunnelling has only been reported in the literature to be occurring in the regions very close to percolation, where inter-particle separation is a few nanometres or less. Electron microscope images from chapters 4 and 5 show particles separated by distances comparable to the dimensions of the metallic grains themselves (i.e. a few microns). At these distances tunnelling would be entirely negligible, and this is reflected by the fact that intrinsically, QTC is highly resistive. Inter-particle separation will of course depend upon metallic loading and compression. QTC requires between 5% and 50% compression (depending upon sample sensitivity) for conduction to occur. If we once again assume that compression is wholly within the polymer regions, particle separations will still only reduce to a minimum of several tens or hundreds of nanometres under compression. Tunnelling probabilities at these distances are still low. However, the high field densities, generated by the spikes on the metallic particles within QTC, promote the tunnelling mechanism. By focussing many electrons at small

tunnel junctions, the number of successful tunnelling events will be increased, even if the tunnelling probability remains the same. In addition, conduction will occur using only the narrowest of junctions. The above approximation of tunnelling distances (calculated using the average particle separation) may indeed be reduced further.

Tunnelling is an appealing conduction mechanism for inter-particle charge transfer, as it is able to explain many of the observed characteristics of QTC. However it remains uncertain that inter-particle separations are short enough for tunnelling to occur on a large scale. Temperature dependency studies would again be required to investigate if tunnelling is indeed occurring. Another problem with a simple tunnelling mechanism is that it does not introduce an explanation for the observed trap-filling effects that are clearly taking place. Further complexity is therefore required in our model, which can allow charge injection to occur.

Charge injection mechanisms and Fowler Nordheim tunnelling

In order to facilitate trap-filling and SCLC phenomena, which are thought to be occurring within QTC, charge must first be injected into the conduction band of the polymer regions of the composite. The simplest mechanism by which this may occur is thermionic emission. Neugebauer *et al.* [86] state that at room temperature, thermionic emission currents will exceed simple tunnelling currents when inter-particle separation is greater than 8nm. This would imply that thermionic emission is quite likely in QTC. However, assuming the work function of nickel to be 5eV, substitution into the Richardson-Dushman equation (equation 2.6) implies negligible current injection at room temperatures. Thermionic emission seems therefore to be an unlikely candidate to explain observed currents of up to 3A.

A more likely source of charge injection might be that of field (or Schottky) emission. Schottky emission processes require electric field strengths between 10 and 1000 kV cm^{-1} [78]. It was earlier quoted (within the discussion of dielectric breakdown) that under typical conditions, enhanced field strengths within QTC are in the range of 2.7 kV cm^{-1} to 100 kV cm^{-1}. This is well within the required range for Schottky emission. Indeed, local fields between many grains may be higher than this calculated value when one considers the effects of charge neutralisation, as seen in figure 6.9. The presence of spikes on the metallic particles is essential to help generate such large field strengths. Without them, this conduction mechanism would be impossible. Such a mechanism is therefore in agreement with observations that only spiky powders give rise to the highly sensitive, conducting properties of QTC.

The observed exponential dependence of resistivity upon barrier thickness could be explained by consideration of electrons tunnelling through the Schottky barrier. However, when the barrier occurs at the interface between a metal and a polymer, rather than at a metal-vacuum junction, Schottky emission becomes synonymous to Fowler-Nordheim tunnelling.

Fowler-Nordheim tunnelling combines the desirable sensitivity characteristics associated with tunnelling with the more realistic inter-particle separations within QTC. Spikes on the metallic grains generate the high field intensities required for this process to occur. Tunnelling takes place over only a small length scale, until the conduction band of the insulator is reached. This makes for a more feasible tunnelling theory, compared to the simple tunnelling model described earlier.
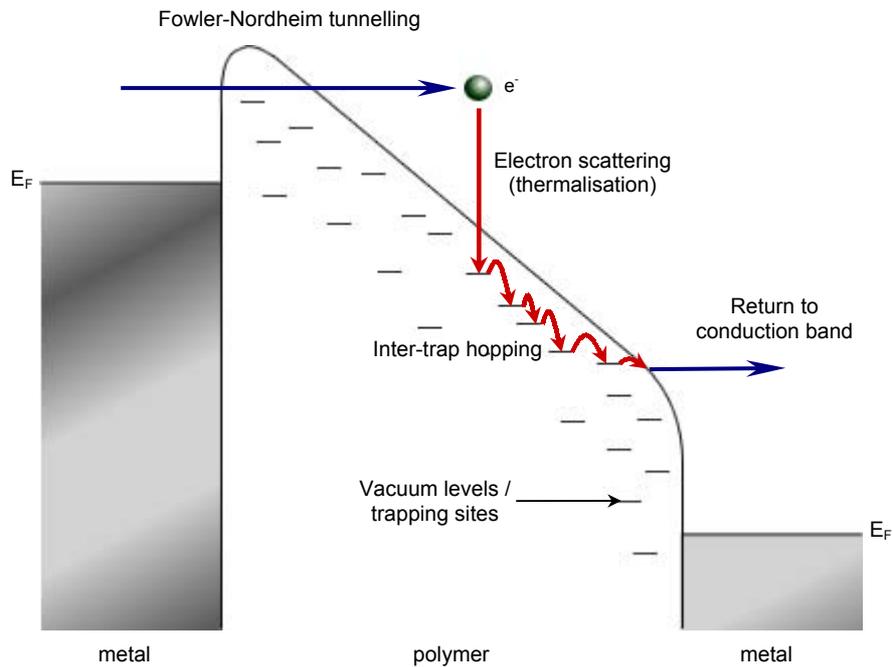
Fig. 6.11: *Fowler Nordheim tunnelling and electron thermalisation into polymer trapping sites allow hopping and other SCLC effects to occur*

In figure 6.11, it can be seen how Fowler-Nordheim tunnelling can also use trapping states within the polymer to influence electrical conduction, giving rise to the observed trap-filling and SCLC effects occurring within QTC. Once electrons have tunnelled through the Schottky barrier, into the conduction band of the polymer, inelastic scattering processes may cause thermalisation of the conducting electrons into lower energy polymer trapping sites. In the polymer used for QTC, a distribution of deep and shallow traps is likely to exist. Vacuum states may therefore be situated within close proximity to the conduction band edge, implying that large quantities of scattering is not necessarily required for this process to occur. Once thermalisation has occurred, the trap filling and SCLC effects that are observed within QTC are free to take place. In addition, hopping between

traps may occur. Electrons may hop back into the conduction band, or continue to jump between trapping sites within the polymer. At very low compressions and applied voltages, when the Schottky barrier is more difficult to tunnel through, electron hopping via trapped sites may even occur from one metallic grain to another. Low temperature conductivity measurements are required to see if conduction mechanisms change from hopping to Fowler-Nordheim tunnelling as applied compression and voltage are increased.

Theoretically calculated plots of resistance against filler fraction are shown in figure 6.12 [62]. The data compares results for four different inter-particle conduction mechanisms. Firstly, an Ohmic mechanism is shown, which treats metal and polymer regions as a linear combination of Ohmic resistances. Secondly, conduction by Schottky field emission is considered. This is followed by a SCLC mechanism. Finally, a model of Fowler-Nordheim tunnelling is shown.

The plots within figure 6.12 illustrate the improved sensitivity to loading (and consequently also to applied pressure) that a tunnelling mechanism provides. Non-tunnelling mechanisms cannot account for the data in figure 3.3, where dramatic changes in resistance occur over a very small range of applied pressures.

Fowler-Nordheim tunnelling appears to combine all of the required features for a successful model of inter-particle charge transfer within QTC, allowing trap-filling and SCLCs to occur freely, along with the high pressure sensitivity associated with a tunnelling mechanism. When combined additionally with a grain charging and 'pinching' mechanism for conduction on the macroscopic scale, all characteristics of QTC can be explained with reasonable confidence.
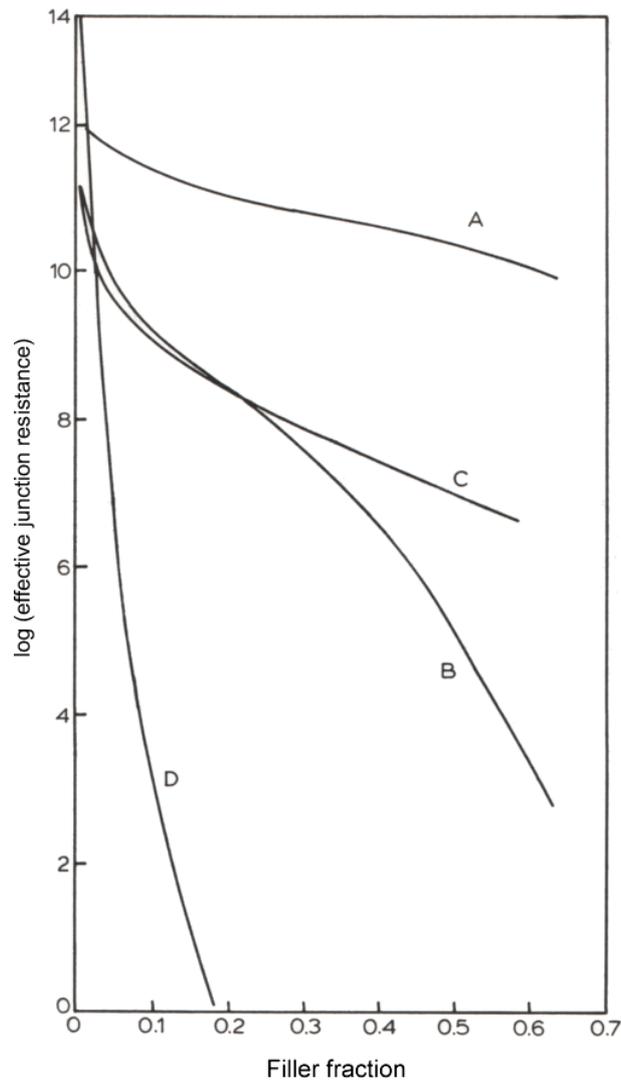
Fig. 6.12: *Theoretical plots of junction resistance as a function of filler
concentration for different conduction mechanisms* [62]*: A: Ohmic,
B: Schottky emission, C: SCLC, D: Fowler-Nordheim tunnelling*

6.4 Conclusions

Current-voltage characteristics of QTC are highly unusual, showing hysteresis, peaks and regions of negative differential resistance. A complex combination of conduction mechanisms is thought to be responsible for these unique electrical characteristics.

Inter-grain charge transfer is thought to be due to Fowler-Nordheim tunnelling. A tunnelling mechanism is required to give rise to the extreme electrical sensitivity to applied pressure, which is characteristic of QTC. Conventional, or simple tunnelling theories cannot account for the currents measured in QTC, due to the large tunnelling distances required. However, a Fowler-Nordheim tunnelling system reduces the required electron tunnelling distance by providing a tunnelling route directly into the conduction band of the polymer. Inelastic scattering processes may then cause electrons to thermalise, dropping into lower energy vacuum states and trapping sites within the polymer. It is then possible for inter-trap hopping to occur, accounting for the trap-filling and SCLC effects that are observed within the composite. High field densities of between 10 and 1000 kV cm^{-1} are required for Fowler-Nordheim tunnelling to occur, which are provided by the uniquely spiky characteristics of the nickel filler powder. Conservative estimates imply that field enhancement factors of approximately 270 to 340 are generated by the sharp points on the surface of the nickel. Without them, these conduction processes cannot occur, and thus composites become far more resistive and highly insensitive to applied pressure.

A new type of mechanism is proposed for the macroscopic effects of charge movement through QTC. Electrostatic charge accumulates in 'dead-end' conductive pathways to a sufficient degree that it eventually prevents the

movement of charge through neighbouring successful conductive pathways. This 'pinching-off' of conductive channels causes currents to fall at higher voltages, giving rise to the peaks and negative-differential resistance observed in current-voltage characteristics. During the first voltage cycle that a sample is subjected to, charging of the metallic grains and of these 'dead-end' channels occur. This accounts for the observed hysteresis and the shift in the current peak position to a higher voltage, compared to peaks occurring during subsequent repeat cycles.

The repetitive charging and discharging of metallic grains within QTC give rise to the occasional regions of noisy current-voltage characteristics, particularly at high voltages, where such processes will be occurring more frequently. Discharging is also thought responsible for RF emissions within QTC. As neighbouring grains neutralise their relative potentials, small bursts of charge may briefly oscillate back and forth, resonating and producing RF emission. Emission frequencies are broad due to the distribution of grain sizes and separations. The neutralisation of charge between adjacent grains may also trigger discharges to occur in neighbouring junctions, causing an avalanche effect of both charge movement and radio frequency white noise.

Section B: Vapour sensing applications of QTC

7 Introduction

Section B of this thesis is an investigation of the development of QTC for use in a commercial application. Specifically, the device that is investigated here is a chemical vapour sensor. By utilising the interaction between polymers and solvent vapours, it was hoped that a sensor could be developed that could detect volatile organic solvent vapours.

An alternative, granular form of QTC is used for vapour sensing tasks, rather than the bulk material that has been the focus of attention in section A. Physically, each QTC granule can be considered to be a small, irregularly shaped sample of the standard bulk composite. Granular QTC consists of clusters of spiky nickel powder particles, coated and bound together by the silicone polymer matrix. Different polymers can also be used to create QTC granules, including poly(urethane), poly(butadiene), poly(vinyl alcohol) as well as the standard silicone. Granule sizes can vary from approximately 50μm to 1mm, but are usually sieved to separate them into several ranges of particle size, each containing a far smaller particle size distribution.

Electrically, granular QTC displays the same properties as exhibited by the bulk form of the material. It is therefore considered a fair assumption that the system is governed by the same conduction mechanisms as within the standard bulk material.

7.1 Types of vapour sensors

When they are exposed to liquids or chemical vapours, many materials will display a change in some of their physical properties. A vapour sensor will detect these changes and convert then to electrical signals via a suitable transduction mechanism. Polymers are particularly useful as vapour sensing elements due to their ease of manufacture and broad chemical variety. Polymers readily exhibit swelling in the presence of solvent vapours, which can be detected in many different ways. Thin film layers of gas-sensitive polymers are therefore at the centre of many gas and vapour sensor systems.

Intrinsically conducting polymers show a change in resistivity in the presence of solvent vapours [102-107]. This is sometimes due to a polymer swelling effect. However, analytes may also cause oxidation or reduction of the polymer chain, giving rise to a change in charge carrier mobility, and therefore a change in conductivity. The three most common polymers used to make such sensors are poly(pyrrole), poly(aniline) and poly(thiophene) [108]. Conducting polymer sensors have the advantage that they are easy to produce and have a rapid response and recovery. However, problems with drift of the electrical baseline and of sensitivity to humidity still need to be addressed.

Some sensors work by detecting mass changes when their surface absorbs chemical vapours [108]. A gas sensitive layer (often a polymer) is bonded to a quartz crystal substrate. Such a device utilises the frequency change of acoustic waves travelling through a crystal when the polymer absorbs molecules of the analyte. Two types of this kind of sensor exist. The quartz crystal microbalance (QMB or QCM) [109] generates bulk acoustic waves (BAW) through a piezoelectric quartz crystal to detect mass changes. Surface acoustic wave (SAW) devices however, use a piezoelectric

substrate to pass Rayleigh waves across the surface [109-112]. A simplified diagram of both types can be seen in figure 7.1.

Acoustic wave sensors usually utilise ultrasonic frequencies in the range of 1 to 500 MHz, and demonstrate response times of the order of 100 to 1000 seconds [108]. Unfortunately they are also highly susceptible to changes in temperature and humidity.
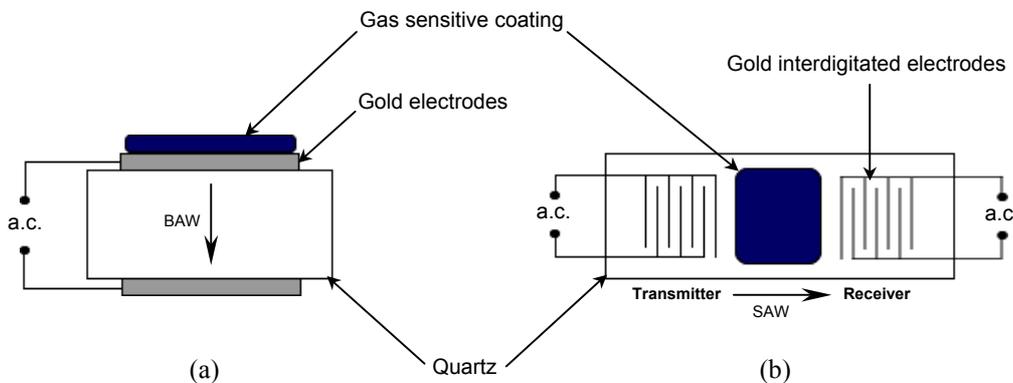
Fig. 7.1: *Mass change vapour detection systems using*
(a) bulk acoustic waves, (b) surface acoustic waves

Gas and vapour sensors that utilise the electrochemical interaction of chemical species with metal-oxide semiconductors are also commercially available, and have been researched extensively [113-117]. The semiconductor's surface (often tin-oxide, doped with small amounts of a palladium or platinum catalyst) may receive or donate electrons from or into vacant orbitals within the semiconductor or adsorbed chemical species. This charge transfer can then be detected as a small current change. The range of detection for metal-oxide gas sensors is between 0.1 parts per million (ppm) and 10 parts per thousand (ppt). However, their response and

recovery speed is no match for other sensor types such as conducting polymers. In addition, elevated temperatures are often required for a significant electrochemical reaction to occur. This results in a sensor system with a relatively high power input requirement.

Metal-insulator-semiconductor structures can be used to construct a type of field-effect gas sensor [108]. The two most common forms of this kind of device are the metal-insulator-semiconductor field effect transistor (MISFET), and the metal-insulator-semiconductor capacitor (MISCAP). Diagrams of these are shown in figure 7.2. In both types of field-effect sensor, the catalytic metal acts as the sensing layer. When analytes adsorb to the sensing layer, the surface potential of the metal is changed. In the MISFET, it is this surface potential that controls the flow of current between the semiconducting drain and source electrodes. In the MISCAP however, a change in the metal's surface potential instead causes a change in the capacitance of the structure. Temperature control of the field-effect gas sensor also affects the device's sensitivity. Sensors typically operate between 50 and 200 °C, and detect gas and vapour concentrations in the range 5 to 100 ppm [108].
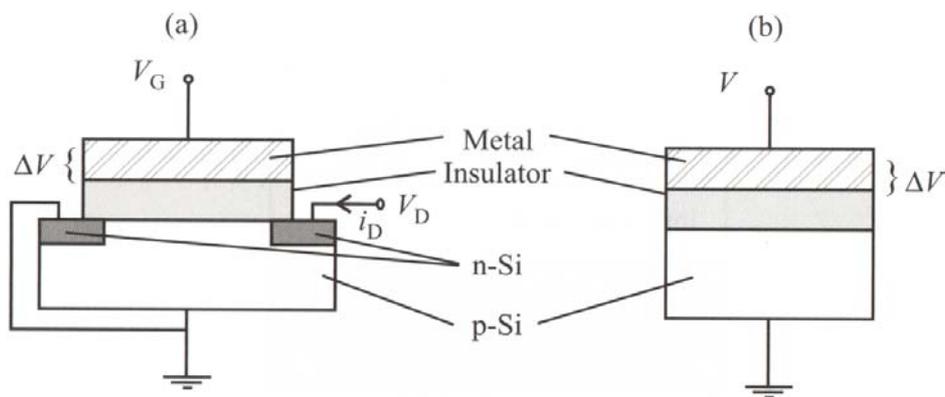
Fig. 7.2: *Field-effect gas detectors, (a) MISFET, (b) MISCAP [108]*

Fibre-optics have also been employed for the purpose of gas and vapour sensing [108] [118] [119]. Polymer waveguides often exhibit a change refractive index, or other optical properties, in the presence of chemical vapours. This is often due to a polymer swelling mechanism. By using measuring techniques such as interferometry [120], reflectance spectroscopy, absorbance and fluorescence, the changes in these optical properties can be measured. This allows information regarding the composition and concentration of the analyte to be processed. Structures of fibre-optic sensors vary widely. Although they have few electrical interference problems, optical sensors require accurate and stable control of temperature and optical outputs. This generates engineering problems, and so sub ppm level detectors are expensive compared to 'solid-state' sensors.

The ultimate low concentration detection system is mass spectroscopy (MS). The analyte molecules are first ionised and then accelerated through a curved path using electric and magnetic fields. The charge to mass ratio of the particles can therefore be deduced, allowing accurate identification of the species. Although highly expensive, it remains the only solution for obtaining high-resolution data, about a complex mixture of gases of vapours, which is both quantitative and qualitative.

Gas chromatography (GC) uses flame ionisation detection (FID) or thermal conductivity detection to detect multiple components within a gaseous mixture. It uses long, narrow capillary columns, with different internal surface treatments along their length. Each component gas is attracted to a different surface treatment according its various physical and chemical parameters, for example polarity, volatility, etc. The tubes are held at a constant temperature whilst the component vapours are separated and detected. A GC-MS feeds the results of the gas chromatogram into a mass

spectrometer for further analysis, enabling high-resolution data to be obtained about each fraction.

Metal-polymer composites may also be used as vapour sensors by utilising polymer swelling as a detection mechanism. In the presence of a chemical solvent, swelling preferentially occurs within the polymer regions of the composite, therefore changing the inter-particle separations of metallic grains within the material. If the metallic loading is set just above the percolation threshold, it is possible for the metal-polymer composite to undergo drastic changes in resistance when it is exposed to specific chemical vapours. This is due to the breaking of conducting pathways as polymer swelling occurs. Several examples of conventional percolating composites being used for vapour sensing tasks can be found in the literature [24] [121-130]. Typical responses to saturated solvent vapour are within the range of 0.05 % to 30 % change in conductivity within 1½ to 2 minutes [122] [123] [130]. However significantly larger responses can be obtained if composites are immersed into liquid baths of appropriate solvents, or have been very carefully manufactured just at the point of percolation [24] [121] [124-129] [131]. Solvent concentration is often found to be proportional to the amount of swelling, giving rise to a sensor that can deliver quantitative information about the analyte in question. Also, different polymers swell by different degrees when different solvents are introduced to them. Qualitative discrimination is therefore also possible.

Thanks to its unique tunnelling conduction mechanism, QTC outperforms standard percolating composites in terms of electrical sensitivity to applied pressure. It is hoped that this conduction mechanism will also give rise to enhanced electrical sensitivity to polymer swelling. A QTC vapour sensor may therefore be able to detect lower concentrations of solvent vapours than similar competitor devices made from conventional composites.

7.2 The electronic nose

Gas and vapour sensors, such as those described in the previous section, can be designed to target a single, specific chemical species.   This is the traditional "lock and key" approach.   Sensitivity to a wider variety of species requires additional sensors for each analyte that is required to be detected. The majority of sensor elements therefore remain inactive until its target chemical is detected.

The "lock and key" approach to sensing can be improved by instead constructing an array of sensors, each of which responds to a different, but wide variety of analyte types. Complex aromas are then introduced to the sensor array, whilst the response to all sensor elements is monitored simultaneously. The result is a combination of responses that is as unique to the aroma as a fingerprint is to a human individual. An odour map can be generated from the pattern of responses. Pattern recognition software then compares the result to a library of pre-programmed aroma responses, and makes a conclusion as to its origin. This is the concept of the electronic nose, resulting in a device that is more flexible and widely applicable than the conventional "lock and key" approach. In addition, techniques such as principle component analysis (PCA) can be used to help classify and distinguish aromas, based upon the combination of responses obtained from the sensor array.

7.2.1 Commercial devices

Numerous examples of commercial electronic nose developments exist, most of which are competing to develop a device capable of accurately distinguishing between a wide variety of complex aromas at the parts per million (ppm) level or lower. Such a device could be used in an enormous

range of applications. Examples include quality control in the cosmetics and the food and drinks industries, leak detection in the petrochemical industry, medical diagnosis, drugs, explosives and gas detection for security and military applications and the environmental monitoring of pollutants. Many of these applications also require low-cost, robust and portable detectors with low power consumption and fast response/recovery times.

Several early commercial devices have been developed by a number of companies, using a variety of vapour detection mechanisms. For example, Osmetech use up to 48 conducting polymer sensors in their device. The Z-Nose from Estcal uses SAW technology, and Alpha-MOS and Applied Sensor use hybrid combinations of MISFET, metal-oxide and QMB sensors. Metal-polymer composite sensors are also being developed into array-based electronic nose systems [25] [132] [130]. The most notable of these is the Cyranose, developed by Cyrano Sciences.

The Cyrano electronic nose uses an array of 32 percolating conducting carbon black-polymer composite sensors. Each sensor is very small (typically a few milligrams in weight), which promotes rapid response and recovery times. The resistance of each sensor is measured just before exposure begins to establish a baseline resistance (R_0), and is then compared to the resistance when saturation has occurred (R) a few seconds later (typically between 2 and 10 seconds). The fractional change in resistance, defined as $(R - R_0)/R_0$ is then calculated for each sensor before signal processing occurs. Information regarding minimum detection levels is misleading as the Cyranose is designed primarily as a fast responding qualitative sensing device. However, quantitative capabilities may be extracted from scientific publications, which detail results from recent research data [25] [133-146].

Typical data show that the Cyranose has good distinguishing ability for a broad variety of solvents in the concentration range between 1% and 100% of SVP. However minimum detection levels may be substantially lower, at the sacrifice of distinguishability. For example, for the solvent 1-pentanol, minimum detection threshold has been quoted at 0.04% of SVP, corresponding to approximately 0.1 ppm, when diluted within a carrier gas flow-rate of several litres per minute [142]. This level of detection is comparable to the performance of the human nose. However, the electrical responses of electronic noses are often found to be proportional to the flow-rate of the test gas, in addition to the analyte concentration within that gas. Therefore, at lower flow-rates minimum detection levels of the Cyranose may be less remarkable.

Concentration levels may be expressed in terms of fractions (or percentages) of room temperature saturated vapour pressure (SVP), or instead in parts per million (ppm) (where ppm are defined as the number of milligrams of dissolved solvent per dm^3 of carrier gas). However, the former is usually favoured when expressing minimum detection levels. Results have shown that for the Cyrano device, electrical response is highly dependent upon the vapour pressure of the analyte being tested [135]. The consequence of this is that all analytes have similar (to within an order of magnitude) minimum detection thresholds when expressed as a fraction of SVP. However, if threshold concentrations are instead expressed in terms of ppm, minimum detection levels are found to be more strongly dependent upon solvent type. It is important to note that this conclusion is a result of the particular swelling and transduction mechanisms appearing within Cyrano composites, and therefore may not necessarily hold true for all vapour detection systems.

8 Theory of vapour sensing in metal-polymer composite systems

Solvent penetration into a metal-polymer composite may cause an electrical conductivity change via many different mechanisms. Electrochemical interactions may occur between solvent and polymer, and also between solvent and metallic filler particles. Charge may be donated or accepted by solvent molecules, resulting in a change in the quantity of charge available for conduction. Alternatively, the work function of the polymer may be modified, thus affecting tunnelling probabilities. In addition, the capacitive and dielectric properties of the material are likely to be modified. Changes in ionic conductivity may also result, especially where polar solvents are concerned. However, all of the above effects are usually negligible compared to the process of polymer swelling, which dominates wherever solvents and elastomers are present within the same system.

Whatever the transduction mechanism, for an effective sensor, the electrical response to the test vapour should be fast-acting and fully reversible. Stable baselines and repeatable responses are required, with large signal to noise ratios. The signal should also be proportional in some way (preferably linearly) to the concentration of the test vapour, if effective quantitative analysis is to be performed. In addition, for qualitative analysis, a wide variety of responses should be obtainable from many different polymer-solvent combinations.

8.1 Polymer swelling

When a polymer is introduced to a compatible solvent, mixing of the two species will occur, and there will usually be a tendency for the polymer to

dissolve. However, by cross-linking the polymer, the structure becomes strengthened and consequentially less soluble. A large amount of empty space exists in-between the random molecular arrangements of polymer chains. This is known as the free volume of the polymer. Solvents penetrate this free volume until the polymer can no longer accommodate the extra molecular species. In order to allow more solvent to be absorbed, the polymer must swell, thus expanding its free volume [147] [148].

It is useful to note that the presence of metallic particles within a polymer will undoubtedly affect the ability of a metal-polymer composite to swell. The following description of homogeneous polymer swelling therefore cannot be applied to composites with total confidence. Berriot *et al.* [149] describe how the strength of bonding between polymer and filler particles is critical in modelling the swelling dynamics of such a system. If bonding is insufficient, cavities surrounding the grains may develop as the polymer expands isotropically. However, strong bonding to the filler particles will result in complex internal stresses and strains, which may also affect the swelling process.

The degree of polymer swelling is controlled by many factors including chemical structure, polarity, molecular mass, pressure, temperature, free volume, porosity, chain flexibility, and cross-link density. The Hansen method, calculates solubility parameters to define the contribution (either positive or negative) of each of these factors towards the swelling of any specific polymer-solvent combination. The result is a multidimensional solubility parameter, representing the overall interaction. A single "Hildebrand" solubility parameter can then be calculated by adding the Hansen parameters in quadrature, and then square-rooting the result. Experimentally, the many different contributions to polymer swelling (and therefore also their corresponding Hansen solubility parameters) are

extremely difficult to evaluate separately from each other, as the observed swelling is a result of the combination of these effects. Instead, a single experimentally observed Hildebrand solubility parameter is therefore normally quoted, which takes into account the many different contributions and describes the overall swelling effect. In order to understand exactly how each of these factors contributes, we must turn to a thermodynamic approach of polymer-solvent interactions.

8.1.1 Thermodynamics of mixtures

In order for a multi-component mixture to form, a fundamental thermodynamic requirement must be fulfilled. Assuming a system of constant pressure and temperature, the Gibbs free energy of the multi-component solution must be less than the sum of the Gibbs free energies of all the individual components. In short, the change in the Gibbs free energy of the system must be negative in order for the mixture to form. This change in Gibbs free energy (ΔG) can be expressed as a combination of two terms, as described in equation 8.1.

$$\Delta G = \Delta H - T\left(\Delta S\right) \tag{8.1}$$

where ΔH is the change in enthalpy (heat of mixing), ΔS is the change in entropy of the system and T is the absolute temperature.

The change in entropy that occurs when a polymer and a solvent are mixed together consists of two mutually opposing components. Firstly, there is a strong desire for the two substances to mix, leading to increased disorder and an entropy increase. The physical mechanism controlling this process is that of diffusion, and is described in more detail in section 8.1.3.

The above process of entropy increase is opposed by a second contribution to entropy change. When swelling occurs, the polymer dilates, resulting in a reduction in the total number of possible polymer chain conformations. Polymer chains become stretched into less entangled states, leading to an increase in the structural order of the polymer. An entropy decrease therefore occurs, which opposes polymer swelling.

The change in enthalpy of the system can be regarded as the chemical energy that is consumed (or liberated) when the components of the mixture are brought together. The reaction can be endothermic or exothermic, and can therefore either oppose or promote the process of mixing. The former of these two cases however, is usually the result. Enthalpy changes within a polymer-solvent mixture can be described by chemisorption and physisorption processes.

8.1.2 Chemisorption and physisorption

Two types of sorption phenomena are possible when a solvent vapour comes into contact with an appropriate polymer. Adsorption occurs when chemicals adhere to the surface of the polymer, whilst penetration into the bulk of the material is described by absorption. Sorption into (or onto) the polymer will occur wherever sites exist that attract the solvent molecules. One of the advantages of polymers for use in sensing applications is the ability to add chemical side-groups. This adds functionality to the polymer, enabling it to have preferential sorption sites for specific chemical types. If the attraction occurs via intermolecular (Van der Waals) forces, the process is called physisorption. The chemical identity of the sorbed molecule remains intact, but is only weakly bound to the surface. Due to the spontaneous nature of this reaction, ΔH is negative, indicating an exothermic reaction, which promotes the mixing process. The alternative

sorption process that may occur at a polymer-solvent interface is chemisorption. In this case, direct chemical bonding takes place between solvent molecules and the polymer. Chemical adsorption such as this is far stronger and more permanent than any physisorption process. This may therefore lead to incomplete recovery of the vapour sensor during purging.
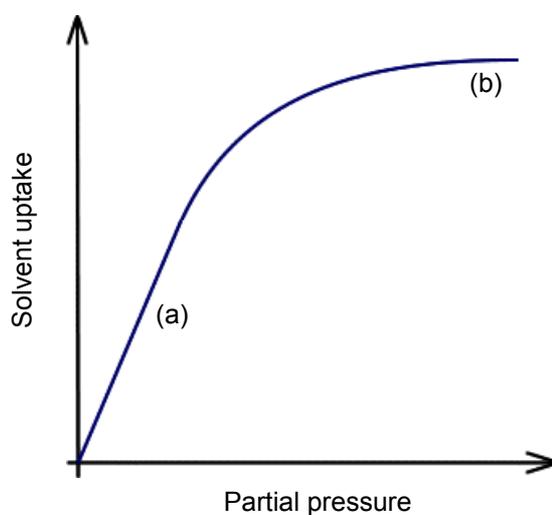
Fig.8.1: *Langmuir isotherm, indicating (a) Henry's law for low partial pressures and (b) saturation at high partial pressures*

Sorption isotherms relate the partial pressure of the analyte vapour to the quantity of sorption that has occurred. The method of measuring the quantity of sorption varies depending upon the system. In the case of surface adsorption, the fractional coverage is measured, whilst for bulk absorption, the volume of the solvent sorbed within the polymer is used. In either case, the sorption quantity will saturate at some limiting value, once all sorption sites have been occupied by the analyte [150]. Therefore, at high partial pressures (and therefore high concentrations of analyte),

sorption isotherms often tend towards a horizontal limit (figure 8.1). This pattern is known as a Langmuir isotherm, and is the most common trend observed for solvent interactions with polymers, including metal-polymer composites [151].

The linear portion of the graph in figure 8.1 at low partial pressures illustrates Henry's law. In this regime, there are far more sorption sites available than there are solvent molecules. Henry's law requires that the gas partition coefficient (κ) (defined in equation 8.2) remains constant during this linear regime.

$$\kappa = \frac{\text{concentration of solvent in gas phase}}{\text{concentration of solvent in solid phase}} = \frac{n_g/V_g}{n_s/V_s} \qquad (8.2)$$

The subscripts g and s denote the gas (vapour) and solid (polymer) components respectively, whilst the letters n and V represent the number of particles present within, and the volume of, that component.

Deviations from the characteristics of the Langmuir and Henry's isotherms frequently occur. This is due to simplifications that have been made whilst constructing the model. The Langmuir isotherm assumes that the probability of occupying a sorption site is equal for all sites, which is clearly not the case for complex polymers with many different active side-chains. The size and distribution of internal voids (or free volume) will also affect the probability of occupying a specific sorption site. Corrections have been made for these shortcomings in the form of the Freundlich and Temkin isotherms. In addition, the Brunnauer, Emmett and Teller (BET) isotherm also considers the added complexity of multi-layer adsorption. However,

the Langmuir isotherm is normally sufficient for the modelling of sorption behaviour in most filled and unfilled polymer-solvent systems [151].

The enthalpy change (ΔH), when the above sorption mechanisms take place, can be determined either by direct experimental measurement, or by determining the difference between the solubility parameters of the polymer and solvent (δ_p and δ_s) [152] [153].

$$\Delta H = V\phi_p\phi_s \left(\delta_p - \delta_s\right)^2 \qquad (8.3)$$

where V is the molar volume and ϕ_p and ϕ_s are the volume fractions of the polymer and solvent respectively. The value of the polymer solubility parameter is usually established experimentally, but is also defined by the following equation:

$$\delta = \sqrt{\text{Cohesive Energy Density}} = \sqrt{\frac{E_{vap}}{V}} \qquad (8.4)$$

where E_{vap} is the molar energy of vaporisation. The implication of equation 8.3 is that ΔH is always positive. Also, as the difference between the solvent and polymer solubility parameters increase, the probability of mixing decreases. This can be considered the mathematical equivalent of the general rule of chemistry that "like dissolves like."

8.1.3 Diffusion and Flory-Huggins theory

When a polymer comes into contact with a solvent vapour there is an entropy increase caused by the desire of the two components to mix together

and thus increase the disorder of the system. The physical process that controls the rate at which this occurs is diffusion.

To simplify the model, at first we assume an ideal mixture in which no swelling and no chemical interactions occur. The change in enthalpy is therefore zero, and the only contribution to entropy change is due to mixing. The polymer neither attracts nor repels the solvent molecules, and therefore the rate at which solvent penetration occurs is controlled directly by the concentration gradient, dn/dx. This is known as Fick's first law of diffusion [154], and is expressed by equation 8.5.

$$F = -D\frac{dn}{dx}$$ (8.5)

where F is the number of particles crossing unit area per unit time (the flux) and D is the diffusion coefficient. The diffusion coefficient is dependent upon several factors. Most notable of these factors is the porosity of the polymer [150]. The average pore size and pore density will clearly affect the rate at which solvent molecules may penetrate the sample.

Equation 8.5 is limited in its application to real polymer swelling systems as it requires a constant concentration gradient. A finite sized polymer sample with limited free volume will clearly not display this behaviour, and so a time dependent version of Fick's equation is required. Consideration of the conservation of matter within the system, combined with Fick's first law yields the Fick's second law of diffusion [155] [97]:

$$\frac{\partial C}{\partial t} = D \, \nabla^2 C$$ (8.6)

where C is the concentration of the solvent in the polymer, and is equal to the volume of the solvent in the polymer divided by the dry volume of the polymer. The implication of equation 8.6 is that the quantity of solvent that has been sorbed into the polymer increases linearly with the square root of the time ($t^{1/2}$). This is known as simple Fickian diffusion.

The entropy change caused by the diffusion and mixing of two molecular species is described in equation 8.7, and is the subject of Flory-Huggins theory.

$$
\begin{aligned}
\Delta S_{\text{mixing}} &= k_B \ln \Omega \\
&= -k_B \left(n_s \ln \phi_s + n_p \ln \phi_p \right)
\end{aligned}
\tag{8.7}
$$

where Ω is the total number of spatial arrangements of the solvent molecules within the polymer (i.e. the degeneracy), which can in turn be expressed in terms of the volume fractions of the polymer and solvent (ϕ_p and ϕ_s) and the number of polymer and solvent molecules (n_p and n_s).

It is important to note that at this point many simplifications have been made. The above theory of diffusion on its own assumes no enthalpy change (athermal mixing). A correction can be made to Flory-Huggins theory to account for this by introducing a Flory-Huggins interaction parameter. However, the theory is still insufficient. It has been assumed that no volume change is occurring within the polymer. The diffusion of liquid into the polymer is accommodated by the free volume of the polymer and the freedom of movement of the polymer chains. Consideration is therefore required of the effect of polymer swelling upon the thermodynamics of the system.

8.1.4 Flory-Rehner theory

Flory-Rehner theory uses a mean-field approach to additionally incorporate the effect of polymer cross-linking upon a polymer-solvent mixture. Previously, Flory-Huggins theory made no consideration of the effect of cross-linking, modelling instead substances that dissolved completely into a liquid solution. Cross-linking adds rigidity and strength to the polymer, making it more resilient to solvent attack. Solvents will still strongly interact with the polymer, however the structure remains intact. The only way for the solvent to be accommodated therefore is for the polymer to swell.

The act of diffusion causes a polymer to expand in the presence of a solvent. When this occurs, polymer chains are stretched to allow for the volume change. This is the source of entropy decrease due to increased order within the polymer network. A counteracting force that resists further swelling is therefore generated, caused by the desire of the polymer network to return to its original unstretched and more highly disordered state. Equilibrium swelling occurs when the two competing effects are in balance with each other.

Characteristic times can be assigned to the two competing effects. The molecular relaxation time, caused by viscoelastic recovery of the polymer, is assigned the symbol τ_m, whilst the characteristic diffusion time is represented by τ_d. The ratio of these two quantities (τ_m / τ_d) is called the Deborah number (D_e) [156]. A small D_e (long diffusion time and short relaxation time) gives rise to a solvent uptake trend that resembles Fickian kinetics. A characteristic $t^{1/2}$ dependency of solvent uptake is therefore observed. Conversely, a large D_e (short diffusion time and long relaxation time) clearly requires greater consideration of the viscoelastic relaxation of

the polymer. Non-Fickian kinetics are therefore observed, and at extreme ratios, solvent uptake is linear with t. For intermediate values of D_e, anomalous diffusion occurs. All cases can be described by the generalised Fickian diffusion equation [155] (a modified form of equation 8.6):

$$J = -D_x \frac{C}{C_x} \frac{\partial C_x}{\partial x} \qquad (8.8)$$

where J is the flux of the solvent and C_x is the local equilibrium concentration at position x into the polymer and D_x is the diffusion coefficient at position x. In the case of Fickian behaviour, $C = C_x$, and D is constant. However, for the more general case of non-Fickian and anomalous behaviour, the diffusion coefficient will change with concentration. This is caused by the alteration of diffusion controlling parameters such as the porosity of the polymer.

The desire to contract back to a smaller volume will depend upon the modulus of elasticity of the polymer. Consideration of this, together with the above diffusion characteristics, allows Flory-Rehner theory to conclude the following equation [147] [148]:

$$G = \frac{RTA}{V_s Q^{5/3}} \qquad (8.9)$$

where G is the shear modulus of the unswollen polymer, V_s is the molar volume of the solvent, A is a constant (incorporating the relative desire of the two substances to mix) and Q is the volume swelling ratio (defined as the volume of the swollen polymer divided by the volume of the unswollen polymer).

One can conclude from the above that a high modulus of elasticity (caused possibly by a high cross-linking density) will inhibit swelling. In addition, if swelling occurs whilst the polymer is under a tensile stress, the equilibrium degree of swelling will increase. Conversely, application of compression to the polymer will restrict the degree of swelling.

9 Summary of previous work

Initial studies have been carried out as part of an undergraduate MSci research project, investigating the vapour sensing properties of QTC granules [157]. The results to that project are briefly summarised here.

QTC granules were made using Silcoset 153 silicone loaded with types 287 and 123 nickel powder. Samples consisting of several grams of QTC granules were subjected to a constant voltage source of 10 V, and were lightly compressed until they passed a current of approximately 1 mA. They were then exposed to a variety of saturated organic solvent vapours at flow-rates of 100 cm^{-3} min^{-1}, whilst simultaneously measuring the current passing through them. After a few minutes of exposure, changes in resistance of up to three or four orders of magnitude were observed (figure 9.1). In the case of exposures to hexane, sample resistance rapidly exceeded the range of measuring equipment (i.e. current $< 10^{-7}$ A). All responses were fully reversible, and showed differential results for different solvent types.
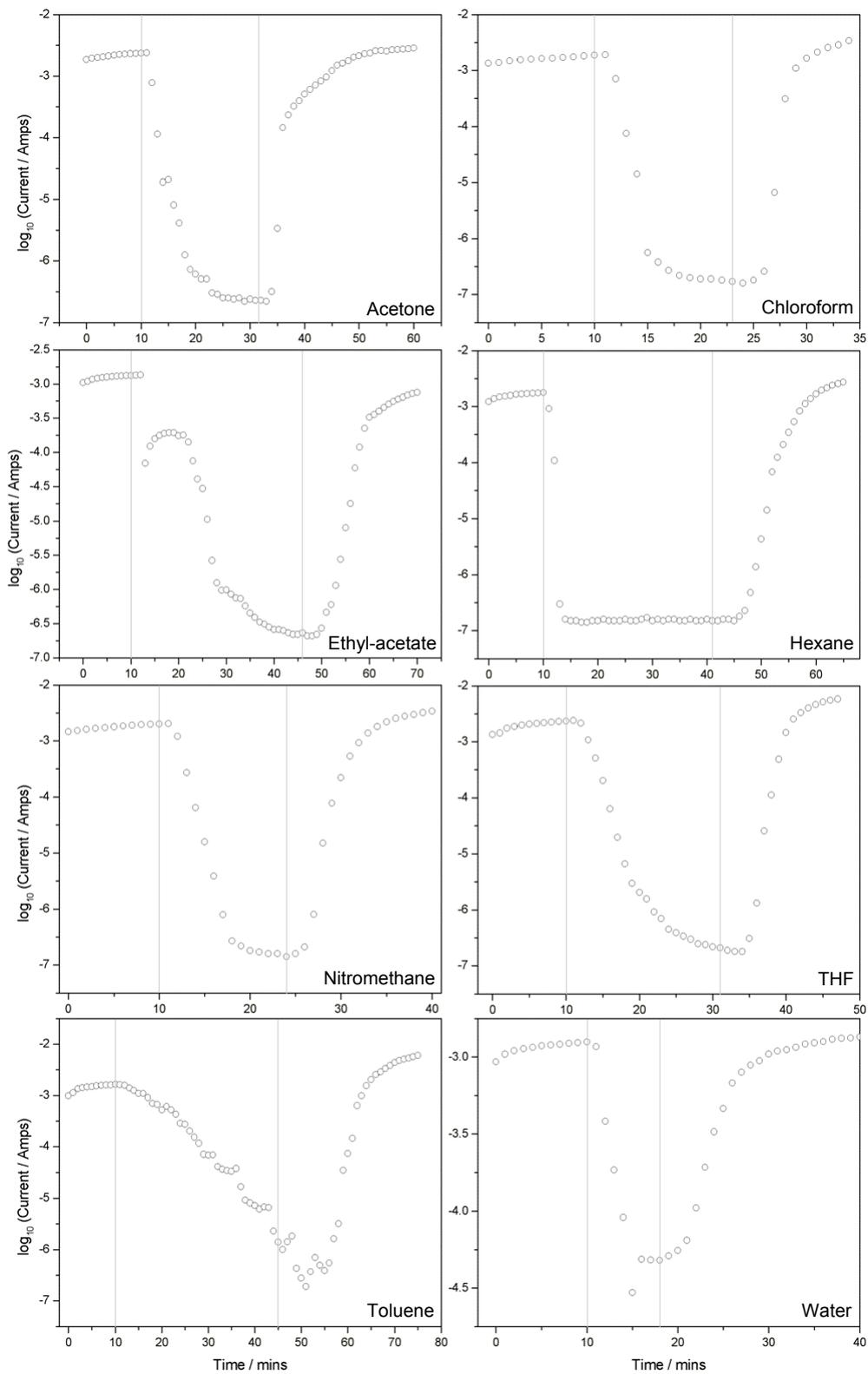
Fig. 9.1: *Response of QTC to different saturated solvent vapours [157]*

10 Response of different QTC polymers to different solvent vapours

10.1 Introduction

A series of experiments were performed to investigate the response of QTC granules, made using different polymers, to a variety of saturated organic solvent vapours. This, in combination with the results to previous sensing work [157], should provide a broad set of response data. This can then be used to determine the practical applicability of QTC for use in a vapour sensing device.

10.2 Experimental

The vapour sensing unit used to expose QTC granules to solvent vapours was designed and built in-house and is shown in figure 10.1. It consists of a Perspex cylinder, into which slide two hollow aluminium pistons. These pistons are mounted vertically, the lower being fixed in position, whilst the upper piston is free to move. QTC granules are placed in the sample space between the two pistons, and a screw mechanism at the top of the structure can then be used to compress the two pistons together, thus making the QTC sample more conducting. The ends of the pistons are covered with a fine nickel gauze mesh, supported underneath by a second more rigid and coarse nickel mesh. These gas-permeable end-caps act as filters, allowing gas and vapour to flow through the pistons and the QTC granules, whilst preventing the granules themselves from being flushed out of the sensor unit. Electrical leads are connected to the two conducting pistons, which allow resistance data to be taken for the granular QTC.
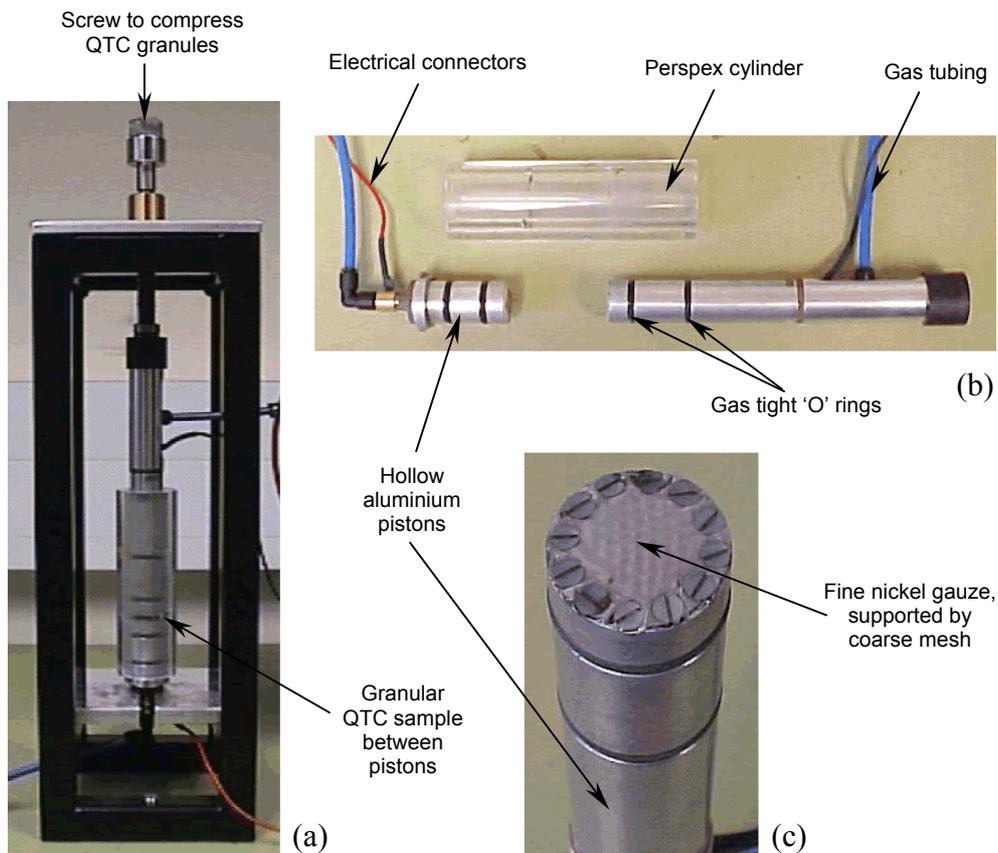
Fig. 10.1: *Three views of the QTC vapour sensor: (a) entire sensor unit, (b) piston electrodes, and Perspex cylinder, (c) nickel gauze end-caps*

Electrical resistance data was taken using a Keithley 2000 multimeter. 3g of QTC granules were placed into the testing chamber, and compressed until resistance reached approximately 20 Ω. In early experiments, a constant voltage of 1 V was applied using a Weir 4000 voltage source, whilst current measurements were taken using the multimeter. However, in later experiments, more consistent and reliable data was obtained when resistance data was taken directly using the multimeter in resistance measuring mode. GPIB communication with a personal computer running LabVIEW software enabled remote data logging at a rate of 1 reading per second
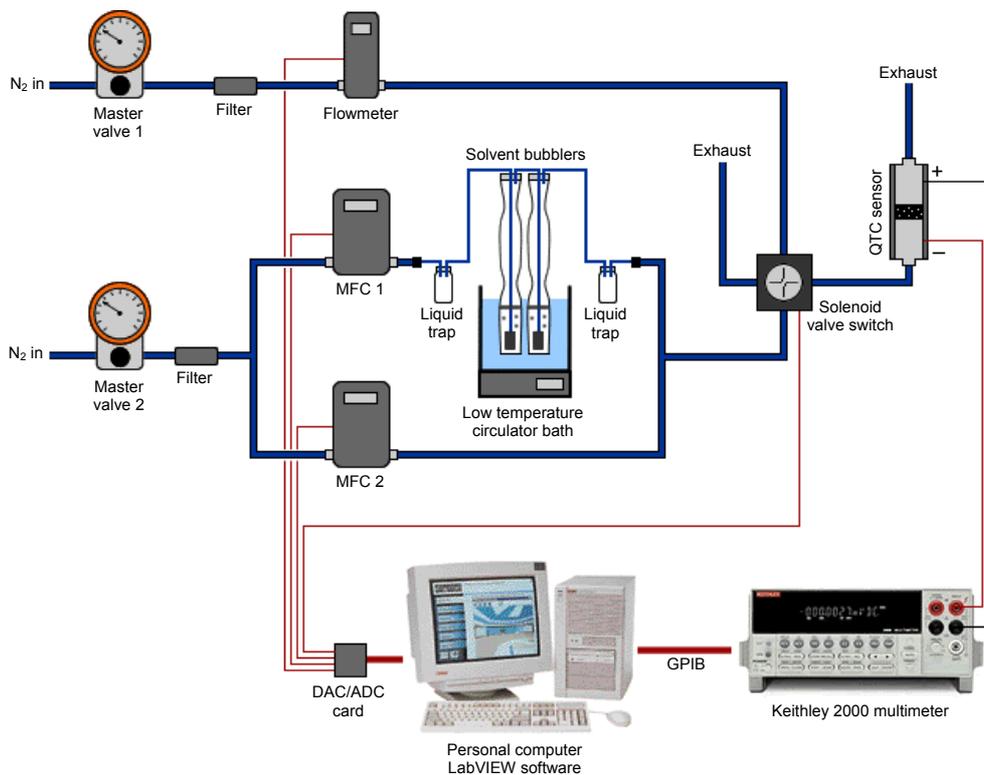
Fig. 10.2: *Experimental setup and control for vapour sensing experiments*

Saturated solvent test vapours were supplied to the sensor unit using nitrogen as a carrier gas. A diagram of the equipment is shown in figure 10.2. Two lines of carrier gas were supplied via the same liquid nitrogen boil-off source, and entered the experimental system at a pressure of approximately 2 bar through two control valves. Both nitrogen lines were then filtered for particulates by means of a 10 μm in-line filter. One line was then split into two paths, going to two separate mass flow controllers (MFCs). Model U-32708-20 MFCs were supplied by Cole-Parmer, and had a flow capacity range of 0 to 50 ml min^{-1}. Remote control of the flow rate was achieved via a personal computer with a digital to analogue converter (DAC) card. Data logging of flow rates was achieved with an analogue to

digital converter (ADC) card. Both ADC and DAC cards were operated using LabVIEW control software written specifically for the task.
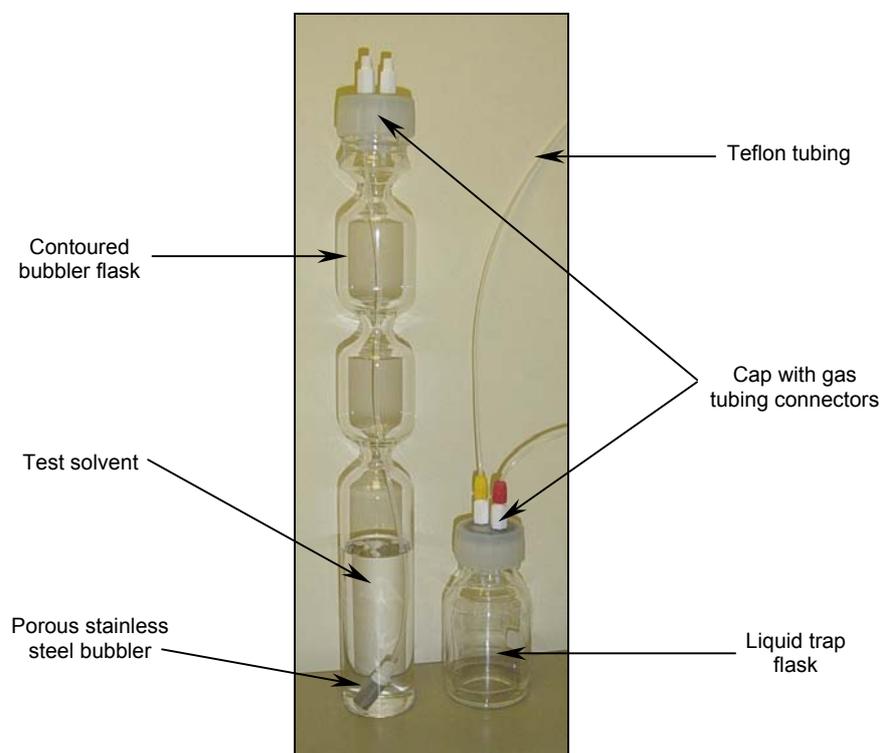
Fig. 10.3: *Bubbler flask (left) containing test solvents, and*
simple liquid trap (right), used to prevent liquid in the gas line

The gas line from the first MFC is then passed through two glass bubbler chambers in series, containing the test solvent in liquid form. Two bubblers were used in order to ensure total saturation of the solvent in the nitrogen carrier gas. The bubblers themselves were porous stainless steel. Glass bubbler flasks were designed and built especially for the task and can be seen in figure 10.3(a). Previous experiments [157] suffered from small quantities of liquid solvent being transported down the gas line towards the

sensor. The narrow restriction sections in the glassware were designed to prevent splashes of liquid solvent from escaping the bubblers. In addition, two liquid traps were placed either side of the bubblers in order to catch any liquid that may still escape. Liquid traps can be seen in figure 10.3(b), and consist simply of a flask with inlet and outlet connections in the cap.

In early experiments, the test solvent was held in the bubble flasks at room temperature. However, daily fluctuations in the ambient temperature strongly affect the vapour pressure of the solvent, and so in later experiments, bubbler flasks were immersed in a variable temperature bath so that solvent temperature may be controlled. The bath was a Grant LTC20-40RS low temperature circulator, with a 20 litre capacity and capable of temperatures in the range –40 °C to 100 °C, and was supplied by VWR International. Baysilone M3 silicone fluid, supplied by Techsil, was used as the heat transfer fluid for the bath.

The gas line from the second MFC acts as a diluent line, and rejoins the solvent saturated bubbler line. Control of the relative flow rates in these two lines enables the concentration of solvent vapour within the carrier gas to be altered. In addition, the low temperature circulator may be used to lower solvent temperatures. This changes the vapour pressure of the solvent in the bubblers, and therefore affects the amount of solvent that can be saturated in the nitrogen flow line.

Once the diluent line and bubbler line have recombined, they connect to a four-way 11500 series electric solenoid rotary valve, supplied by Omnifit. Also connected to this valve is the second nitrogen gas supply line. This acts as a purge line to flush solvent out of the vapour sensor. Large flow rates could be passed though this line to aid effective purging. Flow rates

were monitored using a Cole-Parmer U-32707-22 flowmeter. The remaining two ports on the solenoid valve were connected to an exhaust and to the QTC vapour sensor itself. Two possible valve positions were available, enabling the vapour sensor to be either exposed to solvent vapour, or purged with nitrogen. These two configurations are shown in figure 10.4. Commands to control the valve position could be sent by the personal computer via digital I/O channels on the ADC card. These were also controlled using LabVIEW software, designed specifically for the task. The control software enabled any number of repeat exposures to be performed with variable exposure and purge lengths.
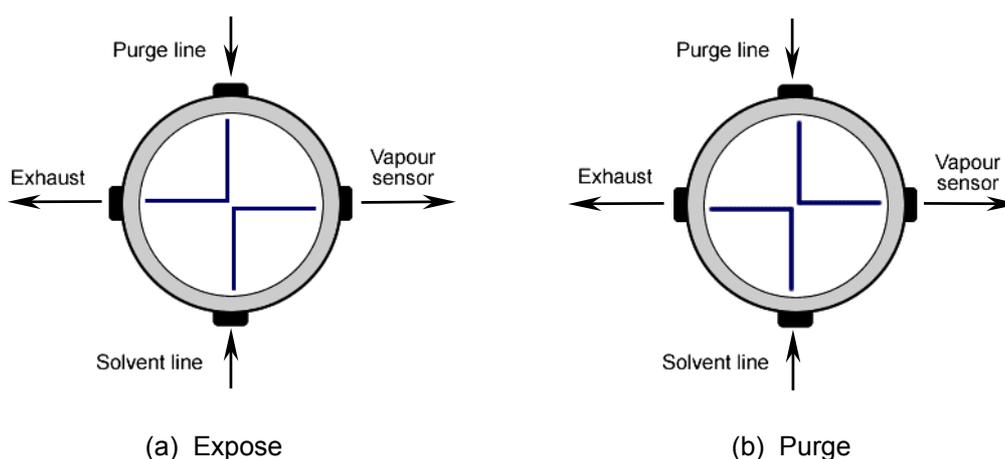
Fig. 10.4: *Two possible configurations of the solenoid valve switch, indicating positions of (a) exposure, and (b) purge*

Early experiments used a manual rotary valve rather than an electrical solenoid valve to switch between purge and exposure settings. However, maintaining consistency in the speed and timing of switching was difficult, and thus a computer-controlled valve was chosen as a more practical alternative. Teflon tubing was used throughout the experimental apparatus to ensure resilience to solvent attack and also to minimise odour tainting.

Confirming solvent saturation

An experiment was first performed to confirm that the nitrogen carrier gas was completely saturated with solvent vapour after passing through the bubblers. The solvent with the highest vapour pressure (hexane) was chosen for this experiment. If saturation could be proven using this solvent, then it should also be true for all the other test solvents too. Nitrogen was allowed to bubble through the hexane for several hours at a fixed flow rate. The mass loss of solvent in the two bubblers over that period of time was then recorded using a microbalance. This was then repeated for several different flow rates, recording the mass loss for each case. From mass loss data, the resulting solvent concentrations for each flow rate could be calculated and compared with each other. The results to this can be seen in Appendix C. Details of how concentration is calculated in terms of both percentage of SVP and ppm is shown in a worked example in Appendix B.

Mass loss from the second downstream bubbler was almost completely negligible when compared to the loss from the first upstream bubbler. This implies that complete saturation of the hexane in the nitrogen is highly probable. The graph in Appendix C also shows that for all flow-rates, solvent was present in the nitrogen carrier gas in equal concentrations. Therefore it was concluded that saturation of the gas with the solvent occurs for all flow rates, and also for all solvents tested.

The concentration for hexane vapour was found experimentally to be 732.3 (± 14.7) ppm, which corresponds to 104% (± 3%) of SVP at 25 °C. The calculated theoretical concentration of hexane at 25 °C (i.e. 100% SVP at 25 °C) implies a level of 700.8 ppm. This is in reasonable agreement with the experimentally determined value. However, allowing for maximum possible errors, all future experiments carried out under these conditions

will therefore assume that bubbler flow rates of 50 ml min^{-1} for any solvent, give rise to 100% ($\pm$ 7%) of SVP at 25 °C. The corresponding ppm levels for a variety of solvents under these conditions can be seen in table 10.1.

Discrepancies between the calculated and experimentally determined concentration can be accommodated for by the fact that the calculation assumes several approximations, such as ideal gas behaviour. In addition, temperature control was not present in the experiment, which may cause larger errors than previously thought.

Solvent	Concentration / ppm (mg solvent per litre N$_2$)	Concentration / % SVP at 25 °C
Ethanol	146.3 ($\pm$ 10.3)	100 ($\pm$ 7) %
Hexane	700.8 ($\pm$ 49.6)	100 ($\pm$ 7) %
THF	628.3 ($\pm$ 44.4)	100 ($\pm$ 7) %
Water	23.0 ($\pm$ 1.6)	100 ($\pm$ 7) %

Table 10.1: *Calculated room temperature saturated vapour concentrations*

Response of different polymer QTC granules to different solvents

A control experiment was first performed, exposing 3g of raw 123 nickel powder to saturated THF vapour at room temperature. This determined if metal-solvent interactions were partly responsible for any changes in electrical response, or if instead the polymer-solvent interaction dominated.

A selection of solvents were chosen for testing the vapour detection properties of QTC granules, including hexane, tetrahydrofuran (THF),

ethanol and water. All solvents were laboratory grade and were supplied by Aldrich. QTC granules made from a variety of different polymer types were manufactured and supplied by Peratech. All granules were 152-300 μm in size, and were made using type 123 nickel powder. Polymer varieties included standard silicone, poly(urethane), poly(vinyl alcohol) (PVA) and poly(butadiene). Specifically, silicone granules were made using Silcoset 153 and Silastic T4, supplied by Ambersil and Dow Corning respectively. The poly(urethane) used was Techsil F42, supplied directly from Techsil, PVA was Universal Bonding Adhesive supplied by Ultrabond, and poly(butadiene) was Krasol LBH 2000 supplied by Kaučuk. Every possible combination of solvent and polymer was tested individually for its effect upon the electrical resistivity of QTC granules.

3g of QTC granules were placed in the sensor and compressed to 20 Ω in the manner described earlier. They were then allowed to relax for at least 15 minutes, so that the effects of viscoelastic drift were minimised. Once a stable baseline resistance was established, exposures could begin. Multiple 1 minute exposures were carried out, followed by a single long exposure until electrical response ceased to change. Purges between exposures were carried out at high pressure (2 bar at master control valve), resulting in purge flow rates beyond the measurement range of the flowmeter (i.e. >> 50 ml min^{-1}). High-pressure purges were used to help encourage complete recovery of the sensor between exposures. Exposures were carried out using room temperature saturated vapour at 50 ml min^{-1}. As explained earlier, this corresponds to 100% (± 7%) of SVP at 25 °C. The equivalent ppm concentration levels can be seen in table 10.1. Experiments were then repeated several times to ensure consistent results. However, repeat experiments were limited due to the relatively small quantity of granules

available for testing. The above was then all repeated until all of the 16 possible polymer-solvent combinations had been tested.

10.3 Results and discussion

The responses of silicone QTC granules to saturated vapours of ethanol, hexane, THF and water can be seen in figure 10.5. In the figure, results can be seen to both multiple 1 minute exposures (left) and also to a single long exposure (right) to the test vapour. Figures 10.6 and 10.7 show similar results for poly(urethane) and PVA granules respectively.

The data presented in figures 10.5 to 10.7 show a wide variety of responses for different combinations of polymer and solvent. Some responses are very large, displaying resistance changes of greater than 6 orders of magnitude, whilst others show virtually no response whatsoever. Some combinations cause rapid responses, with significant resistance change occurring within less than 5 seconds. Other polymer-solvent combinations are slower to respond, requiring several minutes before changes are observed. This broad variety of differential responses is what is required for an effective electronic nose sensing device.

Discontinuities can be seen in a few of the graphs in figures 10.5 to 10.7. One such example is at 45 minutes into the long exposure of ethanol to poly(urethane) granules in figure 10.6. Such irregularities regularly occur at specific decade intervals of resistance values, and are not thought to be characteristics of the vapour sensor. They instead result from the autoranging feature of the multimeter. As the multimeter switches from one measurement range to another, different current sources are used to test for resistance values. Due to the non-Ohmic nature of QTC materials, this results in the observed sudden changes in resistance.
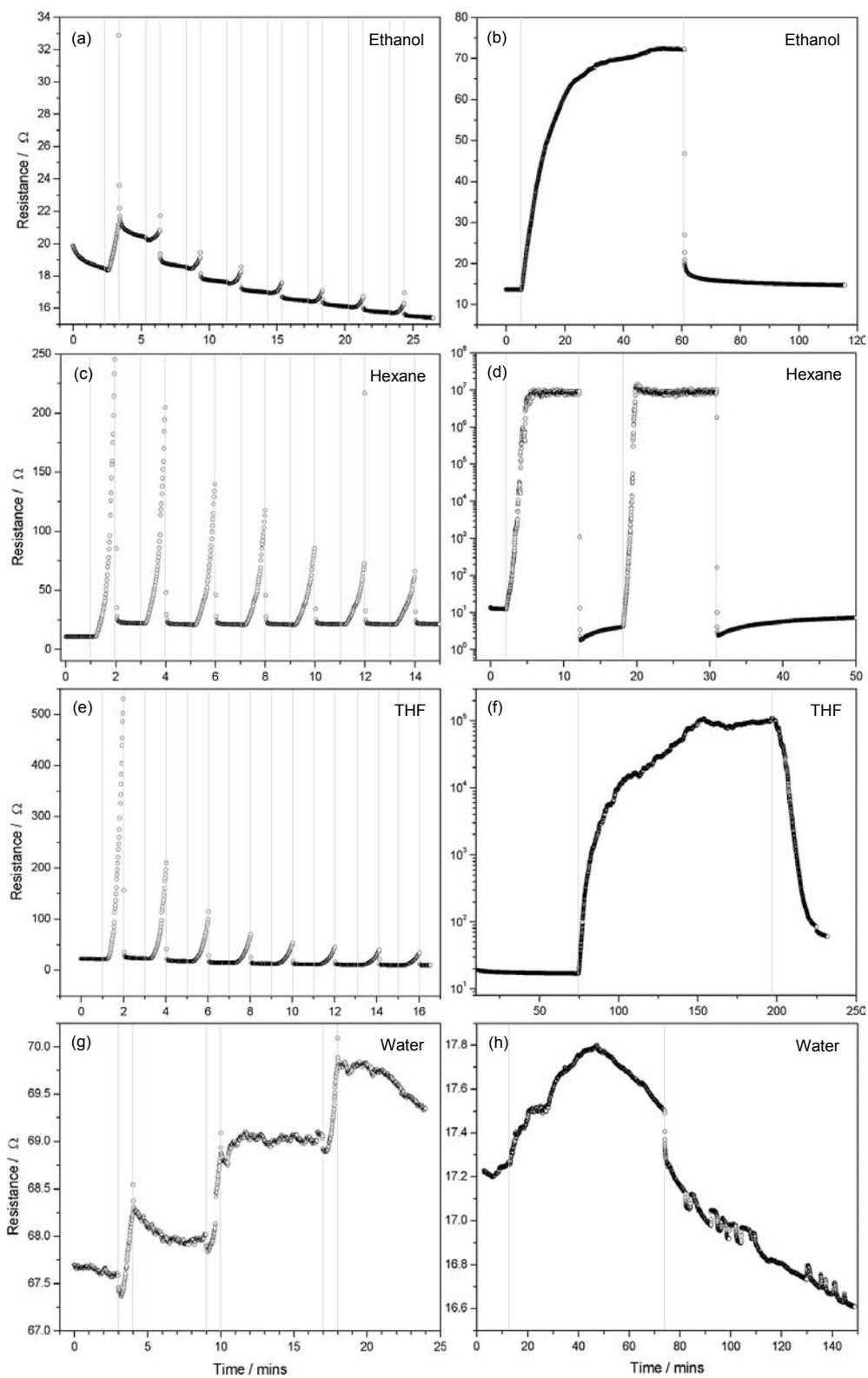
Fig. 10.5: *Response of silicone QTC granules to repeat 1 minute (left)*
and long (right) exposures to different solvent vapours at 100% SVP
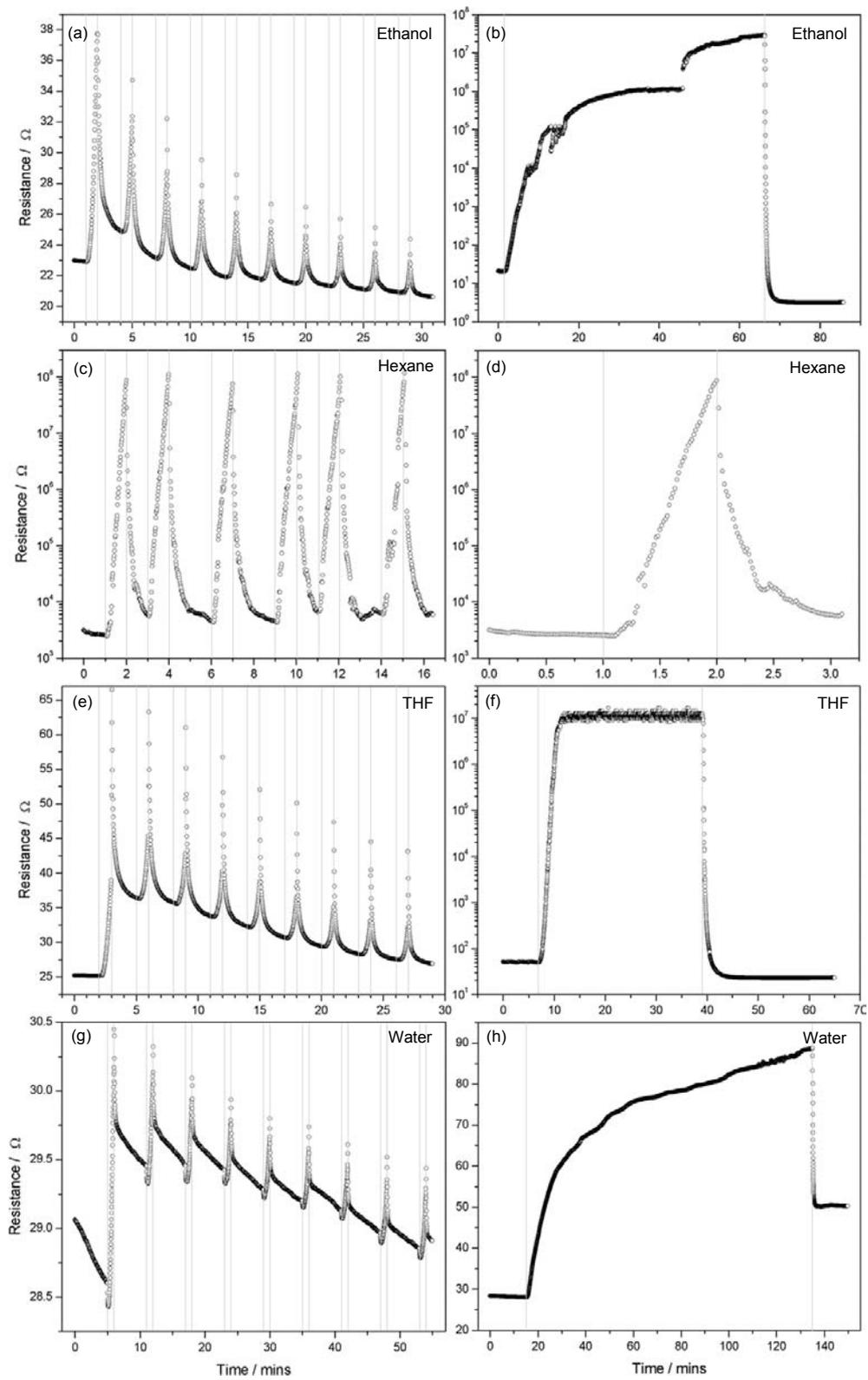
Fig. 10.6: *Response of poly(urethane) QTC granules to repeat 1 minute*
(left) and long (right) exposures to different solvent vapours at 100% SVP
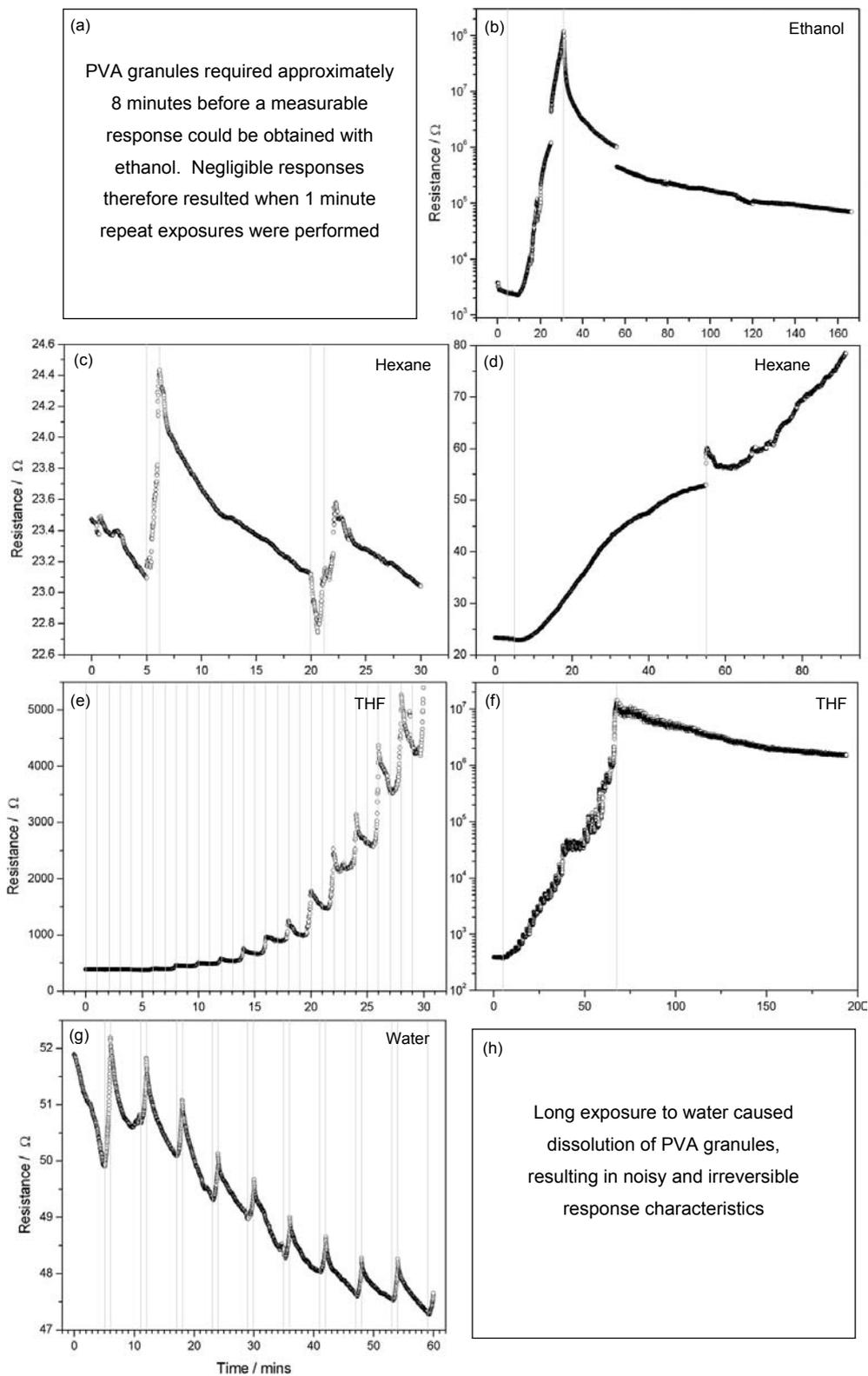
Fig. 10.7: *Response of PVA QTC granules to repeat 1 minute (left) and long (right) exposures to different solvent vapours at 100% SVP*

174
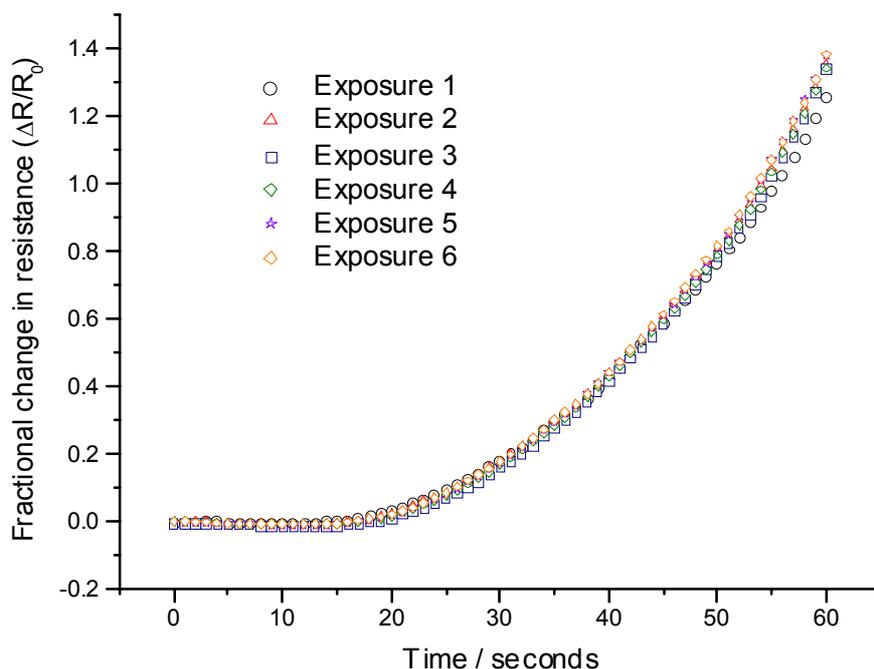
Fig. 10.8: *Example of fractional change in resistance plotted for multiple overlying responses. Data is for silicone granules subjected to 1 minute exposures of THF vapour at 88 (± 7) % SVP at 25°C, or 552.9 (± 39.1) ppm*

Figures 10.5 to 10.7 represent typical results to exposures, however more data was recorded than is shown in the graphs. For each polymer-solvent combination, many exposures were carried out, and an average fractional response ($\Delta R / R_0$) could be calculated. Figure 10.8 shows typical overlying fractional responses for repeat exposures of THF to silicone QTC granules. Similar plots were also generated for all other polymer-solvent combinations. The average fractional responses were recorded at 30 seconds, 1 minute and also at saturation, when, during long exposures, resistance ceased to change. These average fractional responses for all the combinations tested are shown in table 10.2.

	Silicone	Poly(urethane)	PVA	Poly(butadiene)
Ethanol	30s: $1.14\times10^{-3} \to 4.40\times10^{-2}$ 60s: $3.63\times10^{-2} \to 0.251$ Saturation: 6.3	30s: 0.167 60s: 0.811 Saturation: 1.2×10^{6}	30s: 3.02×10^{-2} 60s: 9.67×10^{-2} Saturation: $> 4.8\times10^{4}$	*No measurable response*
Hexane	30s: 4.47 60s: 27.2 Saturation: $> 7.5\times10^{8}$	30s: 281 60s: $> 4.5\times10^{4}$ Saturation: $>> 4.5\times10^{4}$	30s: 1.19×10^{-2} 60s: 3.16×10^{-2} Saturation: 1.6	*No measurable response*
THF	30s: $0.192 \to 4.72$ 60s: $0.731 \to 71.6$ Saturation: 6.3×10^{3}	30s: 9.80×10^{-2} 60s: 0.897 Saturation: 3.7×10^{5}	30s: $6.22\times10^{-2} \to 1.81$ 60s: 3.95 Saturation: $> 3.3\times10^{4}$	*No measurable response*
Water	30s: $0 \to 1.54\times10^{-3}$ 60s: $4.99\times10^{-3} \to 9.83\times10^{-3}$ Saturation: 3.1×10^{-2}	30s: 0 60s: $8.7\times10^{-3} \to 5.5\times10^{-2}$ Saturation: 2.15	30s: 0 60s: $1.0\times10^{-2} \to 3.8\times10^{-2}$ Saturation: -	*No measurable response*

Table 10.2: *Summary of fractional responses ($\Delta R / R_0$), after exposures of 30 seconds, 1 minute and long exposures, for different QTC polymer–solvent combinations*
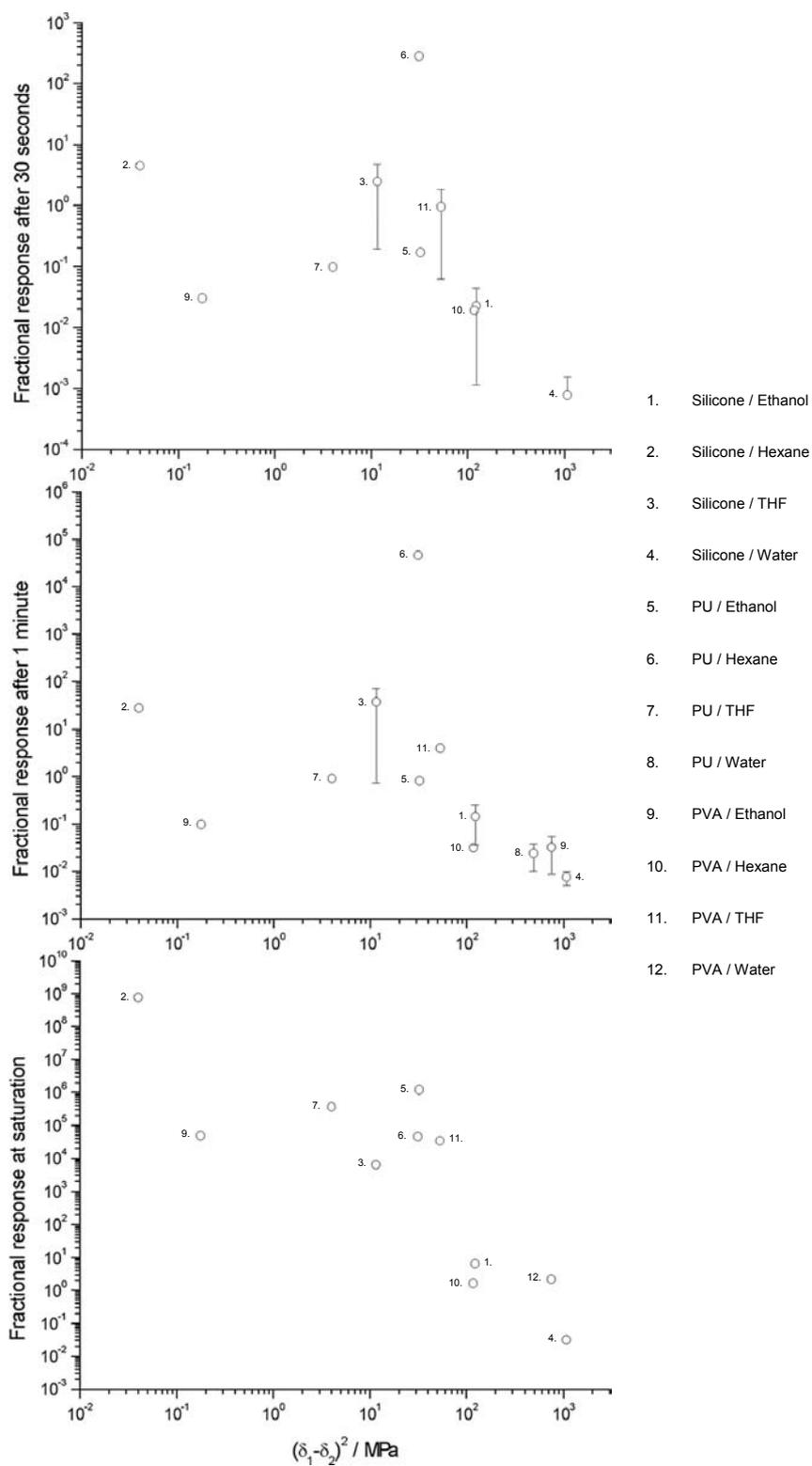
Fig. 10.9: *Correlation of the square of the difference between polymer and solvent solubility parameters with the fractional response at (a) 30 seconds, (b) 1 minute and (c) saturation*

177

Poly(butadiene) data is not present in figures 10.5 to 10.7 nor in table 10.2 and figure 10.9. This is because poly(butadiene) yielded negligible responses for all four test vapours. The polymer is reported to have excellent resistance to a wide variety of organic and inorganic solvents, including strong inorganic acids. The polymer is also resistance to hydrolysis, and is hydrophobic and non-polar. The poor response of poly(butadiene) QTC granules to solvent vapour is therefore to be expected.

Certain polymer-solvent combinations, with large response magnitudes, increased their resistance to values beyond the limiting resolution of the multimeter. In such cases, the resistance appears to suddenly reach a point of saturation at 10^7 Ω, the maximum detection limit for the device. It is important to note that for these examples, seen in figures 10.5(d), 10.6(d) and 10.6(f), the maximum equilibrium response at saturation may be considerably larger than is shown. The fractional response in table 10.2 is therefore quoted as being greater than this corresponding limiting value. Resistance measuring equipment with a wider range of detection is required to observe the full dynamic range of these large response combinations. It is also important to note that response magnitudes of this scale have not been previously reported, except for metal-polymer composites at loadings very close to the critical percolation threshold and for samples actually immersed into liquid baths of a highly miscible solvent [24] [121] [124-129] [131].

Theory suggests that the general trend of response magnitudes can be predicted from the solubility parameters of the respective solvents and polymers. Specifically, if solubility parameters of both the polymer (δ_1) and the solvent (δ_2) have values that are close to one another, then polymer swelling is highly likely. Conversely, if the difference between δ_1 and δ_2 is

large, the combination should produce minimal swelling response. Figure 10.9 plots $(\delta_1 - \delta_2)^2$ against the fractional response for each of the polymer-solvent combinations used in this experiment. Logarithmic scales have been used for convenience, due to the extremely wide range of the data. Three graphs can be seen, representing the responses after exposures of 30 seconds, 1 minute and at saturation. No strong trendline appears to be present on any of the three graphs. However, it can be clearly seen that a correlation between the horizontal and vertical axes does exist, especially for the data at saturation in figure 10.9(c). There is a general grouping from top-left to bottom-right. Simple error analysis shows that error margins are large (typical margins are shown, where appropriate), and so a strong trendline is not to be expected. The deviations and noise within the data arise from many sources. These include inexact solubility parameter data for the specific polymers used, lack of repeatability for specific polymer-solvent combinations, and by inconsistent electrical responses caused by fluctuating temperatures. The correlation is a match to that predicted by theory, that similar solubility parameters give rise to large amounts of swelling. We can therefore conclude that polymer swelling is indeed the predominant transduction mechanism for changes in QTC resistance when exposed to solvent vapours.

The control experiment, where raw nickel 123 powder was exposed to saturated THF vapour, yielded negligible responses after 1 hour of exposure. The result implies that any resistance changes occurring for QTC granules exposed to THF vapour are due exclusively to a polymer-solvent interaction. Any electrochemical effects that may occur between the solvent and the surface of nickel particles are therefore considered negligible. Although not tested with other solvents, it is likely that this is also the case for all of the vapours tested.

Response to ethanol

The fastest and biggest response to ethanol vapour during 1 minute exposures was achieved using poly(urethane) QTC granules. Both silicone and poly(urethane) displayed very rapid recoveries under purging, even after prolonged exposure. PVA granules also gave very large responses during long exposures (possibly due to the polar nature of both PVA and ethanol), but were far slower to react, requiring at least 8 minutes before any observable change could be seen. It is for this reason that no graph is present for 1 minute exposures in figure 10.7(a). PVA was also less efficient in its ability to remove ethanol during purging. This is probably due to the strong affinity between the two species. This gives rise to increased levels of chemisorption and physisorption, which is harder to remove compared to solvent that simply diffuses into the polymer.

Both poly(urethane) and silicone display a decreasing baseline drift. This is the most common type of drift seen in these vapour sensing experiments, and is most almost certainly caused by trap-filling effects within the QTC, as described earlier within this thesis. Nevertheless, the drift observed for ethanol exposures is consistent and predictable, giving rise to consistent and repeatable responses. Examples of baseline drift correction can be seen later in this section.

Response to hexane

Hexane exposures gave rise to probably the largest and fastest acting responses of all, with silicone and poly(urethane) granules quickly reaching the limit of detection for the multimeter within 2 minutes and 1 minute respectively. Hexane results also show improved baseline stability compared to ethanol, caused by improved removal during purging. Such efficient purging is likely to be caused by an exclusively diffusion driven

process. Hexane is therefore probably less attracted to sorption sites within poly(urethane) and silicone than for example ethanol was in PVA.

Recovery was extremely fast for silicone granules, dropping over 6 decades in resistance within less than 5 seconds. Figure 10.5(d) also shows an unusual inverse recovery characteristic, which occurs only for hexane and silicone after long exposures. A similar overshoot in the recovery during purging has also been reported by Hopkins and Lewis [144] for carbon black filled poly(ethylene-co-vinyl acetate) (PEVA) exposed to the nerve agent dimethylmethylphosphonate (DMMP). The cause of the effect is unknown, but it only appears to occur when rapid recoveries are made from very large response magnitudes.

PVA gave a poor response to hexane. Repeat exposures were inconsistent, noisy and showed little repeatability. During long exposures, virtually no recovery was made during purging, implying that long-term damage had been sustained to the granules. Incomplete recovery appears to consistently occur for PVA granules, and is probably due to the fact that the PVA used had very little, or no cross-linking. Solvents would therefore tend to dissolve the polymer rather than cause swelling, thus causing non-reversible sensing characteristics.

Response to THF

THF also shows extremely large and rapid responses with both silicone and polyurethane granules. During 1 minute exposures, silicone reacts faster than poly(urethane), reaching a higher resistance. However, it takes 2 hours to saturate at only 10^5 Ω. Poly(urethane) reacts slightly less quickly than silicone during 1 minute exposures, but in 5 minutes reaches a much larger

saturation resistance of greater than 10^7 Ω. However, poly(urethane) and silicone respond more slowly with THF, compared to exposures of hexane.

The response of PVA to long exposures of THF was also large, reaching 10^7 Ω after approximately 1 hour. Recovery during purging however was incomplete. 1 minute exposures showed very small responses and, once again, incomplete recovery. Dissolution of the polymer is therefore considered likely. The large response after long exposures is therefore misleading due to the permanent damage caused to the granules.

Response to water

Responses to water were small for all the QTC granules tested. This is often a desired characteristic for an electronic nose system, as vapour sensing must give consistent results, regardless of daily humidity fluctuations. Silicone granules appeared to be the most weakly interacting polymer with water, giving rise to the noisiest data, with very slow recovery rates. Poly(urethane) once again displayed the smoothest and most repeatable responses, whilst PVA gave rise to the largest response. This might be expected because of PVA's solubility in water. However, the lack of cross-linking in the PVA granules became apparent again, when long exposures to water were performed. The data was noisy, irreversible and impossible to quantify, implying that the water was beginning to dissolve the polymer.

Common features

The response to water in figure 10.6(g) shows a characteristic that is common to many polymer-solvent combinations. Upon the start of the exposure, resistance often initially falls slightly before rapidly rising as swelling occurs. It would appear that a second mechanism is competing against the predominant effect of polymer swelling, and is attempting to

cause a slight increase in conductivity. The fall in resistance is small and appears to be relatively independent of solvent concentration. It is therefore unnoticeable wherever the subsequent response is very large or fast reacting. Figure 10.10 illustrates this effect more clearly, for 3 repeat 1 minute exposures of silicone granules to THF. The experiment was performed using THF vapour at a slightly reduced concentration, in order to reduce the rate of swelling and to emphasise the initial negative response effect.
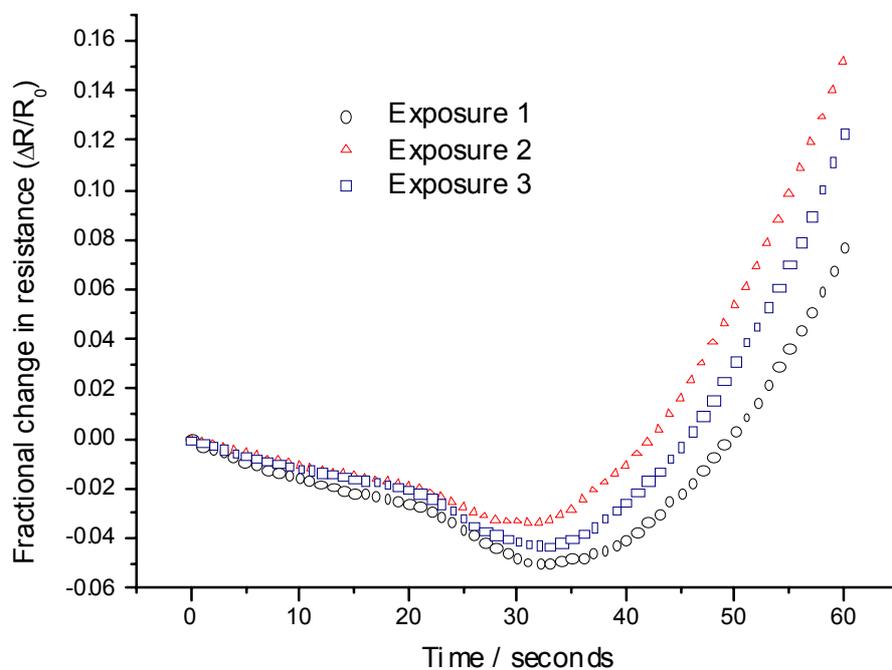
Fig. 10.10: *Example of initial negative response at start of exposure.*
Data is for silicone granules exposed to THF
at 60 (± 7) % of SVP at 25 °C., or 377.0 (± 26.7) ppm

The cause of this unusual initial negative response is uncertain. Initially, flow rate differences between purge (high flow rate) and exposure (low flow

rate) lines were thought to be responsible. However, it was quickly realised that upon exposure, the granules experience a drop in pressure. This would therefore result in a resistance increase, rather than the observed decrease.

Another explanation may be due to static charge, which may accumulate on the surface of the non-conducting regions of polymer granules. As the solvent passes through these granules, it may pick up some of this static charge (especially if the solvent is highly polar), and transport it towards the upper electrode. The charge then is deposited at the electrode as the solvent vapour passes through it, thus increasing the observed current (i.e. decreasing the electrical resistance) flowing through the circuit. However, this process is dependent upon the bias of the electrodes. If the reverse bias was applied, charged species collected by the solvent would no longer be attracted to the upper electrode, and the above effect would not occur. Connections to the multimeter were made with no preference to polarity, resulting in random bias throughout all sensing experiments. However, initial negative responses are seen in nearly all polymer-solvent combinations, except for those with very large response magnitudes and extremely fast response times. The movement of static charge is therefore not considered to be a likely explanation for the cause of this effect.

A more likely mechanism for causing the unusual initial negative responses is provided as follows. As solvent vapour enters the sensor, it is quite likely that small quantities may condense on the surface of the QTC granules. The presence of this liquid within the sensor may improve the electrical conductivity, especially if a polar solvent is being used, enabling an ionic conduction mechanism to be established. Comparison of polar solvent responses compared with non-polar solvent responses would be an ideal way to test this hypothesis. However, analysis of the data proved to be inconclusive. Unfortunately, changing the solvent also changes the speed at

which swelling occurs, and therefore also affects the response curve. Comparisons are therefore very difficult to make, unless solvents can be sourced, with different polarities, but with identical swelling abilities.

Alternatively, solvent polarity may be unimportant in describing the cause of the effects in figure 10.10. Initial penetration of the solvent into the polymer may impart changes upon the dielectric properties of the QTC granules. This might then result in a slight increase in conductivity shortly after the beginning of exposures. However, as time progresses, solvent penetration continues and swelling processes begin to dominate, causing rapid increases in resistance.

Occasionally, at the end of a period of exposure, as the purge begins, a sharp spike is sometimes seen in the electrical response. This sudden rise in electrical resistance occurs only very briefly for approximately 1 second, and is thought to be a result of the different flow rates during purge and exposure. The flow of nitrogen in the purge line is at a considerably higher level than the flow rate in the exposure line. Consequentially, when purging begins, any remaining solvent that is still present in the tubing between the solenoid switch and the sensor is rapidly swept towards the sensor. The resistance suddenly rises as the solvent enters the sensor, followed by a rapid fall in resistance caused by the purge. To minimise this effect, the length of tubing between sensor and solenoid valve was shortened, reducing the quantity of solvent that is swept through at the start of the purge. The data presented in this chapter and the next were all taken using this shortened pipe. Alternatively, the purge and exposure flow rates could be set to equal values, but this would slow recovery rates, and experiments would take much longer to perform.

A common feature to nearly all multiple exposure experiments, regardless of the polymer or solvent used, is that the first exposure usually displays a larger response than subsequent exposures. A good example of this can be seen in figure 10.6(g) for poly(urethane) and water, and also in figure 10.11 for poly(urethane) and THF. When solvents and polymers are mixed together, the processes of chemisorption and physisorption occur simultaneously with the process of diffusion. Bonds are formed between solvent and polymer during chemisorption and physisorption, resulting in a stronger and more permanent binding compared to the wholly reversible process of diffusion. Diffusion will occur whenever a concentration gradient is present, and is therefore constant throughout all exposures. However, chemisorption and physisorption will preferentially occur when sorption sites are vacant. Therefore, during the first exposure, many of these sorption sites will become filled, reducing further chemisorption and physisorption during later exposures, and resulting in diminished responses.

Alternatively, large responses and incomplete recovery during the first exposure could be due to a mechanical polymer ageing effect. During the first exposure and purge cycle, the polymer swells and then relaxes. The state into which the polymer relaxes may be one that has less free volume than before, thus restricting the response in subsequent exposures. Similar mechanical hysteresis has been observed in QTC before [90]. Bulk QTC samples often require a little mechanical exercising to soften the polymer before repeatable pressure sensitivity can be obtained. It is therefore thought that the vapour sensing and polymer swelling equivalent of this effect is being observed in this experiment.

Baseline drift is a common characteristic of many vapour sensors, including those made from QTC. The effect appears to be more problematic when larger currents are passed through the composite, and is therefore likely to

be due to trap-filling effects within the QTC. Lower compressions are therefore found to reduce this problem. Unfortunately, raising the initial resistance in this way has the detrimental effect of limiting the maximum dynamic range of resistance measurement. However, drift can often be compensated for, providing that it occurs in a smoothly predictable manner. To demonstrate this, figure 10.11 shows how a baseline drift function can be subtracted from the repeat exposure to THF data from figure 10.6(e), to produce results with improved repeatability. The baseline drift function was calculated by a best fit to data points taken at the end of each purge cycle.
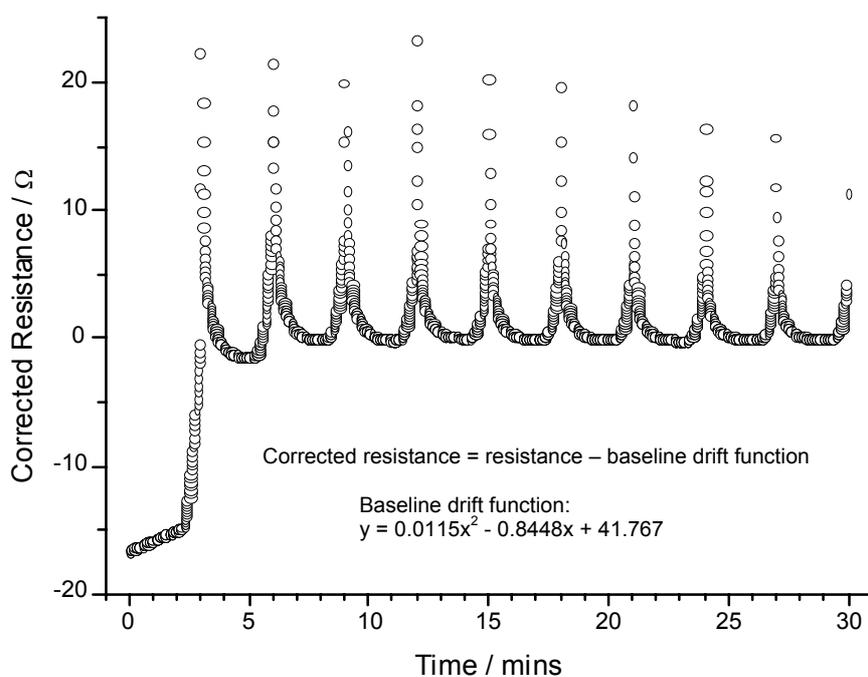
Fig.10.11: *Correction of THF-poly(urethane) response data by subtraction of a quadratic baseline drift function*

Figure 10.11 was created using a quadratic baseline drift function, however in other examples, a linear function is often sufficient. Figure 10.12 shows

linear baseline drift corrected data for a second set of THF exposures to poly(urethane) granules. The results show that by use of simple baseline drift corrections, where necessary, highly repeatable response characteristics can be obtained for a QTC vapour sensor.
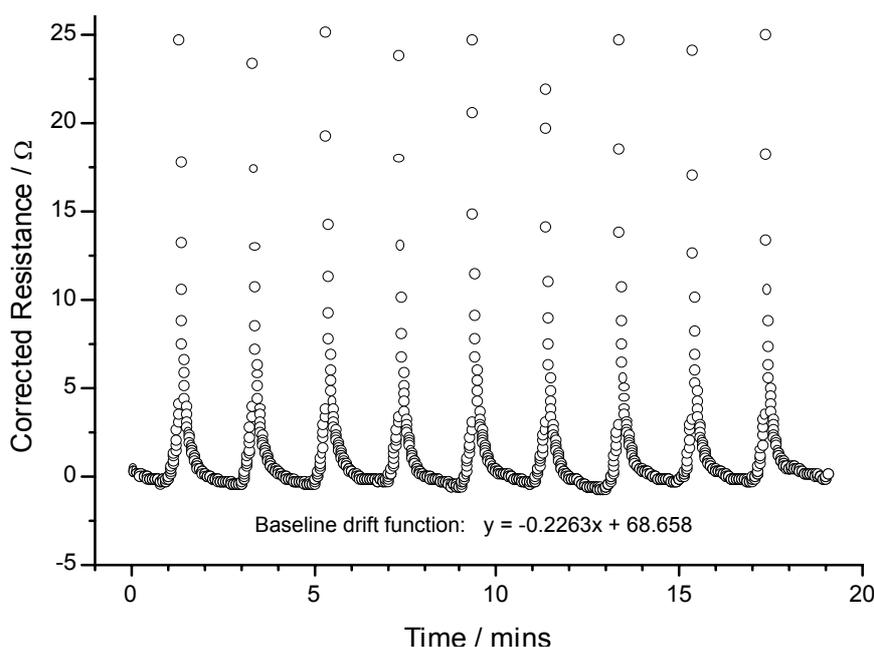
Fig.10.12: *Correction of THF-poly(urethane) response data by subtraction of a linear baseline drift function*

Flory-Rehner theory suggests that swelling in QTC will be restricted by the application of a compressive force. Larger changes in resistivity, and therefore improved detection limits are therefore likely if compression within the sensing unit is reduced. In addition, as previously mentioned, low levels of compression give rise to high baseline resistances, which will minimise trap-filling and baseline drift effects. Low compressions are therefore recommended for improved performance in future experiments.

10.4 Conclusions

When QTC is exposed to saturated organic solvent vapours, electrical resistance is shown to vary strongly with a wide variety of response times and response magnitudes.

Response magnitudes vary from the very large (resistance changes and fractional changes greater than 10^8 for silicone and hexane) down to virtually negligible responses for poly(butadiene). In the particular example of poly(butadiene), exposures to all vapours proved that this particular variety of polymer is unusually resilient to solvent attack. Wide-ranging differential responses are observed across the combinations of solvents and polymers tested, indicating excellent potential for QTC to be used in an array-based vapour detector, or electronic nose. The particularly large and rapid responses for certain vapours show potential for low concentration sensing applications, where signals become greatly reduced

In general, response magnitudes appear to follow the behaviour predicted by their corresponding solubility parameters. Large responses tend to result when solubility parameter differences are small, and poor responses result when solubility parameters differ by large amounts. This indicates that resistance changes in QTC are predominantly caused by a polymer swelling transduction mechanism, as predicted.

Repeat exposures showed that for virtually all experiments, the response magnitude of the first exposure was usually larger than that of subsequent exposures. In addition, first exposures sometimes displayed incomplete recovery, and improved in later exposures. It is thought that during the first exposure, both diffusion and sorption processes are responsible for swelling and resistance changes. Chemisorption and physisorption processes are

comparatively harder to remove, and thus occur less frequently in later exposures, when fewer sorption sites are available. Later exposures instead rely solely upon the reversible process of diffusion to provide swelling, and thus the results show improved recovery and repeatability.

Some polymer-solvent combinations, react very slowly, requiring several minutes to respond, whereas others display changes in resistance that span more than six orders of magnitude within only two minutes of exposure. Similarly, recovery times under purging are also widely varying, with some recovering totally within a few seconds, to some that display virtually no recovery whatsoever. Such variation in response and recovery times may therefore also be used to extract additional qualitative information.

In the specific combination of saturated hexane vapour with silicone QTC granules, unusual recovery characteristics result during purging. Recovery is extremely rapid, reducing back to its baseline value within only a few seconds. However, resistance appears to overshoot this baseline value, and then display an inverse recovery upwards, back towards the baseline. The cause of this strange recovery characteristic is unknown, and only occurs for this specific solvent-polymer combination where the response and recovery is particularly large and rapid. A similar effect has been reported elsewhere by another author [144], following another large and rapid response from a nerve agent exposed to carbon black-filled PEVA. The unique response could be used to provide additional information for qualitative sensing applications.

An unusual response characteristic that occurs immediately after exposure begins is observed for nearly all polymer-solvent combinations. Initially, the resistance appears to fall by a few percent of its starting value, before rapidly rising as swelling occurs. The cause of this effect is uncertain,

although it appears to be independent of concentration, and no obvious connection with either polymer or solvent type has yet been identified. It is possible that static charge on the surface of QTC grains may be swept through the sensor, thus assisting in conduction. However, a more likely mechanism is that the dielectric and conductive properties of the composite are improved, caused by the presence of liquid condensed on the surface or sorbed within the composite. A more detailed investigation into this effect could be carried out by comparing polar and non-polar solvents and their influence upon this initial drop in resistance.

Based upon the data presented in this experiment, it can be concluded that both silicone and poly(urethane) QTC granules show excellent potential for use in vapour sensing tasks. Repeatability is good, and response magnitudes are large when exposed to vapours of ethanol, hexane and THF. Responses to water are small, indicating low sensitivity to variations in humidity. It has also been demonstrated that correction for baseline drift can easily be made by simple subtraction of a drift function from the data.

PVA granules show some potential for vapour sensing tasks, but responses are generally smaller than those observed for silicone and poly(urethane). Unfortunately, PVA displays irreversible changes in resistance caused by dissolution of the polymer in the solvent, especially when the solvent is highly polar. This was due to the low level of cross-linking within the specific variety of PVA used. Future experiments could obtain improved recovery characteristics by increasing the quantity of cross-linking.

It is recommended that future vapour sensing experiments be performed using minimum compression to the QTC sample. The result of this should not only enhance electrical responses, but also minimise baseline drift. Future sensing experiments could also be performed upon other forms of

QTC. The bulk form of the material, for example, when made into thin film samples, would make an ideal sensing element. Such bulk samples would also allow the use of tensile forces to generate the required intrinsic conductivity, thus enhancing swelling further. However, replacing QTC granules with thin-film bulk QTC samples decreases the effective sensing surface area and may therefore compromise sensor performance.

11 Sensitivity of QTC to chemical vapours of differing concentrations

11.1 Introduction

In order for a vapour sensor to display quantitative sensing abilities, the sensitivity of the device must first be characterised. The sensitivity of a vapour sensor is defined by the degree of change in response when exposed to a chemical vapour of differing concentrations. The gradient of a plot of sensor response against analyte concentration is usually used to illustrate this. Ideally, the relationship between these two variables should be linear, although responses will vary for different polymer-solvent combinations. Linearity is not strictly necessary, providing that a consistent and reliable functional trend exists between the two variables, enabling the quantity of analyte to be easily calculated.

11.2 Experimental

Sensitivity experiments were all carried out using the same vapour sensing apparatus described earlier in chapter 10. QTC granules were compressed to approximately 20 Ω and allowed to relax at this compression for a minimum of 15 minutes before exposures began. In each experiment 3g of granules with particle sizes in the range of 152 to 300 μm were used.

Initially, an experiment to characterise sensitivity was carried out on silicone (Alfasil 153) QTC granules (filled with type 287 nickel powder). The experiment used a test vapour of THF at room temperature, using only nitrogen dilution as a method of lowering concentration. Total flow rate through the sensor was maintained at 50 ml min^{-1}, but the relative

proportions flowing through bubbler and diluent lines were changed. In this early test, only three flow rate combinations were tried:

50 ml min^{-1} bubbler, 0 ml min^{-1} diluent: 100 % SVP at 25 °C or 628.3 ppm
40 ml min^{-1} bubbler, 10 ml min^{-1} diluent: 80 % SVP at 25 °C or 502.6 ppm
30 ml min^{-1} bubbler, 20 ml min^{-1} diluent: 60 % SVP at 25 °C or 377.0 ppm

For each concentration, multiple repeat exposures were performed upon a fresh sample of granules, and the resulting responses recorded. The average fractional response ($\Delta R / R_0$) after 1 minute of exposure was then calculated for each concentration, enabling a plot of sensitivity to be produced. In this early experiment, a manual switch valve was used to direct the flow of gas towards the sensor, compared to the solenoid valve detailed in figure 10.2.

Sensitivity data was improved by inclusion of a low temperature circulator bath, into which the solvent bubbler flasks were placed. This introduced greater temperature stability of the solvents. The concentrations of test vapours could now be changed by adjustment of two experimental parameters. Dilution of the vapour with nitrogen provided a concentration range of 2 to 100 % of SVP. Additionally, use of the low temperature bath enabled refrigeration of the solvents to temperatures as low as –30 °C. This reduced solvent vapour pressure and therefore also the amount dissolved in the nitrogen carrier gas. By combining these two variables, concentrations down to 0.8 ppm (approximately 0.1 % of SVP at 25 °C) could be achieved, depending upon solvent type. See Appendix B for calculation details.

In an attempt to further reduce sources of error, an automated solenoid valve was used, replacing the manual switch used in the original test experiment. The number of exposures performed at each concentration could now be

increased to between 30 and 50, with 5 minutes high pressure (2 bar) nitrogen purging between exposures. Data was recorded at as many as 30 different solvent concentrations, and the average fractional response at each concentration after 1 minute was again calculated. In order to reduce data analysis times, a Matlab script was programmed to help extract the relevant data within the original text file, and then to calculate average fractional responses. At each concentration, the experiment was repeated, this time exposing the granules to a single long exposure. Once a saturated equilibrium response had been obtained, the fractional response was also recorded. This enabled two sensitivity plots to be obtained, one for exposures of 1 minute, and one for long exposures.

Polymer-solvent combinations were chosen according to their response size and repeatability. Based upon these considerations, two were chosen: silicone (Silastic T4) with hexane, and poly(urethane) (Techsil F42) with THF. Both granule types used type 123 nickel powder. Sensitivity data for 1 minute exposures and long exposures were collected for both.

11.3 Results and discussion

Results for the initial test experiment for the sensitivity of silicone QTC granules to different concentrations of THF vapour can be seen in figure 11.1. The expected general trend of increasing response with increasing solvent concentration is observed. Unfortunately, this early experiment proved insufficient to enable confident fitting of the data. Error margins, calculated from standard deviations of the multiple responses, are too large, and data points too few. Large error margins were largely caused by fluctuations in temperature due to the lack of control. This affected vapour pressures, which in turn generated uncertainties in concentrations and also deviations in the response. In addition, exposure timings were fairly

inaccurate, as a manual switch valve was used instead of an automated solenoid valve. The experiment was therefore halted after data had been recorded at only 3 concentrations.
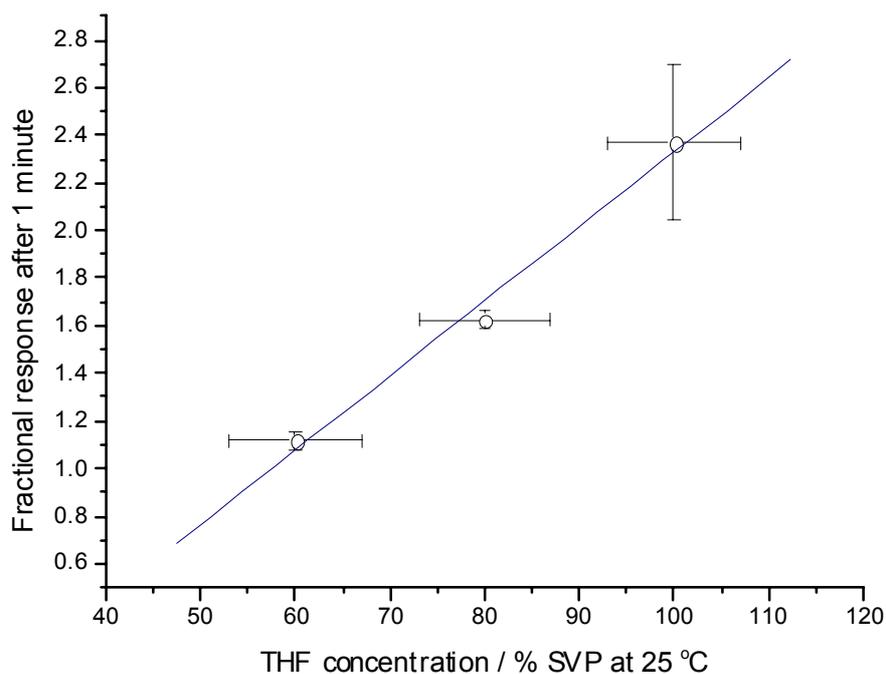
Fig. 11.1: *Sensitivity of silicone QTC granules to THF vapour*
(experiment performed with no temperature control)

Sensitivity of poly(urethane) QTC granules to THF

Temperature control and repeatability were improved greatly by the introduction of the low temperature circulator bath. In addition, by upgrading the manual valve to an automated motorised solenoid valve, consistent exposure timings over many exposures could be achieved more easily. Typical results, showing good repeatability, for 30 repeat 1 minute exposures of THF to poly(urethane) granules are shown in figure 11.2.
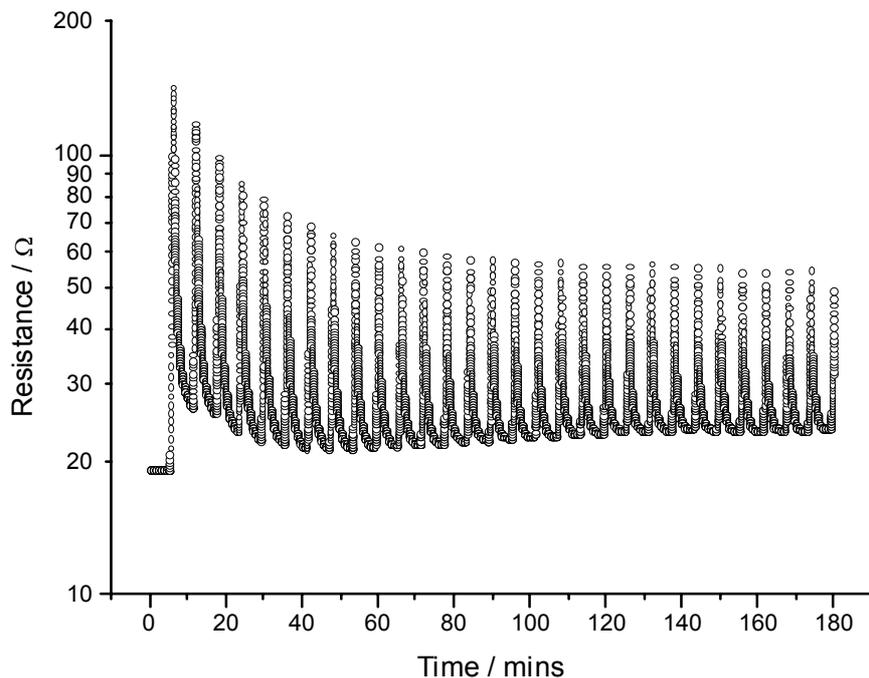
Fig. 11.2: *Typical responses to 30 repeat 1 minute exposures. Data is for poly(urethane) granules exposed to THF at 159 ppm or 26 % SVP at 25 °C (10 °C, 25 ml min^{-1} bubbler line, 25 ml min^{-1} diluent line)*

The sensitivity of poly(urethane) QTC granules using 1 minute repeat exposures to THF is presented in figure 11.3(a). Logarithmic axes have been used so that low concentration and low signal data can be more easily identified. Error margins for each data point were calculated from the standard deviation of the fractional responses during multiple exposures. As can be seen in figure 11.2, multiple exposures improve in repeatability for later exposures. Sensitivity results were therefore also plotted using only data taken from the last 15 exposures at each concentration (figure 11.3(b)). By doing this, error margins are reduced, and tighter grouping of the data into a more linear trend results. However, improvements still need to be made if accurate quantitative analysis is to be performed with this sensor.
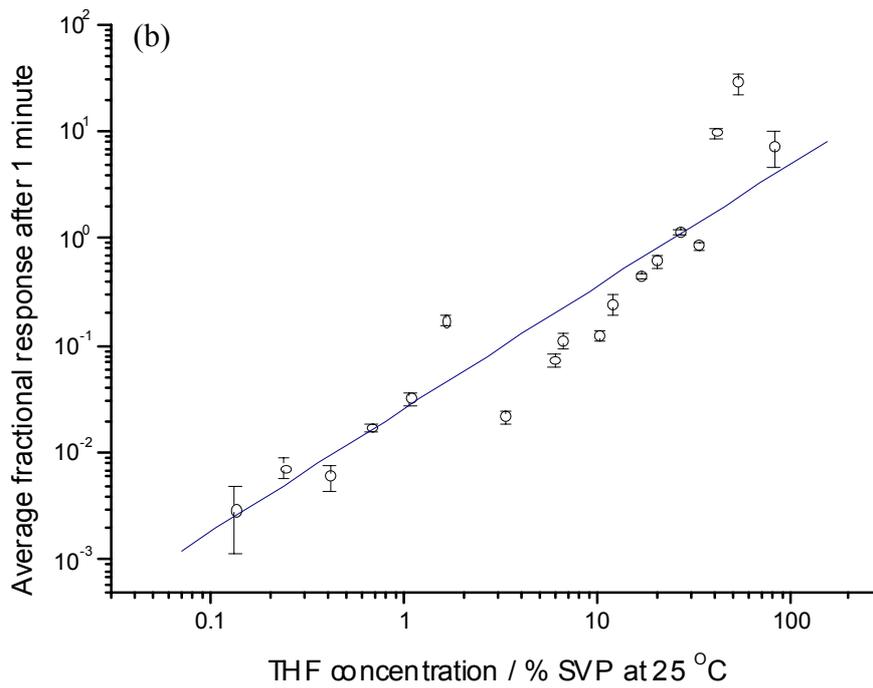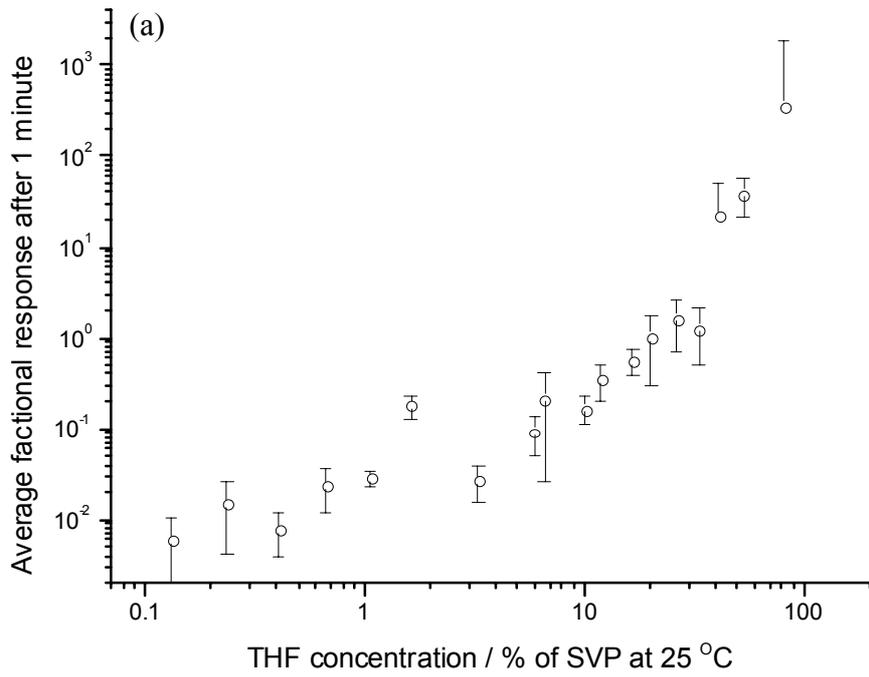
Fig. 11.3: *Sensitivity of poly(urethane) QTC granules*

for 1 minute repeat exposures to THF vapour, using data from

(a) all exposures, and (b) last 15 exposures only
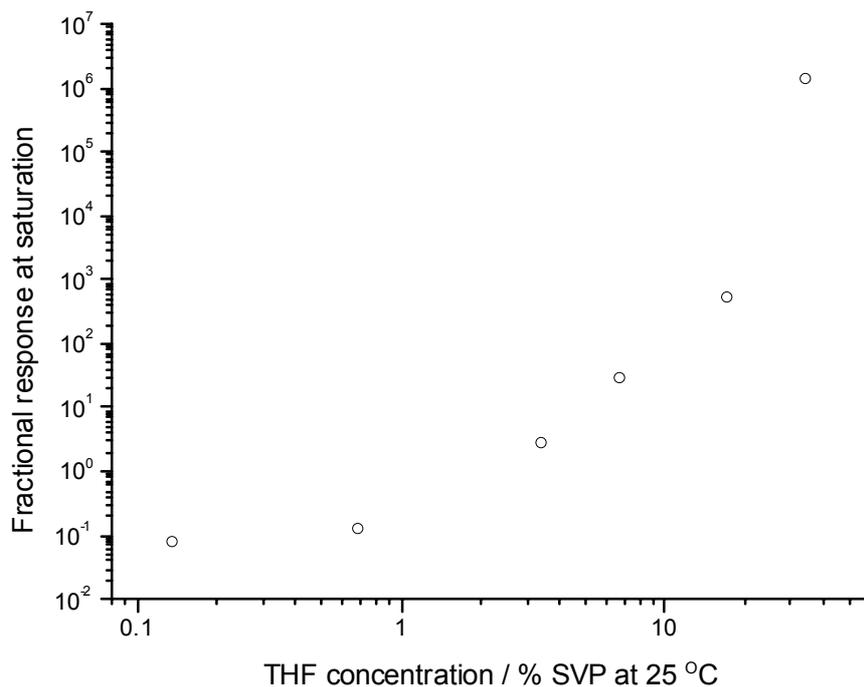
Fig. 11.4: *Sensitivity of poly(urethane) QTC granules*
for long saturating exposures to THF vapour

Sensitivity data for long exposures of THF to poly(urethane) QTC granules can be seen in figure 11.4. In this graph, only single exposures were used for each data point. This was due to the limited quantity of granules available. Error margins therefore cannot be calculated from standard deviations of multiple exposures. The number of data points is also not as large as those seen for 1 minute exposures. This was partly due to the fact that for long exposures at concentrations greater than approximately 30 % of SVP at 25 °C, responses exceeded the range measurable by the Keithley multimeter. The data for these points on the sensitivity plot is therefore not included. In addition, only a limited supply of these QTC granules was available, preventing further experimental analysis.

The sensitivity results for long exposures of THF to poly(urethane) QTC granules show a clear curved trend of increasing fractional response with increasing concentration. A well defined response such as this shows good potential for the use of long exposures to perform quantitative analysis. However, repeat experiments must be performed to ensure the repeatability of this data.

It is interesting to compare the sensitivity trends for long exposures with those obtained for 1 minute exposures. Clearly, larger responses are to be obtained if vapour is sampled for longer periods of time. However, closer inspection of the trends within figures 11.3 and 11.4 implies that at lower concentrations, greater sensitivity (defined by the gradient of the graph) can be obtained by sampling for only 1 minute. In comparison, at higher concentrations, larger gradients and greater sensitivity occur when long exposures are carried out. However, one must also consider that at extremely low concentrations, responses may be too small to detect within 1 minute sampling times, and may therefore require a longer exposure. To obtain maximum sensitivity at these low levels, it is therefore recommended to expose the sensor for a shortest length of time possible before signal to noise ratios become unacceptable.

The cause of the flattening of the sensitivity curve at low concentrations for long exposures gives rise to some interesting ideas of low concentration polymer-solvent interactions, which may not have been previously considered. The flattening (which is considerable when one takes into account the logarithmic axes upon which the graph has been plotted) implies that at very low concentrations, the degree of swelling eventually becomes constant, providing that exposures are performed over long enough sampling times. This is clearly an unusual observation, and is probably controlled by factors not incorporated within the solubility parameter, which

has been calculated based upon swelling measurements at much higher concentrations. Diffusion processes contribute less at low concentrations. In addition, after long exposures, the polymer will have had plenty of time to relax and to accommodate the solvent. Perhaps the polymer has even reached a point of limiting relaxation, unable to expand to contain any more solvent, regardless of small concentration changes. Consequentially, at low concentrations, the swelling mechanism is perhaps no longer driven by thermodynamic mixing requirements, but has instead reached a physisorption and chemisorption saturation limit. This limit would be based upon the specific intermolecular interactions of the polymer and solvent in question, and indeed may not even exist for some combinations. However, closer inspection of the sensitivity at low concentrations is required before any conclusions can be made.

Sensitivity of silicone QTC granules to hexane

Sensitivity plots for silicone QTC granules and 1 minute exposures of hexane vapour can be seen in figure 11.5. Repeatability of these responses between subsequent exposures was more difficult to obtain with the silicone-hexane combination compared to poly(urethane)-THF. Baselines were also less stable. The result is increased noise within the sensitivity plot. Additionally, repeatability showed little improvement after multiple exposures had been performed, unlike poly(urethane) with THF. A second sensitivity plot for the last 15 exposures is therefore not included in figure 11.5. Instead, to improve results, a greater number of experiments at different concentrations were performed.

Again, the expected trend of increasing response at higher concentrations is observed for silicone granules exposed to hexane. However, the range of response magnitudes is slightly smaller than is observed for poly(urethane)

with THF over the same concentration range. This implies that in general, the sensitivity of silicone granules with hexane is slightly lower than the sensitivity of poly(urethane) granules with THF. More combinations must be tested before a full understanding can be obtained of how sensitivity varies between polymer and solvent varieties.
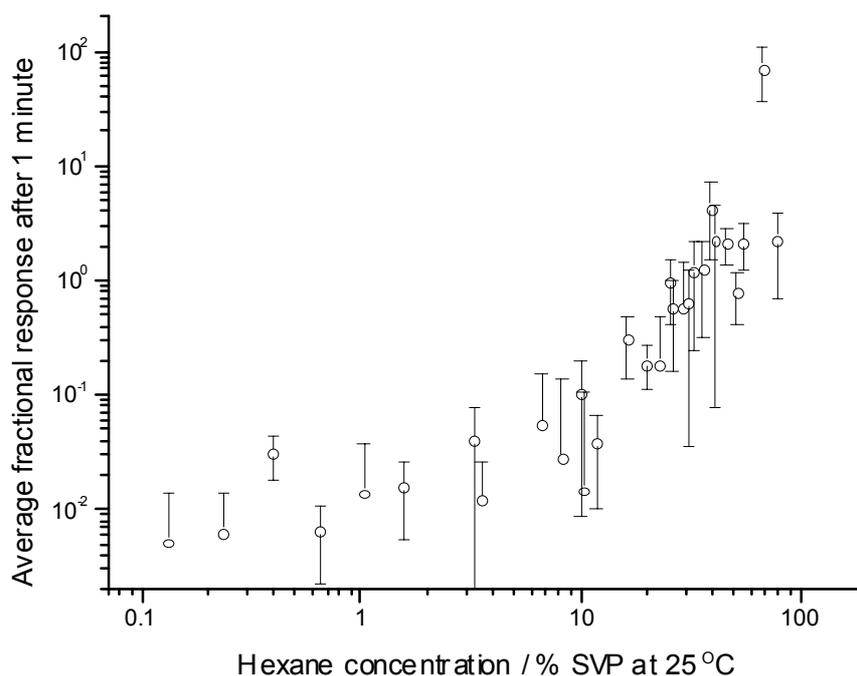
Fig. 11.5: Sensitivity of silicone QTC granules
for 1 minute repeat exposures to hexane vapour

Figure 11.6 shows sensitivity data taken for long exposures of hexane to silicone granules. Again, the data is noisier than that obtained for poly(urethane) with THF. Repeat exposures and additional concentrations would reduce the spread of the data, but again could not be performed due to the limited quantity of granules available.
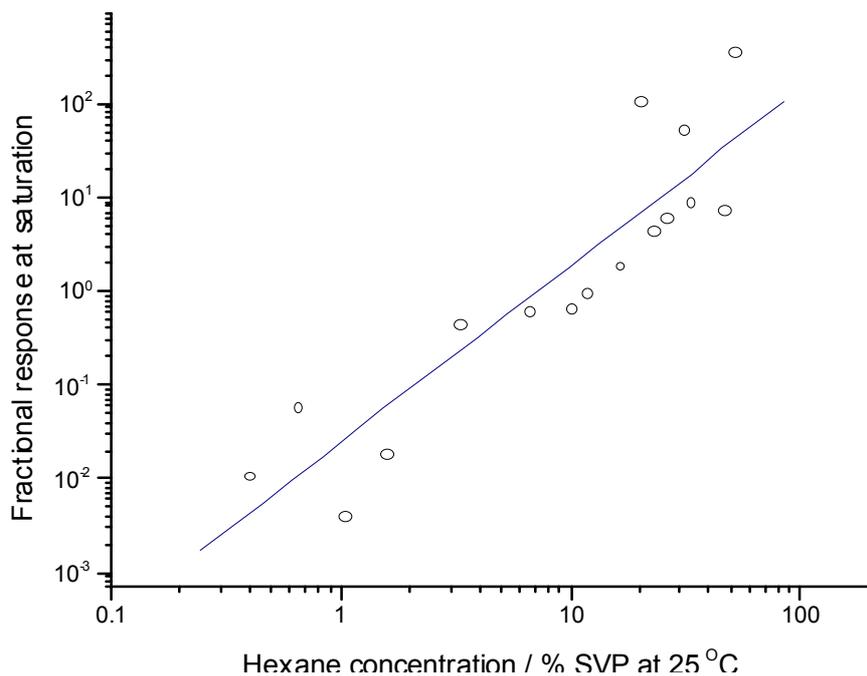
Fig. 11.6: *Sensitivity of silicone QTC granules*
for long saturated exposures to hexane vapour

Comparison of figures 11.5 and 11.6 shows increased linearity in the case of long exposures, compared to 1 minute exposures. This is the reverse result to that obtained for poly(urethane) with THF. Closer inspection of the gradients of figures 11.5 and 11.6 show similar sensitivity at low concentrations, displaying, in both cases, an increase in the fractional response by approximately a factor of ten, within the range 0.1 to 1 % of SVP at 25 °C. This implies that at low concentrations, long sampling and 1 minute sampling both show similar sensitivities. The unusual low concentration effects seen for poly(urethane) and THF are therefore not occurring in the same way for silicone and hexane. However, at high concentrations, 1 minute exposures of hexane to silicone granules clearly show improved sensitivity over long exposures.

11.4 Conclusions

QTC granules made from silicone and poly(urethane) both show wide ranging response magnitudes over changing concentration levels of hexane and THF vapour respectively. Responses considerably above the background noise level are observed down to concentrations as low as 0.8 ppm (0.13 % of SVP at 25 °C), indicating good low concentration detection ability. Modification of the present vapour sensing equipment, so that lower concentrations can be attained, is required, if the lower limit of detection is to be determined.

Repeat multiple exposures show good repeatability. This improves as the number of exposures increases, but sometimes at the expense of signal size. Although repeat results are sometimes noisy, clear trends of increasing response size with increasing concentration can be seen. With additional experiments and further improvements to repeatability, full characterisation of the sensitivity of QTC granules to chemical vapours could be achieved. With appropriate development, QTC therefore shows good potential for use as a quantitative tool in vapour sensing.

Improvements to the sensor could be made in a number of different ways. Increasing the flow rate of vapours passing through the sensor will increase response time, generating larger responses after 1 minute exposures. Lower concentrations may therefore be able to be detected. However, increasing the flow rate will not affect the results obtained for long exposures. Reducing the sensing volume of QTC granules would also have the effect of reducing response and recovery times. Percentage swellings might remain the same, which may mean that little change in the fractional change in resistance would result. However, this is uncertain. Smaller volumes may also affect other factors such as baseline stability or repeatability. It would

also cause saturation of the sensor to occur far sooner than for larger quantities of granules. A new sensing apparatus is currently under development, which has a cylindrical sensing volume of approximately 3mm diameter by 1mm. In addition, multiple versions of this sensor are being made, allowing array-based sensing to also be studied. Future QTC vapour sensing research will be able to compare responses obtained using this miniature sensor with those obtained in this thesis.

The combination of poly(urethane) and THF showed slightly improved sensitivity to concentration changes compared to silicone and hexane. Poly(urethane) granules also showed improved sensitivity to low concentrations of THF using exposures of 1 minute compared to long exposures. Conversely, at higher concentrations, longer sampling times provide greater sensitivity. However, when choosing sampling times, one must also consider that response magnitudes decrease at low concentrations.

For long exposures, poly(urethane) and THF showed a flattening out of the sensitivity curve at low concentrations. This implies that the response undergoes a tendency towards concentration independency at very low concentrations. Long relaxation times may cause deviation away from thermodynamically driven polymer-solvent interactions. Swelling therefore reaches a sorption limited response, beyond which resistance does not change. It is uncertain if this effect has previously been observed due to the difficulty in studying such small polymer expansions. QTC materials may therefore provide a new tool for researching polymer-solvent interactions at very low concentrations.

Silicone granules exposed to low concentrations of hexane vapour showed little difference in the sensitivity obtained using either long or short exposures. However, at higher concentrations, sensitivity was improved by

sampling over 1 minute exposures compared to long exposures. This is the opposite trend to that observed for poly(urethane) and THF, and highlights the different interactions that occur in different polymer-solvent combinations.

12 Polymer-solvent interaction kinematics

12.1 Introduction

In chapter 8 it was described how the penetration of solvent vapour into the volume of a polymer can follow either Fickian or non-Fickian kinetics. Fickian kinetics assume that polymer-solvent mixing is dominated by a constant, but slow, diffusion rate, and that elastic relaxation of the polymer is comparatively fast. The result is that the observed mass change (Δm) of the polymer will increase linearly with $t^{1/2}$, where t is the time. Conversely, non-Fickian kinetics are dominated by very rapid diffusion rates and comparatively slow polymer relaxation rates. Extreme cases of systems such as these display linear increases in mass with t. Intermediate values for the exponent of t represent anomalous diffusion.

It is desirable to characterise the kinematic response of QTC to solvent vapours. This will enable a better understanding of the dominating factors controlling swelling and resistance change within the composite, and will therefore facilitate the maximisation of the potential of QTC as a vapour sensing element. Experiments are therefore performed to record the mass uptake of vapour into a QTC sample during a typical exposure.

12.2 Experimental

The same vapour sensing apparatus, as described in section 10.2, was used to expose QTC samples to solvent vapours. Long exposures of room temperature saturated solvent vapours at flow rates of 50 ml min^{-1} were used in order to maximise mass uptake responses.

The QTC sensor was mounted upon a Status Balances digital balance, capable of recording mass changes as low as approximately 1 mg. However, resolutions of approximately 10 mg were more normally achieved. This limit to experimental accuracy derived from a lack of efficient vibration isolation. In addition, weight measurement was slightly compromised by the inlet and outlet piping, which extended from the sensing unit. Mass readings were recorded manually at approximately 30 second intervals, using a stopwatch as a guide.

To maximise signal to noise ratios, polymer-solvent combinations were chosen that displayed large changes in electrical resistance, and therefore also absorbed large quantities of solvent. Two combinations were chosen, one displaying rapid swelling, and one displaying a slow response. This was to test the full range of kinematic responses observed within QTC. PVA granules with ethanol was chosen for the slowly responding combination, whilst poly(urethane) and THF was chosen as the combination with a rapid response. In both cases, solvent vapours were at 100 ($\pm$ 7) % SVP at 25°C, corresponding to 146.3 ($\pm$ 10.3) ppm for ethanol and 628.3 ($\pm$ 44.4) ppm for THF. In all mass uptake experiments, 3g of QTC granules were used.

12.3 Results and discussion

Earlier electrical response data for PVA QTC granules exposed to ethanol suggest that this combination results in a slow but steady polymer swelling process. Long diffusion times are therefore expected, resulting in plenty of time for polymer relaxation. It is therefore likely that a Fickian trend will be observed in the corresponding mass uptake characteristics.

208

Mass uptake characteristics for PVA granules exposed to room temperature saturated ethanol vapour are presented in figure 12.1. After approximately 1 minute of exposure, a linear response in the change in mass with $t^{1/2}$ results, indicating Fickian diffusion. This trend continues for approximately 30 minutes, at which point an unusual but more rapid rise in mass increase is observed. Finally, after approximately one hour, the change in mass reaches a horizontal limit. At this point the polymer has become saturated with solvent, and has experienced an overall mass increase of about 17 %.
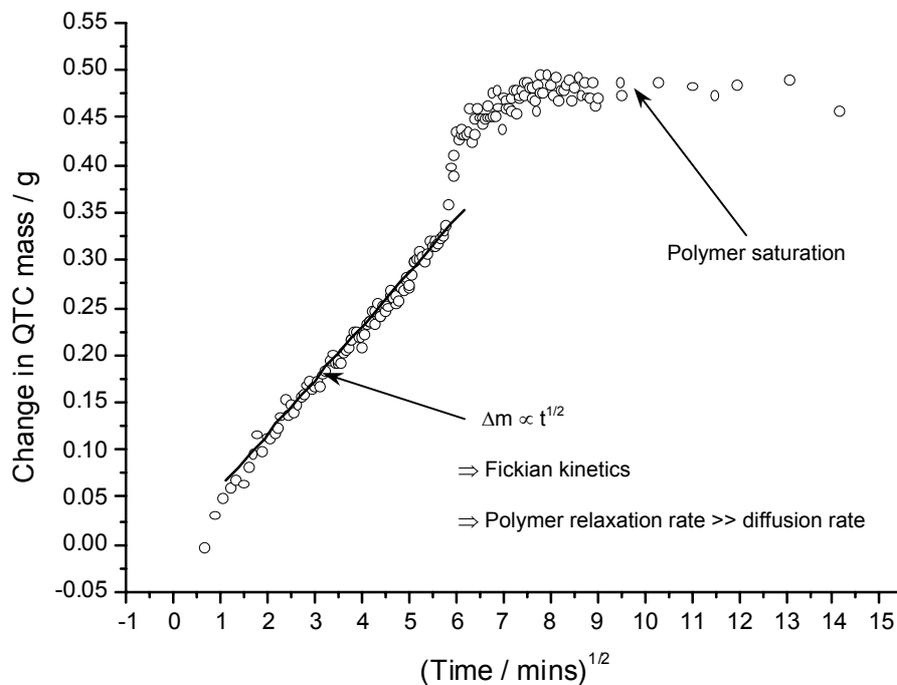
Fig. 12.1: *Mass uptake characteristics for 3g PVA QTC granules exposed to ethanol vapour, showing Fickian diffusion kinetics*

Deviations away from Fickian kinetics are displayed in two small regions of the mass uptake characteristics for PVA and ethanol. Mass uptake is more

209

rapid during the first minute of the exposure, and also for approximately 10 minutes just before saturation occurs. It is likely that for the first minute, polymer-solvent interaction mechanisms are dominated by surface adsorption, and therefore will reflect slightly different mass uptake characteristics to later periods when solvent begins to penetrate into the bulk of the polymer.

The later unusual period of rapid mass increase between approximately 30 and 40 minutes is more difficult to explain. Saturation of the polymer may have begun to occur in some regions of the polymer, but not others, giving rise to a change in diffusion gradients within the composite, and therefore also to the mass uptake characteristics. Some dissolution of the PVA may also have occurred at this point, giving rise to the change in mass uptake characteristics. Alternatively, the anomaly may simply be caused by a vibration and movement of the sensing equipment on the digital scales, or perhaps by a temperature change. However, the latter seems unlikely considering the speed at which the temperature change would need to occur. Repeat experiments under more controlled environmental conditions are required to see if this anomaly occurs consistently.

Figure 12.2 shows mass uptake characteristics for poly(urethane) QTC granules exposed to room temperature saturated THF vapour. Figure 12.2(a) shows the data plotted using time (t) on the x-axis, whilst figure 12.2(b) is plotted against $t^{1/2}$. Neither of the two plots display linear trends, deviating either side of linearity in both cases. Anomalous diffusion is therefore occurring for this polymer-solvent combination, whereby the change in mass (Δm) is proportional to t^{β}, where β is an unknown dimensionless constant with a value between ½ and 1.
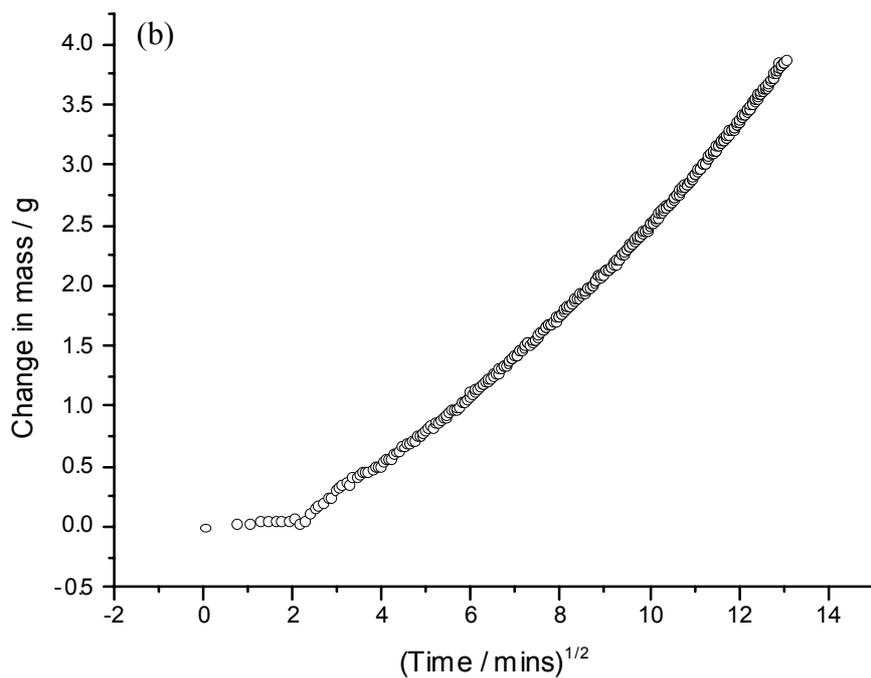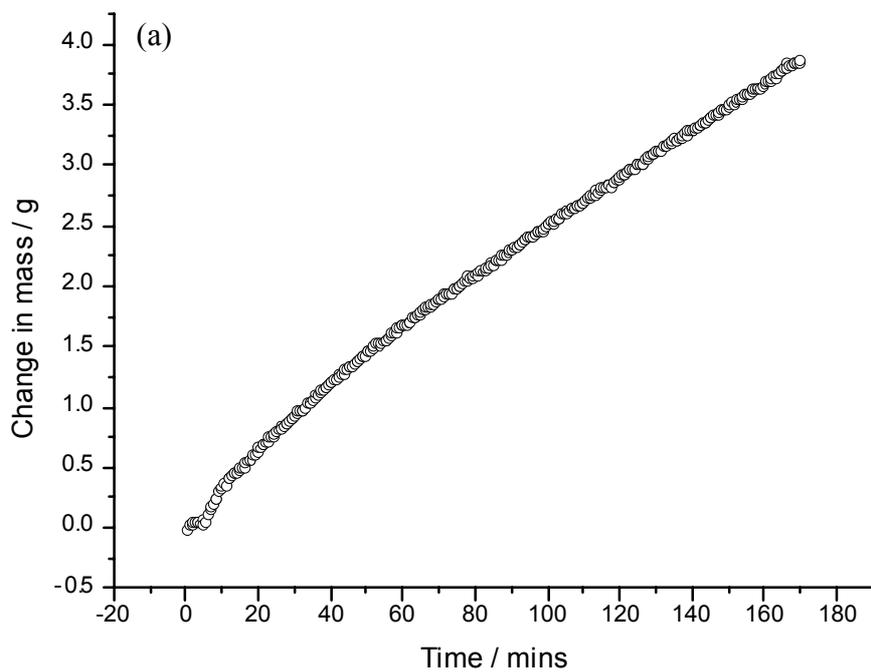
Fig. 12.2: *Anomalous diffusion mass uptake characteristics for 3g*
poly(urethane) QTC granules exposed to THF vapour,
plotted on x-axis scales of (a) t and (b) $t^{1/2}$

Once again, the initial part of the exposure displays different mass uptake characteristics to much of the rest of the exposure. Again, it is likely that surface adsorption kinetics dominate in this early region, followed by bulk absorption processes later in the exposure.

Logarithms of the data in figure 12.2 are taken and replotted in figure 12.3 in order that the unknown exponent, β, can be calculated from the gradient. Linear fitting deduced that β had a value of 0.817 (± 0.001), confirming that anomalous diffusion kinetics occur within the poly(urethane)-THF system.

Linear fit $\Rightarrow \Delta m \propto t^{\beta}$

Where $\beta = 0.817$ ($\pm$ 0.001)

$\Rightarrow$ Non-Fickian kinetics

$\Rightarrow$ Polymer relaxation rate < diffusion rate

Axes: $\log_{10}$(Change in mass / g) versus $\log_{10}$(time / mins)
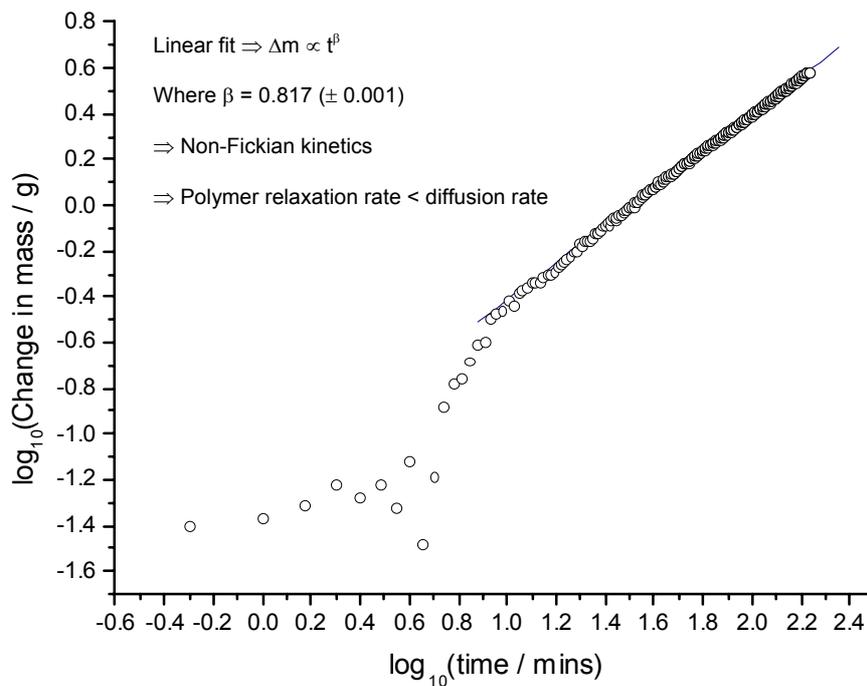
Fig. 12.3: *Log-log plot of mass uptake characteristics for poly(urethane) QTC granules exposed to THF vapour*

212

It is important to note the dramatic difference in the quantity of solvent absorbed in the two polymer-solvent combinations in this experiment. PVA QTC granules reached saturation within approximately 1 hour, having increased in mass by approximately 17%. However, poly(urethane) granules increased in mass by 133% within the same time period (approximately 3 hours), but still had not reached saturation. This large and rapid swelling corresponds well to the large and rapid increase in resistivity observed for the same combination in chapter 10, and further confirms that polymer swelling is indeed the transduction mechanism responsible for electrical responses to vapour in QTC.

12.4 Conclusions

Mass uptake characteristics have given preliminary insight into the kinetics of solvent penetration into QTC. Exposures of saturated ethanol vapour to PVA QTC granules displayed mass changes that were proportional to the square root of the time (i.e. $t^{1/2}$), indicating Fickian diffusion characteristics. Therefore, in this system, diffusion rates are slow and polymer relaxation is relatively fast. This concurs with electrical response data presented in chapter 10 for this polymer-solvent combination. In this system, saturation of the solvent into the polymer occurred after approximately 1 hour of exposure, resulting in a total polymer mass increase of approximately 17%.

Exposures of saturated THF vapour to poly(urethane) QTC granules resulted in far larger mass increases of approximately 60% within 1 hour, increasing to 133% in 3 hours. Saturation still had not occurred after this 3 hour exposure period, indicating a strong mutual affinity for this combination of polymer and solvent. Mass change increased linearly with t^β, where $\beta = 0.817$ ($\pm$ 0.001), indicating anomalous diffusion kinetics.

Deviation away from Fickian behaviour can be explained by the more rapid diffusion rates occurring within this polymer-solvent combination.

The strong agreement between mass uptake characteristics, diffusion rates and electrical responses is further evidence that QTC electrical responses to chemical solvent vapour are transduced via a polymer swelling mechanism.

13 Overall conclusions

A novel metal-polymer composite has been presented, made from combining silicone polymer with a micron-sized nickel powder. The composite is intrinsically electrically insulating, but displays a dramatic increase in conductivity when under compression. Contrary to conventional composites, the material also displays dramatic increases in conductivity under tension and torsion. This thesis has investigated multiple aspects of this novel composite's characteristics, including its microstructure, electrical response to compression and other electrical properties. Novel conduction mechanisms have been suggested based upon the results to above. This thesis has also investigated the potential of using the composite as a chemical vapour sensor, suitable for use in an artificial olfactory device, or electronic nose.

EDAX results show negligible impurities or contamination by other substances. Electron microscopy shows the distribution of nickel powder in the silicone polymer is random and homogeneous, and contains a low distribution of air voids. The nickel powder used to manufacture this composite consists of a uniquely spiky surface morphology, which is retained even after the mixing process. This is thanks to a patented low mechanical energy manufacturing technique. Use of higher mechanical energies or very high metallic loadings, generate larger amounts of friction and abrasion during the mixing process. This damages the spikes, resulting in composites with reduced electrical sensitivity to compression. It is therefore concluded that the spiky surface morphology of the nickel powder particles is crucial to the electrical conduction mechanism.

Electron microscopy also shows that the silicone polymer wets the nickel particles very effectively indeed. Thin layers of polymer persist on the surface of cryo-fractured samples, resulting in SEM image blurring. The consequence of this is that inter-particle contact between nickel grains in the composite is negligible, even at high loadings and compressions. Standard 'percolating' theories of electrical conduction therefore cannot apply.

Electrical characterisation experiments have shown current-voltage characteristics with highly unusual properties. Voltage sweeps generate non-linear changes in current, resulting in peaks, regions of negative differential resistance, hysteresis, time dependency and upward current drift. Conduction is due to a complex combination of mechanisms. Inter-particle conduction is thought occur by field emission and Fowler-Nordheim tunnelling processes, made possible by the strong localised electric field enhancements caused by the spikes on the nickel surfaces. A tunnelling process such as this gives rise to the extreme sensitivity to applied compression that this composite displays. Charge injection processes may be followed by scattering and thermalisation of electrons into trapping sites within the polymer, giving rise to the observed trap-filling and space-charge limited current effects.

On a more macroscopic scale, charge movement is controlled by electrostatic grain charging processes. As conduction occurs, grains charge and discharge, resulting in RF white noise emissions. Due to the random distribution of grains, some conduction channels will not be successful until larger voltages are applied. Therefore, until such a voltage is applied, grain charging occurs. Charge may build up to such an extent that the electric field generated by it may actually prevent charge movement in neighbouring conduction pathways. This electrostatic 'pinching' therefore causes currents to fall at high applied fields, and also to rise again when fields are lowered

and conduction pathways are reinstated. Grain charging is also the cause of electrical hysteresis between initial and repeat voltage sweeps. Under extreme circumstances of high compression and large applied fields, dielectric breakdown of the polymer may also sometimes occur.

Future investigative research into the conduction mechanisms within QTC should include low temperature conductivity measurements. Evidence of tunnelling, field emission, hopping, and many other potential conduction mechanisms could be identified from their characteristic temperature dependencies. However, experiments must be designed with care, as one must also consider the effects of expansion and contraction within the composite, and within the clamp required to compress or stretch the composite. Other areas of interest for future work include detailed analysis of RF emissions from the composite and the effect of applying a magnetic field to the system. Computer simulations of conduction within QTC would also be extremely useful to help test the above theories of charge transfer.

This thesis has also investigated the influence of a variety of chemical solvent vapours upon the electrical conductivity of QTC. A granular form of QTC was used for these experiments. This gave rise to a large surface area and also permitted gas and vapours to pass through the composite whilst it was being compressed, thus aiding response and recovery times. QTC granules were also made using a variety of different polymers, enabling differential responses to solvent vapours to be obtained.

Resistance change is caused by polymer swelling in the presence of solvent vapours. Metallic particle separation within the composite is therefore increased, resulting in a fall in conductivity. Resistance changes of over 6 orders of magnitude have been recorded for exposures of only 2 minutes or less. In comparison, some polymer-solvent combinations resulted in

negligible responses after exposures of several hours. Such a broad variety of response magnitudes and speeds shows great potential for QTC as a qualitative vapour sensor. Responses of different polymer and solvent combinations appear to follow the general trends predicted by their solubility parameters.

Quantitative analysis is also shown to be possible, as response magnitudes were found to increase as solvent concentration was raised. Significant signals were still obtained at concentrations as low as 0.8 ppm (0.13 % of SVP at 25 °C) indicating good potential for low concentration detection systems. The sensitivity at these levels also shows potential for QTC being used as a tool for studying polymer-solvent interactions at very low concentrations. The wide range of response magnitudes between low concentrations and saturated vapours implies that the sensitivity of QTC is very high. It is hoped that future experiments will investigate the minimum limit of detection for a QTC vapour sensor by performing exposures at even lower concentrations. Performance of the sensor may even be improved by use of low compressions or perhaps even samples in tension. In addition, flow rates could be raised and the sensing volume of QTC could be reduced, further increasing response and recovery times, and possibly also improving response magnitudes and signal to noise ratios.

Baseline drift of the QTC vapour sensor does sometimes occur and is caused by the simultaneously occurring processes of viscoelastic drift, trap filling and charge storage within both the polymer and the metallic grains. However this effect can be minimised by allowing relaxation to occur and by using low currents in sensing experiments. This would also have the added benefit of low power consumption in any commercial product. It has also been demonstrated that any remaining drift can usually be easily

corrected for by simple subtraction of either a linear or quadratic baseline drift function.

Mass uptake experiments, monitoring the quantity of solvent absorbed by QTC have also been performed. The two separate processes of surface adsorption and bulk absorption can be identified in these results, the former occurring within the first minute or two of exposure. Slow diffusion rates and fast polymer relaxation times indicated Fickian characteristics amongst the polymer-solvent combinations with the slowest responses. Anomalous diffusion occurred for fast penetrating and responding combinations. This is further evidence of polymer swelling as the transduction mechanism for electrical response in QTC vapour sensing experiments.

In summary, QTC materials show great potential in a wide variety of sensing applications. The unique structure of the material gives rise to an unusual combination of conduction mechanisms within the material, and is responsible for the extreme sensitivity to compression, tension and the presence of chemical vapours. Plenty of research clearly still needs to be undertaken before a full understanding of the electrical conduction mechanisms within QTC can be achieved. However, it is hoped that this thesis has begun to answer some of the questions raised about this remarkable material, and has also highlighted some of the commercial potential held by the composite.

14 Acknowledgements

The production of this thesis would not have been possible without the invaluable help and support of many of my friends, family and colleagues. I would like to use this opportunity to express my gratitude to them all.

I am especially grateful to those who have provided me with financial support throughout my postgraduate studies, namely the Engineering and Physical Sciences Research Council (EPSRC) and Peratech. I would particularly like to thank my industrial supervisor, David Lussey, the managing director of Peratech, who has supported me throughout my time on this project, and without whom, this unique composite and my research project would not even exist. I am also highly grateful to everyone else at Peratech for their assistance and in supplying me with the numerous QTC samples that I have used in my research. I would like to single out Dr. Paul Laughlin especially for his assistance in this area, and also for sharing with me his scientific expertise and experience in the field. I look forward to any future collaboration with Peratech with great enthusiasm.

From the Department of Physics at the University of Durham, I would like to thank Dr. Ken Durose and Andrew Yates for their time and assistance with all the electron microscopy work over the past few years. Thank you also to Prof. Andrew Monkmann and Dr. Joel Foreman for the use of their laser printer to print my thesis. Also from the Department of Physics, I would like to acknowledge the support of the many technical staff who work in both the electronics and mechanical workshops. In addition, I am very grateful to Duncan McCallum, Norman Thompson and David Pattinson for their technical assistance in obtaining and maintaining all of the laboratory equipment.

15 References

1.   Sancaktar, E. and N. Dilsiz, *Pressure-dependent conduction behaviour of various particles for conductive adhesive applications.* Journal of Adhesion Science Technology, 1999. **13**(6): p. 679-693.

2.   Zweifel, Y., C.J.G. Plummer, and H.-H. Kausch, *A microscopic investigation of conducting filled polymers.* Journal of Materials Science, 1998. **33**: p. 1715-1721.

3.   Ota, T., et al., *Control of percolation curve by filler particle shape in Cu-SBR composites.* Journal of Materials Science Letters, 1997. **16**: p. 1182-1183.

4.   Gokturk, H.S., T.J. Fiske, and D.M. Kalyon, *Effects of particle shape and size distributions on the electrical and magnetic properties of nickel/polyethylene composites.* Journal of Applied Polymer Science, 1993. **50**: p. 1891-1901.

5.   Rusu, M., N. Sofian, and D. Rusu, *Mechanical and thermal properties of zinc powder filled high density polyethylene composites.* Polymer Testing, 2001. **20**: p. 409-417.

6.   Abdel-Bary, E.M., *Factors affecting electrical conductivity of carbon black-loaded rubber: 1. Effect of milling conditions and thermal-oxidative aging on electrical conductivity of HAF carbon black-loaded styrene-butadiene rubber.* Journal of Polymer Science, 1977. **15**: p. 197-201.

7.   Balta Calleja, F.J., et al., *Conductive polycarbonate-carbon composites.* Journal of Material Science Letters, 1984. **3**: p. 165-168.

8.   Nasr, G.M., et al., *Material properties: On the percolative behaviour of carbon black-rubber interlinked systems.* Polymer Testing, 1999. **18**: p. 483-493.

9.   Sandler, J., et al., *Development of dispersion process for carbon nanotubes in an epoxy matrix and the resulting electrical properties.* Polymer, 1999. **40**: p. 5967-5971.

10.   Benoit, J.-M., *Transport properties of PMMA-carbon nanotubes composites.* Synthetic metals, 2001. **121**: p. 1215-1216.

11.   Davenport, D.E., *Metalloplastics - high conductivity materials.* Abstracts of Papers of American Chemical Society, 1980. **180**: p. 740-745.

12.   Abrantes, L.M. and J.P. Correia, *Polypyrrole incorporating electroless nickel.* Electrochimica Acta, 2000. **45**: p. 4179-4185.

13.   Cassignol, C., et al., *Microstructure-conductivity relationship in conducting polypyrrole/epoxy composites.* Polymer, 1999. **40**: p. 1139-1151.

14.   Calberg, C., et al., *Electrical and dielectric properties of carbon black filled co-continuous two-phase polymer blends.* Journal of Physics D: Applied Physics, 1999. **32**: p. 1517-1525.

15.   Kost, J., M. Narkis, and A. Foux, *Effects of axial stretching on the resistivity of carbon black filled silicone rubber.* Polymer Engineering and Science, 1983. **23**(10): p. 567-571.

16.   Hindermann-Bischoff, M. and F. Ehrburger-Dolle, *Electrical conductivity of carbon black-polyethylene composites. Experimental evidence of the change of cluster connectivity in the PTC effect.* Carbon, 2001. **39**: p. 375-382.

17.   Comella, T.M., *Elastomers that conduct electricity.* Machine Design, 1975: p. 60-63.

18.   Shahinpoor, M., et al., *Ionic polymer-metal composites (IPMCs) as biomimetic sensors, actuators and artificial muscles - a review.* Smart Mater. Struct., 1998. **7**: p. R15-R30.

19.   Nicholls, H.R. and M.H. Lee, *A survey of robot tactile sensing technology.* The International Journal of Robotics Research, 1989. **8**(3): p. 3-20.

20.   Snyder, W.E. and J. St. Clair, *Conductive elastomers as sensor for industrial parts handling equipment.* IEEE Transactions on Instrumentation and Measurement, 1978. **IM-27**(1): p. 94-99.

21.   Fu, Y., J. Liu, and M. Willander, *Conduction modelling of a conducting adhesive with bimodal distribution of conducting element.* International Journal of Adhesion and Adhesives, 1999. **19**: p. 281-286.

22.   Kathirgamanathan, P., *Unusual electromagnetic shielding characteristics of inherently conducting polymer-coated metal powder / polymer composites.* Journal of Materials Chemistry, 1993. **3**(3): p. 259-262.

23.   Wright, P.V., et al., *Progress in smart microwave materials and structures.* Smart Mater. Struct., 2000. **9**: p. 273-279.

24.   Tsubokawa, N., et al., *Responsibility of electric resistance of polyethyleneimine-grafted carbon black against alcohol vapour and humidity.* Polymer Bulletin, 1997. **39**(2): p. 217-224.

25.   Lonergan, M.C., et al., *Array-based vapour sensing using chemically sensitive carbon black-polymer resistors.* Chemical Materials, 1996. **8**: p. 2298-2312.

26.   Lussey, D. 1998, Peratech Ltd.

27.   Flandin, L., A. Hiltner, and E. Baer, *Interrelationships between electrical and mechanical properties of a carbon black-filled ethylene-octene elastomer.* Polymer, 2001. **42**: p. 827-838.

28.   Flandin, L., et al., *Effect of strain on the properties of an ethylene-octene elastomer with conductive carbon fillers.* Journal of Applied Polmer Science, 2000. **76**: p. 894-905.

29.   Shui, X. and D.D.L. Chung, *A new electromechanical effect in discontinuous-filament elastomer-matrix composites.* Smart Material Structure, 1997. **6**: p. 102-105.

30.   Strumpler, R. and J. Glatz-Reichenbach, *Conducting polymer composites.* Journal of Electroceramics, 1999. **3**(4): p. 329.

31.   Roldughin, V.I. and V.V. Vysotskii, *Percolation properties of metal-filled polymer films, structure and mechanisms of conductivity.* Progress in Organic Coatings, 2000. **39**: p. 81-100.

32.   Broadbent, S.R. and J.M. Hammersley, *Percolation processes.* Proceedings of the Cambridge Philsophical Society, 1957. **53**: p. 629-641.

33.   Sumita, M., et al., *Effect of melt viscosity and surface tension of polymers on the percolation threshold of conductive-particle-filled composites.* J. Macromol. Sci. - Phys., 1986. **B25**(1&2): p. 171-184.

34.   Wang, S.F. and A.A. Ogale, *Continuum space simulation and experimental characterization of electrical percolation behaviour of particulate composites.* Composites Science and Technology, 1993. **46**: p. 93-103.

35.   Flandin, L., et al., *A 3D numerical simulation of AC electrical properties of short fibre composites.* Journal of Polymer Science: Part B: Polymer Physics, 1999. **37**: p. 805-814.

36.   Connor, M.T., et al., *Broadband AC conductivity of conductor-polymer composites.* Physical Review B, 1998. **57**(4): p. 2286-2294.

37.   Flandin, L., et al., *Anomalous percolation transition in carbon-black-epoxy composite materials.* Physical Review B, 1999. **59**(22): p. 14349-14355.

38.   Flandin, L., et al., *AC electrical properties as a sensor of the microstructural evolution in nanocomposite materials: experiment and simulation.* Modelling Simul. Mater. Sci. Eng., 1999. **7**: p. 865-874.

39.   Lux, F., *Models proposed to explain the electrical conductivity of mixtures made of conductive and insulating materials.* Journal of Materials Science, 1993. **28**: p. 285-301.

40.   Bigg, D.M. and E.J. Bradbury, *Conductive polymeric composites from short conductive fibres.* Org Coat '80, 1980. **43**: p. 746-753.

41.   Celzard, A., et al., *Composites based on micron-sized exfoliated graphite particles: Electrical conduction, critical exponents and anisotropy.* Journal of Physics and Chemistry of Solids, 1996. **57**(6-8): p. 715-718.

42.   Krupa, I. and I. Chodak, *Physical properties of thermoplastic/graphite composites.* European Polymer Journal, 2001. **37**: p. 2159-2168.

43.   Mamunya, Y.P., et al., *Electrical and thermal conductivity of polymers filled with metal powders.* European Polymer Journal, 2002. **38**: p. 1887-1897.

44.   Kirkpatrick, S., *Percolation and conduction.* Reviews of modern physics, 1973. **45**(4): p. 574-588.

45.   Zekri, L., et al., *Statistical and scaling properties of the alternating-current conductivity in thin metal-dielectric composites.* Journal of Physics: Condensed Matter, 2000. **12**: p. 293-301.

46.   McLachlan, D.S., *An equation for the conductivity of binary mixtures with anisotropic grain structures.* Journal of Physics C: Solid State Physics, 1987. **20**: p. 865-877.

47.   Celzard, A., J.F. Mareche, and F. Payot, *Simple method for characterizing synthetic graphite powders.* Journal of Physics D: Applied Physics, 2000. **33**: p. 1556-1563.

48.   McLachlan, D.S., *Measurement and analysis of a model dual-conductivity medium using a generalised effective-medium theory.* Journal of Physics C: Solid State Physics, 1988. **21**: p. 1521-1532.

49.   McLachlan, D.S., *Analytical functions for the AC and DC conductivity of conductor-insulator composites.* Journal of Electroceramics, 2000. **5**(2): p. 93-110.

50.   Sixou, B. and J.P. Travers, *Simulation of the temperature dependence of the DC conductivity in granular systems with the effective medium theory.* Journal of Physics: Condensed Matter, 1998. **10**(3): p. 593-600.

51.   Yi, X.-S., G. Wu, and Y. Pan, *Properties and applications of filled conductive polymer composites.* Polymer International, 1997. **44**: p. 117-124.

52.   Youngs, I.J., *Exploring the universal nature of electrical percolation exponents by genetic algorithm fitting with general effective medium theory.* Journal of Physics D: Applied Physics, 2002. **35**: p. 3127-3137.

53.   Van Beek, L.K.H. and B.I.C.F. Van Pul, *Internal field emission in carbon-loaded natural rubber vulcanizates.* Journal of Applied Polymer Science, 1962. **6**(24): p. 651-655.

54.   Bridge, B., M.J. Folkes, and H. Jahankhani, *DC electrical conduction phenomena between two non-contacting stainless steel fibres in a polycarbonate matrix.* Journal of Materials Science, 1990. **25**: p. 3061-3066.

55.   Dani, A. and A.A. Ogale, *Electrical percolation behaviour of short-fibre composites: Experimental characterisation and modelling.* Composites Science and Technology, 1996. **56**: p. 911-926.

56.   Balberg, I., *Tunneling and nonuniversal conductivity in composite materials.* Physical Review Letters, 1987. **59**(12): p. 1305-1308.

57.   Balberg, I., *A comprehensive picture of the electrical phenomena in carbon black - polymer composites.* Carbon, 2002. **40**(139-143).

58.   Ezquerra, T.A., et al., *Memory and switching effects in polycarbonate-graphite composites.* Journal of Applied Physics, 1985. **58**(2): p. 1061-1063.

59.   Ezquerra, T.A., et al., *Alternating-current electrical properties of graphite, carbon-black and carbon-fibre polymeric composites.* Composites Science and Technology, 2001. **61**: p. 903-909.

60.   Gupta, A.K. and A.K. Sen, *Nonlinear DC response in composites: A percolative study.* Physical Review B, 1998. **57**(6): p. 3375-3388.

61.   Jager, K.-M., et al., *Electron transport and ac electrical properties of carbon black polymer composites.* Journal of Physics D: Applied Physics, 2001. **34**: p. 2699-2707.

62.   Radhakrishnan, S., *Effect of fillers on the electrical conduction in polymers: Theory of internal conduction mechanism.* Polymer Communications, 1985. **26**: p. 153-157.

63.   Sherman, R.D., L.M. Middleman, and S.M. Jacobs, *Electron transport processes in conductor-filled polymers.* Polymer Engineering and Science, 1983. **23**(1): p. 36-46.

64.   Van Beek, L.K.H. and B.I.C.F. Van Pul, *Non-ohmic behaviour of carbon black-loaded rubbers.* Carbon, 1964. **2**: p. 121-126.

65.   Miyauchi, S. and E. Togashi, *The conduction mechanism of polymer-filler particles.* Journal of Applied Polymer Science, 1985. **30**: p. 2743-2751.

66.   Celzard, A., et al., *Conduction mechanisms in some graphite-polymer composites: Effects of temperature and hydrostatic pressure.* Journal of Applied Physics, 1998. **83**(3): p. 1410-1419.

67.   Sichel, E.K., J.I. Gittleman, and P. Sheng, *Transport properties of the composite material carbon-poly(vinyl chloride).* Physical Review B, 1978. **18**(10): p. 5712-5716.

68.   Sheng, P., E.K. Sichel, and J.I. Gittleman, *Fluctuation induced tunnelling conduction in carbon-polyvinylchloride composites.* Physical Review Letters, 1978. **40**(18): p. 1197-1200.

69.   Sheng, P., *Fluctuation-induced tunnelling conduction in disordered systems.* Physical Review B, 1980. **21**(6): p. 2180-2195.

70.   Paschen, S., et al., *Tunnel junctions in a polymer composite.* Journal of Applied Physics, 1995. **78**(5): p. 3230-3237.

71.   Kim, G.T., et al., *Non-ohmic current-voltage characteristics in single-wall carbon nanotube network.* Synthetic Metals, 2001. **117**: p. 123-126.

72.   Mehbod, M., et al., *Temperature dependence of the resistivity in polymer-conducting-carbon-black composites.* Physical Review B, 1987. **36**(14): p. 7627-7630.

73.   Pike, G.E. and C.H. Seager, *Electrical properties and conduction mechanisms of Ru-based thick-film (cermet) resistors.* Journal of Applied Physics, 1977. **48**(12): p. 5152-5169.

74.   Isayeva, O.B., et al., *Properties of electron field emission from a fractal surface.* Solid-State Electronics, 2001. **45**: p. 871-877.

75.   Lampert, M.A. and P. Mark, *Current injection in solids.* Electrical Science, ed. H.G. Booker and N. DeClaris. 1970, New York & London: Academic Press. 351.

76.   Pope, M. and C.E. Swenberg, *Electronic processes in organic crystals and polymers.* 2nd ed. Monographs on the Physics and Chemistry of Materials, ed. R.J. Brook, et al. 1999, New York: Oxford University Press. 1328.

77.   Rosenberg, H.M., *The solid state.* 3rd ed. Oxford Physics Series. 1988, Oxford: Oxford University Press. 315.

78.   Celzard, A., et al., *Conduction mechanisms in some graphite-polymer composites: The effect of a direct-current electric field.* Journal of Physics: Condensed Matter, 1997. **9**: p. 2225-2237.

79.   Jain, S.C., et al., *Trap filled limit of conducting organic materials.* Journal of Applied Physics, 2002. **92**(7): p. 3752-3754.

80.   Dissado, L.A. and J.C. Fothergill, *Electrical degradation and breakdown in polymers.* IEE Materials and Devices Series 9, ed. D.V. Morgan, N. Parkman, and K. Overshott. 1992: Peter Peregrinus Ltd. 601.

81.   Sheng, P., B. Abeles, and Y. Arie, *Hopping conductivity in granular metals.* Physical Review Letters, 1973. **31**(1): p. 44-47.

82.   Sheng, P. and J. Klafter, *Hopping conductivity in granular disordered systems.* Physical Review B, 1983. **27**(4): p. 2583-2586.

83.   Sarchev, A.K. and F. Brouers, *New scaling for AC properties of percolating composite materials.* Physical Review Letters, 1994. **73**(21): p. 2895-2898.

84.   Cashell, E.M., et al., *DC electrical conduction in carbon black filled cis-polybutadiene.* Journal of Applied Physics, 1981. **52**(3): p. 1542-1547.

85.   Sheng, P. and B. Abeles, *Voltage-induced tunnelling conduction in granular metals at low temperatures.* Physical Review Letters, 1972. **28**(1): p. 34-37.

86.   Neugebauer, C.A. and M.B. Webb, *Electrical conduction mechanism in ultrathin, evaporated metal films.* Journal of Applied Physics, 1961. **33**(1): p. 74-82.

87.   Grabert, H. and M.H. Devoret, *Single charge tunnelling coulomb blockade phenomena in nanostructures.* NATO Advance Scientific Institutes Series B: Physics. Vol. 294. 1992: Plenum Press. 335.

88.   Hands, P.J.W., *The characterisation of metal-insulator composites*, in *Department of Physics*. 1999, University of Durham.

89.   Bloor, D., *Initial investigation into the properties of the Peratech metal-polymer composite*. 1998.

90.   Laughlin, P.J., *Electrical response of QTC to compression*. 2002.

91.   Gordon, R., *An investigation into the manufacture and hysteresis properties of the Peratech metal-insulator composite*, in *Department of Physics*. 2000, University of Durham.

92.   Boonham, G., et al., *Peratech EMI shielding project*. 2000, Department of Physics, University of Durham.

93.   Yeomans, M., et al., *An investigation into radio frequency emission from a quantum tunnelling composite*. 2001, Department of Physics, University of Durham.

94.   Donnelly, K.P., *Novel metal-polymer conductive composites: Progress report*. 2002, Department of Physics. University of Durham.

95.   Pottage, J.T., *Characterisation of bilayer polymeric light-emitting diodes*, in *Department of Physics*. 1998, University of Durham.

96.   Jonscher, A.K., *Electronic conduction in dielectric films*. Journal of the Electrochemical Society, 1969. **116**: p. 217C-226C.

97.   Sze, S.M., *VLSI technology*. 2nd edition ed. McGraw-Hill series in electrical engineering, ed. S.W. Director. 1988: McGraw-Hill. 676.

98.   Murarka, S.P. and M.C. Peckerar, *Electronic materials science and technology*. 1989: Academic Press. 622.

99.   Grovenor, C.R.M., *Microelectronic materials*. Graduate student series in materials science and engineering, ed. B. Cantor. 1989: IOP. 544.

100.   Edgcombe, C.J. and U. Valdre, *Microscopy and computational modelling to elucidate the enhancement factor for field electron emitters*. Journal of Microscopy, 2000. **203**(2): p. 188-194.

101.   Edgcombe, C.J. and U. Valdre, *The enhancement factor and the characterisation of amorphous carbon field emitters*. Solid-State Electronics, 2001. **45**: p. 857-863.

102.   Bailey, R.A. and K.C. Persaud, *Sensing volatile chemicals using conducting polymer arrays*, in *Polymer sensors and actuators*, Y. Osada and D.E. Derossi, Editors. 2000, Spinger Verlay. p. 149-181.

103.   Barisci, J.N., et al., *Conducting polymer sensors for monitoring aromatic hydrocarbons using an electric nose*. Sensors and Actuators B, 2002. **84**: p. 252-257.

104.   Fang, Q., et al., *Micro-gas-sensor with conducting polymers*. Sensors and Actuators B, 2002. **84**: p. 66-71.

105.   Freund, M.S. and N. Lewis, *A chemically diverse conducting polymer-based "electronic nose".* Proc. Natl. Acad. Sci. USA, 1995. **92**: p. 2652-2656.

106.   Partridge, A.C., M.L. Jansen, and W.M. Arnold, *Conducting polymer-based sensors.* Materials Science and Engineering C, 2000. **12**: p. 37-42.

107.   Gangopadhyay, R. and A. De, *Conducting polymer composites: novel materials for gas sensing.* Sensors and Actuators B, 2001. **77**: p. 326-329.

108.   Gardner, J.W. and P.N. Bartlett, *Electronic noses: Principles and applications.* 1999: Oxford University Press. 245.

109.   Chang, S.-M., et al., *The principle and applications of piezoelectric crystal sensors.* Materials Science and Engineering C, 2000. **12**: p. 111-123.

110.   Wagner, J. and M. Von Schickfus, *Inductively coupled polymer coated surface acoustic wave sensor for organic vapours.* Sensors and Actuators B, 2001. **76**: p. 58-63.

111.   Patrash, S.J. and E. Zellers, *Characterisation of polymeric surface acoustic wave sensor coatings and semiempirical models of sensor responses to organic vapours.* Analytical Chemistry, 1993. **65**: p. 2055-2066.

112.   Park, J., W.A. Groves, and E.T. Zellers, *Vapour recognition with small arrays of polymer-coated microsensors. A comprehensive analysis.* Analytical Chemistry, 1999. **71**: p. 3877-3886.

113.   Oliveros, M.C.C., et al., *Electronic nose based upon metal oxide semiconductor sensors as a fast alternative for the detection of adulteration of virgin olive oils.* Analytica Chimica Acta, 2002. **459**: p. 219-228.

114.   Romain, A.-C. and P.A.J. Nicolas, *Three years experiment with the same tin oxide sensor arrays for the identification of malodorous sources in the environment.* Sensors and Actuators B, 2002. **84**: p. 271-277.

115.   Skubal, L.R., N.K. Meshkov, and M.C. Vogt, *Detection and identification of gaseous organics using a TiO2 sensor.* Journal of Photochemistry and Photobiology A: Chemistry, 2002. **148**: p. 103-108.

116.   Adu, C.K.W., et al., *Carbon nanotubes: A thermoelectric nano-nose.* Chemical Physics Letters, 2001. **337**: p. 31-35.

117.   Hammond, J., et al., *A semiconducting metal-oxide array for monitoring fish freshness.* Sensors and Actuators B, 2002. **84**: p. 113-122.

118.   Culshaw, B., *Optical systems and sensors for measurement and control.* Journal of Physics E: Scientific Instrumentation, 1983. **16**: p. 978-986.

119.   Narayanaswamy, R. and F. Sevilla III, *Optical fibre sensors for chemical species.* Journal of Physics E: Scientific Instrumentation, 1988. **21**: p. 10-17.

120. Fabricius, N., G. Gauglitz, and J. Ingenhoff, *A gas sensor based on an integrated optical Mach-Zehnder interferometer.* Sensors and Actuators B, 1992. **7**: p. 672-676.

121. Chen, J., et al., *Novel vapour sensor from polymer-grafted carbon black: effects of heat-treatment and gamma ray radiation-treatment on the response of sensor material in cyclohexane vapour.* Polymer, 2002. **43**: p. 2201-2206.

122. Marquez, A., J. Uribe, and R. Cruz, *Conductivity variation induced by solvent swelling of an elastomer-carbon black-graphite composite.* Journal of Applied Polymer Science, 1997. **66**: p. 2221-2232.

123. Mabrook, M. and P. Hawkins, *A rapidly-responding sensor for benzene, methanol and ethanol vapours based on films of titanium dioxide dispersed in a polymer operating at room temperature.* Sensors and Actuators B, 2001. **75**: p. 197-202.

124. Chen, J. and N. Tsubokawa, *Novel gas sensor from polymer-grafted carbon black: Vapour response of electric resistance of conducting composites prepared from poly(ethylene-block-ethylene oxide)-grafted carbon black.* Journal of Applied Polymer Science, 2000. **77**(11): p. 2437-2447.

125. Chen, J. and N. Tsubokawa, *Electric properties of conducting composite from poly(ethylene oxide) and poly(ethylene oxide)-grafted carbon black in solvent vapour.* Polymer Journal, 2000. **32**(9): p. 729-736.

126. Chen, J. and N. Tsubokawa, *A novel gas sensor from polymer-grafted carbon black: Effects of polymer, crystalline organic compound and carbon black on electrical response to tetrahydrofuran vapour.* Journal of Macromolecular Science - Pure and Applied Chemistry, 2001. **A38**(4): p. 383-398.

127. Tsubokawa, N., et al., *A novel gas sensor from crystalline polymer-grafted carbon black: responsibility of electric resistance of composite from crystalline polymer-grafted carbon black against solvent vapour.* Polymer Bulletin, 1999. **42**: p. 425-431.

128. Tsubokawa, N., et al., *A novel contamination sensor in solution: the response of the electric resistance of a composite based on crystalline polymer-grafted carbon black.* Sensors and Actuators B, 2001. **79**: p. 92-97.

129. Hassan, H.H., *Electrical conductance of fast extrusion furnace carbon black-loaded styrene butadiene rubber.* Journal Macromol. Sci.-Chem., 1982. **A18**(4): p. 535-543.

130. Zee, F. and J.W. Judy, *Micromachined polymer-based chemical gas sensor array.* Sensors and Actuators B, 2001. **72**: p. 120-128.

131. Chen, X., et al., *Morphology and gas-sensitive properties of polymer based composite films.* Sensors and Actuators B, 2000. **66**: p. 37-39.

132. Ho, C.K. and R.C. Hughes, *In-situ chemiresistor sensor package for real-time detection of volatile organic compounds in soil and groundwater.* Sensors, 2002. **2**: p. 23-24.

133. Doleman, B.J., et al., *Quantitative study of the resolving power of arrays of carbon black-polymer composites in various vapour-sensing tasks.* Analytical Chemistry, 1998. **70**(19): p. 4177-4190.

134. Doleman, B.J., et al., *Use of compatible polymer blends to fabricate arrays of carbon black - polymer composite vapour detectors.* Analytical Chemistry, 1998. **70**: p. 2560-2564.

135. Doleman, B.J., E.J. Severin, and N.S. Lewis, *Trends in odour intensity for human and electronic noses: Relative roles of odourant vapour pressure vs. molecularly specific odourant binding.* Proc. Natl. Acad. Sci. USA, 1998. **95**: p. 5442-5447.

136. Severin, E.J., et al., *Differential detection of enatiomeric gaseous analytes using carbon black - chiral polymer composite, chemically sensitive resistors.* Analytical Chemistry, 1998. **70**: p. 1440-1443.

137. Vaid, T.P. and N.S. Lewis, *The use of "electronic nose" sensor responses to predict the inhibition activity of alcohols on the cytochrome P-450 catalysed p-Hydroxylation of Aniline.* Bioorganic & Medicinal Chemistry, 2000. **8**: p. 795-805.

138. Albert, K.J., et al., *Cross-reactive chemical sensor arrays.* Chemical Reviews, 2000. **100**(7): p. 2595-2626.

139. Severin, E.J., B.J. Doleman, and N.S. Lewis, *An investigation of the concentration dependence and response to analyte mixtures of carbon black/insulating organic polymer composite vapour detectors.* Analytical Chemistry, 2000. **72**: p. 658-668.

140. Sotzing, G.A., et al., *Preparation and properties of vapour detector arrays formed from poly(3,4-ethylenedioxy)thiophene-poly(styrene sulfonate)/insulating polymer composites.* Analytical Chemistry, 2000. **72**(14): p. 3181-3190.

141. Sotzing, G.A., et al., *Highly sensitive detection and discrimination of biogenic amines utilising arrays of polyaniline/carbon black composite vapour detectors.* Chem. Mater., 2000. **12**(3): p. 593-595.

142. Doleman, B.J. and N.S. Lewis, *Comparison of odour detection thresholds and odour discriminabilities of a conducting polymer composite electronic nose versus mammalian olfaction.* Sensors and Actuators B, 2001. **72**: p. 41-50.

143. Vaid, T.P., M.C. Burl, and N.S. Lewis, *Comparison of the performance of different discriminant algorithms in analyte discrimination tasks using an array of carbon black-polymer composite vapour detectors.* Analytical Chemistry, 2001. **73**(2): p. 321-331.

144. Hopkins, A.R. and N.S. Lewis, *Detection and classification characteristics of arrays of carbon black/organic polymer composite chemiresistive vapour detectors for the nerve agent simulants dimethylmethylphosphonate and diisopropylmethylphosphonate.* Analytical Chemistry, 2001. **73**: p. 884-892.

145. Burl, M.C., et al., *Assessing the ability to predict human percepts of odour quality from the detector responses of a conducting polymer composite-based electronic nose.* Sensors and Actuators B, 2001. **72**: p. 149-159.

146. Burl, M.C., et al., *Classification performance of carbon black-polymer composite vapour detector arrays as a function of array size and detector composition.* Sensors and Actuators B, 2002. **87**: p. 130-149.

147. Taylor, L.R.G., *Introduction to polymer science*. 149-162.

148. Cowie, J.M.G., *Polymers: Chemistry and physics of modern materials*. 2 ed. 1991: Blackie Academic & Professional. 431.

149. Berriot, J., et al., *Reinforcement of model filled elastomers: experimental and theoretical approach of swelling properties*. Polymer, 2002. **43**: p. 6131-6138.

150. Buchold, R., et al., *Swelling behaviour of thin anisotropic polymer layers*. Thin Solid Films, 1999. **350**: p. 178-185.

151. Booth, C. and C. Price, *Polymer Properties*. Comprehensive polymer science: The synthesis, characterisation, reactions & applications of polymers, ed. G. Allen and J.C. Bevington. Vol. 2. 1989: Pergamon Press.

152. Barry, A.J. and H.N. Beck, *Silicone polymers*. p. 272-275.

153. Tobolsky, A.V., *Properties of polymers*. p. 17-19.

154. Tanner, B.K., *Introduction to the physics of electrons in solids*. 1995: Cambridge University Press. 246.

155. Gao, P. and M.R. Mackley, *A general model for the diffusion and swelling of polymers and its application to ultra-high molecular mass polyethylene*. Proc. R. Soc. Lond. A, 1994: p. 267-285.

156. Wypych, G., *Handbook of solvents*. Vol. 1st ed. 2001, Toronto: Chem Tec Pub.

157. Noble, M., *Vapour sensing with a novel metal-polymer composite*, in *Department of Physics*. 2001, University of Durham.

158. *Handbook of Chemistry and Physics*. 66th ed, ed. R.C. Weast. 1986: CRC Press.

Appendix A

Reduction of General Effective Medium (GEM) equation
to Percolation theory in the case of an infinite conductivity ratio

GEM equation:
$$\frac{f\left(\Sigma_l - \Sigma_m\right)}{\Sigma_l + \left[f_c/(1-f_c)\right]\Sigma_m} + \frac{(1-f)\left(\Sigma_h - \Sigma_m\right)}{\Sigma_h + \left[f_c/(1-f_c)\right]\Sigma_m} = 0$$

where,
$$\Sigma_l = \sigma_l^{1/t} \qquad \Sigma_h = \sigma_h^{1/t} \qquad \Sigma_m = \sigma_m^{1/t}$$

For an infinite conductivity ratio, $\dfrac{\sigma_h}{\sigma_l}$, σ_h is finite, and $\sigma_l = 0, \Rightarrow \Sigma_l = 0$

Therefore, the GEM equation becomes:

$$\frac{-f}{f_c/(1-f_c)} + \frac{(1-f)\left(\Sigma_h - \Sigma_m\right)}{\Sigma_h + \left[f_c/(1-f_c)\right]\Sigma_m} = 0$$

$$\frac{(1-f)\left(\Sigma_h - \Sigma_m\right)}{\Sigma_h + \left[f_c/(1-f_c)\right]\Sigma_m} = \frac{f}{f_c}(1-f_c)$$

$$\frac{(1-f)\left(\Sigma_h - \Sigma_m\right)}{(1-f_c)\Sigma_h + \Sigma_m f_c} = \frac{f}{f_c}$$

$$\frac{(1-f)\left(\Sigma_h - \Sigma_m\right)}{\Sigma_h - \Sigma_h f_c + \Sigma_m f_c} = \frac{f}{f_c}$$

$$\Sigma_h f - \Sigma_h f_c f + \Sigma_m f_c f = f_c(1-f)\left(\Sigma_h - \Sigma_m\right)$$

$$\Sigma_h f - \Sigma_h f_c f + \Sigma_m f_c f = f_c\left(\Sigma_h - \Sigma_h f + \Sigma_m f - \Sigma_m\right)$$

$$\Sigma_h f - \Sigma_h f_c f + \Sigma_m f_c f = \Sigma_h f_c - \Sigma_h f_c f + \Sigma_m f_c f - \Sigma_m f_c$$

$$\Sigma_h\left(\frac{f}{f_c}\right) = \Sigma_h - \Sigma_m$$

$$\frac{f}{f_c} = 1 - \frac{\Sigma_m}{\Sigma_h}$$

Substituting for Σ_m and Σ_h gives: $\quad \dfrac{\sigma_m^{1/t}}{\sigma_h^{1/t}} = 1 - \dfrac{f}{f_c}$

Taking natural logarithms gives: $\quad \ln\left(\sigma_m^{1/t}\right) - \ln\left(\sigma_h^{1/t}\right) = \ln\left(1 - \dfrac{f}{f_c}\right)$

$$\ln\sigma_m - \ln\sigma_h = t\ln\left(1 - \frac{f}{f_c}\right)$$

Taking anti-logarithms gives: $\qquad\qquad \dfrac{\sigma_m}{\sigma_h} = \left(1 - \dfrac{f}{f_c}\right)^t$

$$\frac{\sigma_m}{\sigma_h} = \left(\frac{f_c - f}{f_c}\right)^t$$

$$\sigma_m = \frac{\sigma_h}{f_c^t}\left(f_c - f\right)^t$$

where f is the volume fraction of the low conductivity component, and f_c is the critical volume fraction of the low conductivity component.

In Percolation Theory,

p is the volume fraction of the high conductivity component, and

p_c is the critical volume fraction of the high conductivity component.

$$\therefore \qquad f = 1 - p \qquad \text{and} \qquad f_c = 1 - p_c$$

Substituting for f and f_c gives the result: $\quad \sigma_m = \dfrac{\sigma_h}{f_c^t}\left(p - p_c\right)^t$

or: $\qquad\qquad\qquad\qquad\qquad\qquad \sigma_m \propto \left(p - p_c\right)^t$

the result obtained for percolation theory,

where $\sigma_m = \sigma_{DC}$ the DC conductivity of the composite.

Appendix B

Calculating vapour concentrations

Vapour pressures at specific temperatures (0 °C and 25 °C) for known solvents were taken from the Handbook of Chemistry and Physics [158]. Corrections for solvents at different temperatures could be made by application of the Clausius-Clapeyron equation:

$$\ln p_i = \frac{-\Delta H_v}{RT_{solvent}} + \left(\text{a constant} \right)$$

where p_i is the vapour pressure, ΔH_v is the enthalpy of vaporisation (taken also from reference [158]) and T is the absolute temperature of the solvent. R is the universal gas constant. The unknown constant can be determined for each solvent by substitution into the Clausius-Clapeyron equation of a known vapour pressure at a specific temperature. Note that this equation assumes that ΔH_v is constant for all temperatures and that the solvent vapour behaves as an ideal gas.

Once the vapour pressure for the desired solvent (at the required temperature) has been calculated, the concentration of the solvent in the carrier gas can be calculated by use of the ideal gas equation:

$$n_i = \frac{p_i V_{gas}}{RT_{gas}}$$

where n_i is the number of moles of solvent dissolved in a volume of gas, V_{gas}, at temperature T_{gas}. The temperature of the gas is assumed to be the same as the temperature of the solvent. This assumption is considered fair due to the low flow rate of gas passing through multiple solvent bubblers. The volume of gas, V_{gas}, is measured in m^3 and can be deduced from the volume flow rate (given in ml min^{-1}), controlled by the mass flow controller on the bubbler line. The resulting value of n_i therefore has units of moles per minute, and represents the number of moles of solvent that are dissolved in the carrier gas per minute within the bubbler line.

Multiplication of n_i by the molecular mass of the solvent allows the number of grams (or milligrams) of solvent per minute passing through the bubbler line to be calculated. To then convert this to the number of milligrams of solvent per litre of carrier gas, one must multiply by the total volume flow rate (measured in litres per minute). The total volume flow rate will be the sum of the bubbler and diluent lines (although dilution of the vapour may not occur in all experiments). The result is now the mass of solvent dissolved in every litre of carrier gas (measured in mg litre^{-1}). This is also the definition of ppm.

Comparison of the above calculated ppm concentration can now be made to the calculated ppm level for SVP of the same solvent at 25 °C with no dilution. Solvent concentration at any flow rate, any amount of dilution and at any temperature can then be expressed as a percentage of SVP at 25 °C.

Worked example:

Solvent: Hexane	Solvent molecular mass: 86g
Solvent temperature: -30 °C	SVP at 25 °C: 20.2 kPa
Bubbler flow rate: 10 ml min^{-1}	Enthalpy vaporisation: 31.56 kJ mol^{-1}
Diluent flow rate: 40 ml min^{-1}	

At 25 °C, vapour pressure = 20.2 kPa. Substituting in Clausius-Clapeyron equation gives:

$$\ln\left(20.2 \text{ kPa}\right) = \frac{-31.56 \text{ kJ mol}^{-1}}{\left(8.31 \text{ J mol}^{-1} \text{ K}^{-1}\right) \times \left(298.15 \text{ K}\right)} + \left(\text{a constant}\right)$$

$$\therefore \left(\text{a constant}\right) = 22.6447$$

Calculate vapour pressure at −30 °C by using this constant and again substituting into Clausius-Clapeyron equation:

$$\ln p_i = \frac{-31.56 \text{ kJ mol}^{-1}}{\left(8.31 \text{ J mol}^{-1} \text{ K}^{-1}\right) \times \left(243.15 \text{ K}\right)} + 22.6447$$

$$\therefore p_i = 1.1342 \text{ kPa} \ (\text{at} -30 \text{ °C})$$

Now use this calculated vapour pressure in the ideal gas equation to calculate n_i, the number of dissolved moles of hexane in the bubbler line:

$$n_i = \frac{(1.1342 \text{ kPa}) \times (10 \text{ ml min}^{-1})}{(8.31 \text{ J mol}^{-1} \text{ K}^{-1}) \times (243.15 \text{ K})}$$

(Remembering that 1 ml = 10^{-6} m^3)

$$n_i = 5.6102 \times 10^{-6} \text{ moles min}^{-1}$$

$\therefore$ 5.6102 x 10^{-6} moles of hexane are dissolved in the bubbler line per minute

Multiplying by molecular mass of hexane (86g), gives:

0.48248 mg of hexane dissolved in the bubbler line per minute

In one minute, total flow (diluent + bubbler) = 50 ml, giving:

0.48248 mg of hexane dissolved in every 50 ml of nitrogen carrier gas

Dividing by 50 ml gives:

9.6497 mg of hexane per litre of nitrogen

ppm are defined as the number of milligrams of solvent dissolved per dm^3 (or litre) of carrier gas. Therefore, to 3 significant figures, the calculated concentration is 9.65 ppm.

Repeating the above calculation for hexane at 25 °C, in 50 ml min^{-1} carrier gas and no diluent, gives a SVP concentration of 700.78 ppm. The lower temperature and diluted value of 9.65 ppm is 1.3 % of this value. Therefore:

Concentration of hexane vapour in nitrogen carrier gas is: **9.65 ppm**

or: **1.3% of SVP at 25 °C**

Appendix C

Confirmation of saturated vapour by mass loss experiment

Nitrogen gas was bubbled through two hexane bubblers in series at ten different flow-rates. The mass of solvent in each of the bubblers was recorded beforehand, and then again after approximately 4 hours of bubbling. The mass loss (and therefore also the ppm concentration) for each flow rate was then calculated. The graph illustrates how flow rate affects the ppm concentration of hexane. If saturation of the vapour is occurring at all flow rates, then the resulting graph should appear horizontal. Incomplete saturation would cause the ppm concentration to fall at high flow rates.
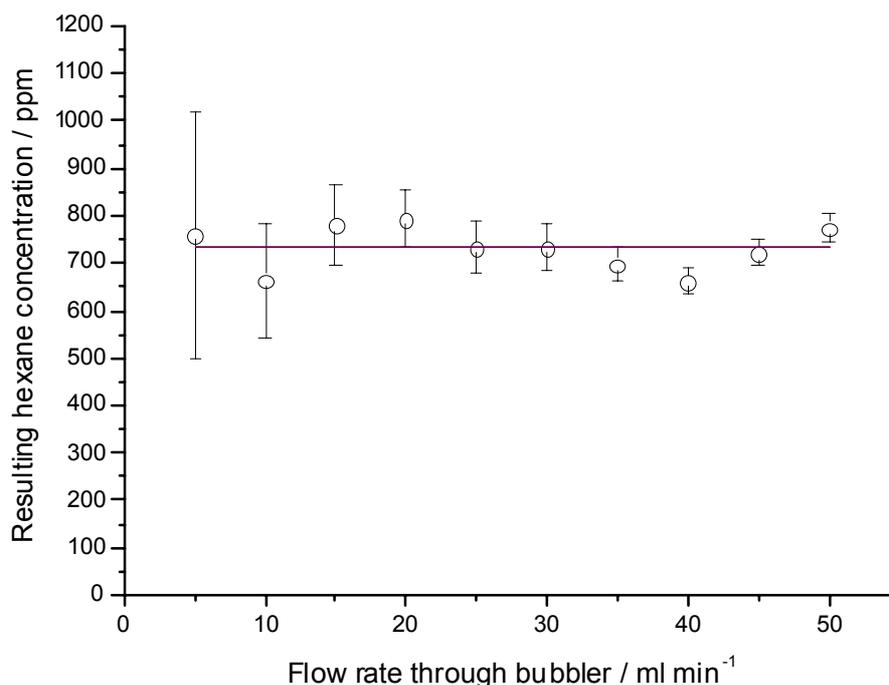
Deviations form horizontal linearity in the above graph are most probably due to temperature fluctuations over the several days taken to perform the experiment. For example, at 20 °C, a 5 °C change can affect concentration levels by more than 100 ppm. The graph implies saturated vapour for all flow rates at a concentration of **732.3 (±14.7) ppm**, which corresponds to **104% (± 3%) of SVP at 25 °C**.